POLITECNICO DI TORINO

ÉCOLE POLYTECHNIQUE FÉDÉRALE DE LAUSANNE

Master's Degree in Environmental and Land Engineering

Assessing the effect of pore-scale heterogeneity on glass beads treated with microbially induced calcite precipitation

Supervisors:

Prof. Lyesse Laloui, EPFL

Prof. Daniele Peila, Politecnico di Torino

Dr. Dimitrios Terzis, EPFL

Ariadni Elmaloglou, EPFL

Candidate:

Paolo Gandolfi

Academic Year 2020/2021

Abstract

Traditional soil improvement techniques have negative impact in a world that is seeing an extreme demographic growth, with consequent larger land use and need for infrastructure. In recent years, the growing need to find alternative has led to the development of new technologies in the fields of civil and environmental engineering.

Among these, Microbially Induced Calcite Precipitation (MICP), represents a technology capable of improving the mechanical characteristics of soils of even fine granulometries, conferring them a greater strength, with a lower environmental impact.

The technology is still in an experimental state and extensive research has been conducted to fully understand the processes behind it, from the laboratory to the field scale. Numerous unknowns related to understanding MICP at the microscale are still present today. These are related to the challenges of the treatment homogeneity and calcium carbonate deposition mechanism.

The present study focuses on the experimental investigation of the effects of pore-scale heterogeneities on MICP treatment results. Previous works have studied the influence of different grain sizes and porosities, or were limited to one-dimensional media.

This thesis aims to investigate the influence that the soil heterogeneity has on microscopic and macroscopic outcomes. For this purpose, three granulometries of increasing grain size distribution gradation (one uniform, one poorly-graded and one well-graded) were tested with a two-phase injection of bacteria solution from top and cementation solution from bottom.

The results were investigated by means of chemical monitoring of the effluents, calcite content physical calculation and numerical analysis of its distribution along the treated columns, correlating it to the changes in permeability and pore size, which are in turn a function of the variability of the granulometries under study. The results were then verified by means of qualitative scanning electron microscopy (SEM) observations.

Chemical monitoring revealed a reaction efficiency greater than 50% for all 11 days of cementation solution injection, demonstrating decreasing but always present bacterial activity. The calcite content estimates coming from the ions in solution concentrations proved to be strongly consistent with the empirical measurements, suggesting that chemical monitoring is a highly effective tool for a non-invasive reaction control and for

the prediction of the result. The calcite content was estimated between 2.5% (in the well-graded granulometry) and 5.3% (in the uniform granulometry) by means of the empirical calculation, while the chemical monitoring reported values on average 20% higher.

The results clearly brought to light an increasing treatment inhomogeneity for increased granulometry variability, highlighting the great influence of permeability variation on the pathways followed by the reactants inside the solid matrix. The presence of preferential or obligatory flow paths in the most heterogeneous granulometries was observed, in which the flow slowdowns and filtering effects caused non-uniform $CaCO_3$ precipitation.

The SEM observations confirmed most of the results obtained numerically, starting from the preferential distribution of the crystals on the beads of intermediate size, up to the explanation of the limited decrease in permeability following the treatment. This outcome obtained from the numerical analysis was explained by the absence of agglomerates capable of occluding the pores.

Finally, a UCS test was performed on a sub-sample of uniform granulometry, demonstrating an excellent improvement in mechanical properties. The specimen went from zero strength prior to treatment to a UCS of approximately 250 kPa following bio-cementation, reporting a failure mechanism of brittle type.

This study therefore provides a greater understanding of the interactions between soil pore-scale heterogeneities and MICP, representing a starting point for the development of new research that would allow to reach a full understanding of the process at the microscale.

Keywords

microbially induced calcite precipitation, MICP, soil improvement, microstructure, image processing, numerical analysis, microscopy, bonded geo-materials, glass beads, strength, permeability, kinetics

Riassunto

Le tecniche tradizionali di miglioramento del suolo hanno impatto negativo in un mondo che sta vedendo un'estrema crescita demografica, con conseguente maggiore utilizzo del suolo e bisogno di infrastrutture. Negli ultimi anni, la necessità crescente di trovare alternative ha portato allo sviluppo di nuove tecnologie nei campi dell'ingegneria civile e ambientale.

Tra queste, la Microbially Induced Calcite Precipitation (MICP), rappresenta una tecnica in grado di migliorare le caratteristiche meccaniche dei terreni di granulometrie anche fini, conferendo una buona resistenza a fronte di un minore impatto ambientale.

La tecnologia si trova ancora allo stato sperimentale, e numerose ricerche sono state condotte per comprendere appieno i processi alla sua base, dalla scala di laboratorio a quella reale. Diverse incognite legate alla comprensione dell'MICP alla micro-scala sono ancora presenti al giorno d'oggi. Queste sono legate al problema dell'omogeneità della cementazione e ai meccanismi di deposizione dei cristalli di carbonato di calcio.

Il presente studio si pone come ricerca sperimentale sugli effetti delle eterogeneità a livello dei pori sui risultati del trattamento di MICP. Precedenti lavori hanno investigato l'influenza di differenti dimensioni dei grani e porosità del terreno, o si sono limitati a indagini unidimensionali.

Questa tesi si pone l'obiettivo di approfondire l'influenza che le eterogeneità dei suoli hanno sui risultati micro e macroscopici. A questo scopo, tre granulometrie di diversa gradazione in distribuzione granulometrica (una uniforme, una poco gradata e una ben gradata) sono state testate con un iniezione in due fasi: una soluzione batterica dall'estremità superiore delle colonne e una soluzione cementizia da quella inferiore.

I risultati sono stati investigati per mezzo di monitoraggio chimico degli effluenti, calcolo empirico del contenuto di calcite e analisi numerica della sua distribuzione lungo le colonne trattate, correlandola ai cambiamenti di permeabilità e di dimensione dei pori, i quali sono a loro volta risultati funzione della variabilità delle granulometrie in studio. I risultati così ottenuti sono stati comparati con osservazioni qualitative al microscopio elettronico.

I monitoraggi chimici hanno rivelato un'efficienza di reazione maggiore del 50% per tutti gli 11 giorni di iniezione della soluzione cementizia, dimostrando un'attività batterica in

diminuzione ma sempre presente. Le stime del contenuto di calcite provenienti dalle concentrazioni degli ioni in soluzione si sono rivelate fortemente coerenti con le misure empiriche, facendo del monitoraggio chimico uno strumento di grande efficacia per un controllo non invasivo della reazione e una previsione del risultato. Il contenuto di calcite si è stimato tra il 2.5 % della granulometria ben gradata e il 5.3% di quella uniforme per mezzo del calcolo empirico, mentre il monitoraggio chimico riportava valori più elevati in media del 20%.

I risultati hanno portato alla luce una chiara disomogeneità del trattamento crescente per variabilità della granulometria crescente, evidenziando la grande influenza della variazione di permeabilità nei confronti dei percorsi seguiti dai reagenti all'interno della matrice solida. Si è osservato l'instaurarsi di percorsi preferenziali o obbligati nelle granulometrie più eterogenee, in cui i rallentamenti nel flusso ed effetti di filtraggio causavano la precipitazione disomogenea del $CaCO_3$.

Le osservazioni SEM hanno fornito la possibilità di confermare gran parte dei risultati ottenuti numericamente, a cominciare dalla distribuzione preferenziale dei cristalli sulle sfere di dimensioni intermedie, fino alla spiegazione della limitata diminuzione di permeabilità in seguito al trattamento. Questo risultato, ottenuto per mezzo dell'analisi numerica, è stato spiegato dall'assenza di agglomerati in grado di occludere i pori.

Infine, una prova UCS è stata eseguita su un provino di granulometria uniforme, dimostrando un ottimo miglioramento delle proprietà meccaniche. Il provino è passato da una resistenza nulla prima del trattamento a un UCS di circa 250 kPa a seguito della bio-cementazione, mostrando un meccanismo di rottura di tipo fragile.

Questo studio fornisce dunque una maggiore comprensione delle interazioni tra eterogeneità alla scala dei pori e l'MICP, ponendosi come punto di partenza per lo sviluppo di nuove ricerche che permettano di raggiungere una piena comprensione del processo alla micro-scala.

Parole chiave

precipitazione di calcite indotta microbiologicamente, miglioramento del suolo, microstruttura, elaborazione delle immagini, analisi numerica, microscopia, geo-materiali cementati, perline di vetro, resistenza, permeabilità, cinetica

Acknowledgements

Having reached the end of these five years of study, it's time to enjoy the finish line, and thank those who helped me get here.

This thesis represents the conclusive point of a path I have never regretted. I would like to thank Prof. Lyesse Laloui for giving me the opportunity to carry out this project and for having immediately instilled in me the right approach and the best attitude. Likewise, I thank Prof. Daniele Peila for not hesitating to supervise me, remaining available for all my uncertainties.

A huge thanks must go to Ariadni, constant presence during these four months of work, who, with her great availability, helped me in every phase of the project and for any kind of problem. Thanks also to Dr. Dimitrios Terzis, a fundamental point of reference on whom I could count for any issue of a practical or technical nature, always being sure of receiving an effective solution.

I thank all the LMS team, from technicians to researchers, a group of talented people, full of experience and expertise, who supported me in the laboratory activities.

If I got this far I also owe it to the one who understands me better than anyone else, thank you Chiara for always being there. Thanks to my true friends, for reminding me of my identity and relieving me in the most difficult moments.

This last year in Lausanne represents the last of the ambitious decisions I have made in my life so far, starting from enrolment in the first year of engineering. For this I have to thank my parents, who made me what I am, who made me aim high, without pushing. Thanks to them and to my sister also for the never lacking and blind support.

Finally, with unpretentiousness, thank to myself, to my realism and pragmatism, that led me to overcome many difficulties on my own. In life there are always simpler paths, but getting involved is never the wrong choice.

Table of Contents

List of Figures

List of Tables

List of Equations

1. Introduction

World population is expected to increase from 7 billion today to over 9 billion in 2050 ("OECD Environmental Outlook to 2050," 2012). This continued growth will inevitably lead to greater energy and water demand, as well as larger consumption of raw materials and land use, negatively affecting the ongoing climate crisis.

One of the sectors that will inevitably follow the population growth is that of civil engineering, and consequently the production of cement. This latter is a widely used material in construction processes, including ground improvement.

The procedures related to the production of cement alone are responsible for around 8% of global CO_2 emissions (Proaño et al., 2020) and, by the year 2050, world cement production is expected to increase between 12% and 23%, considering the rate of population growth and urbanization ("Cement Sustainability Initiative," 2018).

According to the IEA Reference Technology Scenario (RTS) estimates, this would lead to an increase in CO_2 emissions from the cement industry equal to 4% ("Cement technology roadmap plots path to cutting CO_2 emissions 24% by 2050 - News," 2018).

In order to meet one of the requirements imposed by the Paris Agreement, that is to guarantee a temperature increase below 2 °C, it is necessary to intervene in the sectors most influential on the climate crisis, starting from the cement industry and the civil engineering in general. New proposals have already been developed for improving the cement production technology and carbon sequestration (Proaño et al., 2020).

Referring in particular to soil improvement, various technologies, alternative to Portland cement treatment, have been developed, starting from the injection of acrylic or polyurethane resins and silicates (Karol, 2003) inside the ground voids to bind the solid grains.

However, these are still materials whose production and use are expensive and which (with the exception of silicates (Karol, 2003)) have a great impact on the environment.

An alternative that has begun to be studied in recent years is the use of biological processes to mediate the soil improvement. This technology combines notions of microbiology, geochemistry, and civil engineering, to create a natural binding material, the production of which has much less impact on the environment.

1.1. Principles of Bio-geotechnical engineering

By bio-geotechnical engineering we mean all the technologies used for modifying the geotechnical properties of a soil, implemented by means of chemical reactions and mediated by biological activity.

The usefulness of these chemical processes are their by-products, which have the ability to improve the soil engineering properties. These are reactions that occur naturally in nature. The purpose of biological mediation is to make them economically exploitable in the soil improvement, by controlling their timing, rate and spatial distribution. Some of these by-products comprehend inorganic precipitation, organic precipitation and gas generation (Figure 1.1).

As for inorganic precipitations, when mediated by biological activity, it can be defined as bio-mineralization. One of the most studied and used outcomes of this process is calcite.

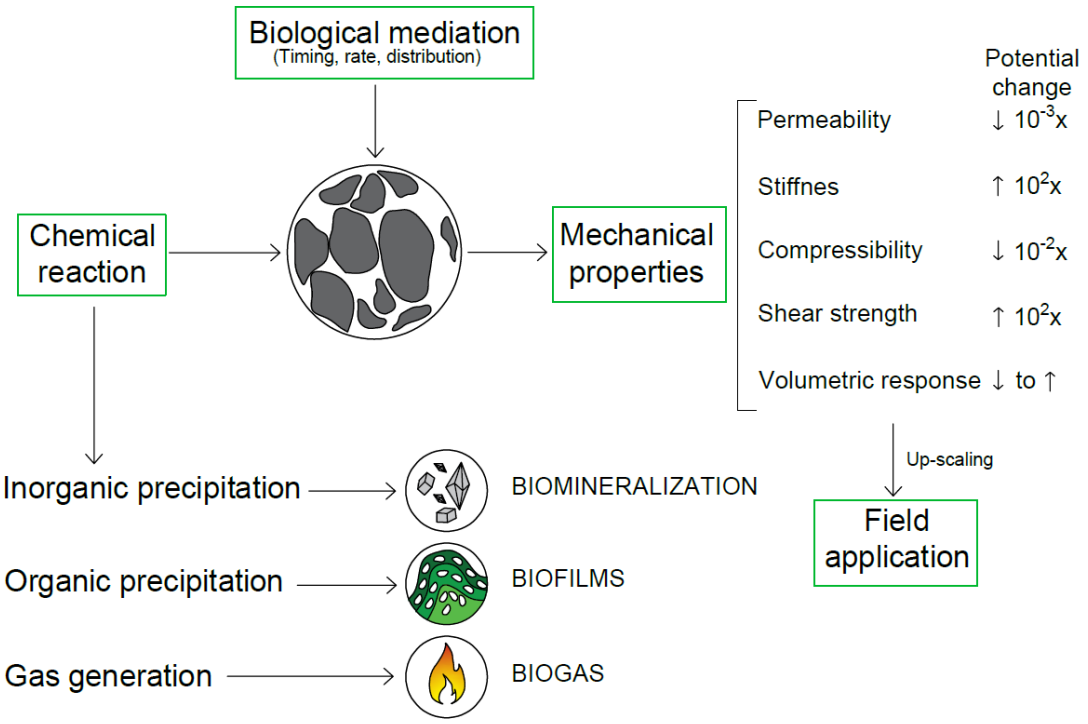

Figure 1.1 - Overview of bio-mediated soil improvement systems. Adapted from DeJong et al. (2010)

A bio-mediated soil improvement technology that makes use of calcite as a by-product is the microbially-induced calcite precipitation (MICP), in which the activity of some bacterial species is exploited to create a $CaCO_3$ over-saturated environment and induce its precipitation (Stocks-Fischer et al., 1999).

Although there are in turn many techniques to induce this process, one of the most studied and applied is certainly the urea hydrolysis, or ureolysis. It provides for the exploitation of biological activity to increase the pH, in order to create the over-saturated environment.

The process, normally taking place in nature, is mediated and catalysed (accelerating it by a factor 10^{14} (Terzis and Laloui, 2019)) by the urease enzyme, excreted by some bacteria. Among these, the most commonly used, given the high activity of its urease enzyme, are the bacteria of the genus *Sporosarcina Pasteurii*.

The enzyme decomposes urea into ammonia and CO_2, which in water are converted into ammonium and carbonic acid, bicarbonate or carbonate ions, depending on the pH. In the presence of a source of calcium ions, Ca^{2+} joins CO_3^- and precipitates in the form of calcium carbonate crystals. The increase in pH causing the over-saturation of the environment is due to the production of ammonium which generates hydroxyl ions. The main ingredients for the treatment are therefore a bacterial solution, a source of calcium ions and urea.

The precipitated calcite crystals form bridges between the soil grains, creating strong bonds that cement the solid matrix, resulting in the bio-mediated soil improvement (DeJong et al., 2010, 2006).

Although the technique presents some weaknesses, including the production of hazardous by-products such as ammonium, the studies related to this technology are multiple and promising. The convenience is linked to the lower impact on the environment compared to traditional technologies, combined with the possibility of treating fine soils, given the low viscosity of the employed reactants.

The improvement of the engineering properties of the soils by means of MICP is mainly linked to the increase in strength (Cheng et al., 2013; Cui et al., 2017; Gao et al., 2019; Konstantinou et al., 2021a; Mahawish et al., 2018; Mortensen and DeJong, 2012; Mujah et al., 2019; Qabany and Soga, 2013; Terzis et al., 2016; Terzis, 2017; Terzis and Laloui, 2019; Van Paassen, 2009; Xiao et al., 2021), maintaining adequate permeability (Qabany and Soga, 2013; Whiffin et al., 2007) and efficiently monitoring the process. The main geotechnical applications include soil stabilization (DeJong et al., 2010), erosion prevention (Anbu et al., 2016), slope stabilization (Cheng, 2012), liquefaction prevention (Dejong et al., 2013), clogging (Ivanov and Chu, 2008) and hydraulic control (Qabany and Soga, 2013).

1.2. A multi-scale problem

One of the most important challenges towards the consolidation and affirmation of the MICP technique is the upscaling to real applications. Among the limits currently imposed by the technology: the production and storage of the bacterial solution, the treatment homogeneity, the biological process randomness, the lack of a standard design technique to get the desired result, the production of dangerous by-products.

Most of the studies related to bio-mediated soil improvement are therefore carried out at the laboratory scale, which can even approach the treatment of considerable volumes (Martinez and DeJong, 2012; Van Paassen et al., 2010; Whiffin et al., 2007). However, studies relating to field applications remain rare (Gomez et al., 2015).

One of the domains in which the research still needs expansion is the study of the physical-biological mechanism at the microscale, and in particular the cultivation, growth and behavior of bacteria, and their interaction with the solid matrix, as regards the biological part and the formation, growth, morphology, spatial distribution and mechanical properties of $CaCO_3$ crystals for the physical context.

Further insights are then needed in themes ranging from the monitoring of the chemical reactions, to the geophysical analysis for the evaluation of the mechanical improvement, to the numerical modelling for the prediction of the treatment results and to the mechanical tests for the understanding of the strength improvement mechanism as a function of treatment strategy and boundary conditions.

All these investigations, already widely developed at the laboratory scale, need then to be transferred to the field scale, where treatment homogeneity, process efficiency and increase in strength are the most important results to be obtained and the most important subjects to be investigated.

For the moment, however, it remains important to proceed with the two scales in parallel, as many variables have not yet been clarified, and reaching a full understanding of the MICP effects and of the chemical-physical-biological process is imperative to definitively transfer this technology at the field scale, where there is a strong need for innovation in standard soil improvement techniques.

1.3. Research objectives

This work follows the need to deepen the study of biological, chemical and physical processes at the microscale. To do this, an experimental research on the effects of MICP technology at the pore scale was conducted.

To evaluate the response of the treatment to the microscopic heterogeneities of the soil, three different granulometries of increasing heterogeneity and grain/pore size distribution variability, were artificially created. To do this, acid-washed glass beads were used instead of soil, in order to avoid the effects of preferential precipitation due to grains shape and material variability.

As regards the shape, it influences the total surface energy, which plays a role in the $CaCO_3$ crystals nucleation (Stack, 2015). The material of which the soil particles are made has also resulted to cause calcite crystals preferential precipitation: Oliveira et al. (2017), for example, reported a detrimental effect of the MICP on organic soils, while Mortensen et al. (2011) highlighted how different minerals can lead to more favourable nucleation sites, directly influencing the thermodynamics of the precipitation and dissolution reactions.

Once the soil material to be used in the study was decided, in order to bring to light the effects of the pore scale heterogeneity, the glass beads were dosed in different percentages of variable size from 1180 um to less than 106 um, obtaining two granulometries: one poorly graded and one well graded. To these was added a uniform granulometry, whose grain size distribution fell within the range of 212-300 μm.

These three mediums were the basis of the investigations. In previous studies (Mortensen et al., 2011) the soil particle size had already been identified to influence calcium carbonate precipitation, with well graded and coarser sands having a higher rate of precipitation than finer and poorly graded soils.

Rebata-Landa (2007) also investigated the MICP efficiency using different soils with varying grain sizes and porosities. In very fine soils, the bacterial activity was limited by the space available in the small pores, resulting in low calcium carbonate concentration. In coarse soils, a low cementation was found, attributed to the formation of a thin distributed layer of calcium carbonate, which was not sufficient to increase the strength of the specimens.

In this study, greater precipitation was found in soils with higher uniformity, while less cementation was confirmed in portions of soil with great fines content. The grain size distribution variability, on the other hand, was found to have an effect mostly on the crystals distribution within the solid skeleton.

As for the porosity in absolute terms, the greater the volume of the voids, the greater the cementation. The areas characterized by very small pores showed cementation only when the flow was channelled towards them, with the forced passage of the reactants therein. In these portions the precipitation was exclusively found at the contact points, while, where the porosity was greater, a uniform layer of small crystals was observed, similarly to what Rebata-Landa (2007) highlighted.

According to Konstantinou et al. (2021a), the MICP treatment effectiveness and the resulting mechanical properties were significantly influenced by the matrix pore size distribution, which is dependent on the GSD. The same injection strategy resulted in different levels of calcium carbonate concentration due to variations in chemical efficiency. Furthermore, even at similar concentrations, the properties of the cemented material varied for the different PSDs.

In this work, the efficiency was found to vary with the GSD, albeit in an unclear manner. At the end of the treatment, the amount of $CaCO_3$ crystals revealed to be a function of the granulometry, and in particular of its porosity.

Furthermore, the matrix heterogeneities have an effect on the calcite distribution homogeneity within the solid matrix. Coarser or less dense soils (less variable in grain size) are characterized by higher flow rates and therefore more uniform cementation (Konstantinou et al., 2021a). This study investigates these effects also at the pore-scale, revealing how local alterations in the flow can lead to increased preferential deposition of $CaCO_3$ and to more or less uniform results.

Another aspect that the soil samples employed in this study allowed to investigate is the effect of the particle contacts number on the calcium carbonate precipitation. Some works have in fact highlighted the preferential $CaCO_3$ deposition at the grains contact points (DeJong et al., 2010; Gao et al., 2019; Mitchell and Santamarina, 2005), a trend that was confirmed by this study. The greater the variability of the grain size distribution, the more numerous are the particle-particle contacts (Mortensen et al., 2011), and this effect is evident in the analyses of our granulometries.

Finally, the ability for MICP to be effective is dependent on the permeability of the soil being sufficient to allow injected chemicals to flow towards the bacteria sites (Mitchell and Santamarina, 2005). In this study, the variations in permeability due to the samples' heterogeneity, were analysed numerically and led to observe their influence both on the quantity and on the distribution of the $CaCO_3$ crystals.

The observation of the effects that the pore-scale heterogeneities have on the bio-cementation behaviour was based on an experimental analysis which followed all the MICP treatment steps, from the biological part to the chemical and physical investigation, up to the mechanical study.

The work began with the cultivation of bacteria and the analysis of their ureolytic activity, and then moved on to the preparation of the cementation solution, to be used together with the bacterial one in the treatment of samples.

The following step was the injection of the two solutions with a two-phase technique. The treatment was accompanied by chemical monitoring, which allowed to quite accurately predict the efficiency and extent of the reaction. The quantity of calcium carbonate actually precipitated was verified empirically, observing its peculiar distribution along the vertical direction. These analyses allowed to evaluate the influence of the granulometry variability on the MICP treatment, at the specimen scale.

To go down to the pore scale, numerical analysis was employed, by means of XRCT image investigation. It allowed for the study of porosity, permeability and calcite content to be caried out with precision, providing useful results, in a mostly qualitative way.

The outcomes obtained from the numerical, chemical and physical investigations were effectively integrated by the observation of scanning electron microscope images, which consented to qualitatively evaluate the morphological characteristics of grains and crystals, and their spatial distribution.

To conclude, a brief study on the mechanical properties acquired following the MICP treatment was performed on a specimen of uniform granulometry. The analysis was carried out by means of a micro-UCS test, accompanied by the observation of the load response, via XRCT images.

1.4. Structure of the thesis

Following this introduction, Chapter 2 represents a brief collection of basic knowledge related to the technology of the MICP. It is an overview on the bio-cementation world, which highlights its limitations and advantages, by means of the presentation of the most important results existing so far in the literature. These latter mostly refer to laboratory-scale studies and are intended to concisely present the scientific basis behind MICP.

A more in-depth focus is devoted to the treatment techniques and to the reaction monitoring and uniformity. Finally, some of the most common results regarding the improvement of the engineering properties of the soil, and in particular the strength and permeability, are synthesized.

By means of this theoretical background of the most recent studies, the reader will be able to better understand the purpose of this work, and the analysis method followed in processing the results.

Subsequently, Chapter 3 contains the explanation of the materials and methods used in the study. How the samples were prepared and how the treatment took place, is there presented. The main procedures followed in monitoring the processes and the chemical properties, together with the methods for evaluating the final result, in terms of calcite content, are here reported.

This is followed by an explanation of the utilised numerical techniques and the software used to process the XRCT images, the presentation of the materials used for the micro-UCS test and the SEM analyses.

Chapter 4 represents a brief reflection on the setup employed as basis for the MICP treatment, necessary for a better understanding of the results.

The thesis investigational part is divided between chapters 5 and 6. The former contains the actual experimental part, showing the results of the chemical analyses of pH, electrical conductivity, ammonium, calcium and TIC. These were caried out in order to monitor the treatment and to make a prediction of the results, while accomplishing a first evaluation on the effect of the different granulometries.

The chemical analysis is followed by the measurement of the calcite content, in which, through the acid digestion technique, the mass of $CaCO_3$ contained in the different

portions of the column is empirically measured, and correlated with the pore-scale characteristics of the bio-cemented samples.

The results obtained up to this point are immediately verified by means of electron microscope investigations, which have provided an interesting practical inspection at the pore-scale. Chapter 5 concludes with the discussion of the mechanical results deriving from the micro-UCS test, carried out on a single sample.

Chapter 6 contains the most important part of the treatment results analysis, which is carried out by means of numerical computation applied to XRCT images. In this context, grain size distribution, porosity, calcite content and permeability have been thoroughly investigated, both at the scale of the column and at that of the pore.

The investigations were achieved by means of the Avizo numerical analysis software, which provided an excellent tool for validating or refuting the experimentally obtained results. The last part of this chapter is dedicated to the observation of the sample deformation response to loading, during the micro-UCS test. The discussion deepens into the failure mode, by means of the analysis of XRCT images deriving from different loading phases.

Chapter 7 is dedicated to the final discussion of the results, deduced from the two parts of experimental and numerical investigation. Here we try to summarize the main outcomes obtained from the analysis on the effects that the pore-scale heterogeneities have on the MICP treatment. In addition to this, we bring to light the major problems encountered in the study and the main advantages of the different techniques employed.

2. MICP literature review

The aim of this chapter is to present the state of the art of the MICP technique, through a brief review of the major studies conducted so far, in order to clarify the process of bio-mediated soil improvement, of which this thesis specifically investigates the pore scale.

2.1. Introduction

To address the need for alternative solutions to common engineering practices, methods less impacting on the environment are evolving today, some of which exploit living organisms, such as bacteria. Among others, applications range from agriculture and crop protection (Amarger, 2002) to wastewater treatment (Hammes et al., 2003) and biodegradation of organic pollutants (Bajaj and Singh, 2015; Castillo-Carvajal et al., 2014; Van Hamme, 2004), but also concrete reinforcement (Kim et al., 2013) or repair (Van Tittelboom et al., 2010), and selective plugging of microbial enhanced oil recovery (Gao and Zekri, 2011; Lazar et al., 2007).

One of the most promising applications is the bio-mediated soil improvement through bio-mineralization, which has been considered as an inventive and new approach in geotechnical engineering, able to improve the mechanical characteristics of the medium. The main results are an increase in strength (DeJong et al., 2010; Qabany and Soga, 2013; Venda Oliveira et al., 2015; Whiffin et al., 2007) and stiffness (Mortensen et al., 2011; Van Paassen et al., 2010; Venda Oliveira et al., 2015; Whiffin et al., 2007), a decrease in porosity (Whiffin et al., 2007) and in some cases in permeability (Chou et al., 2011; Cui et al., 2017; Dadda et al., 2017; Nemati and Voordouw, 2003; Qabany and Soga, 2013), an improvement of the load bearing capacity (DeJong et al., 2010; Van Paassen, 2009; Whiffin et al., 2007).

In our case, bio-mineralization concerns the precipitation of calcium carbonate ($CaCO_3$) which, contrary to traditional materials used in soil stabilization, such as micro-cement or synthetic resins, represents a natural mineral, abundant in geologies. If we consider that almost all chemical grouting techniques, except sodium silicate, are toxic or harmful, this technique is definitely a valid environmental-friendly alternative. Last but not least, colloidal silicates are susceptible to wetting and drying cycles, a risk which does not impact bio-cemented soils.

2.2. Bio-mediated soil improvement system

Bio-mediated soil improvement is a technology whose fundamental concept is the bio-mineralization of calcium carbonate, through the catalysis of ureolytic bacteria: the mechanism underlying this process and the microorganisms involved in it are briefly described in the next two sub-chapters.

2.2.1. Biomineralization

Biomineralization is the process by which living forms influence the precipitation of mineral materials (Skinner and Jahren, 2003). The latter can then be integrated as a part of the organism itself, forming bones or tissues, or can nucleate and grow around the microbe which mediates their precipitation: in this case, we speak of bio-mediated mineralization, which is the mechanism of our interest.

The main application is the bio-mineralization of calcium carbonate, which is characterized by two main steps: nucleation and growth (Fauriel, 2012).

The nucleation starts upon reaching of a certain degree of supersaturation with respect to calcium and carbonate ions (DeJong et al., 2010), following which, the spontaneous growth of a certain number of metastable nuclei starts. We can furthermore distinguish between homogeneous nucleation and heterogeneous nucleation The former applies when the solution is pure and consisting of mineral constituents only, and the latter when foreign nuclei (bacteria, dust, existing calcite clusters, etc.) are present in solution, lowering the energy necessary for the nucleation, which takes place on their surface.

Once seed nucleation occurs, additional ions in solution are continuously adsorbed by the previously precipitated nuclei, increasing the size of the $CaCO_3$ crystals (Mujah et al., 2019), until the decreasing supply of ions hinders further growth and reaction reaches its equilibrium.

The mineralization is enormously accelerated by the activity of some bacteria, which can catalyse the reaction described in chapter 2.3.1.

2.2.2. Microbes in soils

Soil contains a higher quantity of microbes than any other terrestrial habitats, as they have favourable characteristics towards the proliferation of microorganisms, given their high content of nutrients and retained water. It is estimated there are between 10^9 to 10^{12} organisms per kilogram of mass in areas close to the Earth's surface (Mitchell and

Santamarina, 2005). These are both prokaryotes, such as bacteria and archaea, and eukaryotes, such as algae, fungi and protozoa. In particular, the most widespread species is that of bacteria, which can survive in various environmental conditions, withstanding variations in acidity and salinity, but also significant temperature and barometric excursions.

An important bacteria characteristic is their dimension: an average cell measures between 0.5 and 1 μm in diameter and 2-5 μm in length (Srivastava, 2003) and this allows these microorganisms to move freely in the pore space of soils from coarse to fine grained (DeJong et al., 2010, 2006). But, as reported by Mitchell and Santamarina, (2005), a primary restriction on microbial transport is the size of the pore throats within the soil matrix through which the microbes must pass as they move from one pore space to another. The size of these throats is dependent on the smaller fraction of particles in soil. Soil treatment through bio-mineralization could therefore be extended to sandy-silty soils (DeJong et al., 2010; Zamani and Montoya, 2018), as reported in Figure 2.1.

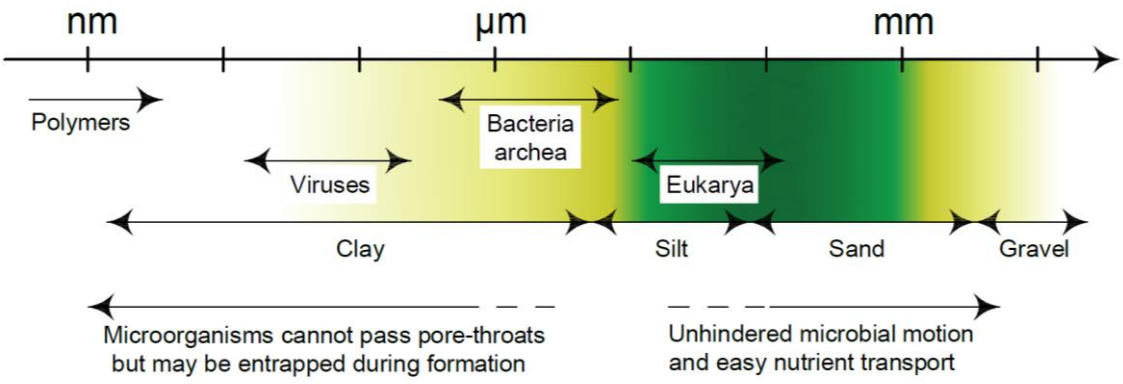

Figure 2.1 - Microbes - Grain size relationship (modified after Mitchell and Santamarina, 2005). The green and yellow areas indicate respectively the biomineralization application range and its possible extension

The microorganisms involved in the bio-mineralization process are those that possess the ability to produce the urease enzyme, among others, genera *Bacillus*, *Sporosarcina*, *Spoloactobacilus*, *Clostridium* and *Desulfotomaculum* (Kucharski et al., 2006).

However, some of these microbes are negatively influenced by the presence of ammonium, which limits their urease activity. Such examples are *Klebsiella aerogenes*, *Bacillus megaterium*, *Alcaligenes eutrophus*, and *Pseudomonas aeruginosa* (Kaltwasser et al., 1972; Friedrich and Magasanik, 1977). But others, like *Sporosarcina* or *Proteus vulgaris* are not affected by the presence of NH_4^+ (Mortensen et al., 2011; Whiffin, 2004) and can be effectively used for the bio-mediated soil improvement, whose process

produces considerable quantities of this ion (DeJong et al., 2010; Mortensen et al., 2011; Whiffin, 2004).

Among the species able to produce the urease enzyme and withstand the presence of ammonium, the genus *Sporosarcina Pasteurii* (Yoon et al., 2001) is nowadays considered as the most efficient, as it is found to yield the highest urea hydrolysis rates and due to its wall electronegativity which enhances attachment on soil grains (Terzis and Laloui, 2019). Other genera of the same family have been studied, such as *Sporosarcina newyorkensis* and *Sporosarcina aquamarina*, which also offer possibilities of use (Clarà Saracho et al., 2020b; Yoon et al., 2001).

2.3. Microbially Induced Calcite Precipitation (MICP)

We can now move on to describe in more detail the Microbial Induced Calcite-Precipitation (MICP): namely the process that leads to soil bio-cementation through the precipitation of calcium carbonate inside the soil matrix, mediated by specific microorganisms (in our case we will always refer to the activity of the most commonly used species, i.e., *Sporosarcina Pasteurii)*.

While in traditionally used injection processes by permeation, cement is used as a binding element, bio-cementation exploits the cementitious action provided by the $CaCO_3$ crystals precipitated on the soil grains.

2.3.1. Process description

The treatment is based on the precipitation of calcite caused by ametabolic process (ureolysis) in which biological activity is used to raise the pH of the environment in order to create supersaturated carbonate conditions. Three main elements are involved in the mechanism of $CaCO_3$ crystals formation: (i) urea, $CO(NH_2)_2$, and its breakdown to form CO_3^{2-}, through a reaction commonly referred to as ureolysis, catalysed by (ii) the urease enzyme, which accelerated the process up to a factor of 10^{14} (Terzis and Laloui, 2019), compared to non-catalysed reaction, and (iii) a calcium ions source, Ca^{2+}.

Ureolysis

MICP is driven by the process of urea hydrolysis (or ureolysis), which naturally occurs in the environment, but is efficiently exploitable only thanks to the catalysis of the urease enzyme. This chemical reaction indirectly conducts to bio-mineralization by generating favourable conditions, which lead to the precipitation of calcium carbonate, as described in the following equations (Hammes and Verstraete*, 2002):

$$CO(NH_2)_2 + H_2O \xrightarrow{\text{Urease enzyme}} 2NH_4^+ + CO_3^{2-} \quad [pH \uparrow] \tag{2.1}$$

Hydrolysis of urea is an irreversible reaction in which urea reacts with water to form ammonium and carbonate (2.1). At neutral pH, bicarbonate (HCO_3^-) is the dominant carbonate species rather than carbonate (CO_3^{2-}), causing a rise in pH to maintain charge balance. As a result of the increasing pH, ammonium (NH^{4+}) starts to dissociate to ammonia (NH_3) until equilibrium is reached between NH_4^+/NH_3 and HCO_3^-/CO_3^{2-} at a pH of about 9.25 (Van Paassen, 2009). The new basic environment creates a supersaturated condition which leads to the precipitation of $CaCO_3$. Stocks-Fischer et al. (1999) determined that precipitation begins at a pH level of 8.3 and occurs at an increasing rate up to a pH value of 9.0. Under these conditions and upon introduction of a calcium source into the system – usually derived from a calcium chloride solution, (2.2) – the carbonate ion reacts spontaneously with Ca^{2+} and thus calcium carbonate is produced, following the reaction given in (2.3) (Chou et al., 2011).

$$CaCl_2 \rightarrow Ca^{2+}(aq) + Cl_2^-(aq) \tag{2.2}$$

$$Ca^{2+}(aq) + CO_3^{2-}(aq) \rightarrow CaCO_3(s) \downarrow \tag{2.3}$$

To produce 1 M of $CaCO_3$, 1 M of $CaCl_2$ and 1 M of urea are required. The remaining chloride and ammonium ions lead to the formation of ammonium chloride (NH_4Cl) by the reaction in (2.4), inducing a decrease in pH. (Mortensen et al., 2011; Oliveira et al., 2017).

$$2Cl^2(aq) + 2NH_4^+(aq) \rightarrow NH_4Cl(aq) \quad [pH \downarrow] \tag{2.4}$$

The rate of ureolysis is defined as the rate of decrease in the concentration of urea with respect to time. It is an important measure to understand the state of our reaction and to have an indication of the activity of the bacteria. It also gives an idea of the possible amount of $CaCO_3$ precipitated.

Measurement and monitoring of the ureolysis rate are important elements of the MICP process. The most common techniques used for this purpose are described in chapter 2.5.4

The urease activity and the MICP process inside the soil matrix, are influenced by several factors such as initial concentration of urea, bacterial density, calcium ions concentration, temperature, pH, oxygen concentration and pore space (Mortensen et al., 2011; Stocks-Fischer et al., 1999; Van Paassen, 2009; Wang, 2019).

In particular:

- Urea concentration positively influences urease as found by Van Paassen, 2009 and Whiffin, 2004. Furthermore, Lauchnor et al. (2015), found that the ureolysis rate increased as the concentration of urea increased up to 423 mM, beyond which the ureolysis rate stayed approximately constant.
- A high bacterial density is correlated to an increased hydrolysis rate (Lauchnor et al., 2015; Martinez et al., 2013).
- Calcium concentration was found to have discordant effects in different studies. Van Paassen (2009), found that increasing the calcium concentration up to 1.5 M resulted in a decrease in ureolytic activity to a point at which ureolysis was almost completely inhibited, while Whiffin (2004), found that the rate of ureolysis was not affected by a calcium concentration up to 50 mM.
- Temperature certainly plays a role in the metabolism of bacteria and therefore in the ureolysis rate. Many studies have observed a correlation between temperature and urease activity (Van Paassen, 2009; Wang et al., 2019; Whiffin, 2004). In particular, (Whiffin, 2004), found that the ureolytic activity was stable between 15 and 25°C and exhibited a linear increase between 25 and 60°C, reaching an optimum at 70°C, above which the urease activity quickly decreased. Wang et al., 2019 observed instead that urease activity was almost inhibited for temperatures below 10°C and reached its peak around 33°C (Figure 2.2).

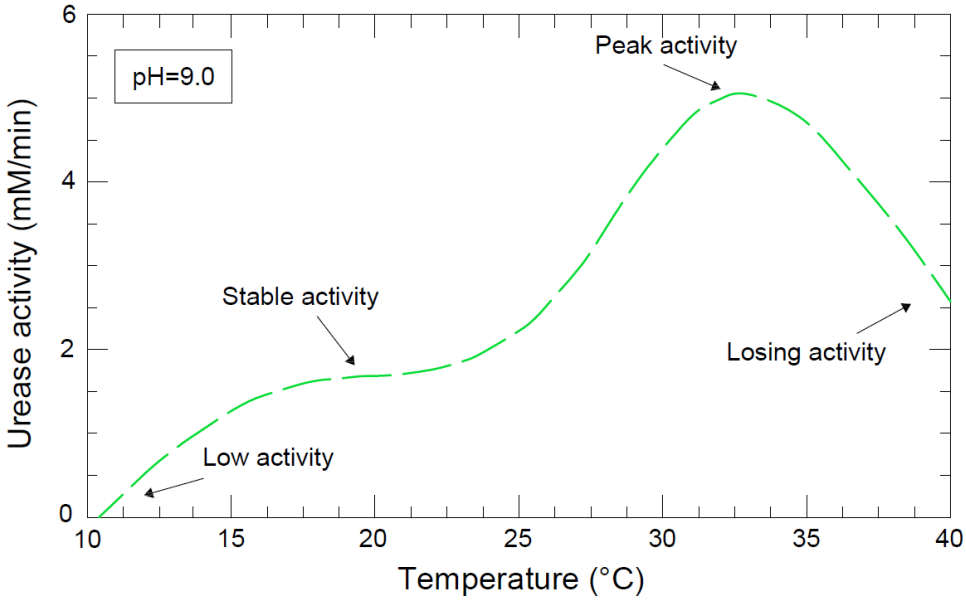

Figure 2.2 - Evolution of urease activity for Sporosarcina Pasteurii with varied temperature (modified after Xiao et al., 2021)

- pH was found to influence the urease activity, which reached the optimum at pH between 7 and 8 and decreased with decreasing and increasing pH beyond this range (Whiffin, 2004).
- Oxygen concentration can have an influence on bacteria growth. Mortensen et al. (2011), showed that anoxic environments didn't hinder the ureolysis rate. Similarly, Whiffin (2004) found that low oxygen supply limited the growth of *Sporosarcina Pasteurii* but did not reduce the level of specific urease activity but, nevertheless, extended periods of oxygen limitation resulted in a reduction of in ureolysis rate.
- The pore space reduction has a negative influence on ureolysis rate. When crystals fill up the pores, they reduce the porosity, and can hinder the liquid flow, creating stagnant areas within the pore network or zone of preferential flow. Furthermore, if a constant flow rate is applied this reduction in porosity leads to an increase in the average flow velocity and to a reduction of the residence time of the substrates within the soil volume, therefore decreasing the urease activity per soil volume (Van Paassen, 2009).

2.4. Bio-improved soils microstructure

The calcium carbonate that precipitates during the MICP process offers the binding agent to induce soil bio-cementation. The principal bond growth mechanism has been identified by Terzis and Laloui (2018) as the deposition of precipitated nuclei. Crystals tend to precipitate by nucleation and settle in different parts of the solid matrix where they subsequently grow, forming larger agglomerates. The sites in which a greater formation of crystals, and therefore of bonds, has been observed are the particle-particle contact points (DeJong et al., 2010; Gao et al., 2019). As explained by DeJong et al. (2010), this could be due to two causes: one biological and one physical. Bacteria generally prefer to settle in areas of the solid matrix not excessively exposed to the advective flux, and therefore position themselves in smaller surface features, as are the points of contact between the grains, where they find shelter and a greater availability of nutrients. Since calcium carbonate preferably precipitates on bacterial cells (Cui et al., 2017), the greatest concentration will occur precisely at the particle to particle contacts. In addition to this biological cause, DeJong et al. (2010) also bring into light a physical motivation due to a filtering process, for which the crystals that precipitate in areas other than the contact points but subsequently resuspend in the flow, tend to be transported and re-deposited

precisely at the contact point between the grains, which act as sieves for the suspended solid part. This preferential deposition is not always that obvious: for example, Cui et al. (2017) and Dadda et al. (2017) observed in their studies that for low calcite content, the crystals were generally sparsely adsorbed on the grains surface, and particle-particle crystals were not considerable.

It is important to make the distinction in the calcite deposition zone, since it is decisive in the mechanical properties acquired by the treated soil. The calcium carbonate crystals that are deposited at the particle-particle contacts and form effective bonds between the grains in the form of solid calcite bridges, contribute to the so-called effective calcite content, which is considered to be the main contributor to soil bio-improvement. The remaining part concurs only in a secondary way to the purpose, and it's not considered as effective calcite content.

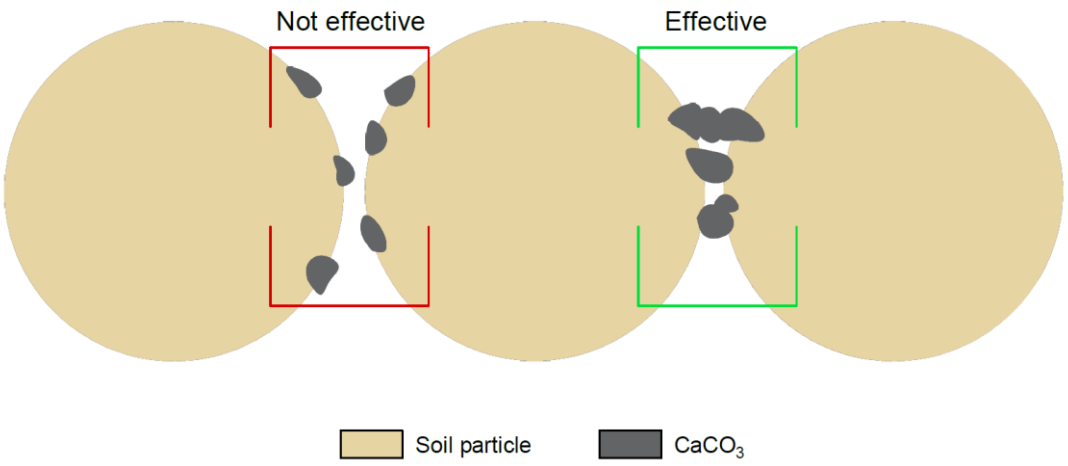

Figure 2.3 - Representation of effective (right) and not effective (left) calcite crystals

The effectiveness of calcium carbonate crystals also depends on their size. At this regards, Cui et al. (2017) observed that at a low level of cementation, the size of the clusters was relatively small but, by continuing the bio-cementation process and therefore, increasing the calcite content, the size of the clusters also increased, transforming previously inactive crystals into active bonds. Similarly, taking into account the concentration of the reactants, Dadda et al. (2017), Qabany and Soga (2013) and Al Qabany et al. 2012, observed smaller single particles for low concentrations and larger mesocrystals for higher concentrations.

Another element that influences the deposition of calcium carbonate is the morphology of the soil grains. According to Xiao et al. (2021), calcium carbonate preferably

precipitates on particles with an irregular surface, compared to smoother grains. A similar result was previously observed by Noiriel et al. (2016), where a reduction of the grains' free surface was observed, which reached between 92% and 100% in the case of irregular particles. For glass beads, the respective reduction was determined to only 11% following the MICP treatment, according to the same study.

To conclude, another aspect to take into consideration when talking about calcite content is that crystals can precipitate into different phases, with different intrinsic characteristics. Studies have shown the existence of three most common phases: vaterite, aragonite and the much more stable calcite, with different geometric structures and in order of decreasing solubility and increasing thermodynamic stability. Amorphous calcium carbonate, with a complex hybrid structure, has also been observed among other forms (Clarà Saracho et al., 2020a; Wang, 2019), but it's considered as a metastable phase. The desired structure for geotechnical applications is the most stable calcite, and the actualization of a certain polymorph has been shown to depend on reaction kinetics and degree of supersaturation (Clarà Saracho et al., 2020a; Van Paassen, 2009), on the microbial agent responsible for urea hydrolysis (Clarà Saracho et al., 2020a; Dupraz and Visscher, 2005), but also on environmental conditions such as temperature, pH and pressure (Terzis and Laloui, 2019).

Therefore, to produce the desired $CaCO_3$ content and achieve the wanted mineral form, it is essential to know how much urea and Ca^{2+} to inject and the amount of time required for the reactions to complete, which is dependent on both the ureolysis rate and precipitation rate.

2.5. Laboratory scale treatment

Having explained the process underlying the MICP technology, it is now possible to provide a description of the main techniques for performing the treatment at the laboratory scale.

As already mentioned, the most common elements used for the treatment are a bacterial solution and a cementation solution. Their common ingredients and preparation are briefly summarized in the following two chapters.

Some variations in the composition, typology and concentration of these solutions are possible and numerous in the literature, but the principle is common and pursues the

objective of having a cementing solution to precipitate under the catalysis of the enzyme urease.

2.5.1. Bacteria solution

The most common bacteria used are those of the genus *Sporosarcina Pasteurii*, which have been found to produce the highest rate of ureolysis compared to other strains that possess the urease enzyme (Whiffin, 2004). Its designation number is ATCC®11859 ™ and it belongs to the family of *Bacilli*, which are typical non-pathogenic soil bacteria, with biosafety level 1.

The bacterial solution (BS) is usually composed by bacteria cells immersed in a growth medium. For *Sporosarcina Pasteurii*, the optimal growth medium recipe involves a mix of deionized water, yeast extract, tris base and NH_4Cl or $(NH_4)_2SO_4$ (ATCC® 11859™). Ammonium, from ammonium sulphate / chloride or from urea, is essential for bacteria growth (Whiffin, 2004), as well as yeast extract, which represents a complex source of nutrients. The tris base is used to target the desired pH for bacteria growth, which must then be lowered to 9 by adding HCl. The detailed procedure followed in this study for the preparation of the bacterial solution is reported in Chapter 3.2.1.

Regarding the cultivation of bacteria, there are several techniques, which vary in practicality and cost. The cells are initially frozen, at -80 °C or in freeze-dried form stored at -20°C. Optimal growth conditions are aerobic, at a temperature of 30 °C. The aeration ratio is a factor that greatly influences the growth of bacteria and is generally chosen equal to 1:5 (Terzis, 2017). The monitoring of bacterial growth is carried out by measuring the optical density at the wavelength of 600 nm (OD600). It is a measure of the opacity of the growth liquid, which can be related to the number of cells present, according to equation (2.5) (Santosh et al., 2001).

$$\text{Concentration of cells per mL} = 8.59 \cdot 10^7 \cdot \text{OD}_{600}^{1.3627} \qquad (2.5)$$

Typically, bacterial species grow according to three distinct phases (Zwietering et al., 1990):

1. The lag phase, during which the micro-organisms must adapt to the new environmental conditions following their extraction from the freezer. During this time, which varies from one to two days, they are unable to multiply and changes in OD600 are not observed.

2. The exponential or logarithmic phase, during which a continuous growth of the OD600 is observed, as the division of the cells takes place at a constant rate. For *Sporosarcina Pasteurii*, the time for cells to double in number at this stage (generation time, or growth rate) is estimated to be around between one and two hours, according to the literature (Mortensen et al., 2011; Terzis, 2017).
3. The stationary phase, during which bacterial multiplication is reduced until it stops, due to the decreased availability of nutrients in the growth medium.

Once the desired number of cells has been reached, the medium can be used for the injection, or it can be centrifuged, in order to separate the solid part (pellet), which can then be resuspended and used, or stored at 4 °C. At this temperature, according to Whiffin, (2004), the bacteria survive, without multiplying, up to 5 days. Alternatively they can be implanted on agar plates, where colonies can survive for up to 20 days if stored in the fridge (Terzis, 2017).

Cells can be harvested at the end of the stationary phase in order to minimize further bacterial growth within the medium matrix. In the literature, values of harvested cells optical densities cells higher than 2 can indeed be observed (Mahawish et al., 2018; Mujah et al., 2019; Rowshanbakht et al., 2016), but also lower values are possible (Cheng et al., 2013; Terzis, 2017), since this parameter also varies according to the initial bacteria density. In the first case the liquid medium should be diluted: in fact, the optimal OD600 values for high urease activity are around 1 (Al Qabany et al., 2012). Stocks-Fischer et al., (1999), reported indeed that the specific rate of ammonium production and $CaCO_3$ precipitation decreases with increased cell concentration, while Konstantinou et al. (2021) suggested that higher bacteria densities should be avoided as they lead to clogging of the pores, preventing free flow.

A strongly characterizing element of the bacteria solution is its urease activity at the time of injection, calculated as explained in Chapter 2.5.4. This parameter varies according to various factors, including those reported in Chapter 2.3, as well as according to the bacteria growth phase and some of their biological features, which vary from population to population. The evaluation of the bacteria activity is important in order to have comparable results.

In the literature, widely varying values between 10^{-1} and 10^{2} mM/min are reported. Whiffin (2004) observed activities between 4 and 18 mM/min, similarly to Gao et al.

(2019) and Mahawish et al., 2018), who reported values respectively in the range of 6.66–11.10 mM/min and 19.38–21.45 mM/min. The measurements of Van Paassen (2009), Cui et al. (2017) and Al Qabany et al. (2012) are slightly lower, respectively 0.67–1.33 mM/min, 0.78 mM/min and 0.08-0-33 mM/min. Finally, Konstantinou et al. (2021b), in their study devoted to the observation of urease activity effects on various parameters related to the MICP, used bacteria solutions with urease activity varying between 0.0075 mM/min and 4.9 mM/min. They were the first to develop a method for obtaining specific urease activity, which is generally a difficult parameter to control.

2.5.2. Cementation solution

The cementation solution is typically a medium containing urea and calcium chloride, i.e. the elements which, once dissolved in water and following the ureolysis reaction, will form calcium carbonate minerals.

Concentrations typically used are less than or equal to 1 M, with equimolar of urea and calcium chloride anhydrous (Al Qabany et al., 2012; Gao et al., 2019; Mujah et al., 2019; Van Paassen, 2009; Whiffin, 2004). Nonetheless, a urea to calcium ratio greater than one is widely used (Clarà Saracho et al., 2020b; Mortensen et al., 2011; Stocks-Fischer et al., 1999) and recommended by Konstantinou et al. (2021) and Martinez et al. (2013) for effective recipe formulations, as it is proven to enhance the ureolysis and calcium carbonate precipitation rates; however, this recipe must be balanced against the environmental impact of increased ammonium being produced.

In case of repeated injections of cement solution, it may be necessary to provide an additional source of nutrients for bacteria attached to the solid matrix of the soil, in order to sustain a good urease activity. For this reason it is possible to integrate a quantity of nutrient broth into the cement solution, generally in the order of 3 g/L. (Al Qabany et al., 2012; Clarà Saracho et al., 2020b; Stocks-Fischer et al., 1999).

Other recipes for preparing the cement solution include varying molar ratios between urea and calcium chloride, or the addition of other elements such as sodium bicarbonate and ammonium chloride (Mortensen et al., 2011; Stocks-Fischer et al., 1999; Wang, 2019).

Various indications are reported in literature, regarding the concentration of the cementation solution. Whiffin (2004) observed that concentrations higher than 1.5 M resulted in reduced $CaCO_3$ content, but is reported by Clarà Saracho et al. (2020b) that the calcium carbonate content increased with the urea–calcium chloride solution molarity

for values lower than 0.15 M. As regards the percentage of precipitated calcium carbonate, Al Qabany et al., 2012 observed that varying chemical concentration (0.1, 0.25, or 0.5 M) did not make a significant difference in the overall efficiency. These differences are due both to the variability of urease activity and to the different injection strategies.

On the other hand, what is definitely influenced by the chemical concentration in the cement solution is the treatment homogeneity. However, this topic will be explored in a separate chapter.

2.5.3. Injection strategies

Injection strategies vary greatly from study to study. One of the needs for which different strategies have been studied is the homogeneity of the treatment. In fact, an accentuated precipitation has often been observed near the injection point, which can cause clogging and limited reactant delivery in the remaining part of the soil, affecting its mechanical and hydraulic properties.

Two major different injection strategies are the two-phase and the single-phase.

The first, and most widespread, was proposed by Whiffin (2007) and involves a first injection of bacteria, a waiting time of about 24 hours to allow the bacteria to attach to the grains of the soil, followed by the injection of various quantities of cement solution. This technique can in turn undergo numerous variations based on the amount of solution that is decided to inject (generally between 1 and 1.5 PV), the alternation and repetition of bacterial and cementation solutions, the injection type (stopped-flow, continuous flow, recirculation) and the waiting time for bacterial attachment, which generally varies from 6 hours to 2 days, depending on the amount of nutrients supplied to the bacteria and the logistical aspects.

Another possible variation, adopted in this study, is the flow reversal of the biological and the cementation solution, which is proven to reduce susceptibility to plugging (Martinez et al., 2013).

As regards the single-phase, it is a technique that involves the injection of a single mixture containing bacteria, urea and calcium chloride. This technique has been optimized by Xiao et al. (2021), who, in their study, have grouted the specimen with the aforementioned solution at low temperatures (less than 10 °C), so that the bacteria were inactive;

subsequently, when the liquid reached relatively high temperatures, the precipitation of calcium carbonate began. This strategy has been shown to lead to a marked improvement in the homogeneity of the $CaCO_3$ distribution in the sample.

In any case, whatever strategy is chosen, the solid matrix must be saturated with variable quantities of water before starting the treatment. Volumes greater than 1 PV are used in order to achieve the greatest possible degree of saturation and ensure the treatment of the entire control volume. Nonetheless, Cheng et al. (2013) demonstrated that soils treated in partially saturated conditions resulted in higher strengths than fully saturated ones, due to the more $CaCO_3$ crystals precipitated at the contact points between the sand grains.

Finally, an important variable is the flow rate. The treatment can in fact be performed by percolation or by adjusting the flow rate with a pump. The latter should be chosen in order to guarantee the homogeneous delivery of the saline solution throughout the sample: Molins et al. (2012) have indeed shown that the rate of dissolution (and so of precipitation) of calcite in water is a function of the Darcy velocity. There is a smooth transition between transport limited and reaction limited dissolution (Figure 2.4), where by reaction rate we mean the speed with which the bacteria in contact with the cement solution are able to catalyse the reaction. The transition gradient between transport limited and reaction limited is due to the existence of a broad range of flow velocities where the rate is transport limited in some pores but limited by reaction kinetics in others.

Since the cementation solution is often left for hours inside the soil, the main objective is to avoid a too low fluid velocity during the injection. As observed by Mortensen et al. (2011) and Stocks-Fischer et al. (1999), if a too low specific discharge is used, the rates of urea consumption and calcium carbonate precipitation are larger than the flow rate, resulting in cementation immediately adjacent to the injection source, while increasing the specific discharge to exceed the reaction rate, allows for a more homogeneous distribution of chemicals along the entire flow path.

However, the drawback of a too high flow rate can be the detachment of bacteria or the displacement of soil grains. Therefore, a correct design of the seepage velocity or flow rate must consider all these situations. In literature, typical values are in the order of 10^{-1} mm/s (Dadda et al., 2017) for the seepage velocity, while flow rates between 0.3 and 1.0 L/h are the most utilized for specimens of typical mechanical testing sizes (Cheng et al., 2013; Mujah et al., 2019; Terzis, 2017).

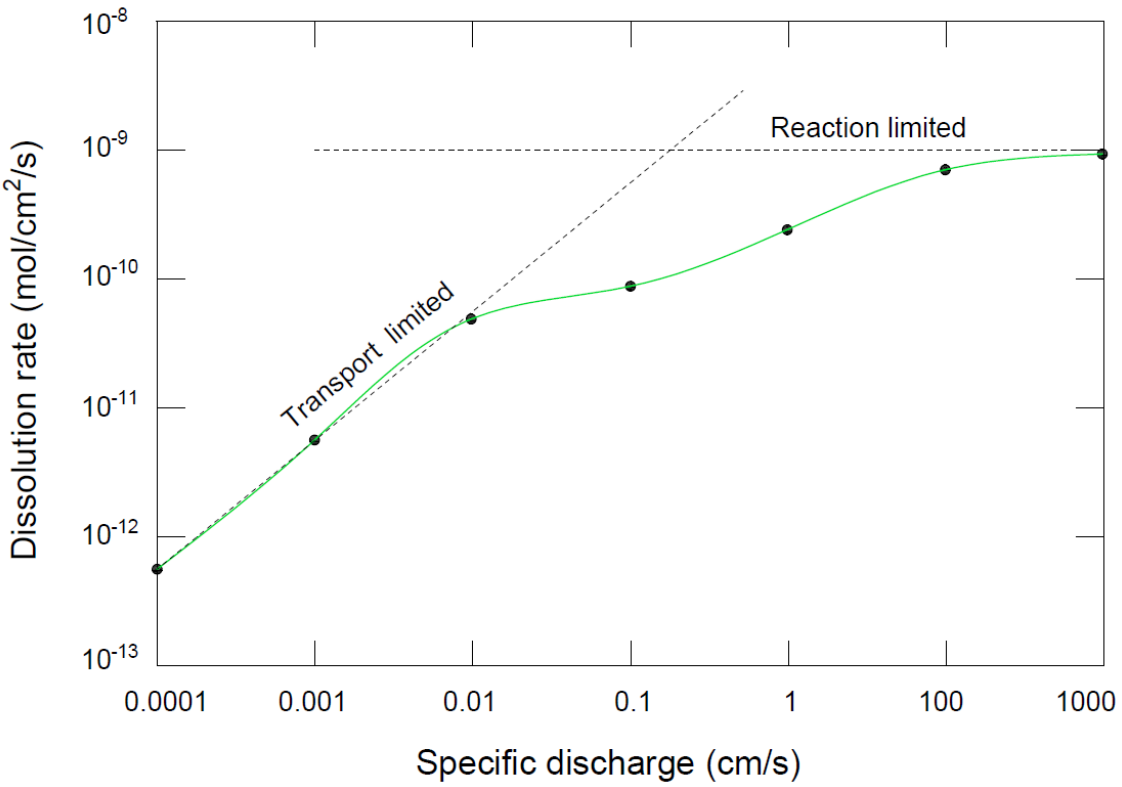

Figure 2.4 - Dissolution rate of calcite as a function of specific discharge. For low velocities, the transport is the limiting factor. Modified after Molins et al. (2012)

2.5.4. Monitoring

Soil treatment via bio-cementation well adapts to a variety of monitoring techniques during injection. These are of extreme importance in order to understand the actual realization of the reaction and its extent. At the laboratory scale, the precipitation monitoring can be carried out in real time through effluent collection and analysis. Geophysical methods are mainly useful for real-scale applications, by observing the change in density in the soil due to solid phase increase following the precipitation of calcium carbonate.

For field-scale monitoring, the most common techniques are the measurements of shear wave velocity, compression wave velocity and resistivity, while as regards the analysis of the aqueous effluents, monitoring mostly refers to pH, electrical conductivity, ammonium, calcium ions, total inorganic carbon and, for the initial phase, of the optical density.

Shear wave velocity

Shear waves do not propagate in fluids and this is advantageous for detecting changes in the solid matrix. The degree of cementation positively influences the shear wave velocity in the soils and their monitoring is particularly useful for determining the effective calcite content, since the crystals present on the grains and not connecting more particles do not significantly influence S-waves velocity (DeJong et al., 2010).

Compression wave velocity

The compression waves velocity is mainly dependent on the porosity, the pore fluid density (related to the degree of saturation), and the solid matrix density.

The use of compression waves velocity can therefore help evaluating the improvement due to cementation but, as reported by DeJong et al., 2010, in loose or lightly cemented soils this measure does not directly correlate with strength unless the soil matrix maintains a constant degree of saturation or until sufficient cementation has occurred.

Resistivity

The resistivity of a soil is a function of various parameters including: the solid matrix resistivity, the pore fluid resistivity, the porosity, the degree of saturation, the clay content and the degree of cementation.

The use of resistivity for calcite content monitoring has not been thoroughly investigated. This is mainly due to the fact that during the treatment this variable changes practically all the other parameters involved in the measure, and it is difficult to isolate the effects actually due to the calcite (DeJong et al., 2010).

Optical density

Before injecting the bacterial solution, it is good practice to know the concentration of microbes present in the liquid. In the same way it can be useful to know their concentration in the effluent, in order to evaluate the quantity of bacteria that have actually attached to the sample solid matrix. This type of analysis can be performed by measuring the optical density of the solution before injection or in the effluent by means of ultraviolet spectrophotometer at wavelength of 600 nm (namely OD600). Equation (2.5), is then an option to evaluate the number of cells.

pH

The pH measurement is a rather empirical tool for quickly monitoring the status of the reaction. It is a good indicator of bacterial activity and is mainly influenced by two phenomena: ureolysis and calcium carbonate precipitation. The first one tends to increase the pH of the solution, according to the reaction of equation (2.1), while the second has the opposite effect, acting as a pH reducer. Martinez et al. (2013), pointed out that if a 1:1 formulation is used between the concentration of calcium chloride and urea, a change in pH should not be observed at the end of the reaction, as the two processes would balance each other. In general, the increase or decrease in pH between the inlet and outlet solution is regulated by the proportion between these two components concentration and an increase or decrease of it can be due both to an increased precipitation and to a reduced bacterial activity. However, if a change in pH is always a sign that the reaction is taking place, its extent cannot be properly estimated with this measurement.

Electrical conductivity

The electrical conductivity (EC) of a fluid is directly related to the number of ions in solution. Its measurement can be useful in evaluating urease activity, mostly in the preparation of the bacterial solution (Whiffin, 2004). If some bacteria are added to a solution containing urea, the ureolysis will take place, with consequent production of ammonium ions (one mole of urea hydrolyses into two moles of ammonium) and an increase in electrical conductivity.

By means of the EC measurement it is therefore possible to evaluate, indirectly, the quantity of urea hydrolysed (2.6), while, by calculating the variation of conductivity in a time interval Δt, one can assess the urease activity (2.7) and possibly, normalizing for amount of bacterial biomass, the specific urease activity (2.8) (Clarà Saracho et al., 2020a).

$$\text{Urea hydrolysed (mM)} = \text{EC (mS cm}^{-1}) \cdot 11.11 \tag{2.6}$$

$$\text{Urease activity (mM h}^{-1}) = \frac{\Delta\text{EC (µS cm}^{-1})}{\Delta\text{t (min)}} \cdot \frac{10^{-3}\ \text{mS}}{1\ \mu\text{S}} \cdot \frac{60\ \text{min}}{1\ \text{h}} \cdot 11.11 \tag{2.7}$$

$$\text{Specific urease activity (mM h}^{-1}\text{OD}_{600}^{-1}) = \frac{\text{Urease activity (mM h}^{-1})}{\text{Biomass (OD}_{600})} \tag{2.8}$$

This measurement is preferably not usable during normal injections with cementation solution, since the calcium ions in turn greatly influence the measurement.

Ammonium

Ammonium concentration is generally measured using a modified Nessler method Whiffin (2004). Its monitoring is the most efficient way to calculate urease activity during injection cycles. In fact, it will be sufficient to divide the quantity of ammonium produced (in mM) by the time interval between injection and measurement (in minutes) to obtain the bacteria activity in mM/min, according to equation (2.9)

$$\text{Urease activity}\left(\frac{\text{M}}{\text{h}}\right) = \frac{0.5\ \text{C}_{\text{NH}_4^+}\left(\frac{\text{mol}}{\text{L}}\right)}{\Delta\text{t(h)}} \tag{2.9}$$

where C_{NH4+} is the ammonium molar concentration and Δt is duration of the reaction. The factor 0.5 is due to the mass balance of the ureolysis reaction, in which each mole of urea is hydrolysed into 2 moles of ammonium.

The ammonium concentration can also be used to evaluate the maximum amount of calcium carbonate that may have formed following the reaction: for every two moles of NH_4^+, in fact, one mole of $CaCO_3$ is formed and the mass of calcite can be determined using the following equation (2.10):

$$\text{CaCO}_3(\downarrow) = \frac{\text{C}_{\text{NH}_4^+}}{2}\left(\frac{\text{mol}}{\text{L}}\right) \cdot \text{M}_{\text{CaCO}_3}\left(\frac{\text{g}}{\text{mol}}\right) \cdot \text{V}_{\text{solution}}(\text{L}) \tag{2.10}$$

where C_{NH4+} is the ammonium molar concentration, M_{CaCO3} is the calcium carbonate mola mass and $V_{solution}$ is the volume of the injected solution.

Finally, if the ammonium measurements are integrated for each injection cycle, the total amount of precipitated calcite is obtained (if all the formed carbonate is considered as precipitated).

Calcium ions

The concentration of Ca^{2+} ions in the effluent solution also provides an estimate of the amount of precipitated calcium carbonate. The calcium ions coming from the calcium chloride in the cementation solution bind to the carbonate ions created after the ureolysis, precipitating as $CaCO_3$. The Ca^{2+} concentration that is measured in the effluent represents the percentage that has not precipitated. Through equation (2.11) it is, therefore, possible to calculate the mass of calcium carbonate that has formed:

$$CaCO_3(\downarrow) = \Delta C_{Ca}\left(\frac{mol}{L}\right) \cdot M_{CaCO_3}\left(\frac{g}{mol}\right) \cdot V_{solution}(L) \quad (2.11)$$

where ΔC_{Ca} is the difference between the calcium molar concentration in the inlet and the outlet solution, M_{CaCO3} is the calcium carbonate molar mass and $V_{solution}$ is the volume of the injected solution.

Total Inorganic Carbon

The last measurement that is most frequently used to monitor in real time the precipitated mass of calcium carbonate is the Total Inorganic Carbon (TIC). This measurement includes the concentration of the three species of the carbonate system, namely carbon dioxide, bicarbonate ion and carbonate ion. The relative concentration of these three species is governed by the pH. In the case of MICP reaction products, the most common forms are carbonate and bicarbonate, given the usually high pH.

The concentration that is measured represents the carbonate that has not precipitated or has not formed (due to an incomplete ureolysis). For the calculation of the precipitated calcite it is therefore necessary to take into account both the concentration of the inlet cementation solution and of the ammonium, since it gives us an estimate of the carbonate not hydrolysed from urea. To go back to the mass of precipitated calcium carbonate it is therefore sufficient to use equation (2.12), paying attention in the calculation of the TIC molar concentration:

$$CaCO_3(\downarrow) = \left[0.5\, C_{NH_4^+}\left(\frac{mol}{L}\right) - TIC\left(\frac{mol}{L}\right)\right] \cdot M_{CaCO_3}\left(\frac{g}{mol}\right) \cdot V_{solution}(L) \quad (2.12)$$

where C_{NH4+} the ammonium molar concentration, TIC is the measured Total Inorganic Carbon, converted in molar concentration depending on the prevalent species, M_{CaCO3} is the calcium carbonate molar mass and $V_{solution}$ is the volume of the injected solution.

Since the TIC is mostly expressed in mg/L it would be necessary to consider the pH, in order to evaluate which is the dominant species and divide the measured concentration for the right molecular mass. Anyway, this last parameter only slightly varies between one carbonate form and another, given the low hydrogen molecular weight.

2.5.5. Calcite content

After the injections, one of the most interesting measures is the calcium carbonate content. Its evaluation is mostly carried out by means of acid digestion and/or numerical analysis, respectively a destructive and non-destructive technique.

Acid digestion

Acid digestion involves the use of a strong acid, usually hydrochloric acid, in order to completely dissolve the calcium carbonate in the sample. The calculation of the effective mass of calcite can therefore be carried out in several ways.

For example, it is possible to measure the mass difference of the dry sample before and after the acid dissolution (Al Qabany et al., 2012; Cui et al., 2017; Mahawish et al., 2018; Martinez et al., 2013; Mortensen et al., 2011; Pan et al., 2020; Xiao et al., 2021): this is the simplest technique and can be quite accurate.

An alternative is to use a U-Tube manometer to measure the pressure increase due to CO_2 production following the $CaCO_3$ dissolution. This measurement is then stoichiometrically correlated with calcium carbonate content.

Less common procedures are the EDTA titration method (Gao et al., 2019) and the inductively coupled plasma optical emission spectrometry (ICP-OES) for the measurement of calcium ions dissolved in the acid (Clarà Saracho et al., 2020b).

Numerical analysis

Numerical analysis, mostly through X-Ray Computed Tomography, is a valid non-invasive alternative (Clarà Saracho et al., 2020b; Dadda et al., 2017; Noiriel et al., 2016, 2012; Terzis and Laloui, 2018). Through the segmentation of grayscale images, it is possible to distinguish the different phases present in the soil (grains, calcite crystals and pores) and numerically calculate the calcium carbonate content. The main limitation of this technique is the resolution, which is inversely proportional to the sample size. To give an example, one of the finest resolutions was employed by Noiriel et al. (2016), reaching 4.46 μm of voxel size for a sample diameter of 6.5 mm. A more in-depth discussion of the technique is present in this study (chapters 3.5 and 6).

Calcite content is not always expressed in the same way in the different studies, as it can refer to ratio between the mass of calcite and the total solid mass or the mass of the soil particles alone, or it can even be expressed as a volume ratio.

In general the most common calcite content values reported in the different studies vary from 0.6 and 1.2% (DeJong et al., 2006) to 25% (Van Paassen, 2009), (from Terzis and Laloui (2019)). It is difficult to define absolute high or low values, as it all depends on the application to be made of the improved soil. Generally, values as low as 2% can

provide sufficient mechanical properties for geotechnical applications, where confinement plays a fundamental role (Terzis and Laloui, 2019).

For other typical values and related mechanical properties refer to Table 2.1

2.5.6. Homogeneity

The spatial uniformity in the calcium carbonate crystals distribution within the sample is one of the most studied aspects in MICP technology (Al Qabany et al., 2012; Chu et al., 2014; Martinez et al., 2013; Mortensen et al., 2011). The treatment often results into non-uniform distribution, with a concentration of calcite at the injection point (Noiriel et al., 2016; Rowshanbakht et al., 2016) or clogging (Whiffin et al., 2007). A non-homogeneous calcite distribution negatively affects the mechanical and hydraulic properties of the soil, whose strength is defined by its weakest point and whose permeability can be limited by localized plugging. This study will investigate calcite distribution for three different base materials composed of idealized glass spheres. The goal is to capture the evolution of calcite content across the reactive flow path and determine changes in rheology (porosity reduction and associated permeability). Finally, the effect of locally varying biocementation will be investigated throughout mechanical loading and study of the volumetric deformation of MICP-treated micro-columns composed of glass spheres.

In the literature, the main variables influencing the treatment uniformity have been identified among the following:

- Solutions concentration
- Precipitation and flow rate balance
- Injection strategy
- Grain size distribution of base material and initial relative density
- Calcite content

Solutions concentration

The most common observation is that a high concentration of reactants leads to a non-homogeneous distribution of calcite, while using lower concentrations the result is more uniform (Al Qabany et al., 2012; Mujah et al., 2019; Qabany and Soga, 2013; Xiao et al., 2021).

Calcite mainly forms in the proximity of the attached microbes, which in turn must be evenly distributed in the solid matrix and uniformly receive nutrients and urea (Martinez

et al., 2013). Higher concentrations of bacteria accompanied by high concentrations of cementation solution would result in localized precipitation at the injection points.

Precipitation and flow rate balance

To achieve a homogeneous distribution it is necessary to limit the precipitation rate (Mortensen et al., 2011; Whiffin et al., 2007). If a slower reaction takes place, the end products can be delivered further away and avoid clogging. The precipitation rate is largely regulated by the concentration of the reactants but also by the bacterial activity. Konstantinou et al. (2021b) observed that the specimens treated with bacteria of higher urease activities had steeper carbonate concentration gradient and highest concentration at the injection point. A lower bacterial activity can therefore lead to a more uniform result (Martinez et al., 2013).

However, what must also be kept under control is the flow rate. In fact, localized deposition occurs if the precipitation rate is higher than the flow rate (Figure 2.4). It is for this reason that the studies by Konstantinou et al. (2021a), Mortensen et al. (2011), Whiffin et al. (2007) and Xiao et al. (2021) have highlighted the importance of this variable in the spatial disposition of calcite crystals. What matters is therefore to balance the ureolysis rate with the delivery of the reactants through the flow rate, in order to obtain a precipitation in the desired places (Whiffin et al., 2007).

Finally, since – as explained in chapter X – bacterial activity is strongly influenced by temperature, Xiao et al. (2021) have proposed a temperature controlled method. They maintained the solution (BS and CS together) at a temperature below 10° C during the injection, in order to delay the reaction until all the reagents were homogeneously arranged in the matrix. When the temperature then returned to compatible values for the microbial activity, the reaction took place, leading to a much more uniform deposition of the $CaCO_3$ crystals.

Injection strategy

The latter technique can also be part of the discussion about the influence of the injection strategy on the homogeneity of the treatment. Previously, Martinez et al. (2013) had also highlighted how the typical technique of injecting both solutions from the same point often led to preferential deposition near the inlet, as urea is consumed more rapidly where the bacteria were present in greater concentrations. They, therefore, noted that by

injecting BS and CS from opposite directions, the reaction was slower, and the plugging reduced, although uniformity was only slightly improved.

In principle, with this method it is possible to reach higher cementation distances, since clogging is greatly reduced: the cementation solution reaches the area with the highest bacterial density having an already reduced concentration itself.

Martinez et al. (2013) also reported that stopped flow was preferable over continuous flow to better distribute nutrients along the sample and hence more uniformly precipitate calcite.

Grain size and relative density

In short, it was observed that coarser materials or materials with low relative density had higher flow rates and this led to more uniform results (Konstantinou et al., 2021a). On the other hand, higher relative densities imply more initial contact point among grains, therefore more potential sites for calcite nucleation and growth. Furthermore, the lower the porosity, the easier it will be to encounter clogging, with its negative effects. Also in this case, therefore, the flow rate must be adjusted effectively. The heterogeneities of the matrix fabric could also play a role in the $CaCO_3$ crystals spatial disposition and an insight into possibility is represented by this study.

Calcite content

Finally, the calcite content itself appears to affect its spatial arrangement in the solid matrix. Konstantinou et al. (2021b) observed that the variance in calcite uniformity in their samples declined as the cementation level increased. Similarly, Cui et al. (2017) showed that the homogeneity increased with the increase of the calcite content. Conversely, Feng and Montoya (2016) and Lin et al. (2015) reported a decrease in homogeneity following an increase in the degree of cementation (from Konstantinou et al. (2021b)).

This parameter does not therefore seem to always have a consistent influence on the calcite crystals disposition in the soil matrix as the other factors could be of greater importance.

2.6. Soil engineering properties improvement

The treatment of a soil through bio-cementation has the potential to improve some important mechanical and hydraulic characteristics. Among the best known effects, an increase in shear strength and stiffness, a reduction in compressibility and permeability (DeJong et al., 2010). The actual realization of a specific improvement depends on the type of treatment, which leads to a different distribution and quantity of calcite within the solid matrix. The macroscopic effects are in fact a function of the conditions that are created at the microscopic level, which in turn derive from the injection strategy used, the concentrations of the reagents and the intrinsic properties of the soil. Therefore, it is possible in a certain sense to control the process, favouring the realization of an improvement rather than another, using methodologies and ingredients similar to those reported in the literature for a certain soil, to have a similar result.

In the next two chapters, we want to explore in particular the effects that the MICP has on strength and stiffness and on the permeability of a soil, for which bio-cementation is most studied in the literature.

2.6.1. Strength and stiffness

(DeJong et al., 2010) reported that biocementation treatment can lead to an increase in shear strength and stiffness by a coefficient of 10^2 for standard soils. Many are the studies in the literature that show an improvement in these soil characteristics, but the results are always characterized by great variability. (Cheng et al., 2013; Cui et al., 2017; Gao et al., 2019; Konstantinou et al., 2021a; Mahawish et al., 2018; Mortensen and DeJong, 2012; Mujah et al., 2019; Qabany and Soga, 2013; Terzis, 2017; Terzis et al., 2016; Terzis and Laloui, 2019; Van Paassen, 2009; Xiao et al., 2021).

At the microscopic scale the strength improvement is due to the calcite crystals that form in the pores, bridging soil grains, and creating a solid interconnected skeleton. The calcium carbonate crystals that effectively connect more grains defines the effective calcite content (Figure 2.3), while the remaining part is not unanimously considered to contribute to the improvement. The real strength enhancing mechanism is, therefore, not completely clear and could be due both to an increase in cohesion, resulting from the effective calcite content, and to an increase in friction, caused by a general increased roughness. Nonetheless, low amounts of calcium carbonate could increase the regularity

of the grains surface, therefore, reducing their roughness and, as observed by Xiao et al., (2021), reducing their residual stress, compared to that of untreated soil.

In the bio-cementation studies, the most common measures of strength improvement are in terms UCS: this is due to the fact that MICP is mainly seen as a useful technology for the treatment of shallow depths (Terzis and Laloui, 2019). However, some studies report results from one-dimensional oedometric compression and triaxial drained tests under confinement. Among the latter, Cui et al., (2017) observed that the variation of the effective friction angle and the effective cohesion are both correlated with an increase in calcite content, respectively via a linear and exponential function (Figure 2.5).

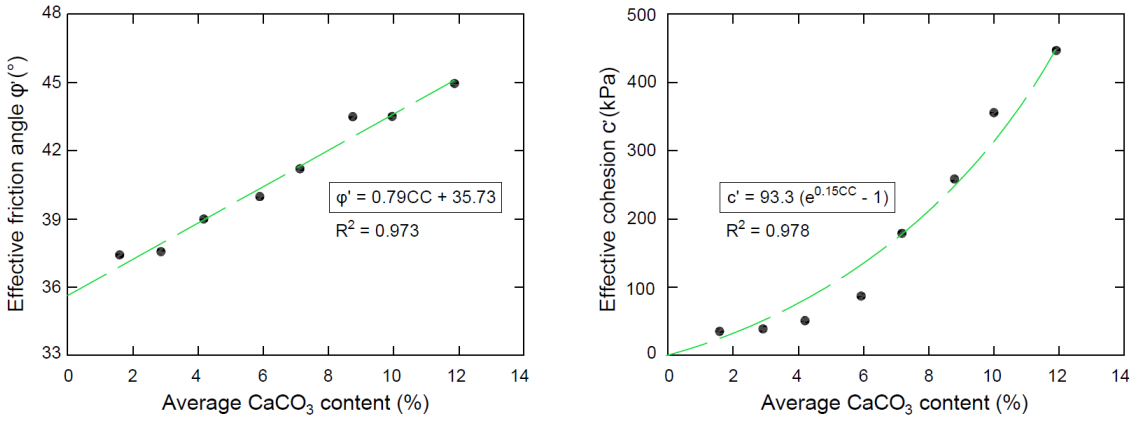

Figure 2.5 - Relationship between $CaCO_3$ content and effective friction angle (left) and effective cohesion (right). Modified after (Cui et al., 2017)

Also regarding the UCS, the general trend is that of higher strength for higher $CaCO_3$ content (Figure 2.6). Table 2.1 reports in turn some UCS test results from literature: we can observe a high variability from one study to another, even with similar calcite contents.

The reasons of this variability are multiple. In addition to calcite content, many are the elements that can influence the final strength acquired by the soil after bio-cementation. Among the most important:

- Degree of saturation
- Concentration of the reactants and treatment homogeneity
- Grain size and relative density

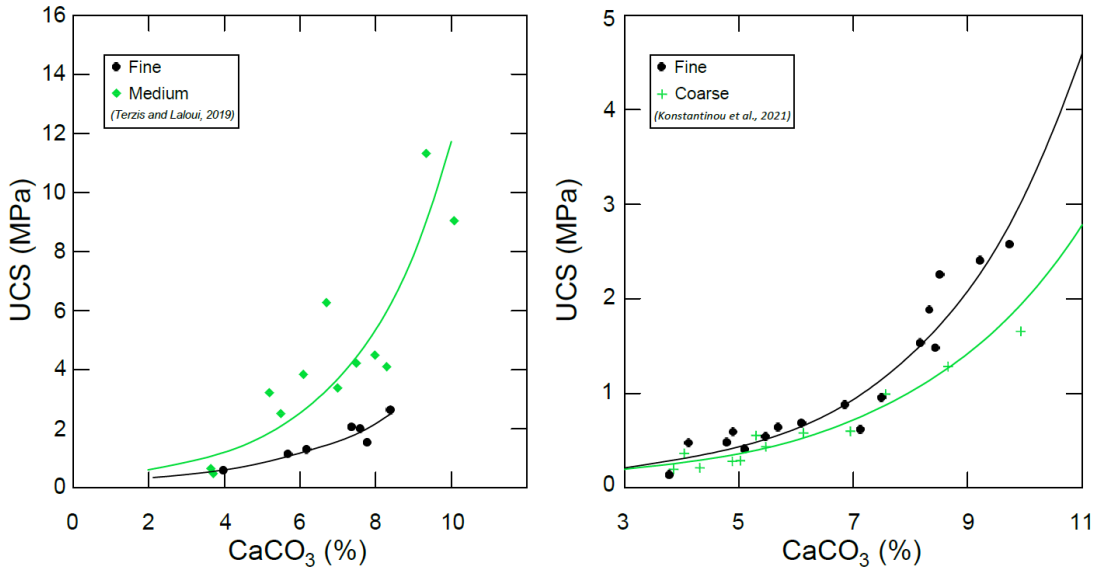

Figure 2.6 - Relationship between $CaCO_3$ content and UCS for fine (black dots) and medium (green squares) granulometries from Terzis and Laloui (2019) on the left and for fine (black dots) and coarse sands from Konstantinou et al. (2021a) on the right.

Table 2.1 – Typical CaCO3 contents in previous studies and related UCS. Modified after Terzis and Laloui (2019)

Source	**$CaCO_3$ (%)**	**UCS (kPa)**
van Paassen et al. (2010)	12–27	700–12000 (UCS and triaxial)
Cheng (2012)	4.5–11.5 (coarse) 0–27.5 (fine)	Up to 2067 (coarse) and up to 3700 (fine)
Cheng et al. (2013)	1–14	150–2300
Qabany and Soga (2013)	0–8	Up to 3000
Duraisamy (2016)	0.26–9.34	50–950
Terzis and Laloui, 2018	3–10	Up to 11400
Konstantinou et al. (2021a)	5–10	500–2500 (fine) 450–1600 (coarse)
Cui et al., 2017	9–13.5	1500–2200

Degree of saturation

In general, strength and stiffness are increased for lower degree of saturation (Cheng et al., 2013). This is due to the influence of water on the distribution of calcite crystals within the solid matrix. At low saturation levels, the water is disposed by forming menisci between one grain of soil and another: the subsequent injections of reactants will therefore lead to the precipitation of calcium carbonate crystals precisely at the particle-particle contact point, mainly resulting in strong effective solid bonds (Figure 2.7). Theoretically, by reducing the saturation level, it is therefore possible to achieve an increased strength

for lower calcite content. However, the control of the degree of saturation in soils with low retention capacity is complex, so most of the results in literature refer to complete saturation conditions.

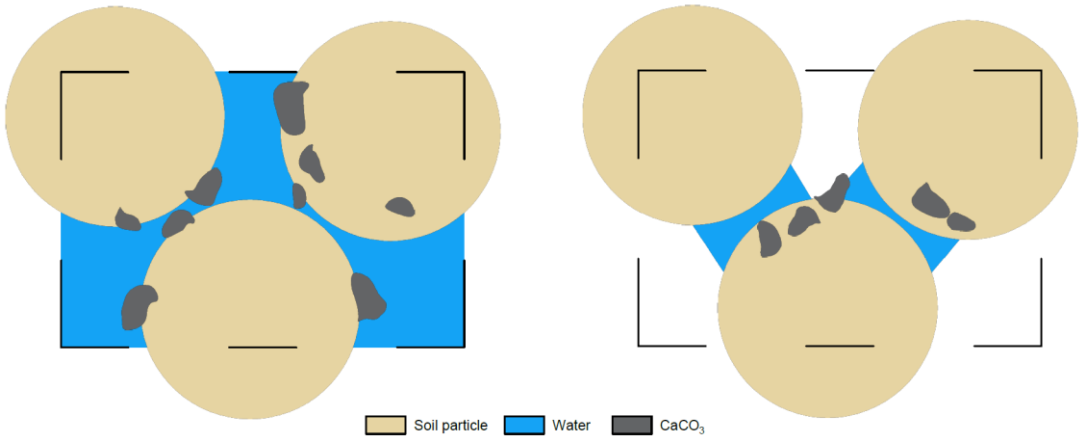

Figure 2.7 - Schematic representation of the water disposition and minerals precipitation behaviour at complete saturation (left) and partial saturation (right). Modified after Terzis and Laloui, (2019)

Concentration of the reactants and treatment homogeneity

Reactants concentration and treatment homogeneity are closely connected, as explained in chapter 2.5.6. Synthetically, a higher solutions concentration can result, with the same injection strategy, to higher calcite contents, thus leading to an increase in strength (Figure 2.5 and Figure 2.6). At the same time, however, more concentrated reactants can cause a heterogeneous distribution of calcium carbonate in the soil, hence, reducing the improvement effectiveness.

As aforementioned, most of the studies observed higher strengths and stiffnesses for higher cementation levels. In particular, Clarà Saracho et al. (2020a), Cui et al. (2017) and Konstantinou et al. (2021a), reported that the increased cementation level led to a stress-strain behaviour transition from ductile to brittle, which may be considered as an unwanted effect in many geotechnical applications. Taking into account the reactants concentration, the same studies observed, for higher salinity, an uneven bonds distribution in the solid matrix, where a few heavily loaded particle contacts were found to transmit a large proportion of the load, with negative effects on the shear strength. Similarly, Qabany and Soga (2013), treating their soil samples at different reagent concentrations – from 0.1 M to 1.0 M – observed a higher UCS for the lower concentrations. The treatment inhomogeneity affects the final strength both if it takes place between the top and the bottom of the specimen (Mahawish et al., 2018), or if it occurs at the microscopic level.

Anyhow, the overall soil strength, controlled by the weakest part, cannot be increased considerably if the treatment is not homogeneous (Xiao et al., 2021).

Grain size and relative density

Finally, the structure itself and the state of the soil at the time of injection can have a significant influence on the final result in mechanical terms. Cheng et al. (2013), and more recently Konstantinou et al. (2021a), observed that the strength is improved with the decrease in particle size (and pore size), for similar $CaCO_3$ contents. On the contrary, according to Terzis and Laloui (2018), the improvement is more pronounced for medium-grained than fine material (Figure 2.6). It could be said that the efficiency of the treatment increases with the increase in particle size from fine to medium, due to the increase in the size of bonds, and then decreases in the coarser granulometries where the distances to be bridged are higher. It is therefore a matter of number and proximity of the particle-particle contacts: the more the contacts, the more effective is the precipitation location. This is the same reason why also the relative density plays a key role in final strength, and it is normally easier to improve the denser sands (Chou et al., 2011; Gao et al., 2019).

At this regard, Rowshanbakht et al. (2016) reported that when the soil was compacted, the sand grains were closer together than in an uncompacted one and the calcite crystals formed over a shorter distance, thus leading to an increased strength. Furthermore, when the soil is compacted, i.e. at a higher relative density, the number of particle-particle contacts increases (Figure 2.8), as the voids are reduced. More contacts means more effective calcite content and therefore higher strength (Qabany and Soga, 2013).

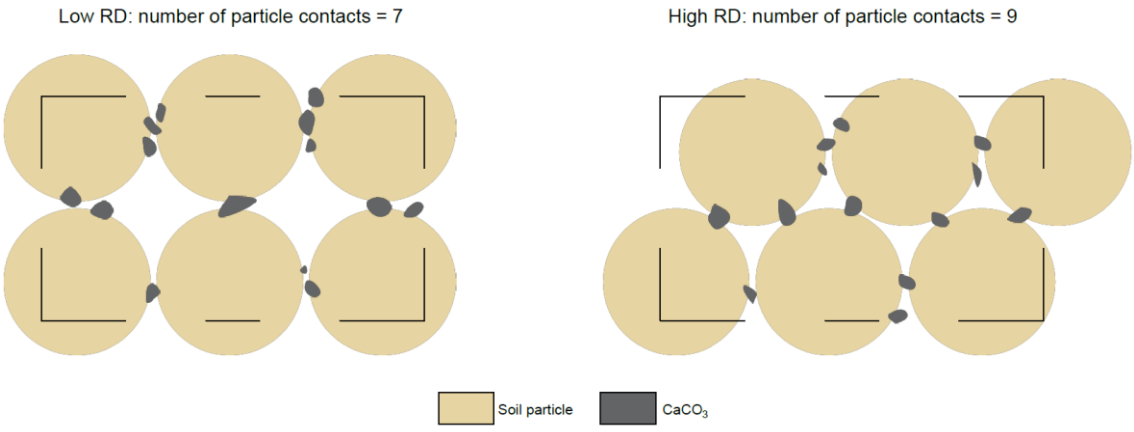

Figure 2.8 - Difference in number of particle-particle contacts points between loose (left) and compacted (right) sands. The number of contacts increases and the distances to be bridged decrease for higher relative densities.

2.6.2. Permeability

In past studies, bio-cementation has produced different and sometimes discordant effects on the treated soil permeability. In general, the most commonly observed effect is a reduction in permeability following cementation (Cheng et al., 2013; Dadda et al., 2017; Nemati et al., 2005; Nemati and Voordouw, 2003; Zamani and Montoya, 2016), although there are studies reporting a minimal reduction or near-maintenance of the pre-treatment hydraulic properties (Whiffin, 2004; Whiffin et al., 2007).

The permeability of a soil is a function of voids connectivity, shape and size of pores and throats, grain shape and size, etc. Precipitated calcite can significantly reduce the permeability by altering all these soil characteristics: for example, the precipitating crystals increase the roughness and at the same time reduce the porosity, reorganizing the flow field (Noiriel et al., 2016).

One of the factors that most influence the reduction of permeability is the calcite content. The higher the quantity of calcium carbonate, the greater the porosity reduction and, even if some studies reported no or little influence of this reduction on the permeability – (Whiffin et al., 2007) – most of the results in the literature find a direct correlation between the amount of calcite content and permeability reduction (Cheng et al., 2013; Dadda et al., 2017; Qabany and Soga, 2013; Zamani and Montoya, 2016).

Dadda et al. (2017) observed in their studies a 70% reduction in permeability for a calcite content of 14% by volume and a 1 M concentration of the reagents: these results are comparable to those obtained by Cheng et al. (2013) in their tests, at 100% degree of saturation, for the same calcite content and with similar concentrations (1.4 M). Van Paassen (2009) in turn observed a reduction of 60% using a concentration of 1 M and with a calcite content equal to 100 kg/m^3. Finally, Qabany and Soga (2013) instead reported a reduction of about 30% with a concentration of 1 M but with a lower calcite content (1%). It can be said that these are all comparable results and the reduction in permeability is substantial. This could be largely due to the high concentrations of reactant used.

In addition to the calcite content per se, other factors play a fundamental role in modifying the hydraulic properties of a MICP treated soil. The size and the spatial distribution of the minerals should also be taken into account for the evaluation of permeability variations (Noiriel et al., 2016), as large crystals that occlude the pore throats have a greater

influence on the reduction of permeability than small crystals uniformly precipitating on the grains surface. The main factors influencing the crystals size and distribution are the concentration of the reactants and the degree of saturation, respectively. The concentration of the reagents is in turn also responsible for the spatial uniformity of the precipitation, as explained in Chapter 2.5.6.

Cheng et al. (2013) reported that it is preferable to perform bio-cementation under lower saturation conditions, as it maintains relatively high residual permeability. The reason is the same for which the increase in strength is greater at low saturation: the crystals concentrate at the grains (Figure 2.7), maintaining a certain connectivity between the larger pores and throats, where most of the fluid flows.

Regarding the concentration of the reactants, Qabany and Soga (2013) observed a higher and faster reduction of permeability for higher concentrations (1 M), although the effect was mainly due to localized clogging – caused by the formation of larger crystals – more than to a general reduction in permeability. For a more uniform result, lower concentrations (0.25 M) are preferred, causing a more uniform cementation and an overall reduction in porosity and connectivity.

Since these two factors (concentrations and degree of saturation) are decided at the design stage, the degree of permeability reduction could be controlled to achieve the desired result. At the same time, the amount of precipitated calcite is largely predictable and multiple injection cycles can be repeated to obtain the desired final calcium carbonate content in the soil. It is therefore clear that the degree of permeability reduction could be controlled both at the design stage and during treatment, although further studies are needed.

This flexibility of use makes out of the MICP a good technique for various engineering applications, which may require different types of results. In fact, depending on the context, permeability may need to be drastically reduced, e.g. to limit the water flow or isolate polluting plumes, or to decrease the infiltration of water in soil slopes and reduce the landslide risk. But in some other cases it may wanted to be maintained, e.g. for soil improvement purposes, in order to keep the drainage capacity and reduce the hydrostatic thrust, while increasing the soil strength.

2.7. Discussion and challenges

The possible applications of MICP in the geotechnical field are manifold. Exploiting the capabilities of this technology to improve the strength and stiffness of a soil and reduce its permeability, promising applications can be seen in the increase in the bearing capacity of the soil (Van Paassen et al., 2010), in slopes stabilization (Cheng, 2012), in the prevention of soil liquefaction (Dejong et al., 2013), for erosion control (Anbu et al., 2016), for clogging (Ivanov and Chu, 2008) and selective plugging (Nemati et al., 2005), in the reduction of permeability (Qabany and Soga, 2013), to improve the mechanical behaviour of sand fills (Gao et al., 2019), etc.

Bio-cementation could be an alternative to the current techniques used in these fields, i.e. soil compaction, traditional grouting, chemical grouting, structural methods. Taking into consideration traditional grouting, which is a widely used and consolidated technique, some studies have compared the latter's characteristics with those of MICP. The key points for which the bio-cementation could be preferable to the traditional permeation grouting with Portland cement, are mainly the permeability retention, a comparable or greater strength, the possibility of treating finer granulometries leaving the soil structure as intact and, obviously, the fact of being environmental friendly.

As already explained, by regulating the concentration of the reactants and the flow rate it is possible to limit the permeability reduction for MICP treated soils. Mujah et al. (2019) showed that the permeability of MICP treated samples was greater than that of Portland treated. Cheng et al. (2013), in addition to confirming this fact, pointed out that a further advantage of permeability retention is that it allows additional treatment cycles, thus allowing to control the final result also in terms of resistance.

This latter, in the works of Mujah et al. (2019) and Qabany and Soga (2013), was always lower or comparable to that of the bio-cemented samples, for Portland treated specimens, in terms of UCS.

The range of grain sizes that can be treated with MICP is much wider than that of Portland. The latter can generally only be applied to grain sizes in the range 4.75–76.2 mm (Pan et al., 2020), while MICP could be used to cement sands with a d_{50} less than 0.6 mm. Regarding the coarser grain sizes, MICP showed limitations, although some studies successfully treated coarse sands with a standard injection technique (Konstantinou et al., 2021b) or developing new methods (Mahawish et al., 2018; Pan et al., 2020). One

limitation that has been observed for MICP is its inability to cement organic soils, which after treatment have shown a loss of strength and stiffness of approximately 50% (Oliveira et al., 2017).

While MICP is proven to have these and many other advantages, as well as a wide range of applications, the actual deployment of the technology at the field scale is still a challenge. Large-scale experiments exist in literature. Whiffin et al. (2007) observed a significant improvement in strength and stiffness over several meters employing five meters columns. Martinez and DeJong (2012) applied the technique at the macro scale for the construction of a shallow foundation, highlighting the problem of the treatment homogeneity. An even larger scale is the one for which the results of van Paassen et al. (2010) are reported, as they biocemented a sandy soil with a volume of about 100 m^3 observing a significant increase in stiffness.

What is missing to reach a consolidated full-scale application technique is a design method that allows to effectively predict the final properties of a soil treated with a certain strategy and certain concentrations. A limit to this need is represented by the great variability of the biological process itself and its variable behaviour when applied to different soils. It is then extremely important to consolidate a method for monitoring the process, to be able to keep under control the extension of the treatment and its homogeneity: two elements that have proved to be problematic. The unevenness of the treatment, in particular, can have negative effects on the final result, in engineering terms. If in the first place it is necessary to design the injection strategy in a coherent way and with adequate concentrations, an anomalous behaviour of the reaction is not excluded. This could lead to increased depositions in a part of the volume to be treated, with consequent clogging and strongly inhomogeneous distribution of the binding crystals. Geophysical methods seem to be a good option in this regard, and can be accompanied by micro invasive techniques, such as micro cores, for their validation. With a good monitoring technique, it would be possible to start the treatment at low concentrations, in order to obtain the best homogeneity, and then increase them according to the obtained results, with new injection cycles. Operational costs must always be kept under control, as they could exponentially grow if the intervention becomes long-lasting. This is mainly related to the reactant preparation.

The solutions used for the MICP seem to be able to be used efficiently from an economic point of view only with an industrial production. We refer in particular to the cultivation of bacteria, the transport and storage of which represents a further aspect to be considered, if we consider the difficulty of on-site cultivation. In this regard, Terzis and Laloui, 2019 reported how the use of freeze-dried cells could facilitate in-situ applications and contribute to overall reproducible results.

The durability of the treatment is another element that has been discussed. DeJong et al. (2010) observed a degrading of the calcite precipitate during loading and similarly Whiffin et al. (2007) showed that once the bonds were broken, the strength improvement of the material was almost completely lost. This is mostly due to the stiffness obtained from the soil following the treatment. The calcite bonds offer a good increase in strength but are subject to a brittle behaviour, especially for high $CaCO_3$ contents (Clarà Saracho et al., 2020a; Cui et al., 2017; Feng et al., 2017). Lower concentrations could increase strength while partially maintaining the soil ductility.

As regards the deterioration of MICP-treated soils to environmental conditions, some studies have observed sensitivity of the treatment to freeze-thaw cycles and acid rain. Cheng et al. (2017) reported that the bonds deterioration after freeze-thaw cycles was a function of the soil granulometry. Well-graded sands are characterized by more particle-particle contacts and therefore more cementitious bonds, still guaranteeing a good permeability. This allowed for a faster water transfer, and therefore a higher durability to freeze-thaw cycles. Liu et al. (2019) showed that the bio-cemented soils well resisted to few freeze-thaw cycles, and only gradually lost strength with repeated rounds. However, multiple MICP treatments contributed to a considerable reduction of the soil susceptibility to this environmental factor.

In the same study, acid rain solutions instead showed a highly detrimental effect on MICP-treated soil, even for high calcite contents. This is due to the high $CaCO_3$ solubility in acid, which, therefore, proves to be a weak point of the technique.

Finally, a topic widely discussed in the literature concerns MICP harmful waste products. The ureolysis process by its nature leads to the formation of ammonia and ammonium (2.1). The production of ammonia can affect the nitrogen cycle: through the nitrification process, in the presence of oxygen, nitrates are produced. These are excellent fertilizing products but also primarily responsible for water eutrophication. Terzis and Laloui (2019)

reported the possibility of capturing and recycling ammonium, which could then be reused. DeJong et al. (2010) instead proposed alternative methods for pH control, e.g. denitrification, iron reduction and sulphate reduction. Even if these are less efficient methods, they are characterized by the production of more benign by-products.

In general, to minimize the amount of ammonium produced it is advisable to reduce the reagents concentration and it is necessary to balance the ratio between the urea and calcium concentrations, even if this reduces the reaction efficiency (Martinez et al., 2013). Alternatively, as shown by Clarà Saracho et al. (2020a), there are bacterial strains of the *Sporosarcina* genus (e.g. *S. Newyorkensis*), capable of guaranteeing a good calcite precipitation efficiency even at lower reactants concentrations, thus decreasing the amount of hazardous by-product being produced.

2.8. Conclusion

The MICP technology has attracted a lot of attention in the last years: many studies have been conducted on this technology, and as many are in development. The need to find alternatives to common grouting techniques, which have proven to have a strong impact on the environment, has prompted to deepen the process of bio-mediated soil improvement, which presents itself as an environmental friendly technique, in particular from the point of view of CO_2 production.

It has shown excellent potential and sometimes better mechanical properties than commonly cement grouted soil. Its possible uses are not limited to the geotechnical field, but range from the environmental, with applications for waste water treatment (Hammes et al., 2003), reactive barriers (DeJong et al., 2010), carbon sequestration (Martinez et al., 2014), to the building field, e.g. for concrete repair (De Belie and Muynck, 2008), to mining applications like selective plugging (Nemati et al., 2005) and tunnels walls stabilization (Fauriel, 2012).

From the geotechnical point of view, the improvement in strength and stiffness and the good control over the permeability are the major results of the MICP. The ability to monitor the process and adjust the injection strategy accordingly to the desired result represent another point of bio-mediated soil improvement.

Further research on the process at the microscopic scale is necessary, in order to fully understand the biological variable and both the chemical and physical process behind the $CaCO_3$ precipitation and its distribution in the soil matrix.

The biggest obstacle towards an effective consolidation of the technique is represented by the upscaling. Full-scale applications remain limited and some issues related to the hazardous by-products and to the production of the solutions in ready to use large quantities do not facilitate the definitive affirmation of the MICP.

Nonetheless, it is worth continuing research in a field so important to today's expanding world that it needs environmentally friendly yet effective alternatives to support the growing construction field.

3. Materials and methods

This chapter aims to present the materials and methods used in this research. The macro-phases that characterized the project were packing, solutions preparation, injection, chemical-physical analysis, numerical analysis, mechanical study and SEM analysis.

3.1. Sample preparation

The preparation of the samples includes the sizing and implementation of the packaging and the choice of particle sizes for the solid matrix.

3.1.1. Artificial soil

In place of a real soil it was decided to use acid-washed soda-lime glass beads (Sigma Aldrich) with density 2.48 g/cm^3. In this way it is possible to standardize the influence of the shape of the particles and of the material of which they are composed.

Three granulometries were artificially created: a uniform sand (UN), a poorly graded sand (PG) and a well-graded sand (WG). The last two are defined according to the ASTM standard (ASTM D2487-17e1, 2017), while the first one represents a distribution with extremely low variability in grain size. To prepare these "soils", different percentages of the different diameters available to us have been dosed. They were defined by the manufacturer in a range, of which the median was chosen for our calculations.

Table 3.1 shows the content in each grain size range, corresponding to the granulometric curves of Figure 3.1. instead shows the artificial granulometries characteristics, as defined by the ASTM standard. The average porosities were roughly calculated by measuring the volume occupied by the known mass.

Table 3.1 - Dosage of each grain size for the granulometries under study

	Bead Size Range [µm]	Sieve size [mm]	Percentage passed [%]	Frequency [%]
UN	212-300	0.3	100	100
PG	710-1180	1.18	100	7
	425-600	0.6	93	63
	212-300	0.3	30	28
	150-212	0.212	2	1
	<=106	0.106	1	1
WG	710-1180	1.18	100	60
	425-600	0.6	40	20
	212-300	0.3	20	5
	150-212	0.212	15	5
	<=106	0.106	10	10

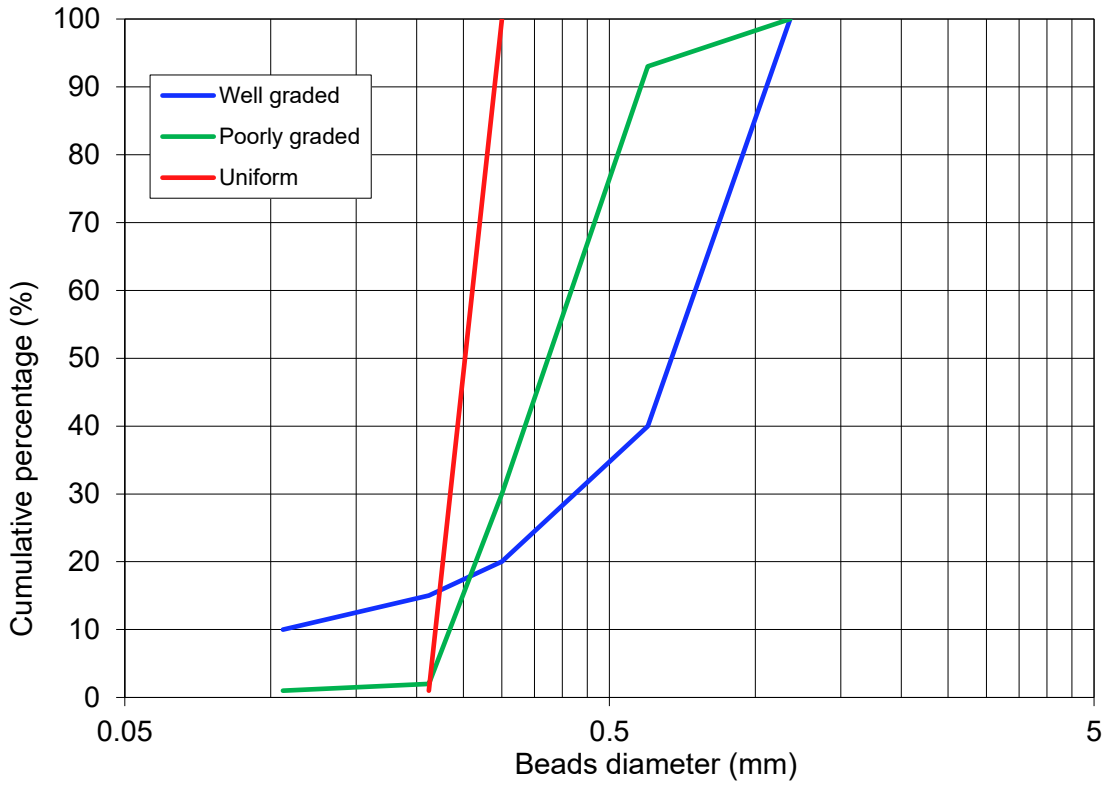

Figure 3.1 - Artificial granulometric curves

Table 3.2 - Artificial soil characteristics and classification according to the ASTM standard (D2487-17e1). Cu stands for coefficient of uniformity, Cc for coefficient of curvature, ε for porosity

	UN	PG	WG
d_{10} [mm]	0.221	0.23	0.1
d_{30} [mm]	0.24	0.30	0.41
d_{50} [mm]	0.256	0.39	0.69
d_{60} [mm]	0.41	0.41	0.75
Cu [-]	1.86	1.78	7.50
Cc [-]	0.63	0.95	2.24
ε [-]	0.36	0.31	0.22

3.1.2. Packaging

The glass beads were packed in centrifuge tubes of two different sizes: 50 ml and 15 ml (Figures Figure 3.2 and Figure 3.3). In this way, three larger columns for the physic-chemical analyses and a duplicate represented by three smaller columns intended for the XRCTs numerical analysis were constructed.

The molds had respectively an internal diameter of 26.5 mm and 14.0 mm, for a height of 120 mm. For the construction of the specimens, the centrifuge tubes were perforated at both ends, so as to be able to insert two valves (Figure 3.3) collected to the 2 mm inlet

and outlet pipes. Subsequently, a filter mesh was placed inside each mold (top and bottom) to prevent the glass beads from escaping. The remaining volume was filled with the previously prepared artificial granular media, weighing each time the mass of glass beads present in each specimen.

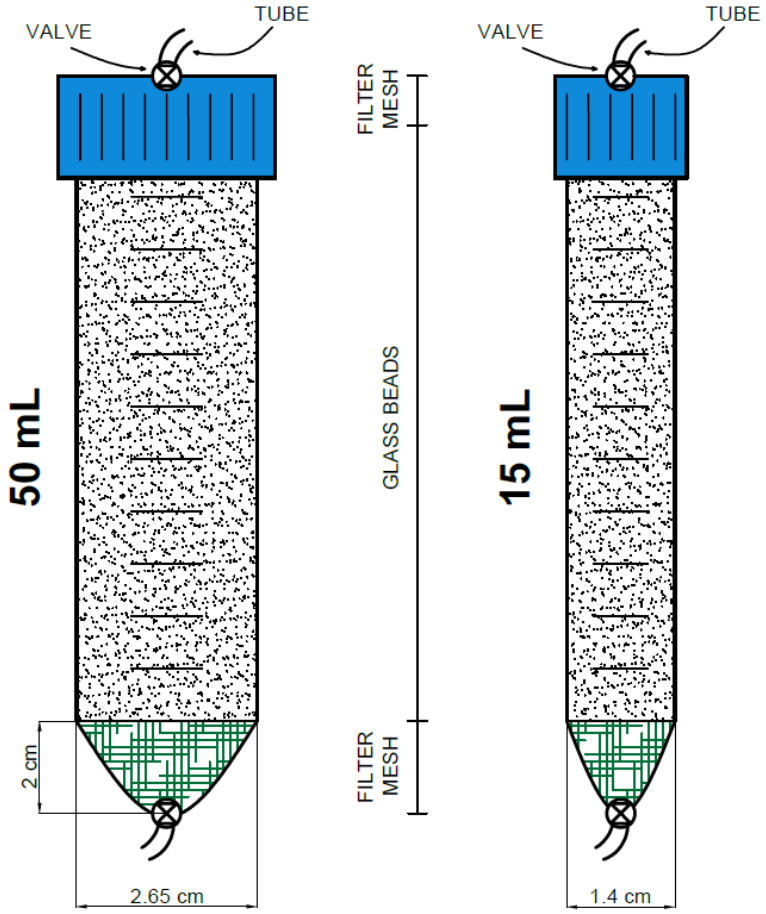

Figure 3.2 - Scheme of the two sample sizes used. The largest (50mL) on the left and the smallest (15mL) on the right. Both had the same height and a filter mesh was placed at top and bottom. Plastic 2-way valves were placed at the insertion of the pipes.

Since acid-washed glass beads, which have zero cohesion, have been used, they have been observed to freely arrange themselves in their more compact structure. Further compression and agitation did not lead to observable compaction changes and it was not even possible to obtain a less dense structure than that naturally obtained from the beads with the force of gravity alone. Therefore, no maximum and minimum void ratio measurements were carried out and the self-compacting of the glass beads was ensured to always lead to the highest possible relative density.

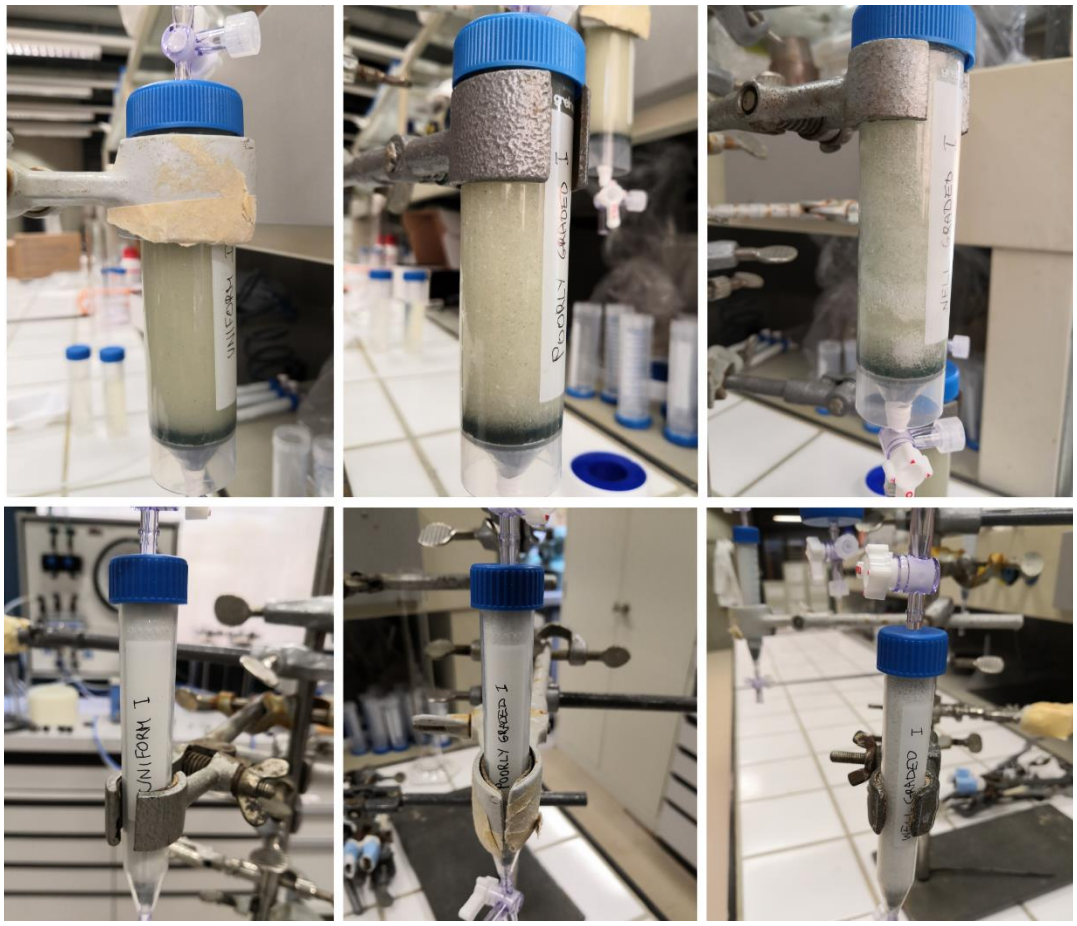

Figure 3.3 - Columns used for injections. On the top row the 50 mL samples and on the bottom row the 15 mL samples. Left to right UN, PG, WG.

The mass of glass beads used for each sample was measured (Table 3.3). Subsequently, knowing the bulk volume occupied by the latter, the porosity of the sample was roughly calculated. The difference in porosity between two samples containing the same granulometry lies in the different disposition of the fines, which easily arrange in the voids of the larger beads.

Table 3.3 - Packings specifications: m_{beads} is the weighted mass of the beads, V_{bulk} is the measured volume (base × height) occupied by the beads. The volume of the voids (V_{voids}) is calculated as the difference between the bulk volume and the volume of the beads.

Sample size	Granulometry	m_{beads} (g)	V_{bulk} (cm^3)	V_{voids} (cm^3)
15 ml	UN	21.37	14.01	6.16
	PG	23.03	14.01	5.39
	WG	27.19	14.16	3.61
50 ml	UN	75.52	47.98	20.46
	PG	81.28	47.98	17.75
	WG	88.85	47.98	14.19

3.2. Reactants

Two reactants were prepared for bio-cementation: the bacterial solution (BS) and the cementation solution (CS).

3.2.1. Bacteria solution

The bacterial solution was prepared from freeze dried *Sporosarcina pasteurii* cells stored at -20 °C, under sterile conditions. The microbes were inoculated in a liquid medium (ATCC 1376), which consisted of 20 g/L yeast extract, 10 g/L ammonium sulphate and 0.13 mol/L Tris buffer aqueous solution (Figure 3.4). The mixture pH was regulated to 9 with HCl and then autoclaved before the insertion of the bacteria. Subsequently, the solution thus created was incubated 30 °C for 72 hours in order to allow bacterial growth. At the end of the incubation (Figure 3.5) the solution had an OD600 of 1.2 and the stationary phase was considered to be reached.

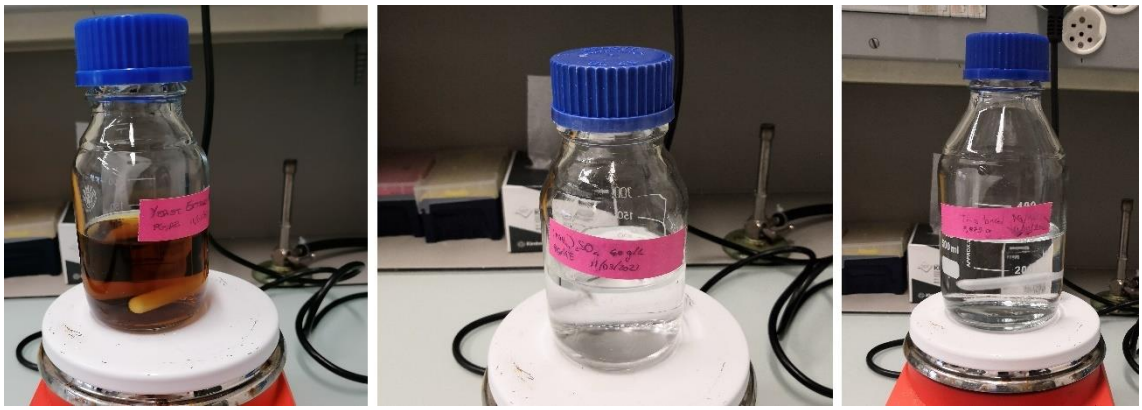

Figure 3.4 - From the left: yeast extract (20 g/L), ammonium sulphate (10 g/L), Tris buffer (0.13 mol/L)

Figure 3.5 - Difference in opacity between two incubated solutions: on the left the negative sample (without inoculated microbes), on the right an effective bacteria solution

The bacteria ureolytic activity was calculated by measuring the electrical conductivity of 27 mL urea solution 1.11 M to which 3 mL of BS were added. Two measurements were taken at a distance of 5 minutes and the rate was calculated. Through the conversion of equations (2.6) and (2.7), it was therefore possible to evaluate bacterial activity, which turned out to be equal to 19.2 mM/h. The specific urease activity was therefore 15.61 mM/h/OD600.

3.2.2. Cementation solution

The cementation solution is composed of urea (CH_4N_2O), calcium chloride ($CaCl_2$) and nutrient broth. An equimolar concentration of $CaCl_2$ and CH_4N_2O of 0.25 mol/L was used. The concentration of the nutrient broth was instead of 3 g/L. The constituents were weighed and combined with a litre of demineralized water and subsequently mixed with a magnetic stirrer for complete dissolution.

3.3. Treatment

A syringe pump (Harvard apparatus, ± 0.25% accuracy) was used for the injections. The flow rate was adjusted according to the porosity and section of each sample, in order to obtain the same seepage velocity within each granulometry (0.024 cm/s), accordingly to the following relation (3.1):

$$q\ (mL\ s^{-1}) = v_{seep}(cm\ s^{-1}) \cdot A(cm^2) \cdot \varepsilon \qquad (3.1)$$

where q is the flow rate, v_{seep} is the target seepage velocity, A is the total section area and ε is the porosity.

The employed flow rates are shown in Table 3.4, together with the volumes used for each injection (1.2 PV). Before each inoculation, the pipes were filled with the proper liquid, in order to guarantee the exact injection of the calculated volume.

Each sample was initially saturated by injecting 2 PV of demineralized water, in order to achieve a relatively controlled flow field. The valves were opened for injections and immediately closed for reaction or attachment time.

A two-phase injection scheme was used for the bacterial and cementation solution. Following saturation, 1.2 PV of BS were immediately injected into each column from the upper valve, collecting the outflow from the lower valve (mainly water). The bacteria were left to attach to the soil grains and grow for 24 h, at the end of which the CS injection was started.

Each sample was treated with 11 CS injections, performed at an interval of 24 h. The same volumes of BS were used for each CS injection, but the flow direction was changed. The CS was inoculated from the lower valve and effluent was collected from the upper valve. The collection took place every day in individual vessels for each sample. All the effluents were stored in the refrigerator at 4 °C (in order to stop the reaction) until the end of the treatment and then sent for chemical analysis. At each injection, the effluent representing the injection of the previous day was collected.

Following the last injection of CS plus the 24 hours of reaction, the samples were flushed by injection of 5 PV of demineralized water in order to eliminate any unconsolidated residues of the reagents and they were put in an oven at 100 °C for drying.

Table 3.4 - Volumes and flow rates needed for the injections. A_{voids} is the area of the void, calculated as section area times the porosity, v_{seep} is the target seepage velocity and $v_{BS/CS}$ is the volume needed for the BS or CS injections (1.2 PV).

Sample size	Granulometry	A_{voids} (cm^2)	v_{seep} (cm/s)	Flow rate (mL/s)	$V_{BS/CS}$ (mL)
15 mL	**UN**	0.59	0.024	0.0142	7.39
	PG	0.52	0.024	0.0125	6.47
	WG	0.35	0.024	0.0083	4.34
50 mL	**UN**	2.02	0.024	0.0484	24.55
	PG	1.75	0.024	0.0420	21.30
	WG	1.40	0.024	0.0335	17.03

Figure 3.6 shows a schematic of the process followed for the treatment.

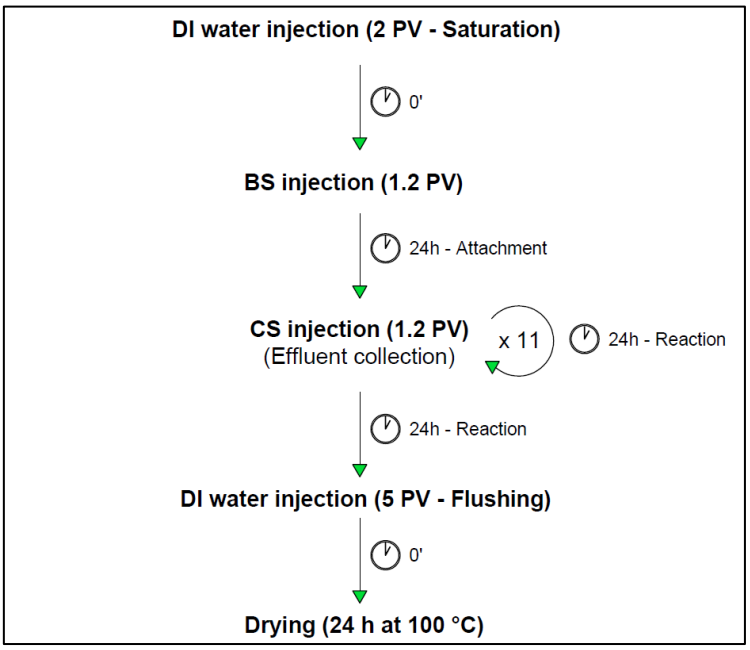

Figure 3.6 - Treatment scheme

3.4. Physico-chemical analysis

The chemical and physical analyses include monitoring the reaction by measuring the concentration of ions in solution and calculating the calcite content by acid digestion.

3.4.1. Chemical monitoring

The chemical monitoring of the reaction consisted of the measurement of pH, electrical conductivity (EC), OD600 and ions concentration in the effluents. The first three measurements were performed manually every day, while the ions concentration was measured by the Central Environmental Laboratory of the EPFL at the end of the treatment on the effluents stored in the fridge (11 for every granulometry). This latter involved the analysis of ammonium (NH_4^+), calcium ion (Ca^{2+}) and Total Inorganic Carbon (TIC).

The pH and the EC were measured by means of the respective probes which a digital multiparameter benchtop meter (Orion ™ Versa Star Pro ™ - Thermo Scientific ™) was equipped with. In the days when access to the laboratory where the instrument was stored (CEMBL - EPFL) was limited, the pH was measured via pH test strips with sensitivity 0.1, while the electrical conductivity was not recorded. These two measures were also partially collected for the influent CS of the specific day.

Ammonium, calcium and TIC results were used to calculate the theoretical amount of precipitated $CaCO_3$ (equations (2.10), (2.11) and (2.12) and the reaction efficiency by means of the following equations (3.2), (3.3) and (3.4) :

$$\eta_{NH_4^+}(\%) = 0.5\frac{C_{NH_4^+}(\text{mol L}^{-1})}{C_{CS}(\text{mol L}^{-1})} \cdot 100 \tag{3.2}$$

$$\eta_{Ca}(\%) = \left(1 - \frac{C_{Ca^{2+}}(\text{mol L}^{-1})}{C_{CS}(\text{mol L}^{-1})}\right) \cdot 100 \tag{3.3}$$

$$\eta_{TIC}(\%) = \left(1 - \frac{0.5\ C_{NH_4^+}(\text{mol L}^{-1}) - C_{TIC}(\text{mol L}^{-1})}{C_{CS}(\text{mol L}^{-1})}\right) \cdot 100 \tag{3.4}$$

where η_{NH4+} is the ammonium conversion efficiency, η_{Ca2+} is the calcium precipitation efficiency and η_{TIC} is the carbonate precipitation efficiency; C_{NH4+}, C_{Ca2+} and C_{TIC} are the ammonium, calcium and TIC molar concentration in the effluent, respectively; C_{CS} is the urea and calcium chloride molar concentration in the influent (0.25 mol/L).

3.4.2. Calcite content empirical measure

Calcite content (CC) was physically measured at this stage in both sample sizes via acid digestion. The procedure, described in detail below, involves measuring the mass of the samples before and after the treatment with hydrochloric acid, which dissolves the precipitated calcium carbonate. The difference in weight is therefore equivalent to the mass of calcite.

The procedure is slightly different between the two column sizes. The 50 mL samples were divided into three parts (top, center and bottom), which were in turn divided into two parts for consistency: the respective CC was then averaged, and the variance of the measurement obtained. In the 15 mL columns the $CaCO_3$ was still estimated on top, center and bottom part but without further splitting each part in two, because of their already small size. The fragments were first placed in special labelled bowls and then weighed.

Inside a fume hood, the necessary amount of HCl (1 M) was added to the bowls (Figure 3.7) and 30 minutes were waited for the dissolution reaction to stop. Subsequently, the excess acid containing the dissolved $CaCO_3$ ions was removed with a syringe, taking care not to remove the glass beads too. After that, more acid was added again for a second dissolution, lasting 2 hours, after which all the $CaCO_3$ was considered dissolved. The liquid was then removed again, and deionized water was added to rinse the glass beads.

Figure 3.7 - Labelled glass bowls for acid digestion, containing columns portions immersed in HCl

Once having removed as much water as possible with the syringe, the measurement cups with the glass beads were placed in the oven at 100 °C for 24 h to dry.

The following day the weight of the fragments was measured again and the difference between the two measurements provided the calcite content, according to the equation (3.5):

$$CC(\%) = \frac{m_{CaCO_3}(g)}{m_{matrix}(g)} \cdot 100 \qquad (3.5)$$

where CC is the calcite content, m_{CaCO3} is the mass of calcium carbonate, calculated as the difference between the sample weight before and after acid dissolution, m_{matrix} is the mass of the solid matrix as weighted after dissolution.

The calcite content thus obtained was used to evaluate the efficiency of the chemical reaction and precipitation of calcium carbonate, comparing it to the maximum quantity that could have formed if all the $CaCl_2$ had been converted into $CaCO_3$ (Al Qabany et al., 2012; Wang, 2019). The resulting relation is as follows (3.6):

$$\eta(\%) = \frac{m_{CaCO_3}(g)/m_{matrix}(g)}{C_{CaCl_2}(mol\ L^{-1}) \cdot V(L) \cdot M_{CaCO_3}(g\ mol^{-1})/m_{matrix}(g)} \cdot 100 \qquad (3.6)$$

3.5. Numerical analysis

Numerical analyses were performed on high resolution X-ray computed micro-tomographies performed at EPFL's PIXE laboratory (RX-SOLUTIONS Ultratom micro CT system). The samples used were those of 15 mL (diameter 14 mm). The image processing was then performed with the Amira-Avizo software (ThermoFisher SCIENTIFIC).

Scanning takes place by means of an X-ray beam incident on the slowly rotating sample. The result is a stack of 2D TIFF images representing as many slices of the column. The distance between the images is a function of the resolution of the scan, which depends on the distance of the source from the sample. The smaller the sample diameter, the closer the source can be placed and the more concentrated the ray beam will be, thus increasing the resolution.

The incident X-rays are partly absorbed and partly transmitted by a material according to its attenuation coefficient. Afterwards, they reach a detector and the set of projections

acquired at each sample rotation step allows a software to reconstruct a picture, returning the three-dimensional distribution of the attenuation coefficients throughout the sample. Figure 3.8 shows the synthetic scheme of a micro tomography functioning.

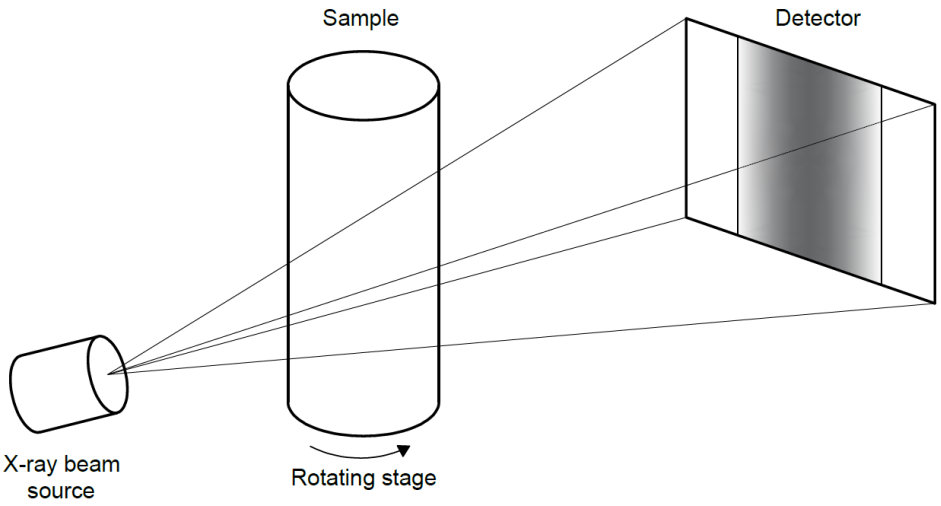

Figure 3.8 - Synthetic scheme of a micro tomography system operation

3.5.1. Initial considerations

In this study a resolution of 8.3 µm was achieved and the X-ray beam was set to an intensity 150µA and a voltage o 55 kV.

The identification and separation of the calcium carbonate crystals from the glass beads was the main challenge to address, as the linear attenuation coefficients and densities of the two materials are very similar (Bam et al., 2020) and the initial resolution was not sufficient to clearly distinguish the calcite bonds.

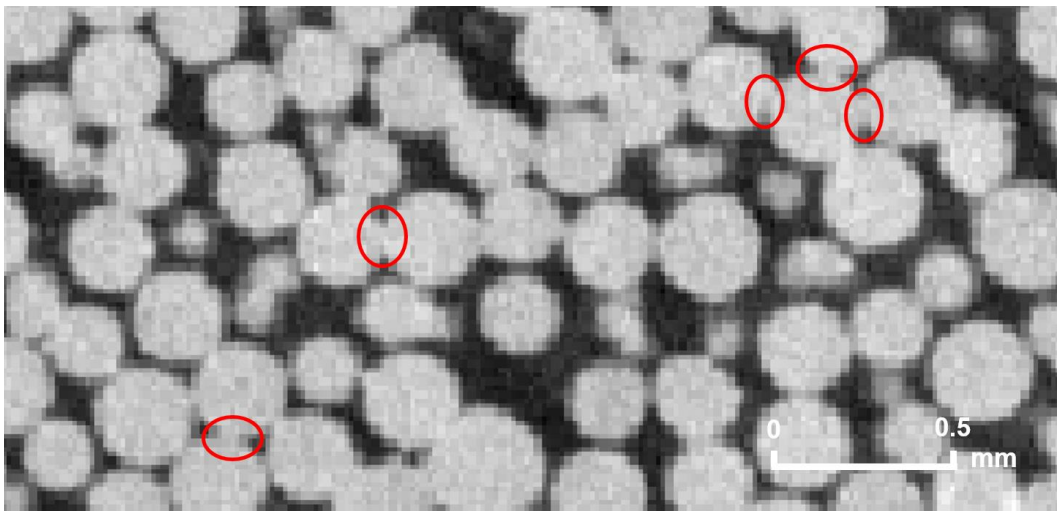

Figure 3.9 - Grayscale image of the cemented uniform sample. One can guess the presence of bonds when the union between the glass beads is more marked (red circles). The resolution is not sufficient to distinguish the calcite crystals and the contrast between the two solid phases is absent.

The presence of calcite can be assessed with the postulate that the existence of bonds results into glass beads having a clearer surface contact, as shown in the Figure 3.9 rather than a single contact point. This latter corresponds to untreated spheres.

Circle Hough Transform

A Hough Transform (HT) was also attempted to extract the spheres (Yadav et al., 2014), in order to separate the calcite crystals by subtraction of the latter from a binary image representing the whole solid phase. The attempt was made using a Phyton script from Amira-Avizo Xtra Library, but the result was not satisfactory.

The algorithm is designed to detect circles in imperfect images. The user must provide an estimate of the number of circles (or spheres) present and the range in which their radius falls. Although some tests have been made with even reduced radius ranges, it has not been possible to correctly isolate the spheres.

An extract of the best obtained result is shown in the Figure 3.10: some circles are identified and well fitted, but a good part is badly fitted or not identified at all. The problem seemed to be that same circles were fitted multiple times while others never were. This led not only to the incompleteness in spheres identification, but also to an incorrect size and overlapping of those correctly found. By solving these problems, the calcite crystals could probably have been separated effectively.

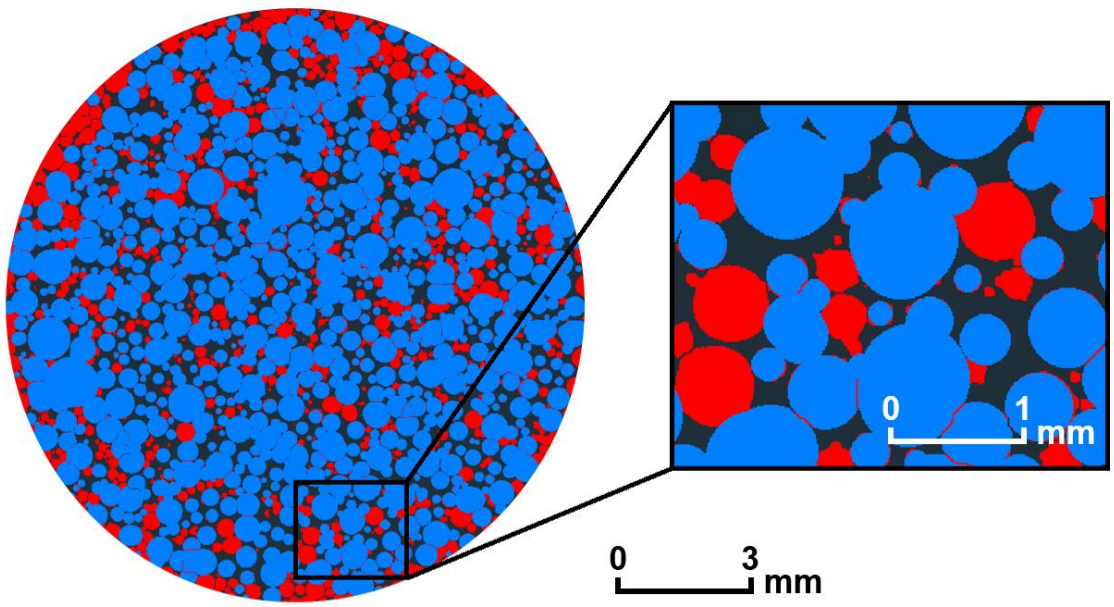

Figure 3.10 - Attempt to HT circles fitting in a cemented uniform sample slice. In red the binarized image representing the whole solid phase, in blue the circles found by the algorithm. Many spheres are not fitted and just as many are incorrectly identified

Filtering

Different filtering methods have also been tested, but without obtaining any advantages. Median and Non-Local Means filters were not necessary, as the image did not have much noise and the edges were well delineated. Edge enhancement filters, such as “Unsharp masking”, did not provide any advantage to calcite detection. In conclusion, no filtering method was employed.

Final solution

Once the extreme difficulty in separating the solid phases was ascertained, it was decided to keep glass beads and calcium carbonate crystals as a unique solid phase and to carry out a binarization between the latter and the voids. In this way a qualitative comparative analysis was achieved between a cemented and a not cemented MICP sample of the same granulometry. Therefore, absolute results are not available, as the treated and the untreated sample do not exactly have the same topological characteristics and grain distribution. However, comparing the same granulometry with and without cementation, was still possible to trace the effect of the treatment in a qualitative way.

The datasets referred to below are therefore six: uniform treated (UN 1), uniform untreated (UN 2), poorly graded treated (PG 1), poorly graded untreated (PG 2), well graded treated (WG 1), well graded untreated (WG 2).

We clarify that the wording “treated” and “untreated” does not refer to the same sample before and after cementation but to two different but statistically similar samples of same granulometry.

3.5.2. Pre-processing and segmentation

Each tomography was composed of about 10 thousand TIFF images. To carry out an analysis of the sample properties variation along its entire length, it was necessary to convert each dataset into LDA (Large Data Access) format to optimize computational time. This step required about one hour and a half of processing for each column, but significantly speeded up the following operations.

Once the datasets were converted, a sub-sizing through the *Extract Subvolume* module was made to obtain lightweight files and allow the operations to be carried out in good time. The result was the union of voxel pairs, resulting in a halving of the resolution to 16.6 μm. The processing speed benefited a lot, while image quality was not essentially affected.

For each file thus processed, two different types of sub-samples were extracted:

1. One 75 mm high parallelepiped, representing approximately the entire length of the column, designed for continuous analyses along sample. Having a square base, it excluded most of the column boundaries. The latter was achieved with the *Extract Subvolume* module.
2. Three cylinders with a diameter equal to the diameter of the sample and a height of 15 mm, designed for discrete analyses at the top, center and bottom of the samples. In this case the *Volume Edit* module was used for cropping.

Figure 3.11 shows a scheme of the sub-samples thus extracted, together with their dimensions. Since no filters were used, the following step was image binarization, meant to separate the solid phase (glass + $CaCO_3$) from the voids. To do this, Avizo's *Interactive Thresholding* module was used, in order to isolate a certain grey level interval to which the binary value 1 is assigned, from the rest of the image, which assumes a value of 0. The histogram interval corresponding to the solid phase is easily identifiable, given the contrast with the voids. The only difficulty lies in the halo at the grains' edges, which reflects intermediate grayscale levels. After several attempts, the thresholding values shown in the Table 3.5 were used.

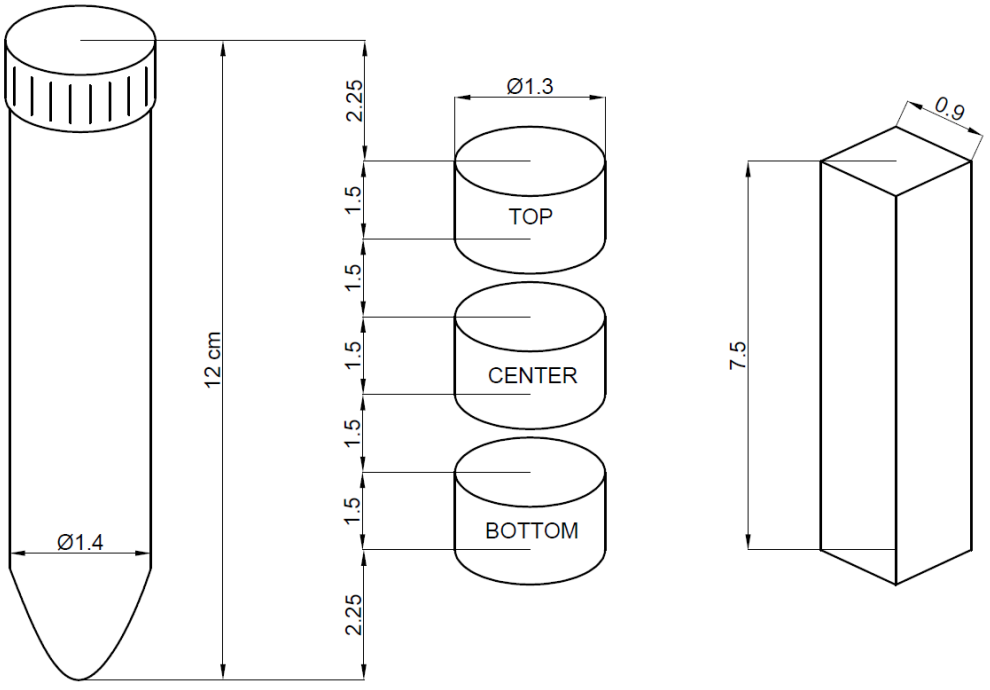

Figure 3.11 - Scheme of the extracted sub-samples used for the calculations, measures in cm. A space is left from top and bottom to avoid considering the filter mesh and the cap. Every sub-cylinder is equispaced of 1.5 cm (904 voxels) and has a height of 1.5 cm and a diameter of 1.3 cm. The inscribed parallelepiped instead has a side of 0.9 cm (540 voxels) and a height of 7.5 cm (4522 voxels).

Table 3.5 - Thresholding values for the six datasets

Granulometry	MIN grey value	MAX grey value
UN 1	31000	65535
UN 2	31000	65535
PG 1	34000	65535
PG 2	34000	65535
WG 1	35000	65535
WG 2	29000	65535

Since the contact points between the grains are not detected by the micro tomography due to resolution limitations, an image separation was carried out to divide the individual glass beads. This method is based on the principle of watershed lines and distance transformation and aims to identify the lines that separate the grains. An advantage of this technique is the pixel preservation, so that the volume of the particle does not change. The *Separate Objects* module, with the *Chamfer conservative* method was used for the image separation settings, with a 3D interpretation and a number of neighbourhood equal to 26. A particular of the conversion from grayscale to binary and to separate image is shown in Figure 3.12 for the three treated granulometries.

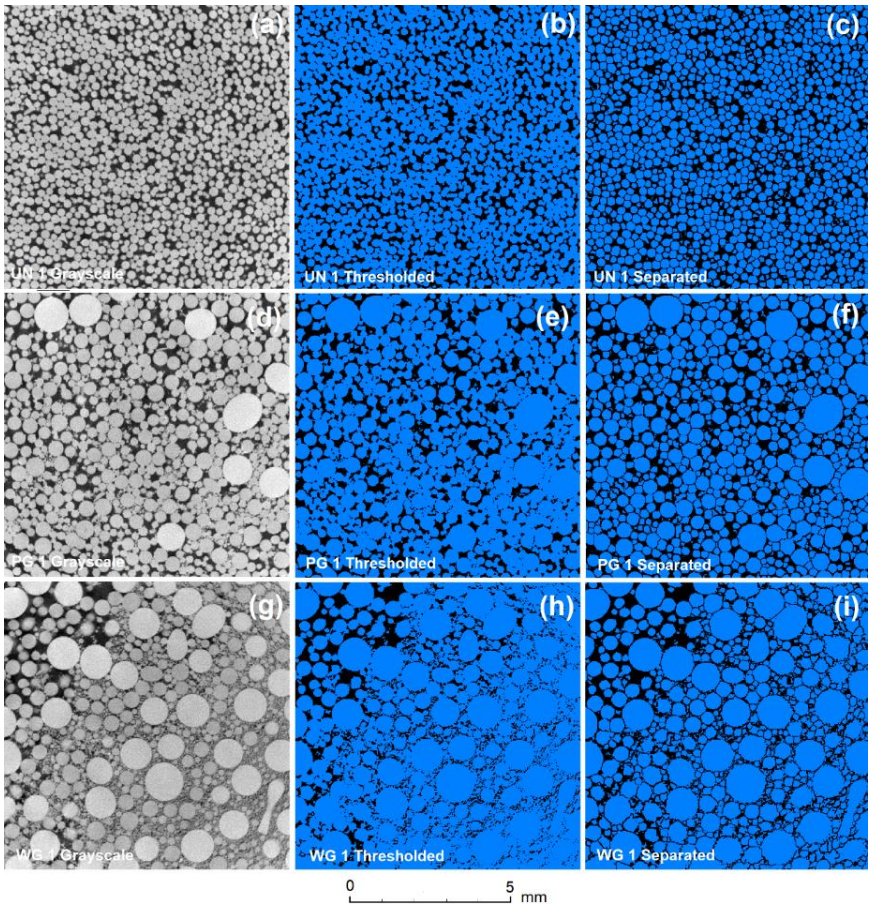

Figure 3.12 - Grayscale images for the three granulometries (a = UN 1, d = PG 1, g = WG 1), with respective binary (b, e, h) and separate (c, f, i) images

Figure 3.13 in turn shows the result of the segmentation process with a zoom to the particle size, again for the all the granulometries.

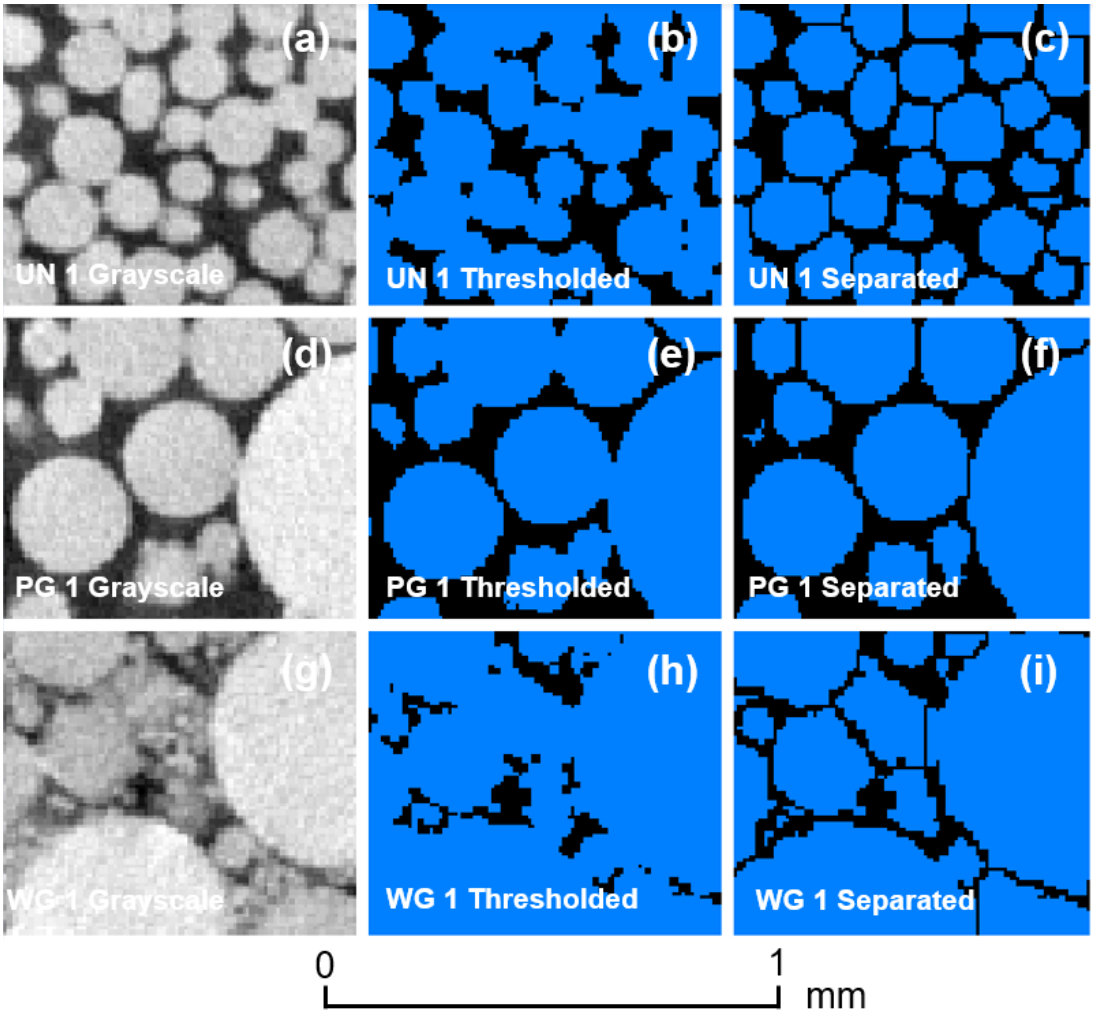

Figure 3.13 - Separation process: zoom to the particle size for the uniform (a, b, c), poorly graded (d, e, f) and well graded (g, h, i) granulometries

In Figure 3.14 below is reported the synthetic scheme followed for the dataset preparation. At this point the numerical analyses could begin.

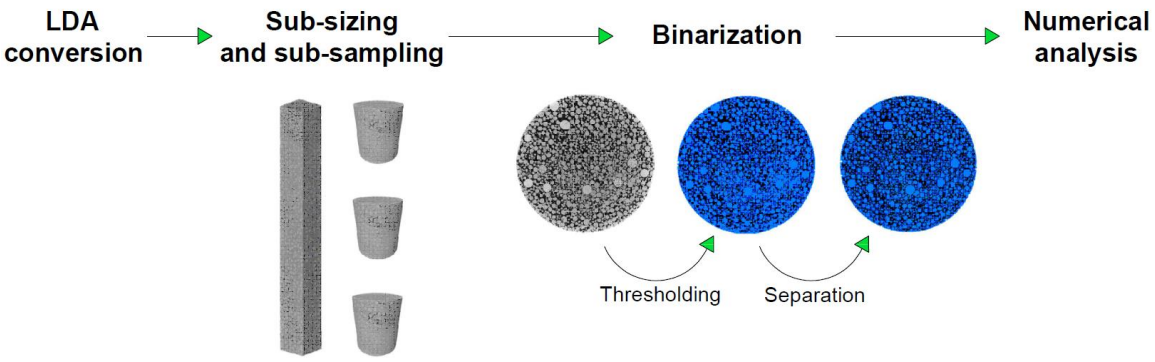

Figure 3.14 - Scheme of the binary data preparation for numerical analysis

3.5.3. Grain-size distribution

The grain-size distribution analysis was carried out using Avizo's *Label Analysis* module. The measure on which the study is based is the particles equivalent diameter. It is calculated as follows (3.7):

$$D_{eq} = \sqrt[3]{6 \cdot \frac{Volume3d}{\pi}} \tag{3.7}$$

where Volume3d is the computed volume of each separated particle.

The granulometric curves were then calculated with MATLAB, comparing the size of the grains between the treated and untreated samples (since calcite is part of the single solid phase, it increases the size of the grains). To smooth the granulometric curve, the numerically calculated equivalent diameter (too high in number) were averaged in order to obtain only 10,000 different values and a more regular curve.

3.5.4. Porosity and pore skeleton

Porosity was numerically calculated in different ways for the different binary sub-volumes. In the case of the parallelepiped, the volume fraction was calculated according to a 2D interpenetration, in order to obtain the fraction of solids, and therefore of voids, for each slice of the scan. The result is therefore the porosity variation along the sample, with a resolution equal to the number of slices of the sub-volume (4522).

In the case of cylindrical sub-samples, the volume fraction was calculated according to a 3D interpretation, eventually obtaining the total porosity of the portion.

The skeletonization is a tool used to observe the sample void network and the path a fluid might follow in it. The technique consists in extracting the centreline of the sample interconnected regions, such as the pores and pore throats. This "skeleton" of the pore network that is thus created also contains information about the size of the void space in that point, which is shown via colormap and thickness of the skeleton.

The *Auto Skeleton* module was used to extract the pore space network of our granulometries on cubic-shape sub-volumes, of 1.5 mm side. Bigger volumes gave confusing interpretations. The process was carried out on the untreated samples only, because no differences were highlighted with the cemented ones and the aim was not the comparison.

3.5.5. Calcite content

The calcite content was evaluated starting from the numerical results of the porosity on the parallelepipeds and on the sub-cylinders.

The volume of calcium carbonate was calculated as the difference between the solid volume of the cemented sample and that of the uncemented one of same granulometry. Since the distribution of the glass beads is not the same between treated and untreated samples, it was decided to always subtract the average solid volume value of an untreated sample from the treated ones. The calculations were performed using the fraction of solids in the unit reference volume. The calcite content in mass is then obtained through $CaCO_3$ and glass densities.

Equations (3.8) and (3.9) clarify the method used:

$$CC = \frac{V_{S\,1} - \overline{V}_{S\,2}}{\overline{V}_{S\,2}} \cdot \frac{\rho_{CaCO_3}}{\rho_{glass}} \cdot 100 \tag{3.8}$$

$$CC = \frac{|\Delta\varepsilon|}{1 - \overline{\varepsilon}_2} \cdot \frac{\rho_{CaCO_3}}{\rho_{glass}} \cdot 100 \tag{3.9}$$

where $V_{S\,1}$ is the volume of solids of the treated sample, $\overline{V}_{S\,2}$ is the volume of solids of the untreated sample of same granulometry. $\Delta\varepsilon$ is the difference between the mean porosity of the untreated sample and the porosity of the treated sample of same granulometry, $\overline{\varepsilon}_2$ is the mean porosity of the untreated sample.

For the calculations on the sub-cylinders, the mean untreated porosity was calculated as the average of the porosities of the 3 untreated sub-cylinders (top, center and bottom), while for the calculations on the parallelepipeds the mean porosity of the cemented sample was the average of the porosities along that sub-volume.

The results were therefore the variation of CC along the parallelepipeds and the total CC in the different sub-cylinders.

3.5.6. Permeability

Permeability analyses were conducted using *Avizo XLabSuite Extension*. With the *Absolute Permeability Experiment Simulation* module, it was possible to numerically simulate a permeability test.

The estimate of absolute permeability is obtained from Darcy's law (3.10):

$$\frac{Q}{S} = -\frac{k}{\mu}\frac{\Delta P}{L} \tag{3.10}$$

where Q is the flow in the pore space ($m^3\ s^{-1}$), S is the sample cross section subjected to flow (m^2), k is the absolute permeability (m^2), μ is the dynamic viscosity of the flowing fluid (Pa s), ΔP is the pressure drop from between top and bottom of the sample, (Pa), L is the sample length in the flow direction (m).

S, L and μ are boundary conditions, while Q and ΔP are the unknowns which are deduced with a finite volume method by numerically solving the Stokes equations (3.11):

$$\begin{cases} \operatorname{div} \vec{V} = 0 \\ \mu\vec{\nabla}^2\vec{V} - \vec{\nabla}P = \vec{0} \end{cases} \tag{3.11}$$

where $\vec{V}$ is the fluid velocity in the pore space, μ is the fluid dynamic viscosity and P is fluid pressure.

The system in (3.11) is a simplification of the Navier-Stokes equations, according to the hypothesis of incompressible Newtonian fluid and steady-state laminar flow. This means respectively that the density and the dynamic viscosity are constant, the velocity does not vary over time and no turbulence is produced.

For our study, once having made sure to use the correct spatial units of measures with respect to the declared voxel size (mm in our case), the datasets on which to perform the permeability analyses were prepared.

The tests were performed on different samples than those previously used. In fact, simulation is a highly time-demanding process, given the required computations. Therefore, starting from the thresholded and separated sub-cylinders, cubic sub-volumes of 7 mm side (420 voxels) were extracted. These can be considered REV, as they have a size ten times greater than the greater of the d_{50} (that of the WG sample), which is 0.69 mm. The analysis was therefore made again on the top, center and bottom of each column, comparing treated and untreated samples of the same granulometry.

Using the *Invert* module on the binary sub-samples a new binary image was obtained, where the value “1” represents the pore space.

The *Axis connectivity* module was applied to the latter in order to exclude isolated pores from the calculation. This step did not change the final result in our case, as all the pores

were connected. The simulation of the permeability test was then performed on these datasets.

For each cubic sub-sample, the inputs for the simulations were:

- Pressure at the top = 130,000 Pa
- Pressure at the bottom = 100,000 Pa
- Dynamic viscosity of the fluid (water) = 0.001 Pa·s

The outputs were:

- The absolute permeability
- The flow path and velocity simulation
- The pressure drop simulation

Since the study used glass beads (sphericity ≈ 1), it was possible to compare the numerically calculated permeabilities with those calculated using the Kozeny-Carman equation (3.12) (Kruczek, 2014):

$$k = \frac{1}{K}\frac{\varepsilon^3}{(1-\varepsilon)^2}d^2 \tag{3.12}$$

where K is an empirical constant, which depends on the tortuosity and is assumed equal to 150 (Ergun, 1952); ε is the numerically computed porosity for the specific column part and d is the mean numerically calculated equivalent diameter of the granulometry.

3.6. Mechanical study

A micro UCS test on a bio-cemented sample of uniform granulometry (UN 1) was performed at the PIXE laboratory of the EPFL, monitoring its evolution through XRCT.

The sample was obtained from a 15 mL cemented column fragment, which was cored to obtain a shape suitable for the test and to which cement paste was applied to provide smooth planar surfaces.

The maximum height allowed by the compression cell was 15 mm: the sample under study had a height of about 9 mm, including the paste, and a width of 6 mm, for a length to diameter ratio of 1.5. These dimensions were therefore within a REV, as the d_{50} of the UN 1 sample was equal to 0.256 mm.

The uniform granulometry was the only one to be mechanically tested as the other samples did not have fragments of sufficient size to fit into a REV (Figure 3.15).

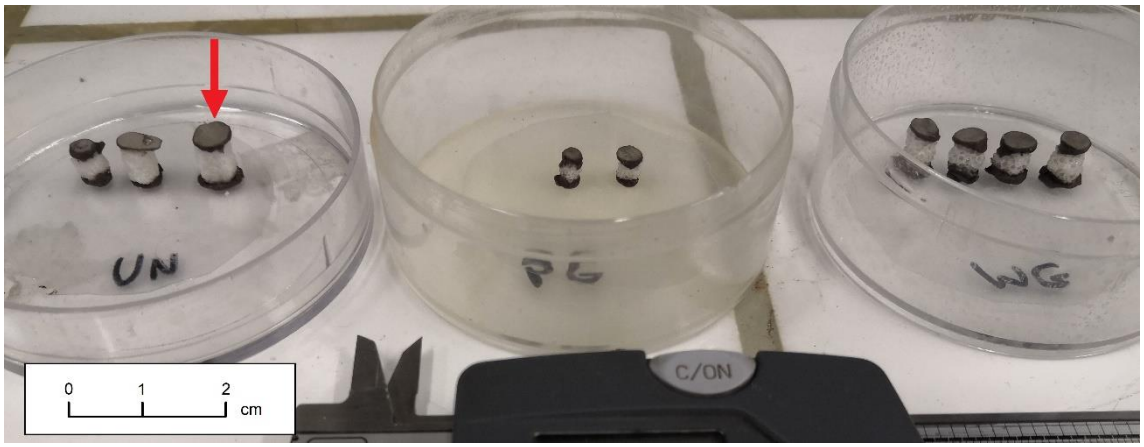

Figure 3.15 - All the samples cored for the UCS test. From the left, the uniform, the poorly graded and the well graded granulometries. Among these, only samples from the uniform distribution were suitable for the test and only the one indicated by the red arrow was used

A constant strain rate equal to 0.1 mm / min was imposed (ASTM D2166 / D2166M-16, 2016) and a stress-strain curve was obtained, from which the UCS could be estimated.

In addition to that, 4 tomographic scans were performed, with a quite low resolution equal to 17.2 µm, due to the test setup. They were carried out as follows:

1. The first scan on the undisturbed sample, with no forces applied
2. The second scan within the postulated elastic branch, at 0.4% axial strain
3. One immediately after failure
4. One in the softening part, at 1.5% axial strain, when the test was stopped

The tomographic images were analysed both three-dimensionally and by investigating the same 2D vertical section, in order to observe the volumetric deformation of the sample and the development of the failure mechanism.

The preparation of the latter followed the premises illustrated in the chapter 3.5.1. The pre-processing did not require a conversion to LDA, given the smaller sample size and low resolution. No sub-sizing or sub-sampling were performed, since the resolution was already quite low, and all the sample volume was of interest. The thresholding values for binarization were in this case 36000-65535 and no image separation was carried out, since only the relative movement of the grains has been studied.

Figure 3.16 shows a slice of the undisturbed sample on an XZ plane in gray scale and after binarization.

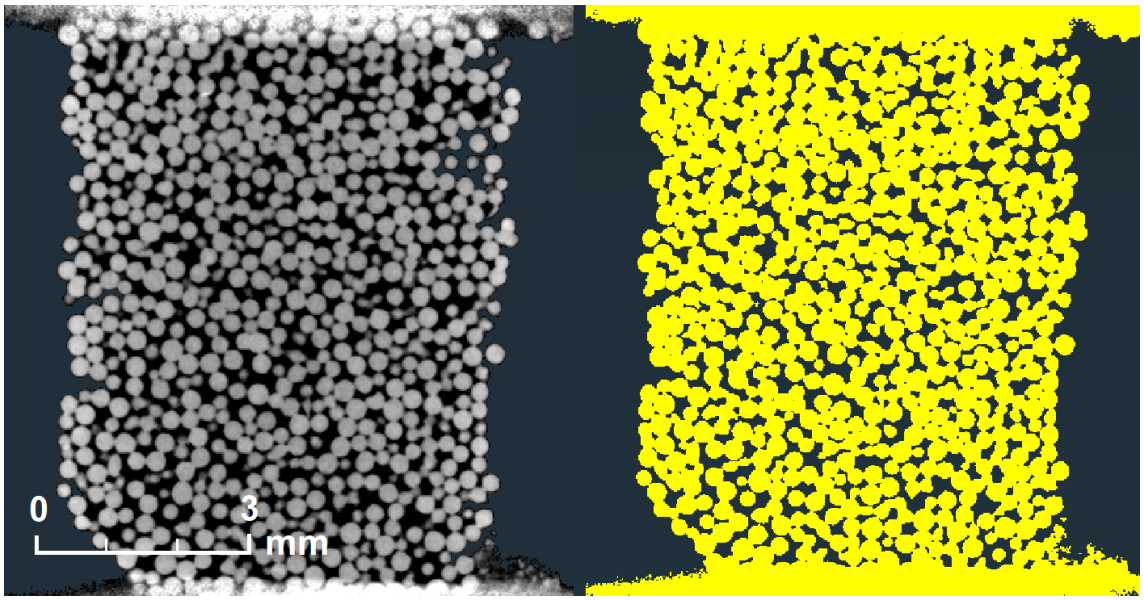

Figure 3.16 - Uniform sample for UCS test before loading. On the left the grayscale image, on the right the thresholded one

3.7. SEM

In order to observe surface and textural characteristics of the calcium carbonate crystals precipitated on the glass beads, a scanning electron microscopy (SEM) investigation was conducted. The intent was to verify the actual presence and disposition of the crystals, their bonding effect, as well as to evaluate the prevailing $CaCO_3$ polymorphs. The analysis was carried out in the EPFL CIME laboratory. Small aggregates of each granulometry were collected and covered by a 100 nm-thick gold coating (Figure 3.17) using the sputter coating technique in order to ensure a proper conductivity for the microscope electron beam. They were then observed under the electron microscope in a purely qualitative manner.

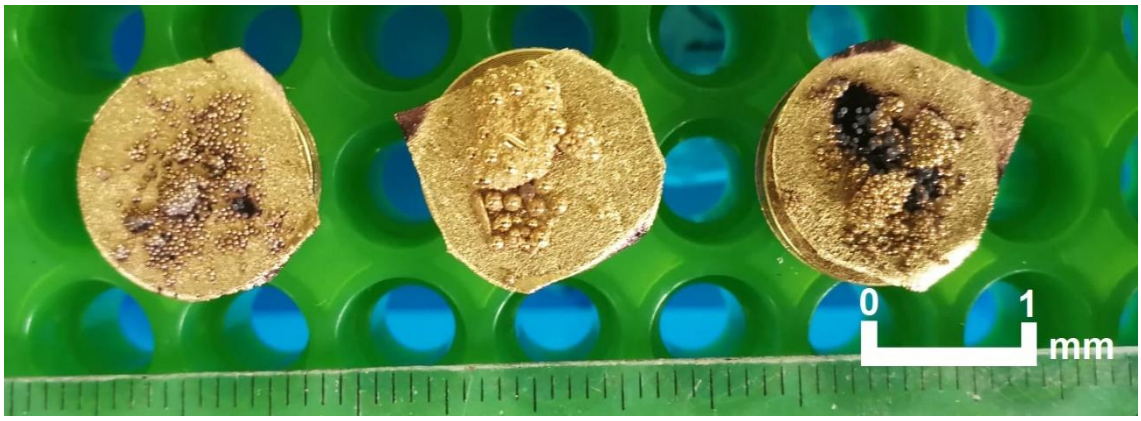

Figure 3.17 - SEM ready gold coated samples. From the left: UN, WG, PG

4. Considerations on the setup

4.1. Glass beads compaction

In order to obtain consistent results in the various experiment duplicates and in reference to other studies, the soil samples subject to analysis are usually compacted to a certain relative density, to which the properties and characteristic behaviour patterns of granular materials are connected (Cui et al., 2017; Dadda et al., 2017; DeJong et al., 2010; Fauriel, 2012; Terzis et al., 2016). This measure indicates the relative position of the current void ratio, between the minimum and maximum void ratios of the soil (Lade et al., 1998) (4.1):

$$Relative\ Density = \frac{e_{max} - e}{e_{max} - e_{min}} \tag{4.1}$$

where e_{max} is the soil void ratio in its loosest state, e_{min} is the soil void ratio in its densest state and e is the soil void ratio in the current state.

In this study it was not possible to appreciably change the degree of compaction of the glass beads, so the relative density of the different samples is not the same and neither is their porosity.

As observed by Onoda and Liniger (1990), in fact, the loosest possible packing of spheres in a container depends on the magnitude of the gravitational forces.

Spherical particles can be arranged in 5 idealized packings. The loosest is the cubic with solid volume fraction of 0.91, while the densest are the face-centred cubical and the close-packed hexagonal, both with a solid volume fraction of 0.35 (McGeary, 1961).

Pouliquen et al. (1997) reported that in reality, the volume fraction of the spheres, cannot exceed 0.74, but spheres simply released in a box do not spontaneously arrange into a crystalline formation. Even when vibrations are imposed to compact the arrangement, the maximum volume fraction obtained was 0.64. The matter is slightly different for distributions of spheres with different diameters, as is the case in this study, but it is clear that there are minimum and maximum compaction limits that are difficult to govern with respect to the case of a real soil, in which the particles can be rearranged to obtain a higher density.

It is believed that this difference is dictated by the shape of the grains, which in the case of spherical beads limits the possibilities of rearrangement of the particles, compared with the structures that a soil with irregular grains can assume (Figure 4.1).

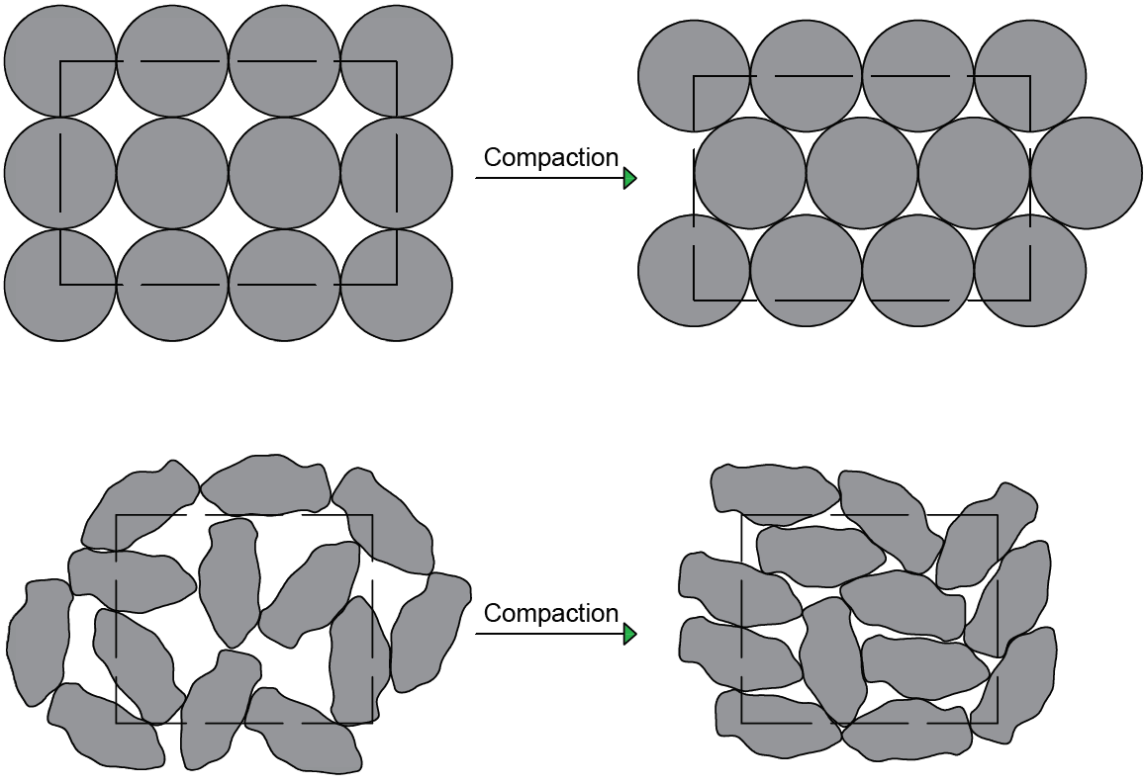

Figure 4.1 - Effects of compaction on glass beads (top) and on uniform size irregular particles (bottom). The possibilities of rearrangement for a real soil are greater than for spheres, due to the influence of the of grains rotation.

In practical terms, once the granulometries were created and the artificial soil inserted into the columns, any attempt at compaction or mixing has never led to appreciable changes in relative density, and this is why our samples were considered to be at their at the lowest possible porosity.

4.2. Granulometries

The granulometries created according to the distributions shown in Table 3.1 have in some cases encountered some practical problems. This consideration is mostly valid for well graded distribution (WG), and in particular in its dosage of fine and coarse grains. Given the large difference in diameter between the glass beads, the smaller particles tended to segregate in some areas of the column, within the voids of the larger beads. This trend led to a largely heterogeneous porosity within the WG samples due to the increased presence of solids in some areas. Although a variable porosity was sought, as an intrinsic characteristic of a well graded soil, this segregation of the fines led to abrupt changes of solid content and therefore of porosity which influenced the final cementation, the interpretation of the results and their reproducibility, as the reactants used to follow preferential paths during the injections (Figure 4.2).

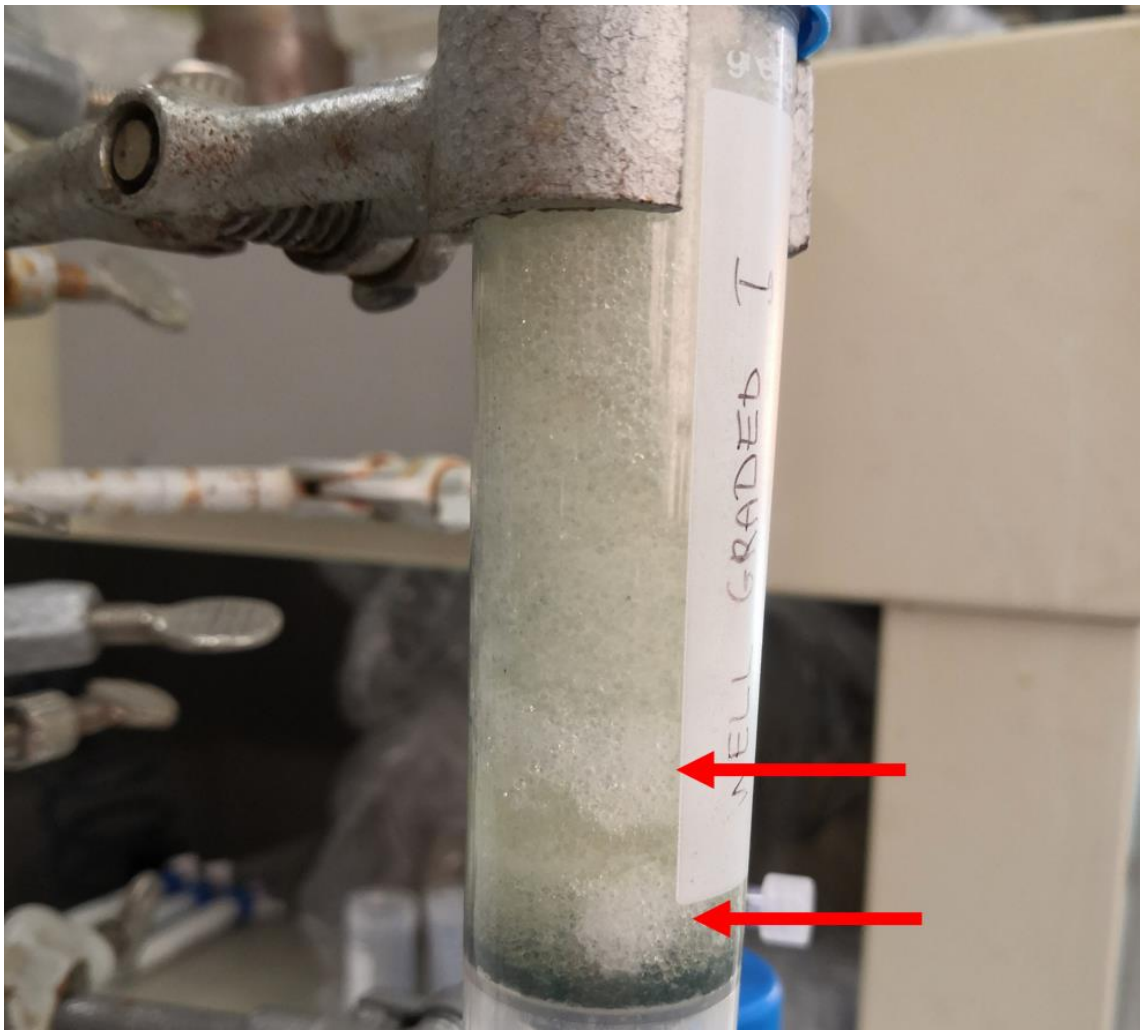

Figure 4.2 - WG sample during treatment: areas with increased fines (red arrows) hindered the passage of the reactants and led to an inhomogeneous cementation

This aspect of the WG samples will be clearly shown in Chapter 6, thanks to numerical analysis.

Apart from this observation, the granulometries proved to be representative of real soils with different porosities and degrees of uniformity. In particular, these two properties were strongly interconnected, being the degree of heterogeneity the determining factor of our soils' intrinsic porosity. Since this latter parameter was not modified by compaction and the different granulometries' d_{50} did not differ in an essential way, the large differences in volume of voids were mostly dictated by the variance in the grain size. This last observation is in agreement with what was observed by Das and Sivakugan (2011), which reported a decrease in void ratio as the soil coefficient of uniformity increased.

The quickly measured porosities used for the calculation of the flow rate are therefore shown in Table 4.1: they clearly decrease as the variability of the grain size increases.

The difference between the 50 mL and 15 mL samples lies in the increased influence of boundary effects in the smaller ones and in the different fine segregation in the WG samples.

Table 4.1. Roughly calculated porosities ε

Sample size	Granulometry	ε (-)
15 ml	UN	0.39
	PG	0.34
	WG	0.23
50 ml	UN	0.37
	PG	0.32
	WG	0.25

4.3. Conclusion

The initial intent was to compact the samples at the same void ratio, but the physical characteristics of the glass beads did not prove suitable for this purpose. Maintaining different porosities and consequently changing the flow rate was considered a good solution.

By targeting the same seepage velocity in all samples (0.024 cm/s) it was in fact possible to consider the bacteria attached to the soil grains as exposed to similar advective fluxes, which is a factor proved to influence the degree and distribution of the cementation (Martinez et al., 2014; Mortensen et al., 2011; Stack, 2015).

In this way the influence of the pore-scale heterogeneities could be isolated and investigated in a separate and autonomous way, and the different results of the treatment could be attributed to these different properties.

A more representative well graded sample could have been fabricated using a greater quantity of beads of intermediate size between fine and coarse, in order to limit the freedom of movement of the grains smaller than 106 μm and their uncontrolled segregation.

5. Experimental Characterization

This section contains the experimental analyses carried out on the 50 mL (UN 1, PG 1 and WG 1) and 15mL (UN 1s, PG 1s, WG 1s) specimens. The results mainly concern the treatment chemical monitoring, the calcite content, the qualitative microscopic analysis and a mechanical test.

5.1. Chemical analysis

In this chapter we intend to present and discuss the results relating to the chemical analyses of pH, electrical conductivity, ammonium, calcium and total inorganic carbon concentration on the effluents of the 50 mL samples.

As already explained, these analyses were performed on the effluents of the 11 CS injections. This means that the first effluent represents the BS injected on the first day, while the last volume of CS injected was not collected, because it was diluted in 2 PV of water. The monitoring allowed us to understand if and to what extent the reaction took place.

Within the effluents of the first CS injection (therefore representing the BS), calcium carbonate precipitates were already observable in the outlet pipes and storage containers (Figure 5.1), indicating that the reaction started already in the first half hour.

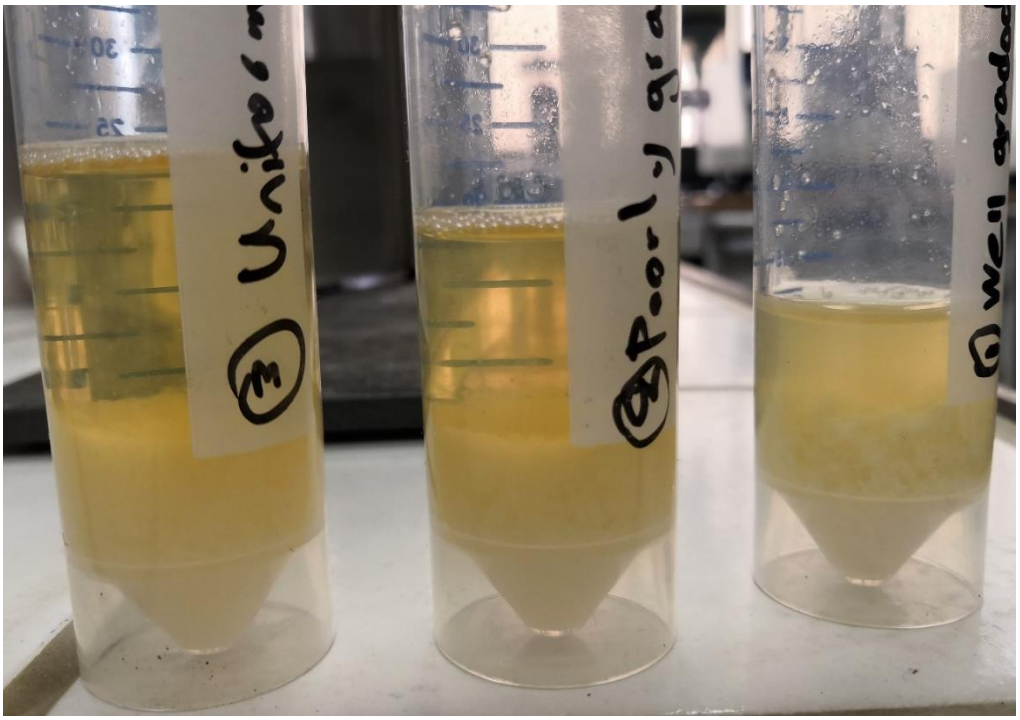

Figure 5.1 - Calcium carbonate precipitates on the bottom of the falcon tubes containing the first effluent (mostly BS). From the left: WG, PG, UN

An attempt was made to measure the OD600 on effluents, with the aim of measuring the number of bacteria remained attached on the solid matrix. However, the results were not usable, given the increased opacity of the effluent due to the suspended $CaCO_3$ crystals.

5.1.1. pH and Electrical Conductivity

The pH and EC monitoring is a real-time control tool of the reaction. The precipitation of calcium carbonate in fact leads to a reduction in pH and salinity in the fluid (and therefore of its electrical conductivity), while the ureolysis process increases them.

These alterations are to be evaluated in relation to the pH and EC of the influent CS. In this study, the pH before injection was not always measured, but it is known that it was equal to 7 on the first day and stabilized at around 6 in the rest of the treatment campaign. The electrical conductivity of the influent CS has always remained unchanged, around 42 mS/cm. This last measurement was not carried out in the last four days due to the impossibility of accessing the laboratory for analysis.

Figure 5.2 shows the trend of the measured pH and EC during the treatment, while Table 5.1 reports the exact values.

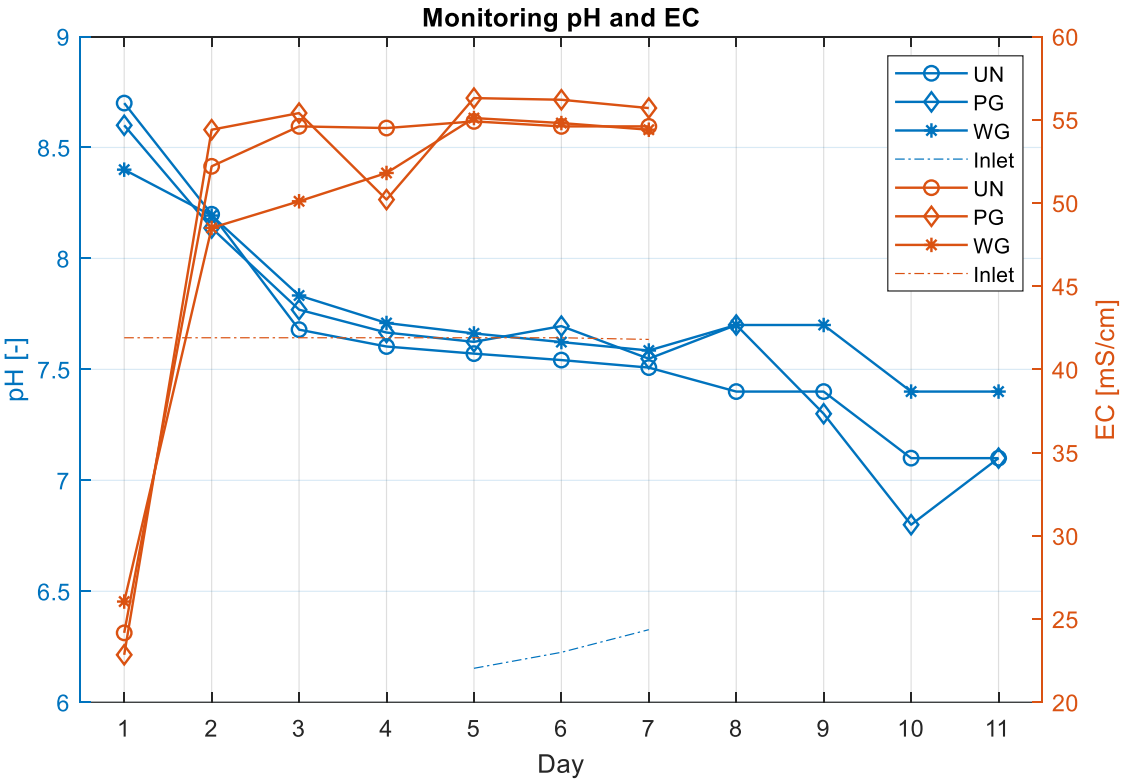

Figure 5.2 - Trend of pH and EC measurements. On the left y-axis the pH, on the right one the EC

Table 5.1 - Results of pH and EC monitoring

Day	1	2	3	4	5	6	7	8	9	10	11
					EC [mS/cm]						
CS IN	41.9	41.9	41.9	41.9	41.9	41.9	41.8	-	-	-	-
UN 1	24.2	52.2	54.6	54.5	54.9	54.6	54.6	-	-	-	-
PG 1	22.9	54.4	55.4	50.2	56.3	56.2	55.7	-	-	-	-
WG 1	26.1	48.5	50.1	51.8	55.1	54.8	54.4	-	-	-	-
					pH [-]						
CS IN	7.0	-	-	-	6.2	6.2	6.3	-	-	-	-
UN 1	8.7	8.2	7.7	7.6	7.6	7.6	7.5	7.4	7.4	7.1	7.1
PG 1	8.6	8.1	7.8	7.7	7.6	7.7	7.5	7.7	7.3	6.8	7.1
WG 1	8.4	8.2	7.8	7.7	7.7	7.6	7.6	7.7	7.7	7.4	7.4

By looking at the electrical conductivity results, it can be observed that on the first day it is very low as there are no ions in the BS. On the second day there is an average increase of about 30 mS/cm, with the PG having the greatest increase and the WG the least. On the third day the EC of the UN reaches 55 mS/cm and then remains almost constant for the rest of the measurements. The WG, on the other hand, shows linearly increasing EC values from 48 mS/cm to 55 mS/cm from the second to the fifth day, and then remains constant. The EC of the PG is in general the highest of the three from the second day onwards, with the exception of the fourth, in which it has a fall of about 5 mS/cm, and then returns constant around 55-56 mS/cm for the other measures.

If we exclude the outlier on the fourth day, the EC of PG is on average the highest of the three granulometries, followed by UN and WG. In particular, the first two report a more sudden increase in EC in a single day and then remain constant, while the EC of the WG grows more slowly from the second to the fifth day, to then reach the same values as the UN.

As regards the pH, for all the granulometries it is very high on the first day, as the BS itself had a pH of 9. It then decreases until the third day, starting from which, it remains constant until the seventh. From this moment the pH of the UN begins to decrease until it reaches a value of 7.1 on the last day of monitoring. The WG instead shows slightly increasing values from day 7 to day 9, and then decreases to a pH of 7.4. Finally, the pH of the PG increases from the seventh to the eighth day and then sharply decreases to 6.8 on day 10 and back to 7.1 on the last day.

On average, the highest pH is that of WG and the lowest that of UN. The PG values are instead more variable and the lowest only in the last three days. In general, if up to day 7

the pHs are all similar and on average stable, from day 8 to 11 the gaps widen and the trend becomes more irregular, although always decreasing.

5.1.2. Calcium, ammonium and TIC

Measurements of ammonium and calcium ions and of total inorganic carbon concentration are the first useful tool for estimating the quantity of precipitated calcium carbonate. Figure 5.3 shows the trends of Ca^{2+} and NH_4^+ in the 11 analysed effluents. The exact values are instead shown in the Table 5.2.

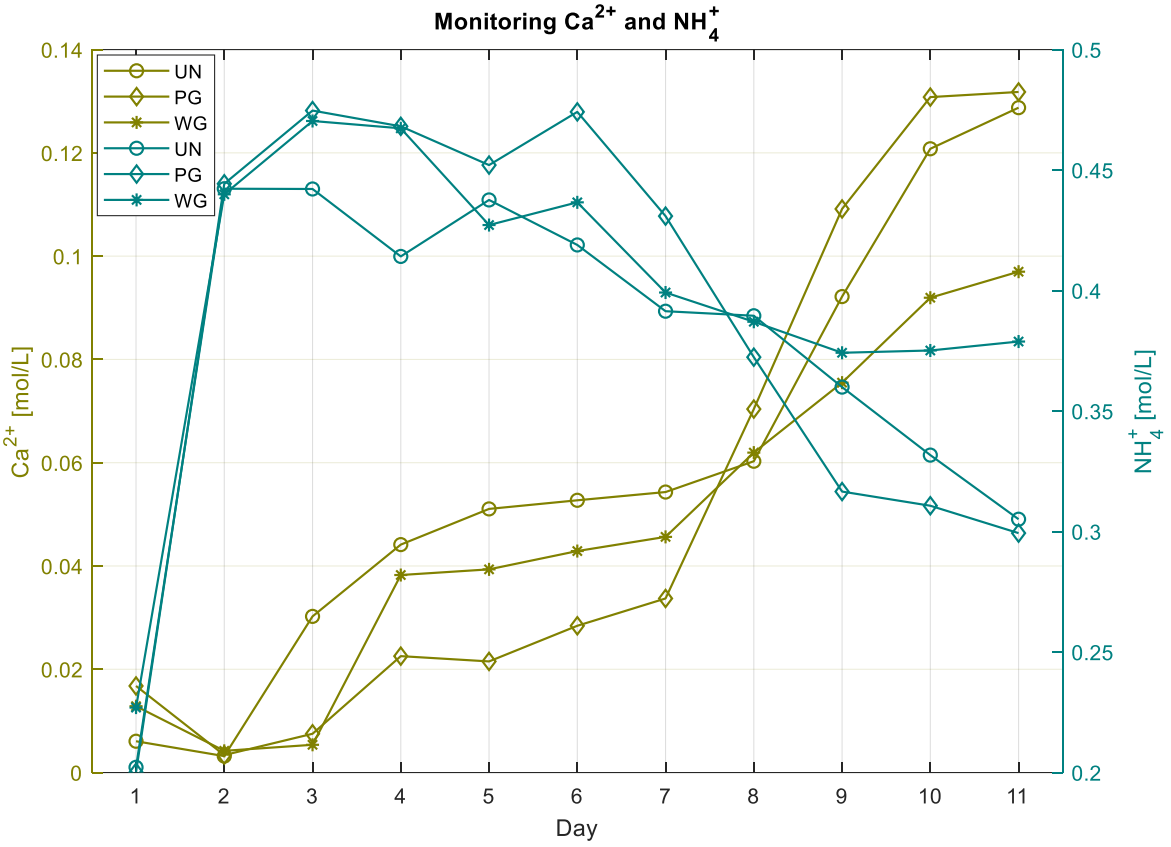

Figure 5.3 – Trend of calcium and ammonium concentrations in mol/L. On the left y-axis the Ca^{2+}, on the right one the NH_4^+

Calcium is low on the first day (BS) and even decreases the following day. From day 3 it starts to increase, with the UN sample reporting the greatest increase in concentration from day 2 to 3. The increase is almost constant for all the granulometries up to day 7, starting from which, there is a surge in the curve , with concentrations tending more rapidly to those of the inlet CS.

On the last day of monitoring, the granulometry with Ca^{2+} concentration in the effluent closest to the concentration in the inlet CS is PG, followed with little difference by UN

(both about 0.13 mol / L). The WG, on the other hand, remains on lower values, around 0.1 mol/L. It is observed that the Ca^{2+} concentration is not distinctively higher for any of the grain-size distributions for the whole duration of the MICP treatment. From day 3 to 7, however, the UN has the higher concentrations, followed by the WG and the PG. From the 8th day onwards the order becomes PG, UN, WG.

As regards the ammonium, the first day it is low, as it is absent in the BS. For all samples, from day 2 the concentration increases and remains almost constant until day 6, from which it begins to decrease. The values in the PG decrease more abruptly than the others, passing from concentrations of about 0.47 mol/L on day 6 to 0.30 mol/L on the last day analysed.

Similarly to the case of calcium, at the end of the monitoring, PG and UN have similar ammonium concentrations (about 0.3 mol/L) while the WG shows this time higher values, around 0.38 mol/L. For the latter, the NH_4^+ concentration stops decreasing and even slightly increases from the ninth to the eleventh day. Again, it is difficult to identify a granulometry showing ammonium concentrations always higher than the others.

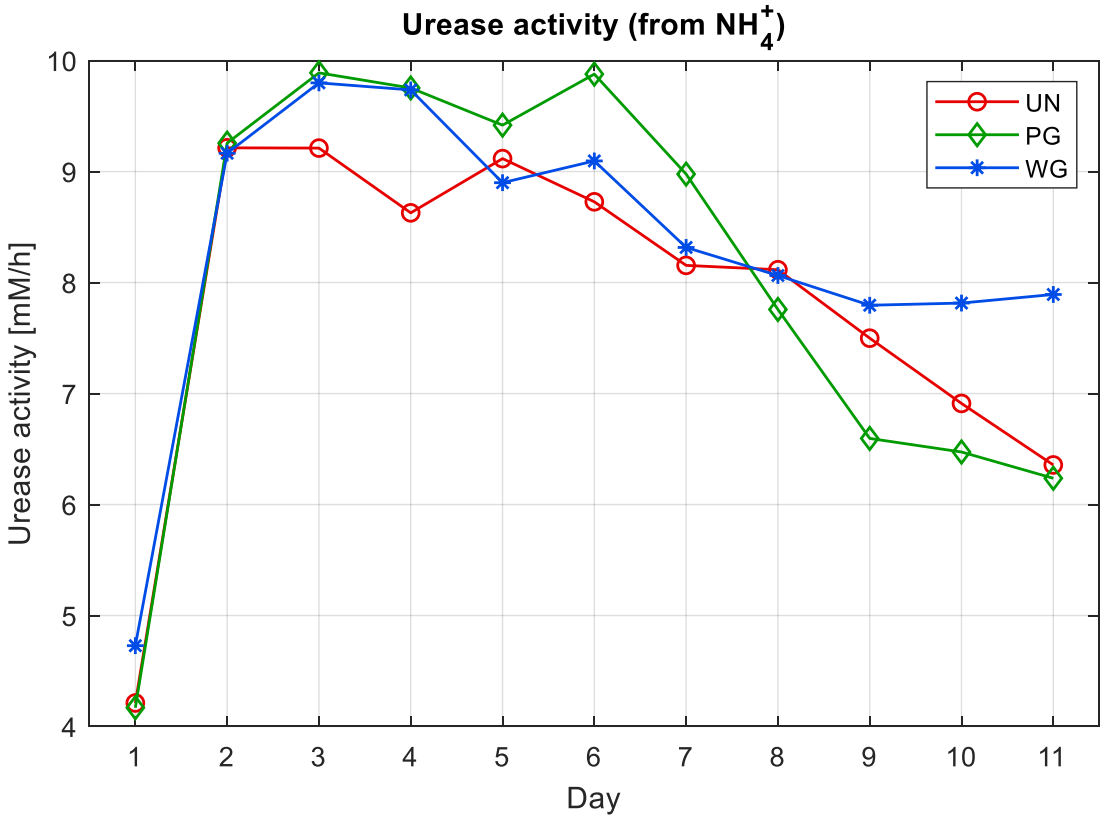

Figure 5.4 - Urease activity trend during the treatment (in mM/h) calculated from the ammonium concentration values

Starting from the ammonium concentration it is possible to trace the urease activity during the treatment, by means of the equation (2.9), where the duration of the reaction is 24 hours.

The bacterial activity trend during the treatment is shown in Figure 5.4.

The tendency is identical to that of ammonium, as the relationship with the latter is linear. Excluding the first day, the general observation is that urease activity increased slightly between the second and third injection, after which, it decreased uniformly in the WG and instead remained initially higher and only from the day 6 sharply decreased for the PG and UN granulometries.

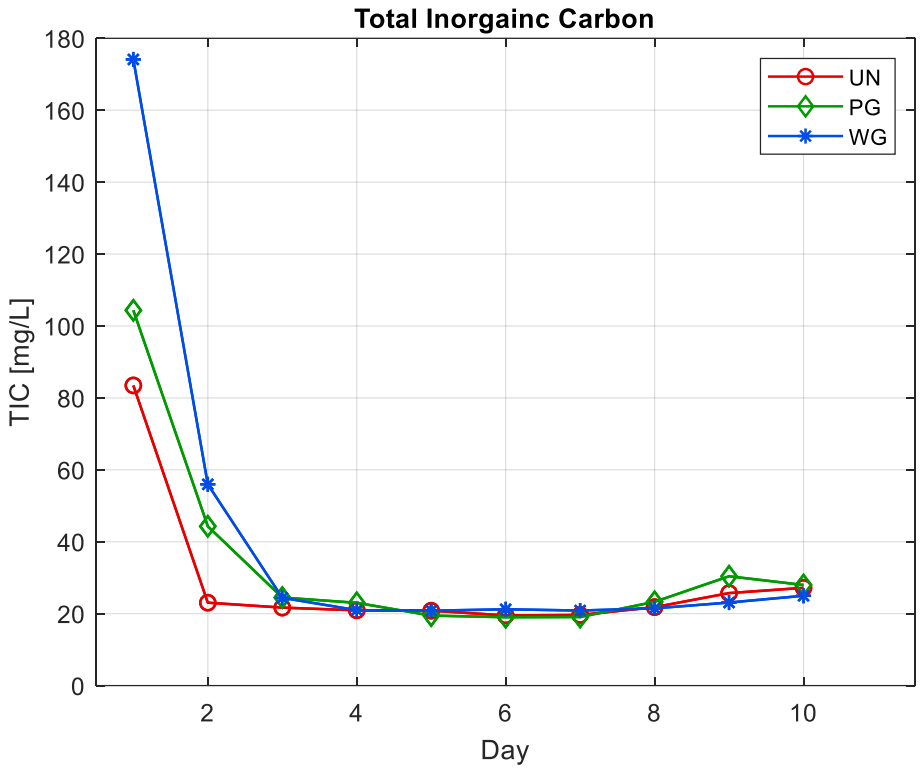

Figure 5.5 - TIC concentration trend in mg/L for the three granulometries

The total inorganic carbon trend can be seen in the Figure 5.5 above, while the exact values of concentration are shown in Table 5.2. In this case the results are reported in mg/L.

The trend of the TIC is different from previous concentrations. The high values of the first day partially hide the behaviour from the remaining part of the treatment. In any case, even starting from the second day the concentrations immediately decrease abruptly, and then remain constant from day 3 to day 8 (about 20 mg/L), starting from which, they grow again slightly up to about 27 mg/L.

Table 5.2 - Concentrations of calcium, ammonium and TIC in the three granulometries

Day	1	2	3	4	5	6	7	8	9	10	11
						Ca^{2+} [mol/L]					
UN 1	0.006	0.003	0.030	0.044	0.051	0.053	0.054	0.060	0.092	0.121	0.129
PG 1	0.017	0.003	0.008	0.023	0.022	0.028	0.034	0.070	0.109	0.131	0.132
WG 1	0.013	0.004	0.005	0.038	0.039	0.043	0.046	0.062	0.076	0.092	0.097
						NH_4^+ [mol/L]					
UN 1	0.202	0.442	0.442	0.414	0.438	0.419	0.391	0.390	0.360	0.332	0.305
PG 1	0.200	0.444	0.475	0.468	0.452	0.474	0.431	0.372	0.317	0.311	0.299
WG 1	0.227	0.440	0.470	0.467	0.427	0.437	0.399	0.387	0.374	0.375	0.379
						TIC [mg/L]					
UN 1	210.25	83.48	23.05	21.68	20.92	20.82	19.52	19.63	21.81	25.72	27.19
PG 1	252.20	104.37	44.30	24.48	23.01	19.46	19.01	19.06	23.29	30.40	27.97
WG 1	512.65	174.12	55.98	24.41	20.97	20.83	21.21	20.87	21.48	23.09	24.98

Chemical efficiency

The following calculations exclude the measurements of the first day, which refer mainly to the BS. Therefore, the results are reported starting from the first effluent CS, for each granulometry.

The reaction chemical efficiency can be evaluated, by using the relations in (3.2), (3.3) and (3.4), respectively as regards the conversion efficiency of urea into ammonium and the precipitation efficiency of calcium from Ca^{2+} and carbonate from hydrolysed urea.

Table 5.5 shows the efficiency values day by day, while in the Figure 5.6 their development can be observed.

Table 5.3 - Chemical efficiency day by day for the three granulometries

Day	2	3	4	5	6	7	8	9	10	11
					Precipitation efficiency from Ca^{2+} [%]					
UN 1	98.73	87.90	82.34	79.58	78.91	78.27	75.89	63.13	51.68	48.50
PG 1	98.65	97.00	90.98	91.39	88.63	86.52	71.84	56.35	47.68	47.28
WG 1	98.32	97.85	84.70	84.26	82.84	81.75	75.22	69.80	63.22	61.21
					Conversion efficiency NH_4^+ [%]					
UN 1	88.45	88.43	82.83	87.52	83.79	78.29	77.91	71.99	66.35	61.02
PG 1	88.86	94.94	93.63	90.42	94.83	86.18	74.47	63.32	62.14	59.87
WG 1	87.99	94.07	93.46	85.44	87.32	79.84	77.41	74.84	75.03	75.77
					Precipitation efficiency from TIC [%]					
UN 1	87.91	88.28	82.69	87.39	83.65	78.16	77.78	71.85	66.18	60.85
PG 1	88.19	94.65	93.47	90.27	94.70	86.06	74.35	63.17	61.95	59.69
WG 1	86.86	93.71	93.31	85.30	87.19	79.70	77.28	74.70	74.88	75.61

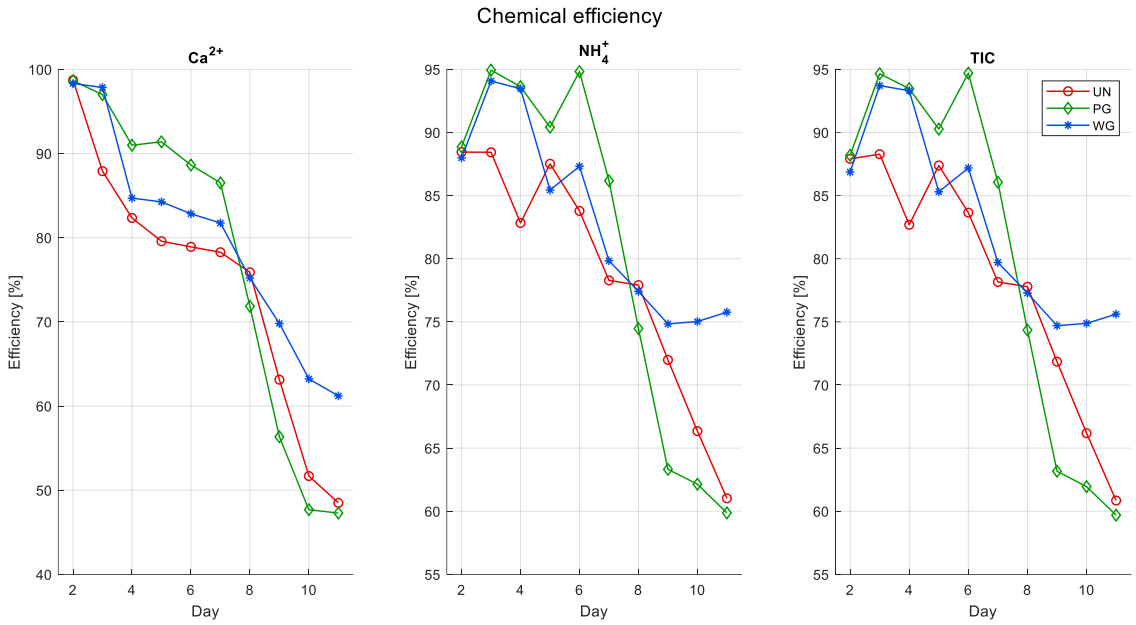

Figure 5.6 - Reaction efficiency from chemical results. Linear interpolation

In all estimates, the chemical efficiency of the PG sample is the highest for days 2, 3 and 4 (up to 99% on day 2 in the case of calcium) and then decreases more sharply than the others, until it becomes the lowest on the 11th day (48.5% in the case of Ca^{2+}). The chemical efficiency in the WG sample is, on the other hand, always higher than the UN one, for the whole treatment and for each measurement.

The precipitation efficiency of Ca^{2+} is the one which, starting from the highest values (close to 100%) decreases more abruptly, to efficiencies lower than the others. Ammonium conversion and carbonate precipitation efficiencies, on the other hand, have similar trends and magnitudes.

To conclude, in the cases of NH_4^+ and TIC, the efficiency in the WG sample slightly increases the last 3 days of monitoring by about one percentage point. Furthermore, for all granulometries, around days 5-6 the efficiency of the reactions begins to decrease faster.

Precipitated $CaCO_3$ and calcite content

Also in this case the results exclude the measurements of the first day. Starting from the measured concentrations and thanks to equations (2.10), (2.11) and (2.12), it was possible to trace the total amount of $CaCO_3$ that should be precipitated during the treatment, according to the estimates suggested respectively by NH_4^+, Ca^{2+} and TIC.

The results are reported in Table 5.4, while the trend is shown in Figure 5.7.

Table 5.4 - Precipitated $CaCO_3$ (mg) from ammonium, calcium and TIC estimates

Day	2	3	4	5	6	7	8	9	10	11
$CaCO_3$ from Ca^{2+} [mg]										
UN 1	606.57	540.07	505.91	488.93	484.82	480.89	466.24	387.87	317.54	297.98
PG 1	525.79	516.98	484.93	487.11	472.4	461.12	382.92	300.31	254.14	252.01
WG 1	418.88	416.89	360.86	358.99	352.95	348.27	320.46	297.37	269.35	260.76
$CaCO_3$ from NH_4^+ [mg]										
UN 1	543.44	543.3	508.9	537.72	514.76	480.98	478.66	442.29	407.61	374.92
PG 1	473.63	506.01	499.04	481.9	505.42	459.33	396.93	337.48	331.22	319.1
WG 1	374.86	400.8	398.2	364	372.03	340.15	329.8	318.84	319.65	322.81
$CaCO_3$ from TIC [mg]										
UN 1	540.13	542.39	508.04	536.89	513.94	480.2	477.88	441.42	406.59	373.84
PG 1	470.04	504.49	498.2	481.11	504.75	458.68	396.27	336.68	330.17	318.14
WG 1	370.08	399.26	397.53	363.42	371.46	339.56	329.23	318.25	319.01	322.12

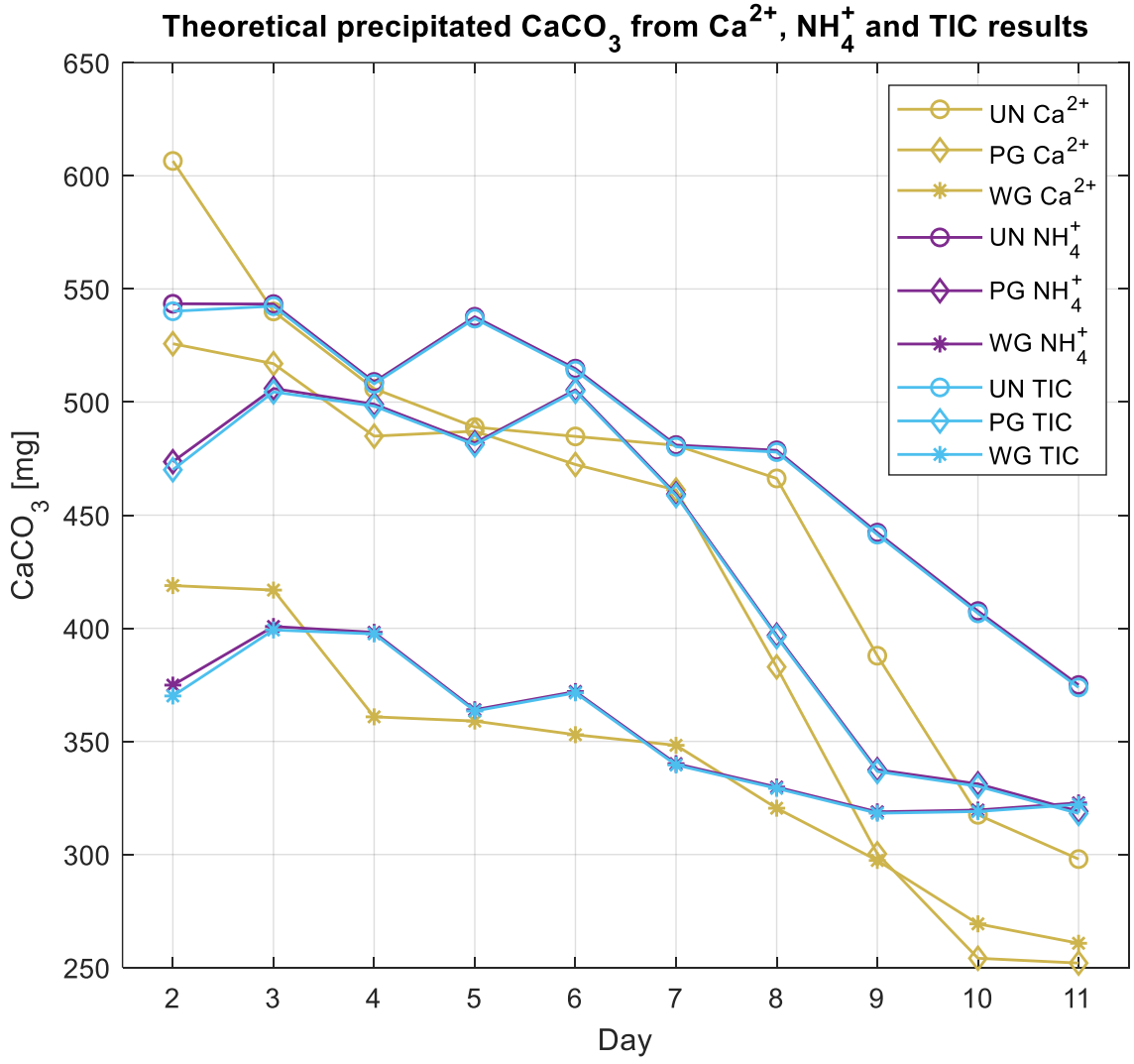

Figure 5.7 - Theoretically precipitated $CaCO_3$ from ammonium, calcium and TIC estimates

From the Figure 5.7 we can observe that the precipitation took place every day of the treatment, decreasing with the passage of time. The estimates provided by ammonium and TIC are very similar, while the concentration of Ca^{2+} seems to overestimate the mass of calcium carbonate precipitated on day 2 (up to 12%) and then underestimates it from the third day on, with values up to 20% lower in the last two days.

On average, the precipitated mass of calcium carbonate is approximately 457 mg/day for the UN, 393 mg/day for the PG and 349 mg/day for the WG.

Finally, by relating the mass of calcium carbonate to the mass of each sample solid skeleton with equation (3.5), the calcite content was obtained, the cumulative trend of which can be observed in Figure 5.8. The final $CaCO_3$ content at the end of the treatment is instead reported in Table 5.5.

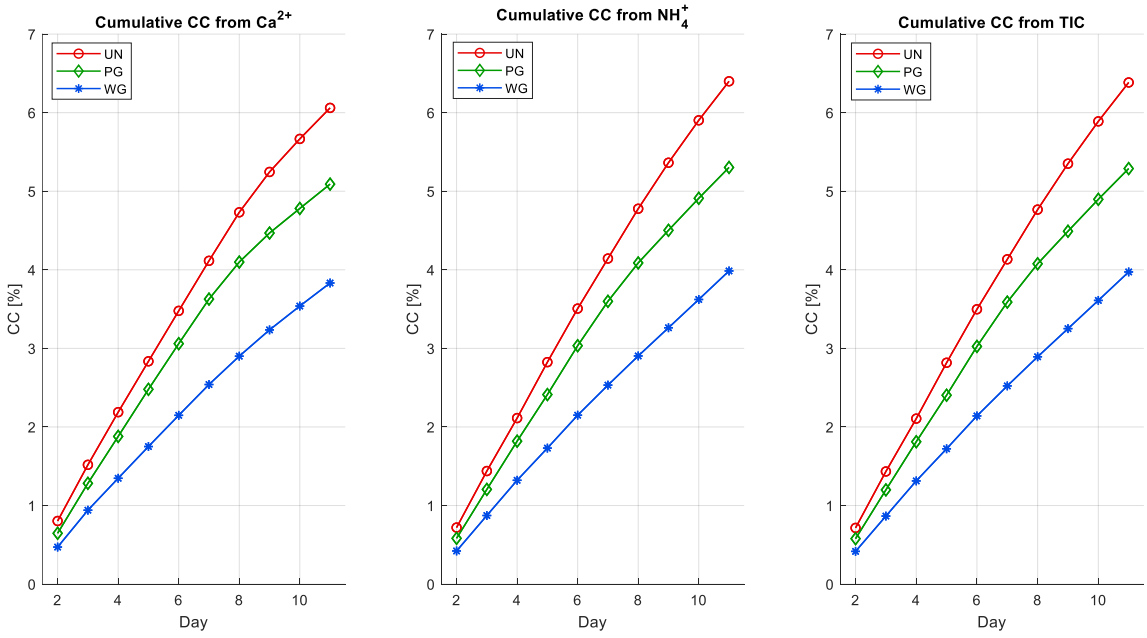

Figure 5.8 - Cumulative calcite content estimates from calcium, ammonium and TIC concentrations

It can be observed how the evaluation starting from calcium results underestimates the calcite content compared to that calculated starting from the concentrations of ammonium and TIC.

Looking instead at the differences between the three granulometries, the uniform is the one in which the calcite content is greater (more than 6% at the end), followed by poorly graded (up to 5.3%) and well graded (almost up to 4%).

Table 5.5 - Final calcite content (%) from chemical estimations, for the three granulometries

	Final calcite content [%]		
	From Ca^{2+}	From NH_4^+	From TIC
UN 1	6.06	6.40	6.38
PG 1	5.09	5.30	5.29
WG 1	3.83	3.99	3.97

5.1.3. Discussion

By means of the results of the chemical analyses it is possible to make some important observations on the treatment.

Bacterial activity

From the pH and EC values (Figure 5.2), it can be confirmed that the reaction actually took place. First, in fact, the effluents always have a pH higher than the influent CSs, and it is clear that this is the result of the ureolysis reaction. Secondly, excluding day 1, the EC is always higher in the effluents, therefore more ions are present in solution than in the influents, and they derive at least in part from the hydrolyzation of urea. Therefore, for all 11 monitored days, the bacteria remained active: the extent of their activity must instead be assessed in more detail.

Looking again at the pH, we notice two major drops at the start of the treatment and towards day 8. We could link this decrease in pH to an increased precipitation of $CaCO_3$, which could be the case with the first drop, but also to a decrease in ureolytic activity, which seems more plausible as the cause of the second decline. In this circumstance, the measurements of EC do not help us to understand which is the real situation.

However, observing the values of the urease activity during the treatment, we can realise that in days 2 and 3 it increases slightly, while it begins to decay decisively only from day 7. This behaviour confirms what assumed for the pH trend: on days 2 and 3 the precipitation of $CaCO_3$ is very high, so much so as to lower the pH, which was raised by a good ureolysis rate (between 9 and 10 mM of urea hydrolysed per hour up to day 6). In the last days, however, the precipitation decreases, but the ureolytic activity does it even faster, so that the pH increases less.

Bacterial activity is in the low average of other studies, similar to the values reported by Al Qabany et al. (2012) and among those used by Konstantinou et al. (2021b). It is important to note that at the end of the treatment an activity between 6 and 8 mM/h is still present.

As for the pH, a comparison with other studies is difficult, as it varies with the variation of the ratio between urea and calcium chloride. Martinez et al. (2013) stated that an equimolar formulation does not induce a change in pH. Although in our study we used a 1:1 proportion between the two solutes, the pH has undergone changes, as hydrolysis and precipitation do not go hand in hand, also because if the environment is not sufficiently basic, precipitation is disadvantaged (it starts at a pH of 8.3 according to Stocks-Fischer et al. (1999)).

Finally, what is important is to relate the pH at the outlet to the one at the inlet. The pH of our CS was around 7 on the first day and then settled around 6. These values are perhaps too low to ensure that sufficient basicity is achieved following the hydrolysis. Probably, in the vicinity of the bacterial cells, the pH has locally reached sufficient values for precipitation, as the other chemical results report a continuous production of calcium carbonate throughout the treatment. Therefore, the fact that the output pH is almost always lower than the threshold value of 8.3, does not mean that the precipitation has not occurred, as localized increases are possible and the pH could also have decreased only following precipitation, as a consequence of it.

As for the differences between the various granulometries, we are not able to derive safe conclusions on the alterations of pH between the three distributions, due to the variability of the results.

It can be observed that the pH values are always very similar and become more variable following the decay of day 8, even if the trend is almost always the same. This offset may be due to the different relative amount of bacteria attached in the solid matrix. In the WG, for example, the pH and the ureolytic activity appear to be higher than in the other granulometries towards the end of the treatment. This could be explained by thinking about the structure of the WG sample, which contains a greater variability of grains size and therefore more contact points between the particles, where the bacteria settle. The segregation zones of the smallest particles could also act as filters against bacteria, causing them to accumulate in the vicinity.

A higher number of bacteria at the end of the treatment could have a more marked influence on the total hydrolysis rate compared to the first days when the activity of the single cells is more variable and important. It is therefore hypothesized that a more

marked activity after some days is due to a greater number of microbes per PV (i.e. bacterial density).

The offset at the end of the treatment between UN and PG is more difficult to interpret. It could be a random occurrence or due to the lower d_{50} of the UN, which provided better attachment conditions for the bacteria, and therefore a higher number of cells in relation to the PV.

Reactions efficiency

Observing the ionic concentrations, it is possible to make some considerations on the progress of the reactions.

In the first CS effluents (days 2 and 3) the molar concentration of calcium at the outlet is always close to zero (Figure 5.3 and Table 5.2). This is a sign of an almost complete precipitation of ions in the form of $CaCO_3$. Only in UN 1, on day 3, the concentration is slightly higher, perhaps limited by the presence of carbonates or a pH that was not high enough. Up to day 7 the concentrations increase only slightly, up to the big increase on day 8, from which less and less calcium precipitates. However, observing the trends of the curves in Figure 5.3, it is clear that an increase in Ca^{2+} corresponds to a decrease in NH_4^+ and bacterial activity.

Comparing Figure 5.3 and Figure 5.5, we can assume that the bacteria were at least partially active for all 11 days. In fact, the TIC increases slightly in the last 3 days, a sign that ureolysis was still going on. However, the extent of this activity was very low, so much so that the carbonates produced by hydrolysis did not precipitate efficiently due to a pH that was not high enough, causing an increase in TIC. Conversely, on days 2 and 3 the TIC has higher values than the following probably due to very high bacterial activity, resulting in increased production of carbonate ions, only a part of which precipitated.

Regarding the reaction's chemical efficiency, Figure 5.6 shows concordant trends according to what is estimated by calcium ammonium and TIC. The conversion efficiency of carbonate into $CaCO_3$ is linked to the hydrolysis of urea, by which it is limited. Very similar values and trends between NH_4 and TIC are the result of a reaction limited by ureolysis. The latter is, therefore, the factor also governing the carbonate precipitation efficiency, since the concentration of these ions is generally 2 orders of magnitude lower than that of ammonium.

Precipitation of calcium slows down more rapidly, probably because it is influenced both by the availability of ions and by the pH and towards the end of the treatment these factors are both limiting.

As already mentioned, from day 8 the greatest drop in chemical efficiency is observed, so it can be said that the bacteria began to decay more markedly after 9 days from their injection.

As for ammonium, the conversion efficiency on the 11th day is still higher than 60% and even around 75% for WG 1. The latter are considerable values, as a reaction still so effective after 11 days highlights a possibility of using bio-cementation also for prolonged cycles. It should be noted that the CS itself contained 3 g/L of nutrient broth of sustenance to the microbes.

However, these observations are derived from the chemical concentrations and the actual assessment of the precipitation efficiency must be based on the actual measured calcite content in the solid matrix.

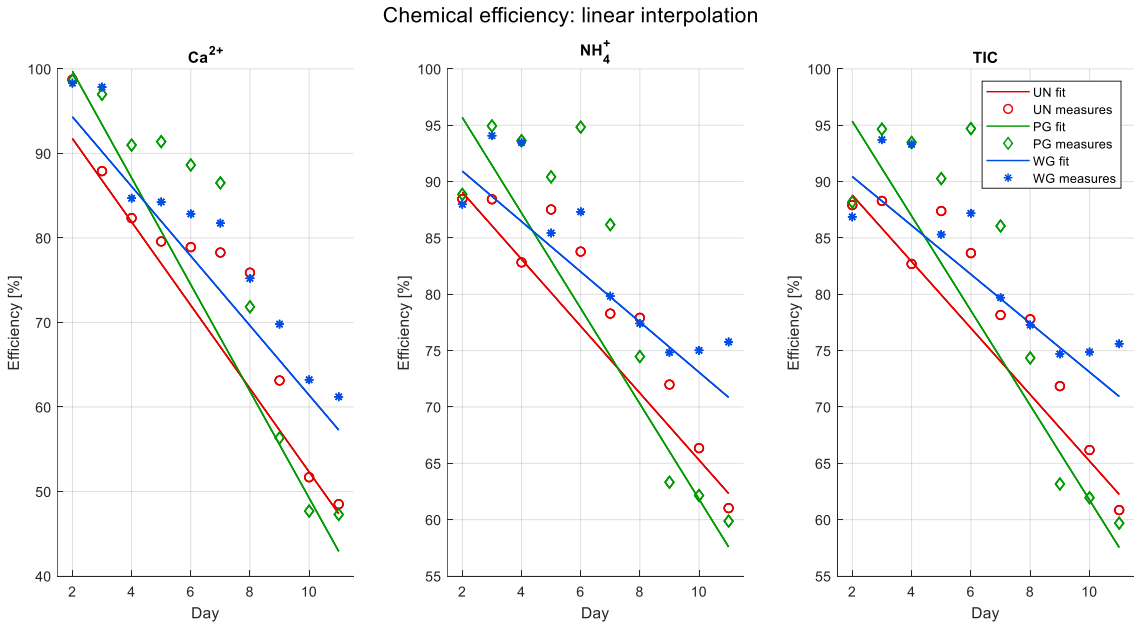

Figure 5.9 - Chemical efficiencies linear interpolation

Figure 5.9 presents the linear interpolation of the calculated chemical efficiency. By looking at it, some observations on the different granulometries can be made. It is interesting to observe that the WG sample is the one that maintains the highest values at the end of the treatment, confirming what was previously said about the relative presence of bacteria on its solid skeleton. On the other hand, the PG seems to have the highest

efficiencies in the first few days, and then collapses starting from day 6. The lowest values at the beginning are registered in the uniform sample: this could be due to the greater ratio between volume of voids and solids, and the fewer contact points, which perhaps led to a lower relative quantity of bacteria, resulting in an inferior reaction efficiency.

These differences could also be due to random factors, always possible in the case of reactions of biological origin and difficult to validate with a limited number of samples.

Calcite content

A great benefit of the ions in solution analysis is the amount of precipitated $CaCO_3$ estimation.

The extreme similarity between ammonium and TIC estimation is due to the observation made above. Although the calcium concentrations suggest a lower $CaCO_3$ content than the others, this difference is small (30% max) and the trend over the days is very similar, making the results reliable.

The trend is also similar to that of concentrations, as it derives directly from them. The days in which the maximum difference between the calcium and ammonium estimates is observed, are the last three. At that time, the pH was probably not sufficient for precipitation.

The least amount of calcite precipitated in the WG sample, followed on average by PG and UN. This result is a function of the fluid volumes: although in the WG the concentrations were sometimes higher, the absolute quantity of calcite is greater where the quantity of reagent is greater.

If the amount of calcium carbonate precipitated according to the estimates is normalized by the void ratio, the result of Figure 5.10 is observed, with the WG reporting the highest values for the entire duration of the treatment, confirming the greater entity of the precipitation in relation to the available volume. Similarly, the PG shows a higher normalized $CaCO_3$ with respect to UN, due to the lower void ratio

When it comes to evaluating the calcite content, since it is by definition related to the weight of the solid matrix, the difference between the granulometries is even more marked. The UN, being the one with the lowest mass, has the highest calcite content, followed by PG and WG. In Figure 5.8 this can be observed through the curve of the calcite content accumulated during the treatment.

Right from the start, the quantity order is the one just mentioned, with the gaps that gradually increase as the days go by.

Obviously, also in this case the CC estimated by calcium is lower than that evaluated from ammonium and TIC. However, the difference between UN and WG remains about two percentage points at the end of the injections.

The results of calcite content at the end of the treatment are in line with what has been reported by other studies, but a more explicit comparison will be only made with the empirically calculated CC (Chapter 5.2).

The cumulative curve growth is logarithmic, suggesting a decrease in the CC increment during treatment.

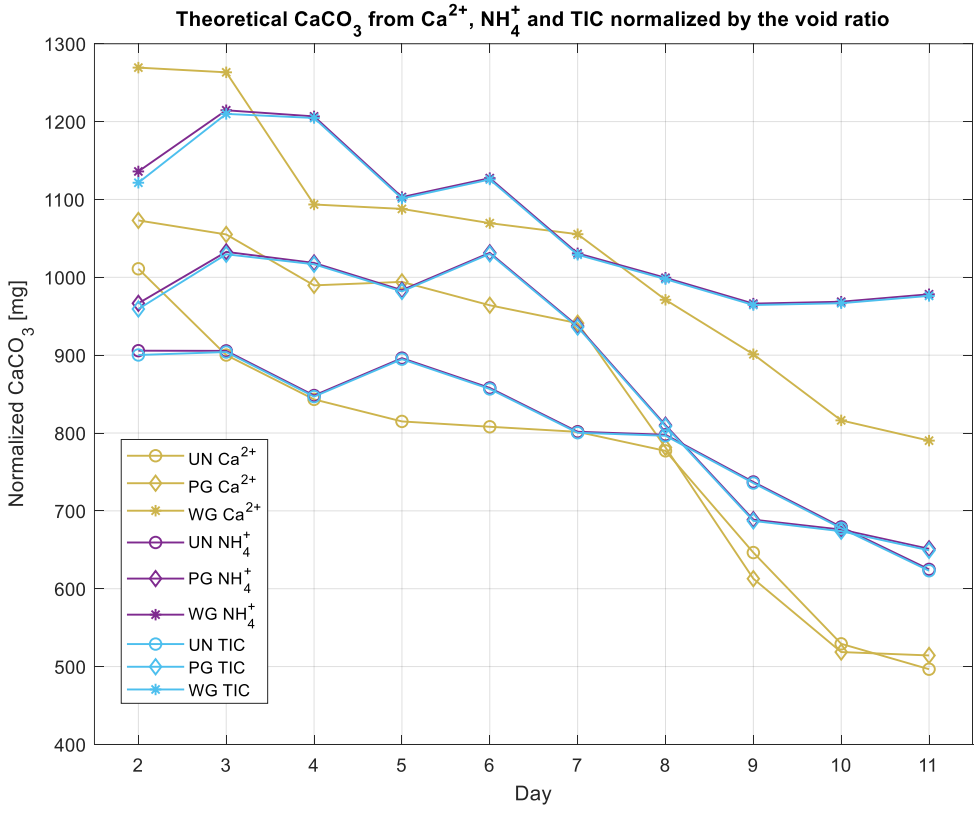

Figure 5.10 - Theoretically precipitated $CaCO_3$ from chemical estimations, normalized by the void ratio

5.1.4. Conclusion

An important conclusion of this first analysis is the ascertained bacterial activity throughout the whole the treatment. Although it appears to be continuously decreasing (especially starting from day 8 from BS injection), the calcite content seems to increase every day.

The combined analysis of ionic concentrations and pH allows to evaluate the extent of reactions during treatment, with the possibility of adjusting the number of injections to reach the desired CC.

The efficiency of the reaction, however, appeared to be continuously decreasing, although it remained almost always greater than 50%. For longer treatments it is advisable to perform an intermediate BS injection, in order to return to higher efficiencies and activities, saving injection cycles.

With 10 injections of CS 0.25 M, a good precipitation of calcium carbonate was obtained, if we consider a geotechnical application, where a CC of 2% can bring sufficient mechanical properties improvement to the soil (Terzis and Laloui, 2019). In this study, the CC varied between 3.83% and 6.40%, depending on the estimates and the granulometries, i.e. the maximum amount of calcite that can actually be present in the solid matrix.

The highest CCs were recorded for the uniform granulometry, followed by the poorly graded and the well graded. These differences are due to the definition of calcite content, which is a relationship of the calcite mass with the solid skeleton masses, increasing from UN to PG, to WG.

Even observing the mass of $CaCO_3$ in absolute terms, however, the final result still sees the UN excel, followed by PG and WG, as the volumes of voids and therefore of reactants in play follow that order

However, the relative concentrations are different. In particular, the increased calcium concentration and the increased urease activity in the WG in the last days of the treatment is explained by a greater absolute bacterial presence, due to the solid matrix internal morphology. The better gradation of WG in fact leads to a much higher number of contact points and a higher content of fines, which can represent favourable elements to an increased attachment of bacteria compared to PG and UN.

5.2. Empirical calcium carbonate content determination

The calcite content was measured with acid digestion method on both 15 mL and 50 mL samples at the top, center and bottom. The larger samples were characterized by two measurements on 2 sub-samples, from which mean and standard deviation are derived.

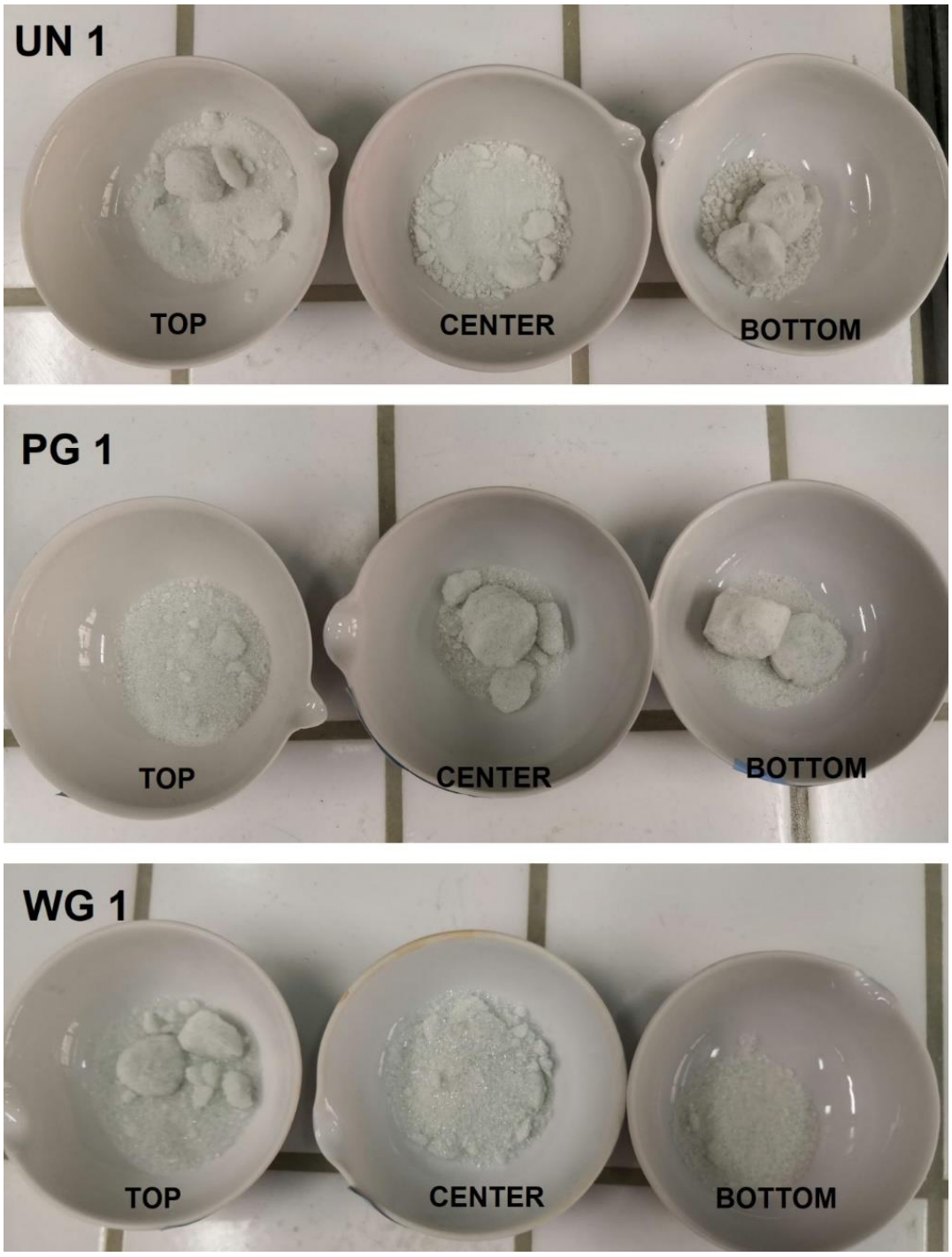

Figure 5.11 - Top, center and bottom cemented fragments for uniform (UN 1), poorly graded (PG 1) and well graded granulometries

Before being treated with HCl, the top, center and bottom sections of the 50 mL granulometries appeared as in Figure 5.11 above.

The larger fragments are found at the center and bottom of PG 1 and at the bottom of UN 1. WG 1 presents some intact pieces only at the top.

The Table 5.6 shows the CC results from acid digestion for both sample sizes, while Figure 5.12 exhibits the CC values along the columns in a discrete way.

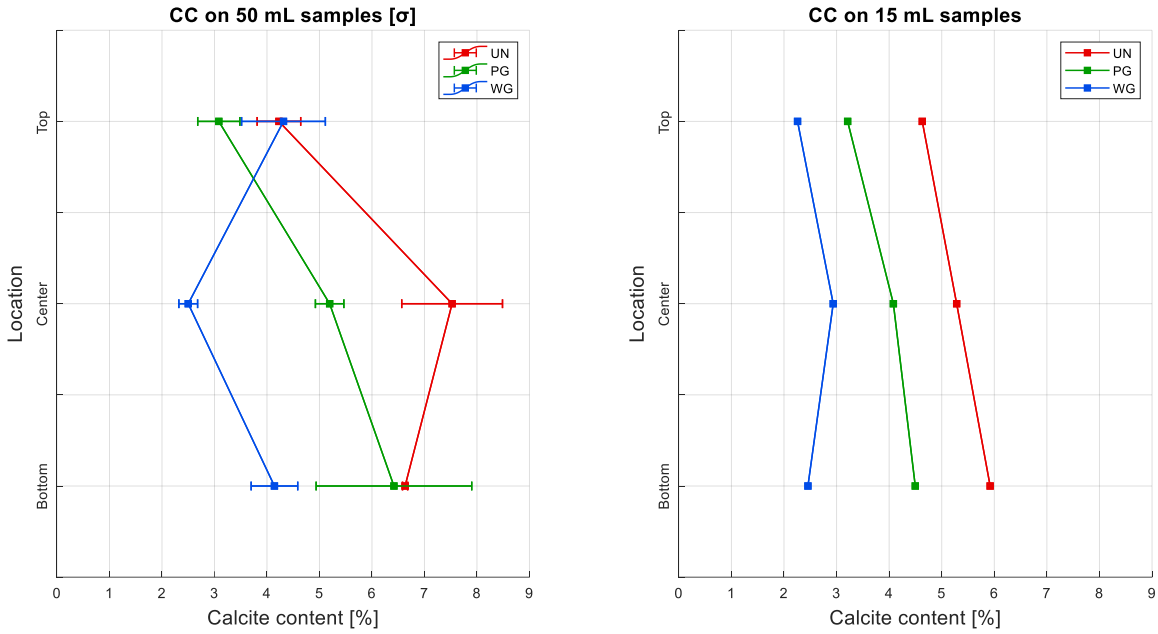

Figure 5.12 - Calcite content trend along the columns for big (left) and small (right) samples. The error bars on the left figure represent the standard deviation

The mass of $CaCO_3$ is greater in larger samples than in smaller ones, but this is due to the size of the analysed fragments. In the 50 mL columns, a total of 4.15 g of $CaCO_3$ were measured in the UN, 3.93 g in the PG and 2.82 g in the WG. In the 15 mL columns, the measured masses are 0.93 g, 0.80 g and 0.61 g respectively.

This results in total calcite contents varying between the 3.44% of the WG and the 5.92% of the UN for the 50 mL columns. The values are slightly reduced for the smaller molds, going from 2.54% for the WG to 5.27% for the UN. The PG always has intermediate contents.

The total standard deviation reaches values equal to 1.61% in the larger columns while slighter variabilities are observed in the smaller samples (0.66% maximum).

From the mass of calcite, it was possible to trace its volume and therefore the volume of solids change in the treated samples. With this data we calculated the porosity reduction, which is variable between 9.29% and 9.80% in the 50 mL molds and between 7.15% and

7.97% in the 15 mL ones. Referring to Figure 5.12, it is possible to perceive the trend of the CC along the columns.

Table 5.6 - Empirical calcite content measurements and porosity decrease for sub-samples placed on top, center and bottom of both big and small samples

BIG SAMPLES (50 mL)							
		$CaCO_3$ mass (g)	CC (%)	σ (%)	Total CC (%)	Total σ (%)	Δε (%)
UN 1	TOP	0.60	4.23	0.41	5.92	1.58	9.41
		0.61					
	CENTER	0.89	7.53	0.96			
		0.70					
	BOTTOM	0.64	6.63	0.05			
		0.71					
PG 1	TOP	0.33	3.08	0.40	4.97	1.61	9.80
		0.41					
	CENTER	0.85	5.19	0.27			
		0.60					
	BOTTOM	1.13	6.42	1.48			
		0.62					
WG 1	TOP	0.79	4.31	0.80	3.44	0.99	9.29
		0.53					
	CENTER	0.49	2.50	0.18			
		0.46					
	BOTTOM	0.31	4.14	0.44			
		0.23					
SMALL SAMPLES (15 mL)							
		$CaCO_3$ mass (g)	CC (%)	σ (%)	Total CC (%)	Total σ (%)	Δε (%)
UN 1s	TOP	0.28	4.63	-	5.27	0.35	7.70
	CENTER	0.31	5.28	-			
	BOTTOM	0.34	5.92	-			
PG 1s	TOP	0.18	3.21	-	3.97	0.66	7.15
	CENTER	0.31	4.08	-			
	BOTTOM	0.31	4.50	-			
WG 1s	TOP	0.20	2.26	-	2.54	0.35	7.97
	CENTER	0.23	2.94	-			
	BOTTOM	0.18	2.46	-			

In the 50 mL samples the WG has the minimum of CC in the middle of the column (2.5%), where the UN has its maximum (7.5%). The PG reports an increase in CC from top (3.1%) to bottom (6.42%). In the 15 mL samples there is an opposite trend for the WG, which in this case has a maximum of CC in the center (2.94%). Both the UN and the PG are characterized by a calcite content increasing towards the bottom of the column. In this case, however, the variability along the sample is limited, if compared to the 50 mL ones.

In the latter, the CC is very similar in the three granulometries at the top, with the WG having the highest.

Concerning the standard deviation, the greatest are observed in the center of the UN and at the bottom of the PG, while the lower are the ones in the middle of WG and PG samples.

In the smaller samples the different CC as a function of the granulometry is clearly evident along the entire length of the columns, with an offset between the three curves of always at least one percentage point.

5.2.1. Discussion

The size and cohesion of the fragments in the Figure 5.11 are not always indicative of high calcium carbonate content. In particular, the integrity of the parts is highly dependent on the disturbance they underwent when opening the molds. However, the fact that big intact fragments were found at the bottom of UN 1 and PG 1 agrees with the results found for the CC.

To effectively compare the calcite contents for the two sizes under analysis, reference can be made to the Figure 5.13. The increasing CC from WG to PG to UN is common to both sizes and is mainly due to the increasing solid matrix mass. The difference that stands out first is the higher CC measured in the larger diameter samples. This fact is always valid, drawn in the center of the WG. To explain the difference, it is possible to hypothesize that, since the smaller samples are more affected by the boundary conditions, a relatively larger part of the crystals has precipitated outside the control volume on which the measurements were made (e.g. in pipes, valves, wire meshes). Although even in the 50 mL columns not all the calcite is precipitated on the glass beads, in proportion to the sample size this quantity is in that case smaller than in the 15 mL samples, considering that the calculations on the injected reactants volumes were made taking into account only the matrixes pore volume and not that of the other portions of the setup.

If we then exclude the WG, the other granulometries have an increasing CC from top to bottom. That is in fact the point from which the CS injections were performed. Previous works have shown an accentuated precipitation at the injection point (Konstantinou et al., 2021b; Noiriel et al., 2016; Rowshanbakht et al., 2016) and this trend is mostly confirmed in this study. Even the 50 mL WG, while not having an increasing trend from top to bottom, reports an augmented CC at the lowermost, after a decrease in the center.

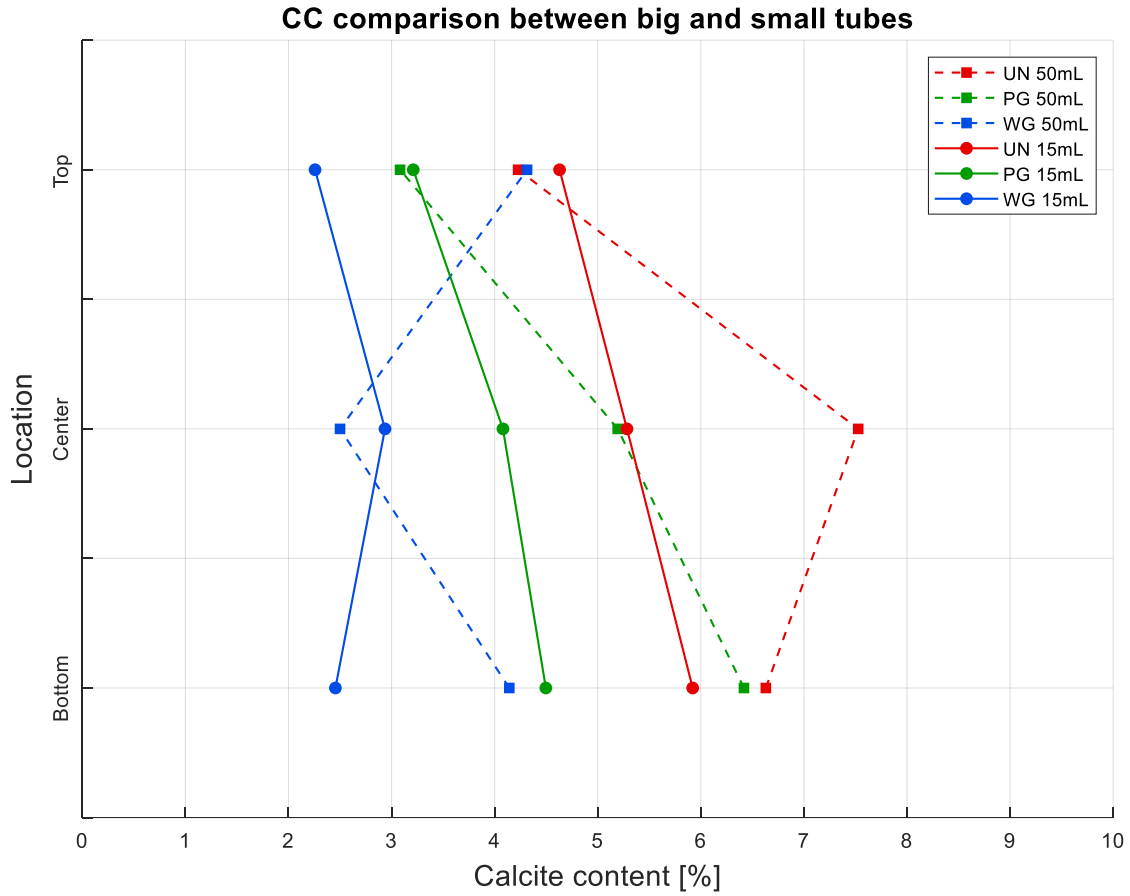

Figure 5.13 - Calcite content comparison along the length of the 50 mL and 15 mL columns

The 50 mL UN and 15 mL WG, in addition to reporting a higher content at the bottom than the top, are characterized by a maximum in the center, particularly evident in the UN. This behaviour was also observed in some cases in Martinez et al. (2013), but both with inverted BS and CS injection, and with inoculation from the same point.

To interpret our results, it could be hypothesized that in these two cases the greatest precipitation took place in the center because ideal conditions of good bacterial presence and high concentration of CS occurred.

In the case of increased precipitation towards the injection point, the simplest explanation is a slight plugging and reduced delivery of the reactants to the areas furthest from the inlet, an effect that occurred in a reduced way for the cases mentioned above. As for the 50 mL UN, it can be thought that the higher porosity reduced the amount of plugging at the source and led to an increase in precipitation where more bacterial sites were present. In the 15 mL WG, perhaps, the bacterial concentration near the CS injection point was

reduced due to filtration phenomena of segregated fines, which prevented the microbes from reaching the same distances as the other samples.

The behaviour of the 50 mL WG is instead the opposite, as a minimum of CC is clearly observed in the center, with values 50% less than top and bottom. This result suggests that the number of bacteria far from their injection point can be sufficient for a good precipitation of $CaCO_3$ and the CS can carry the reactant to the end of the column if large plugging phenomena do not occur. The reduction in the center could be explained by assuming a particular flow path inside the sample, with a reduced presence of fines in the center and consequent easier passage of fluids and less precipitation where the contact points were fewer. A higher content of fines at the CS outlet may then have led to a slowdown of the solutions in that area, where many bacterial cells were present, causing considerable precipitation.

In general, the variability of the WG can be explained by the variability of its morphology, while the consistent results of UN and PG for the two dimensions under study confirm that plugging and non-uniform cementation of the samples are a distinctive MICP feature, with increased concentrations towards the CS injection point.

When comparing the acid digestion results on the 50 mL samples with those from the chemical analysis estimates, the outcomes are highly consistent. The CC calculated from the calcium concentration overestimates the empirically calculated one by 2.36%, 2.41% and 11.34% for UN, PG and WG, respectively. The results obtained from ammonium are instead higher by 8.11%, 6.64% and 15.99% respectively, similarly to TIC approximations.

These limited differences allow to rely on the chemical estimates, which can be performed in real time. Anyway, the spatial distribution of calcite in the soil cannot be known from them.

However, it is necessary to keep in mind that the calcite content calculated with the chemical results does not include the concentrations of the last effluent CS. This means that the approximated CC would have been slightly higher. A linear regression for the CC prediction at the twelfth day (Figure 5.14) leads to higher chemical CC of 15.26%, 17.43% and 23.26% for Ca^{2+} and 18.12%, 18.65% and 24.81% for NH_4^+, for UN, PG and WG respectively. The linear prediction of CS number 11 (day 12) is in any case higher than the probable real value, given the logarithmic increase of the measurements.

These are more important overestimates but still consistent with the empirical results. The difference with respect to the latter may, as previously mentioned, be due to the calcite deposited outside the control volume on which the measurements were made but which is included in the chemical guesses.

The more marked difference in WG may be due to the lower pore volume and therefore greater relative contribution of the calcite precipitated outside the control volume. Massive errors in the CC measurement can be excluded, given the coherent results of the blank samples.

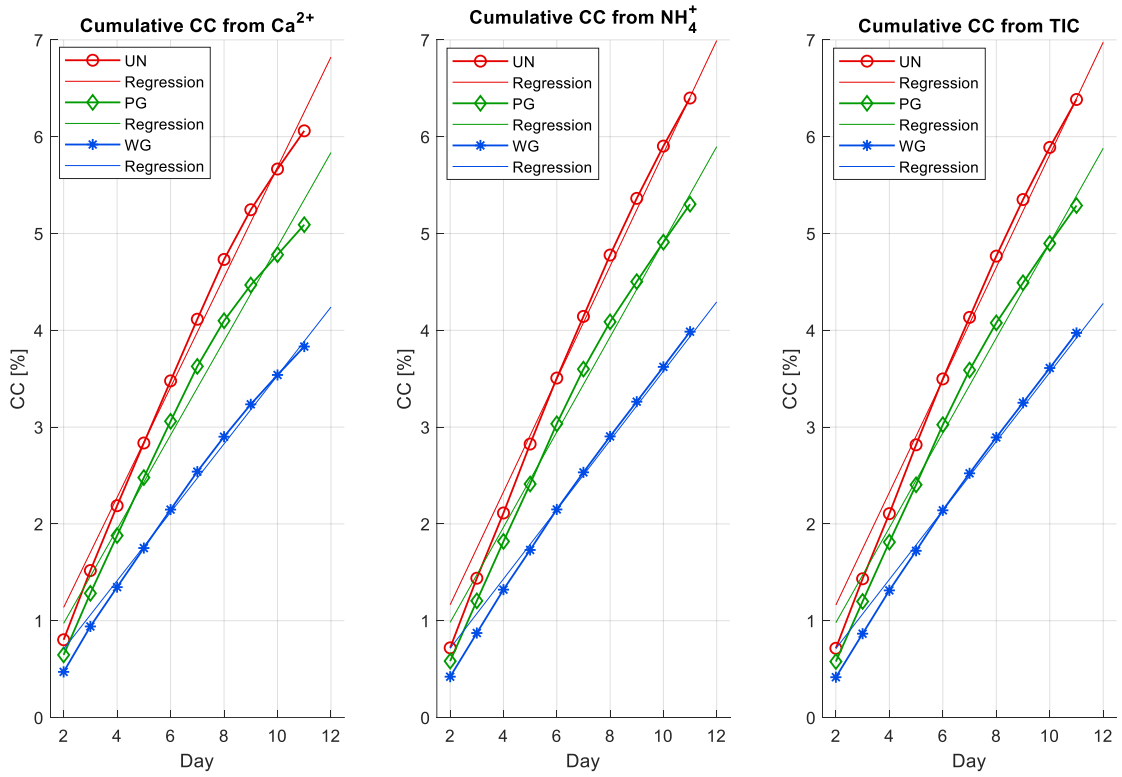

Figure 5.14 - Cumulative CC from chemical estimates with linear regression for the 12th day prediction

Finally, comparing the acid digestion results with previous studies, the CC is analogous to that obtained by Cheng (2012), Cheng et al. (2013), Qabany and Soga (2013) and Terzis and Laloui (2018). Furthermore, with 12 treatment cycles, Cui et al. (2017) reported a CC of about 9% but with higher concentrations of reactants and different injection scheme. Konstantinou et al. (2021b) observed contents between 5% and 9% for bacterial activity similar to this study, but with higher initial bacterial concentrations. For the same number of injections and the same treatment scheme Konstantinou et al. (2021a) reported CC between 4.5 and 6%, with higher amounts in fine sands. Extraordinarily higher values are instead those reported by Van Paassen (2009) (12-27%).

5.2.2. Conclusion

The calcium carbonate content measured with the acid digestion technique turned out to be in agreement with the estimates coming from the calculations on ionic concentrations. This suggests the possibility of using them for real-time monitoring, keeping in mind the overestimation coming from them, due to precipitation outside the control volume.

The calcite distribution trend along the columns showed in general an increase towards the cementation solution injection point, due to a possible plugging. In case of sufficient porosity this effect is less marked, and the reactants can effectively reach more distant areas, but still resulting in a reduced amount of calcite at the opposite end of the CS inlet (Except for the 50 mL WG).

The distribution of bacteria within the solid matrix plays a role in the uniformity of the treatment and can be governed by filtration effects or preferential flows, caused respectively by areas with high and low content of fines.

At the same reactant concentration, the calcite content is higher for more porous soils, characterized by a lower solid mass and a larger volume of solutions. On the other hand, the percentage reduction in porosity is similar, and this is a sign of a rather similar relative quantity of calcite.

Smaller volumes reported lower CCs for the same granulometry and under the same treatment conditions. This may be due to the greater relative importance of external elements volume outside the target one.

To conclude, the total calcite content was found to be in line with previous studies using similar treatment conditions, highlighting a good representativeness of the glass beads with respect to real soil.

5.3. Microscopic characterization with SEM

The observation with the electron microscope of some portions of the bio-cemented samples allowed to identify the prevailing types of calcium carbonate polymorphism. The study is exclusively qualitative and helps to observe the distribution of the crystals on the glass beads. All images represent fragments from the center of the columns.

Figure 5.15, Figure 5.16 and Figure 5.17 are a reference for an understanding of the $CaCO_3$ distribution over a wide field and its crystalline form on a UN, PG and WG sub-sample respectively. In all cases, small crystals are observed distributed more or less

homogeneously, covering the surface of the glass spheres, with sometimes larger agglomerates (mesocrystals) at the contact points. This result has often been observed in other studies for low reactants concentrations (Dadda et al., 2017; Terzis et al., 2016).

Figure 5.15 represents the uniform granulometry, with the crystals scattered over the entire surface of the spheres and a prevalent polymorphism represented by calcite. The image represents a scarcely cohesive portion, but the calcium carbonate is in any case present in a homogeneous way.

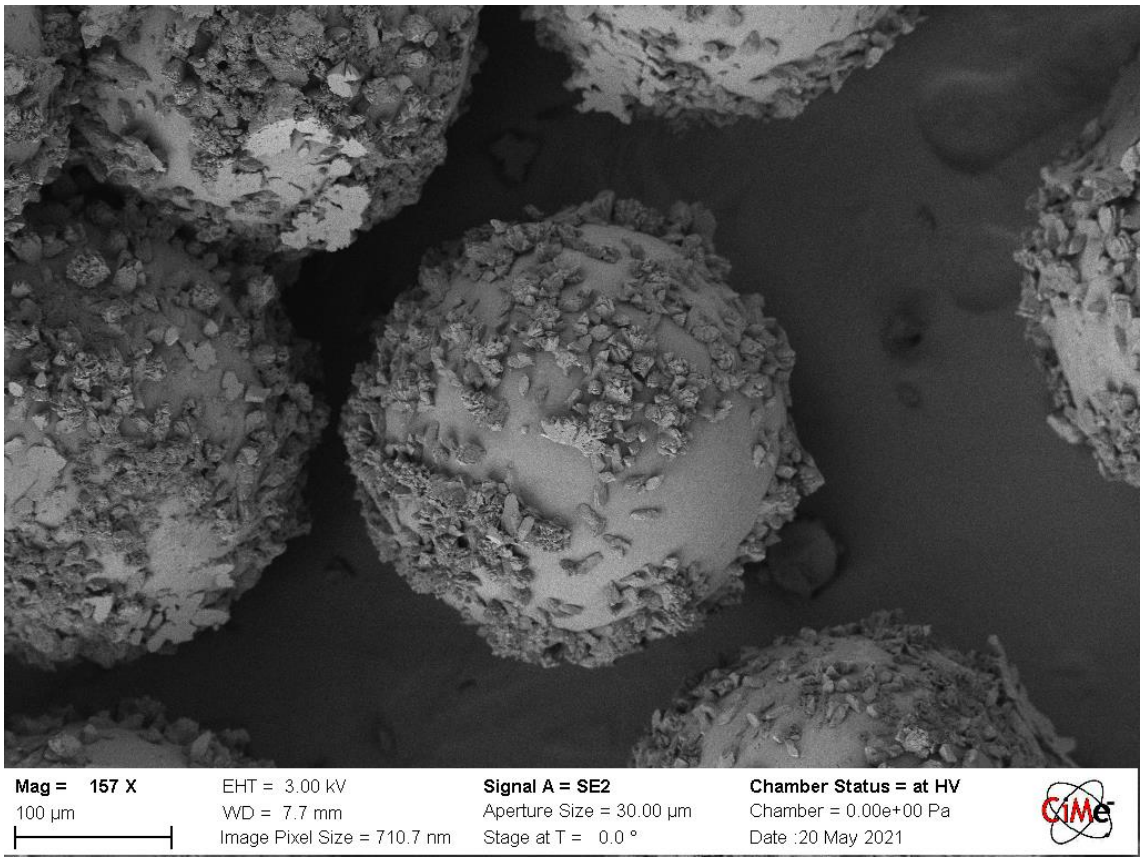

Figure 5.15 - Wide-field image of a UN sample fragment

Figure 5.16 is instead an example of the poorly graded granulometry, in a strongly cemented and cohesive portion. The homogeneous coverage of the larger beads is prevalent, with the smaller spheres cemented to the others with few crystals and typically present at the point of contact. In this case, the only observed polymorph is calcite.

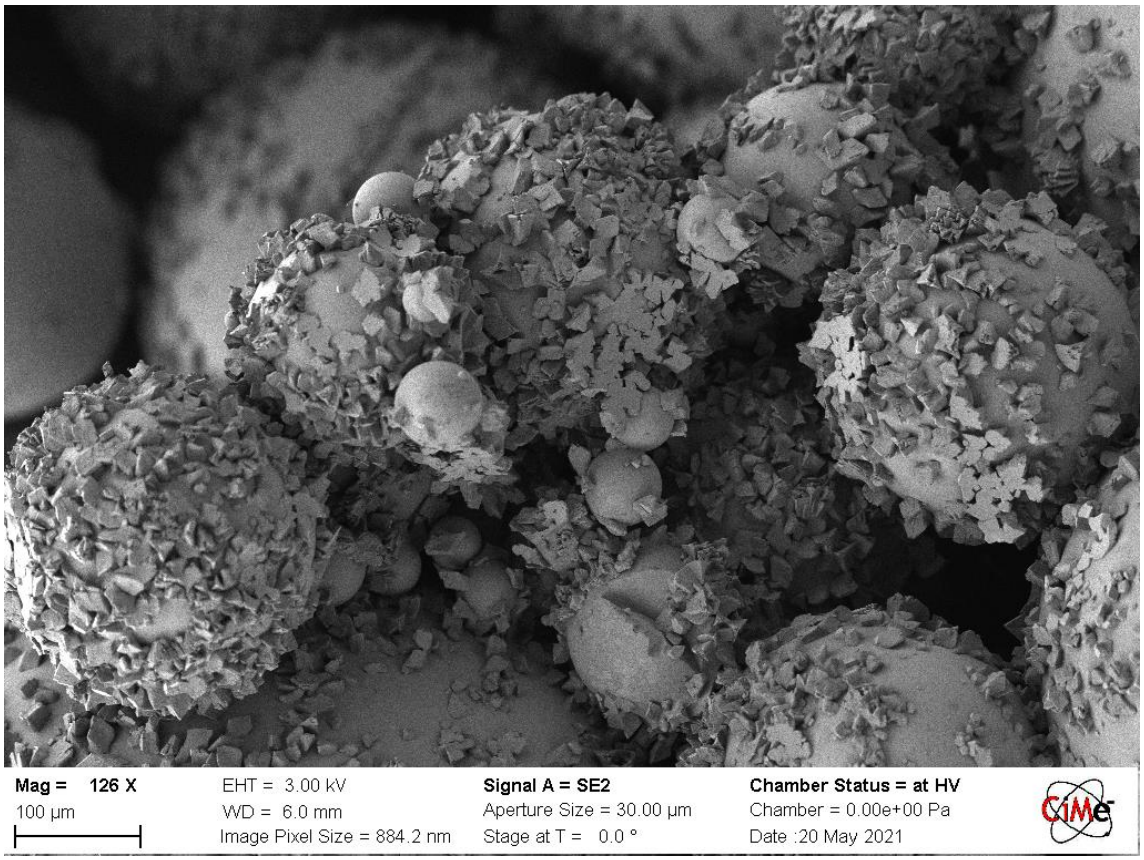

Figure 5.16 - Wide-field image of a PG sample fragment

Finally, Figure 5.17 represents the well graded granulometry. In this case it is evident an inhomogeneous distribution of the crystals and a preferential precipitation on some glass beads.

The central sphere has a complete and homogeneous crystalline coverage, while all the small diameter spheres forming the large agglomerate are characterized by a few crystals located at the contact points.

Bottom right in Figure 5.17 one can see a large diameter bead (probably 1mm) with the presence of crystals distributed fairly evenly but with a decidedly lower density than the central bead. It could be hypothesized that the latter was covered with smaller spheres at whose contact points more calcite precipitated or where biomass filtration effects occurred.

An observation that applies to all granulometries is that the precipitation seems more pronounced on the beads of intermediate size (between 200 and 400 µm), while the crystals are present in lower density on the much smaller and much larger spheres.

One way to explain this pattern could be that, as reported by Stack (2015), there is a threshold supersaturation that is necessary to achieve prior to the nucleation becoming favourable, attributed to a pore-size dependent solubility. The stability of a nucleus is influenced by its surface energy, which also depends on the radius of the pore. The latter can lower the total surface energy, facilitating the precipitation by generating a smaller critical radius, or alternately a lower supersaturation necessary for growth.

As for the mineralogical characterization, also in this case the only observable polymorph is calcite.

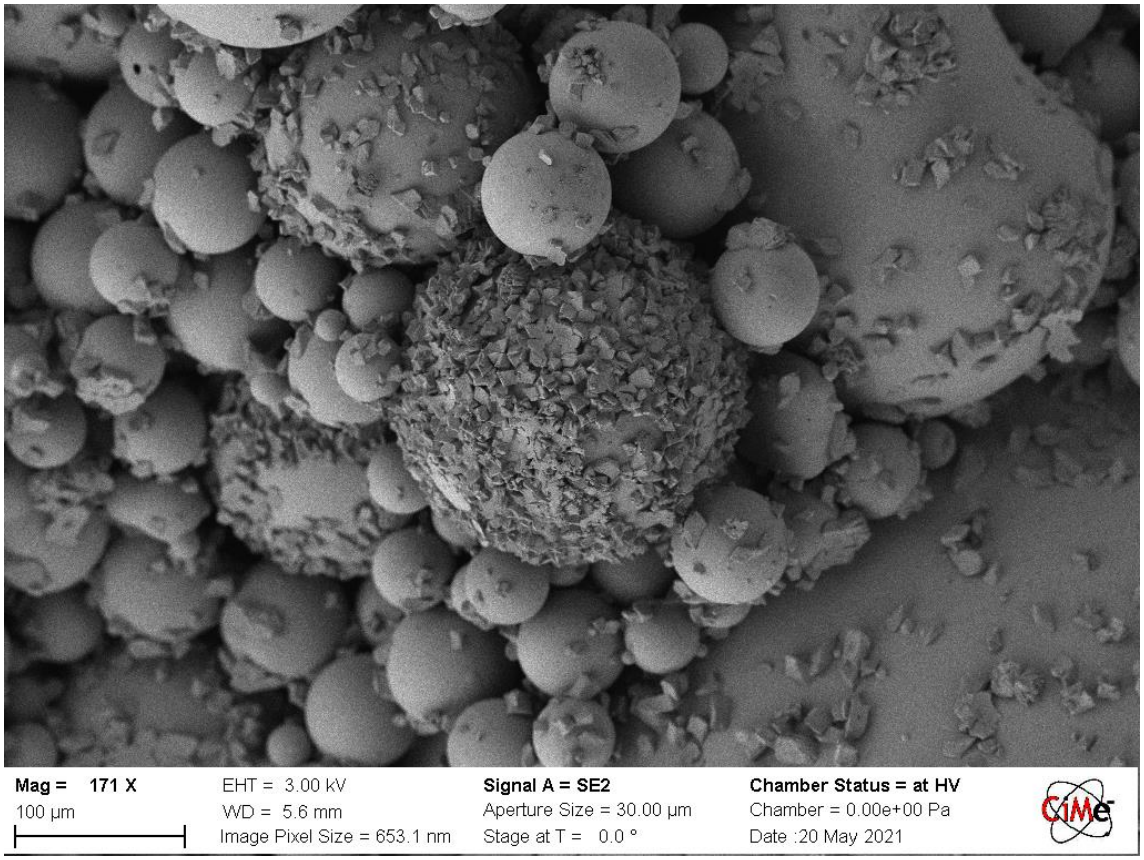

Figure 5.17 - Wide-field image of a WG sample fragment

As far as the mineralogical characterization is concerned, the shapes of the $CaCO_3$ crystals can be observed in Figure 5.18.

In the carried-out observations, calcite was found to be the only crystalline form present on PG and WG samples and the most widespread on the UN.

In Figure 5.18c and 5.16d, however, small agglomerates of amorphous calcite can be observed on the uniform granulometry indicated by the blue circles. These deposits are

found exclusively in this sample, close to the much more numerous calcite crystals and in some cases covering them.

In addition, the amorphous phase was not observed in the whole sub-sample analysed, but in some localities only. This leads to not being able to exclude the presence of this phase also in the other granulometries, in segments not observed under the electron microscope.

What is certain is the prevalence of crystalline calcite, representing the most stable and resistant $CaCO_3$ form, in well distributed and tiny crystals, sometimes forming small aggregates in the contact points.

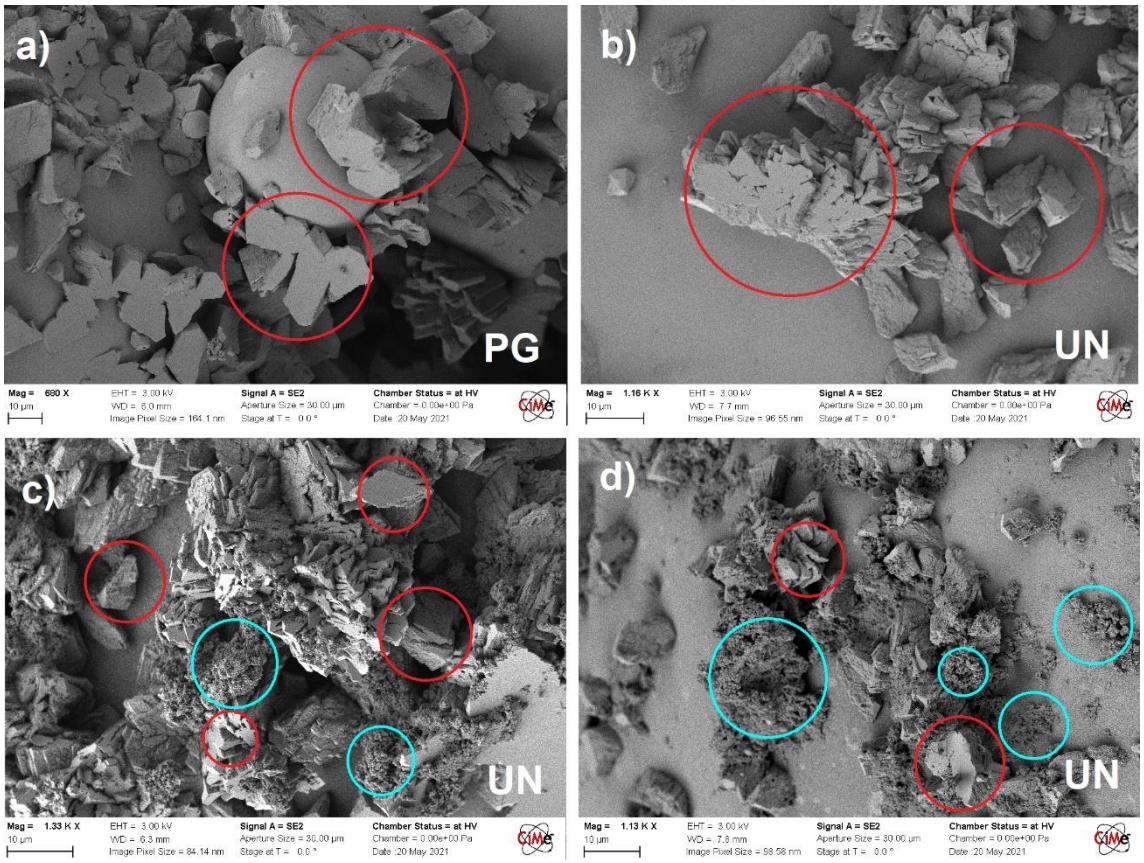

Figure 5.18 - Crystal polymorphism on PG (a) and UN (b, c and d) granulometries. The red circles highlight calcite crystals, the blue ones indicate amorphous calcium carbonate

As regards the effective calcite bonds, in Figure 5.19 some examples can be observed for the UN and PG granulometries, while Figure 5.20 shows the case of the WG.

The medium-large sized beads, shown in Figure 5.19, in addition to being characterized by a more marked and uniform distribution of the crystals, have bonds consisting of

agglomerates of single calcite minerals, which probably bind the spheres more effectively.

More than real clusters, they are rather agglomerations of single crystals precipitated close to each other and then grown up to contact. We can however speak of calcite-calcite cementation, as described by Cui et al. (2017), as the bridge is created by the merger of crystals precipitated on two different spheres.

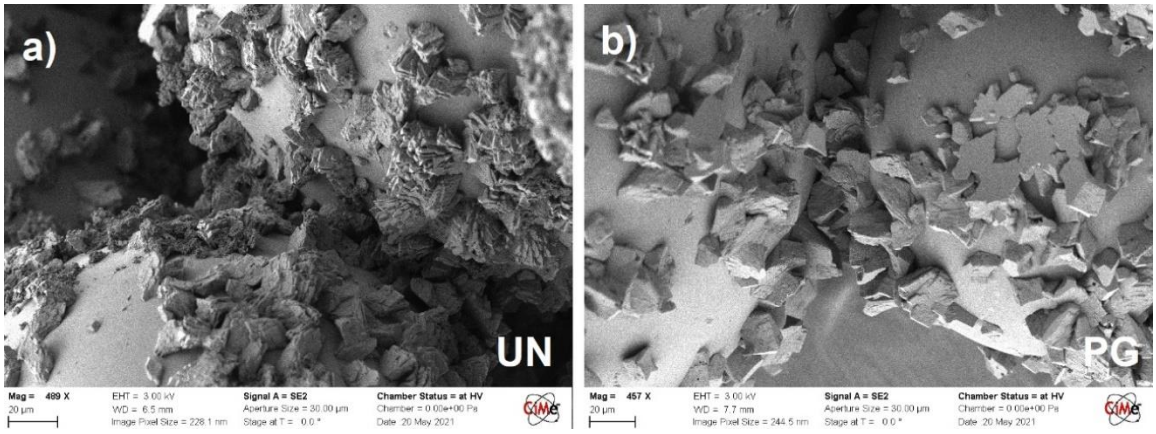

Figure 5.19 - Effective calcite bonds on uniform (left) and poorly graded (right) sub-samples

In the well-graded granulometry (Figure 5.20a), it can be observed how the dense agglomerates formed by the smallest beads (<106 µm) are characterized by bonds of single small crystals, precipitated at contact points (red rectangles). The blue rectangles, on the other hand, highlight areas with a more marked presence of calcite, forming stronger bonds. These areas are always found in correspondence with beads of intermediate dimensions, around which the smaller ones have settled, creating numerous contact points and probably creating a favourable environment for the settlement of bacteria.

Figure 5.20b instead shows even more clearly the typical bonds between the minor spheres (red circles), which in this case are limited to the contact points and had a limited growth, unlike the crystals highlighted by the blue circles which, having nucleated in an open space, have grown to exceed the size of the smaller spheres.

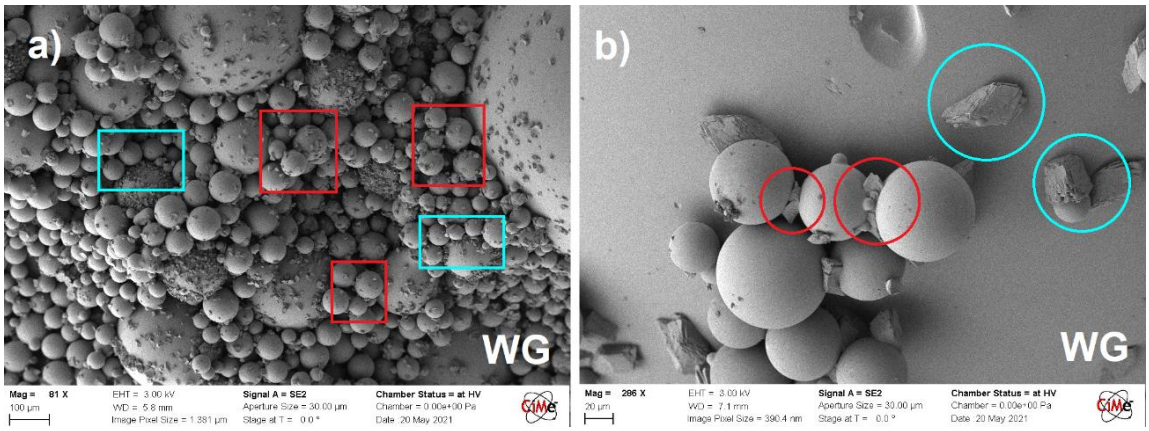

Figure 5.20 - Effective calcite bonds on well graded sub-samples. In a) the red squares indicate single / few little crystals bonds, while the blue squares show area in which the connections are made of bigger clusters. In b) the red circles highlight the tiny crystals between the smallest beads; the blue circles designate bigger crystals on the surface of a large bead

These bridging characteristics of the small radius particles led to the creation of large intact fragments, which were actually found at the opening of the WG (Figure 5.21) and PG columns. The latter, however, despite having sufficient strength to remain intact, crumbled with ease at the slightest disturbance. This fact could be the consequence of these fragments' microstructure, characterized by clusters of small beads, cemented by weak bonds of single crystals, which allowed an extensive and sufficient cementation for integrity but not for good strength.

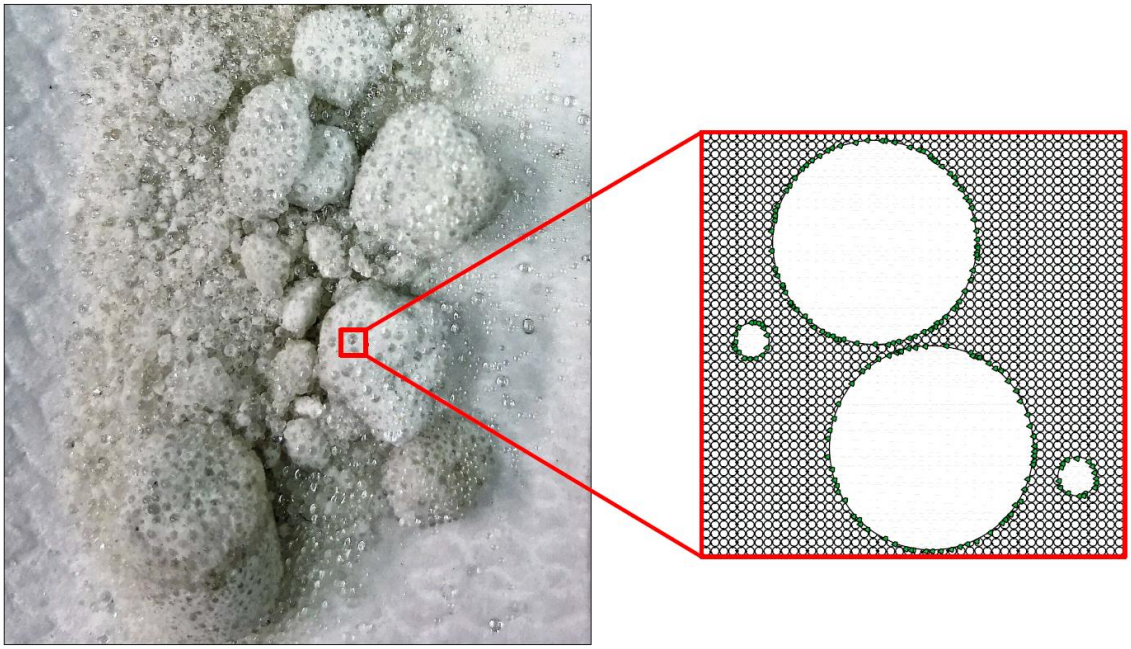

Figure 5.21 - Intact pieces from the 15 mL WG sample. The structure of a fragment is characterized by many weakly cemented small beads, surrounding bigger spheres

This weakness of the few crystals connections is due to the bond failure mechanism. Some SEM images (Figure 5.22) have, in fact, allowed us to understand that breakage occurs due to detachment of the crystals from the glass beads and never due to crystal-crystal separation. This mechanism is evident in the bonds of the calcite-calcite cementation type, as defined by Cui et al. (2017), whereby bridges are formed by connecting two non-tangent spheres.

The cementation failure takes place between crystal and sphere, as the surface of the latter is very smooth, preventing the establishment of a great resistant friction forces between glass and calcite.

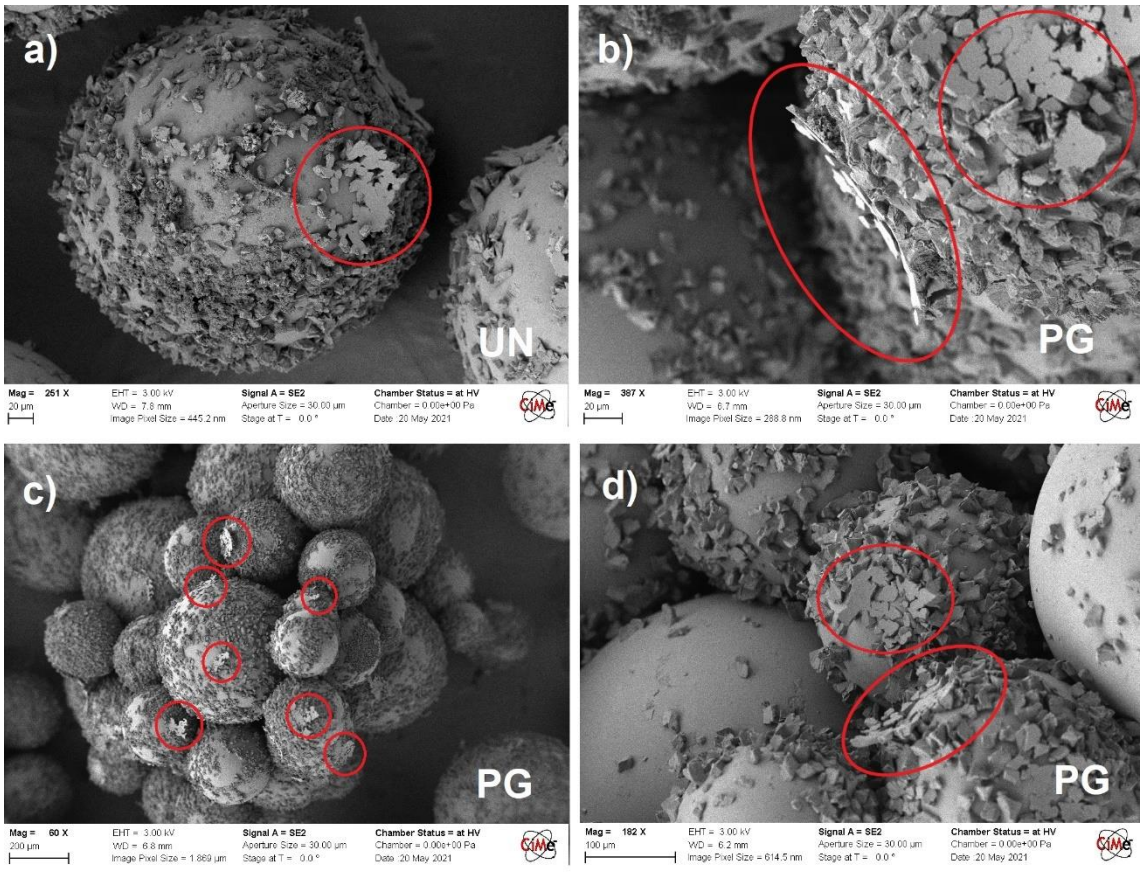

Figure 5.22 - Spheres detachment surfaces in sub-samples of uniform (a) and poorly graded (b, c, d) granulometries, designated by red circles.

Although crystals are present in a widespread way on most of the particles, their uniform distribution and the absence of pore-clogging conglomerates lead to the hypothesis of a minimum change in permeability following the treatment, mainly due to the reduction of porosity and not to a consistent modification of the flow path.

5.3.1. Conclusion

The electron microscope observations are an effective control tool on the precipitation behaviour of $CaCO_3$ crystals and their morphology, after the end of MICP treatment.

The low concentration of the reactants confirmed previous observations which linked it to the formation of small and evenly distributed crystals.

In this study it was possible to observe that most of the glass beads with diameters between 200 μm and 500 μm were uniformly covered by a dense blanket of small crystals, while the others mostly showed the exclusive presence of bonds at the point of contact.

A similar attitude was reported by Konstantinou et al., 2021a, who observed the presence of crystals only at particle-particle contact for fine sands, with limited deposition at noneffective locations. They also reported that few crystals were sufficient to cement these soils, while observed a deposition of the crystals both at the contact points and on the surface of the grains in the coarse sands, requiring in this second case a larger amount of cementation to produce an increase in strength comparable to the fine one.

In our study this difference in strength cannot be verified, but the different distribution of minerals for large and small beads is evident. One reason could be that the voids between the smaller spheres are not sufficient for the settlement of large amounts of bacteria and the growth of crystals.

The uniform or localized distribution of the calcite observed in this study could also be explained by looking at the granulometries degree of uniformity: the more uniform they are, the more uniform the number of contact points and the sites of precipitation. In the case of beads with a diameter less than 106 μm, these are distributed on the larger spheres, creating numerous nucleation points on the latter and maintaining few points of contact between them.

The reason why the large diameter spheres proved to be relatively poor in crystals could be explained by the hypothesis that the small beads were originally cemented to them and then detached, bringing with them the crystals deposited at the contact point, due to the smaller radius of curvature of the latter which leads to a stronger adhesion force.

A discussion on the surface energy and the supersaturation as a function of the pore radius should be further explored but suggests an additional explanation for this apparent preferential deposition.

In any case, the assessed distribution of the crystals, combined with the effortless fragments' disintegration observed empirically, suggest that, although cementation is present throughout the sample, only the most cemented particles transmit most of the loads, with the smaller ones not much contributing to the mechanical improvement, and with the consequence of an uneven distribution of forces. This behaviour also was reported by Clarà Saracho et al. (2020b) for increasing calcite contents.

The observed polymorph is mainly calcite, with the exclusion of few deposits of amorphous $CaCO_3$ in some areas of the uniform granulometry. According to Wang et al. (2021), for low bacteria density (OD_{600} from 0.2 to 1), as the one used in this study, the prevalent polymorph is calcite, already from the beginning of the reaction. For higher OD_{600}, amorphous calcite undergoes to polymorphism to calcite during the 24 hours after the injection. The reason why the amorphous phase was still observed in the UN can be explained by hypothesizing a further bacterial growth after injection, facilitated by the greater porosity and quantity of BS of the uniform granulometry. A higher bacterial density could have accelerated the reaction leading to the formation of amorphous $CaCO_3$, which then would not have completely converted into calcite.

The creation of effective calcite bonds, combined with the increase in the surface roughness of the glass beads, suggest an improvement in the soil mechanical properties, due respectively to an increase in cohesion and friction angle.

Given the crystals distribution in areas with a high presence of small diameters beads, it is thought that soils with a high content of fines can be more easily cemented, with less waste of reagents. The result of the cementation could however be a limited soil strength, given the bonds morphology, consisting of single crystals or agglomerates of a few minerals. This empirically observed low strength in the samples of this study may not be found in the case of a real soils with more pronounced roughness. In that case, in fact, the detachment of the crystals from the surface of the grains would be more difficult and the crystal-crystal breaking mechanism, never called for in this study and which requires a greater load, could come into play.

To conclude, as regards the hydraulic properties of the samples, the permeability following the treatment is not believed to be appreciably reduced. Porosity certainly decreased due to the actual presence of a good amount of crystals which resulted in calcite contents up to 6%. This reduction of the voids is however characterized by the

development of a thin covering of the spheres with the small agglomerates at the contact points never obstructing the pore throats. The flow paths will therefore not be modified and a decrease in permeability will be mainly due to the increase in roughness and the decrease in the pore volume.

A more in-depth numerical analysis of the change in permeability can be found in Chapter 6.5.

5.4. Mechanical results of the micro-UCS test

This chapter presents the results of the micro-UCS test mechanical part, carried out in the EPFL PIXE laboratory. The numerical analyses relating to the failure mechanism carried out at the same time are reported and discussed in Chapter 6.6.

Figure 5.23 shows the result of the unconfined compressive strength test on the uniform granulometry sub-sample. The height of the specimen is 9 mm, including the cement paste at the ends. The load rate is equal to 0.1 mm/min.

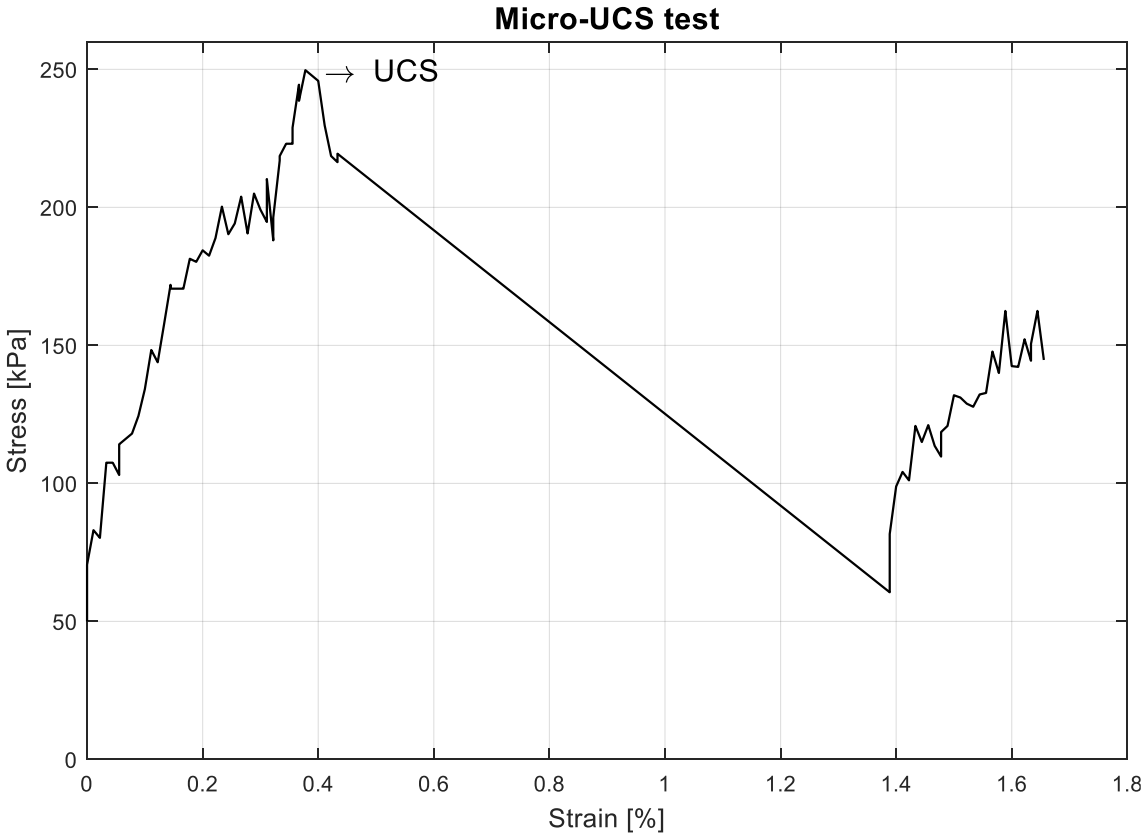

Figure 5.23 - Micro-UCS test results

The steps that are observed are due to the loading process, which occurs in a discreet way, not maintaining the load at each incremental phase. The linear collapse observable starting from a strain equal to 0.4% is instead probably caused by the breaking and disintegration of the specimen, with consequent immediate displacement to a strain of 1.39% where the reloading curve starts, exhibiting a slope similar to that of the elastic phase.

The maximum load applied to the column was 8.99 N which, combined with an average base area of 36 mm^2, led to the definition of a sample UCS equal to 249.72 kPa.

Considering the null strength of the glass beads before bio-cementation, the incidence given by the treatment is important. The specimen also endured a strain of up to 0.4% which, combined with the sudden decrease in load following the failure, make of it a brittle material.

This result is not surprising if we consider the solid matrix architecture, held together exclusively by rigid cement bonds, without which the strength would be zero.

It is interesting to note how the increase in load following the specimen breaking is still consistent and due to the maintenance of intact fragments (Figure 5.24) with mechanical characteristics probably equal to the integral specimen.

Figure 5.24 - Condition of the specimen following the UCS test

Although it is a micro mechanical test, the results of the UCS of the test sample can be compared with previous studies.

For similar calcite contents, Konstantinou et al. (2021a), reported strengths from 500 kPa to 2500 kPa for fine soils and from 450 kPa to 1600 kPa for coarse sands. Cheng et al. (2013) on the other hand, for calcite content around 5% observed UCSs not exceeding 300 kPa for treatment conditions similar to this study. Qabany and Soga (2013), for CC between 2% and 6% experimented UCSs between 200 kPa and 1000 kPa on their sandy samples. Higher values were instead obtained by Terzis and Laloui (2018), with UCSs up to 2 MPa for CC up to 6%. All these and other studies register higher values for higher amounts of calcite.

It can be said that the strength obtained from the glass beads is in some cases close to that of the sands of the other studies, for similar calcite contents. This means that the cohesive role of calcite is of primary importance in improving the soil mechanical properties, as it is the only active mechanism before failure occurs.

By observing Figure 5.24, it can be seen that the specimen has undergone fracture, originating at least two sliding surfaces from which three intact fragments have been created. A clear unique surface of failure is not visible, although it may have been destroyed by the next load. For a more in-depth analysis of the failure behavior, one can refer to the tomographic images discussed in Chapter 6.6.

5.4.1. Conclusion

To briefly summarize what was observed in the micro-UCS test, the strength of the uniform granulometry was defined as about 250 kPa, which represents a result consistent with previous studies.

The collapse behavior is of the brittle type and the specimen does not completely flake off following failure, suggesting the presence of two failure surfaces.

The MICP proves to be a technique capable of conferring good mechanical properties to materials of zero intrinsic strength, through the creation of calcite bonds which increase the cohesion of the soil.

6. Numerical Analysis

In this section we present and discuss the results obtained by numerical analysis of the 15 mL samples, comparing cemented (UN 1, PG 1, WG 1) and untreated (UN 2, PG 2, WG 2) specimens. The study will focus on the grain-size distributions, porosity, calcite content, permeability and breaking mechanism of the three granulometries under analysis.

6.1. Pre-processing considerations

Following the methodology described in Chapter 3.5, the results obtained in the numerical analysis proved to be mostly consistent. Thresholding and solids separation appeared to be quite accurate for almost all granulometries.

The exception is the tomography performed on the cemented well-graded sample. In this case, repeated attempts did not allow to obtain images as sharp and still as for the other granulometries. In particular, the problem was mostly found in the lower part of the column.

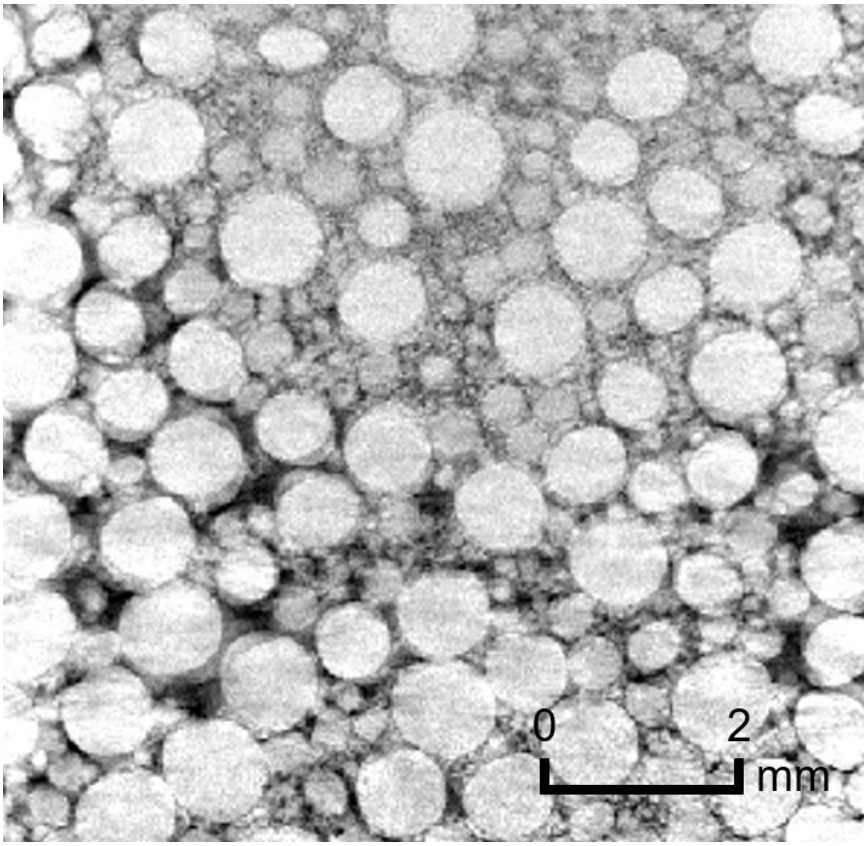

Figure 6.1 - Bad image quality and blur for WG 1 specimen. Grayscale image on the XZ plane, from the bottom of the sample

The reason for this result, which can be observed in Figure 6.1, is not entirely clear. The sample was kept motionless during scanning but some movements imperceptible to the

naked eye may have occurred. An alternative would be the presence of moisture within the sample, but its presence was not subsequently observed, and it is unclear whether its occurrence would have caused that effect.

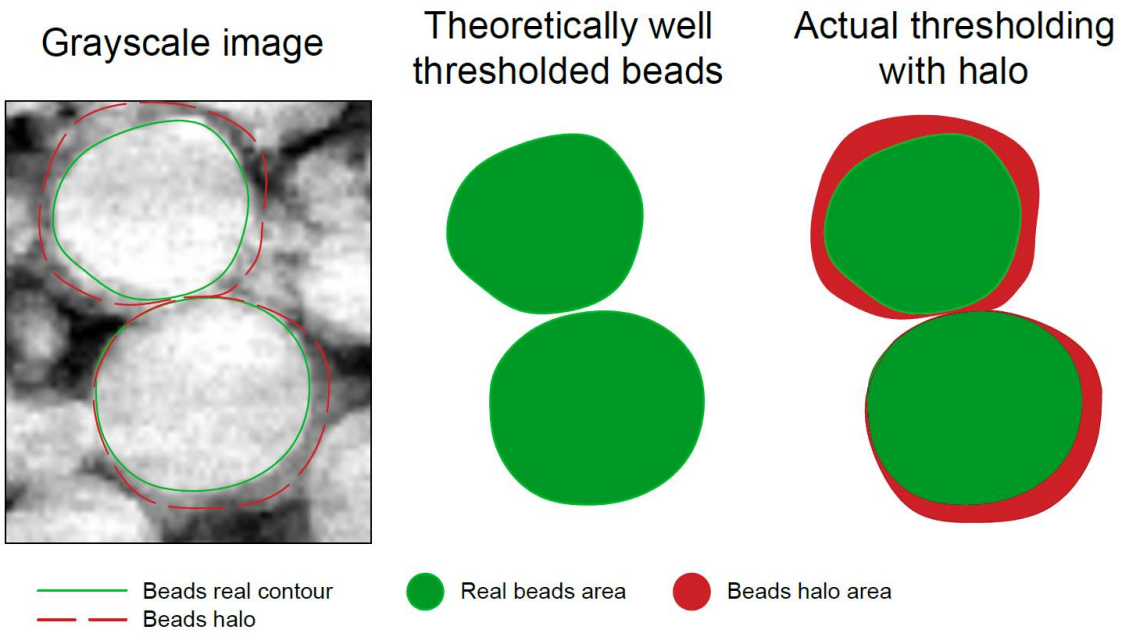

Figure 6.2 - Thresholding issues in the WG blurred image

The solution was not finally found, and the tomographic image was post-processed as best as possible to obtain an acceptable result, on which to perform the calculations.

Nevertheless, the estimate of the solid volume is often higher than the real size (Figure 6.2), with consequent overestimation of the increase in equivalent diameter and calcium carbonate content, as well as under estimation of porosity and permeability.

As described in the following chapters, the outcomes must always be interpreted taking into consideration this WG 1 sample characteristic.

However, as mentioned, these problems did not occur along the entire column, and precisely because of this irregularity in the image quality, it was not possible to homogeneously arrive at an accurate and consistent binarization along the sample length. The consequence is the difficulty in correctly interpreting the results obtained from the numerical analyses, which must sometimes be considered to result from graphic errors and sometimes of real cementation outcomes.

6.2. Grain size distribution

From the measurement of the beads' equivalent diameter, as identified by the thresholding and label analysis, the numerically calculated particle size distribution was obtained.

The raw result was characterized by irregular curves, due to the discreet dosage of the available grain sizes and to the differentiated representation of slightly variable dimensions. The computed equivalent diameters were averaged at ten thousand regular intervals, in order to obtain a trend similar to a normal distribution, through which, the effect of the MICP on the grains size is evident (Figure 6.3).

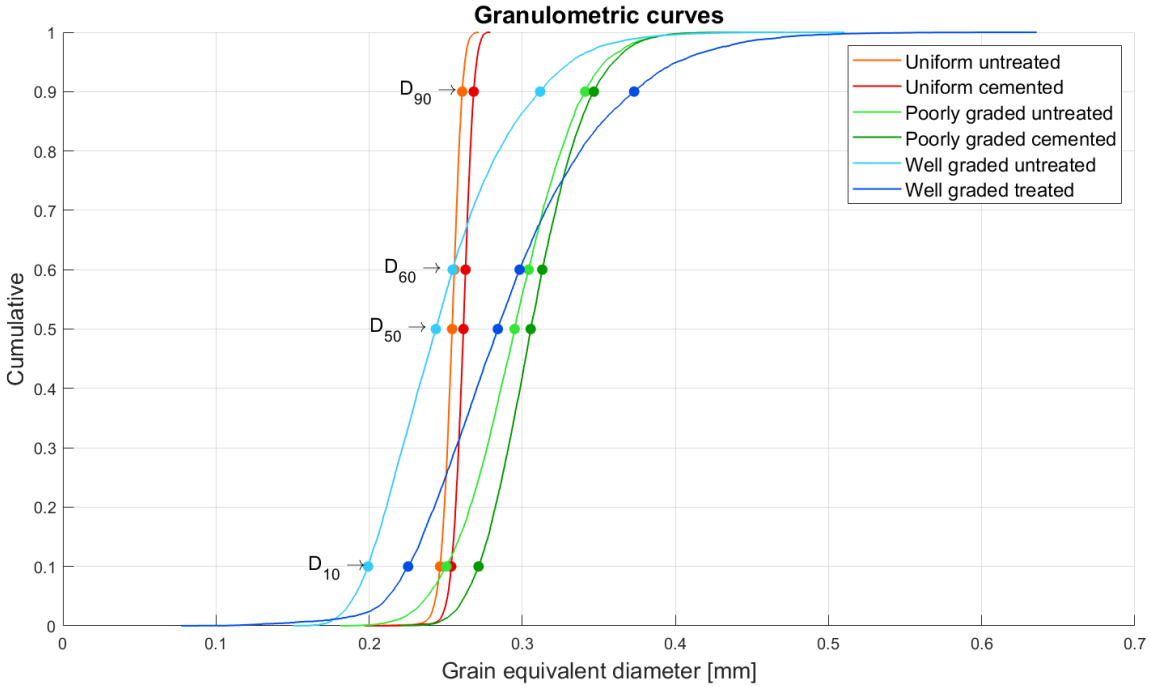

Figure 6.3 - Numerically calculated and averaged granulometric curves for untreated and cemented granulometries. The dots show the representative diameters indicated by the arrows (D_{10}, D_{50}, D_{60} and D_{90})

The greatest quantity of fines is found in the WG, while the different heterogeneity of the granulometries is clearly evident from the slope of the curves and from the range of covered diameters.

As regards the glass beads increase in size following the precipitation of calcium carbonate on them, the shift in the representative diameters can be observed from Figure 6.3 and Table 6.1. In general, the most important increase is related to the WG, followed by the PG and the UN.

Table 6.1 - Representative diameters (D_{10}, D_{50}, D_{60} and D_{90}) and size shift before and after cementation

	D_{10} [mm]	D_{50} [mm]	D_{60} [mm]	D_{90} [mm]
UN 1	0.2536	0.2616	0.2629	0.2683
UN 2	0.2463	0.2542	0.2556	0.2608
ΔUN	0.0073	0.0074	0.0073	0.0075
PG 1	0.2714	0.3055	0.3131	0.3467
PG 2	0.2504	0.2950	0.3041	0.3411
ΔPG	0.0210	0.0105	0.0090	0.0056
WG 1	0.2254	0.2840	0.2982	0.3730
WG 2	0.1993	0.2436	0.2545	0.3117
ΔWG	0.0261	0.0404	0.0437	0.0613

The uniform granulometry is characterized by a constant shift of the curve, of about 7.5 µm. The poorly graded, on the other hand, displays the maximum discrepancy in the D_{10} while the gap decreases in the larger diameters. In contrast, the WG presents a difference in shift increasing as the grain size increases, up to a change of 61.3 µm in the D_{90}.

6.2.1. Discussion

Figure 6.4 reveals some differences between the numerically calculated curves and those defined by the dosage of the different beads' sizes.

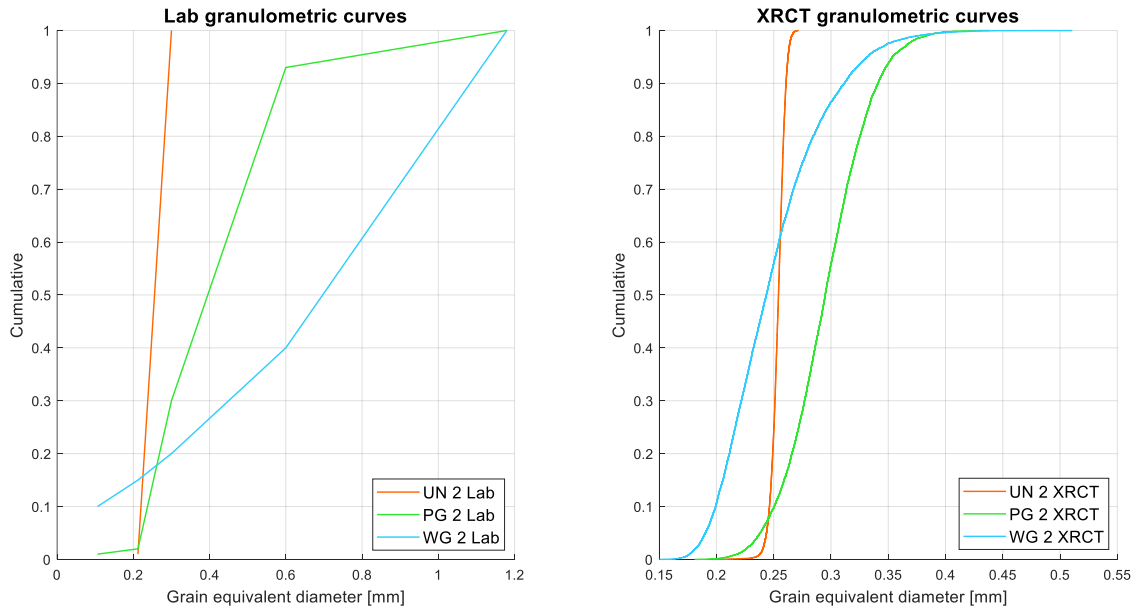

Figure 6.4 - Comparison between the granulometric curves as obtained numerically (left) and as discretely defined according to the dosage used for their creation (right)

The first dissimilarity that is noticed is the maximum grains size, which, according to the real definition, should reach 1.18 mm. Although this was the maximum limit, in the

numerically computed curves it reaches a maximum of 0.5 mm in the WG and 0.44 mm in the PG (untreated). However, this is only the effect of the average that has been applied to the approximately 150 thousand different sizes calculated through XRCT. The maximum diameter evaluated by Avizo before the average reached 1.3 mm for PG and WG, proving to be slightly higher than the real one, but ensuring a fairly precise binarization.

Consistent with the real dosages, the WG curve shows a higher fine content than UN and PG, and a more elongated and distributed distribution.

Unlike the discrete laboratory curve, which shows an almost exponential trend for the WG, the numerical one defines a quasi-normal distribution. This is due to the definition of the lab curve, which takes into account only the maximum value of the different glass beads diameters, which are instead defined in a range of sizes, whose distribution was not known. It can be said that the numerical estimate has well calculated the intermediate diameters, providing a continuous curve, which can be considered representative of the distributions throughout the whole range of definition.

Regarding the modifications caused by cementation, the uniform granulometry appears to have reported a homogeneous cementation, due to the minimal diameters' variability. The magnitude of the increase in grain size is comparable to the size of a single layer of calcite crystals, as observed qualitatively in this study and as reported in other papers (Cui et al., 2017; Dadda et al., 2017), but less than about ten times the average calcite crystal size reported by Clarà Saracho et al. (2020b), for similar reactants concentrations.

The increase in grains size is instead more marked in the D_{10} of the PG, which represent spheres of about 0.25 mm. The shift progressively decreases towards larger diameters. This observation is in line with the preferential deposition observed in the SEM images, confirming a reduced precipitation on the large radius beads. However, this result could also be due to thresholding issues, since tiny spheres are more difficult to identify and smaller beads may have been counted as joined into one solid.

Finally, the WG granulometry shows the most marked increase along the entire curve. In this case, however, the greater shift in the D_{90} compared to the D_{10} and D_{60} is more difficult to explain.

The SEM images provided a discordant result. It can then be confirmed that the thresholding and separation of the WG 1 sample did not lead to the desired results and, given the halo of the images, the larger the blurred beads, the greater the increase in size, as both the bead and its halo are considered as solid parts (value equal to 1 in the binary image).

Furthermore, given the greater number of fines, the same assumption made for PG, according to which agglomerations of very small cemented particles could have been considered as a single solid, holds true.

For these reasons the result shown in Figure 6.4 for the WG is not to be considered completely reliable.

6.2.2. Conclusion

From the results of the numerical analyses it was possible to compare the discrete grain sizes with those measured by the XRCT images. The trend was consistent, although due to the average applied to the numerous measurements, the larger diameters were underestimated. The actual measurements, however, reach and exceed the theoretical dimensions, while remaining decidedly consistent. The averaged curves, as well as the original ones (not reported), prove to be a good tool for the evaluation of a continuous granulometric curve for soils in which it is not known.

Regarding the evaluation of MICP effects, the study of the granulometric curves modification allows to observe in a practical way the grains increase in size due to bio-cementation, and provides a useful tool for the detection of possible preferential precipitations.

Interestingly, the uniform granulometry confirmed a homogeneous cementation result, with an average increase of less than 10 μm, equal to the thickness of a thin crystalline layer. The poorly graded one showed a greater cementation on the small and intermediate beads (21 μm increase in D_{10}, from 250 to 271 μm) with a decrease for the larger diameters. This result is in agreement with the qualitative SEM observations, where the beads of that size were the most cemented.

Finally, the well graded curve was difficult to interpret and showed the greatest increase of all granulometries (up to 61 μm shift in D_{90}), although this result is most likely due to binarization or separation errors.

6.3. Porosity and pore skeleton

The study of the porosity change of a cemented sample was the first step towards the calcite content numerical estimation. The rendering of the pore volume skeleton provided a first understanding of the possible flow paths, which served as a basis for the permeability results interpretation.

One should remember that the comparison between cemented and non-cemented samples does not concern the exact same sample before and after treatment, but two samples of the same granulometry, statistically similar.

The continue analyses along the height of the columns started with a 7.5 cm high sub-sample, but then the 5 mm at the top have been removed, as characterized by an anomalous behavior of high and linear increase in porosity in UN 2, PG 2 and WG 1.

It has not been possible to give physical significance to this result and is thought to be due to Avizo's calculation issues on the volume fraction at the extremity. All the continuous analyses on the parallelepipeds representing the column height were therefore conducted with this premise.

6.3.1. Porosity

The MICP treatment intuitively leads to a reduction in porosity. This was confirmed by the continuous analyses of the pore volume change along the column height (Figure 6.5).

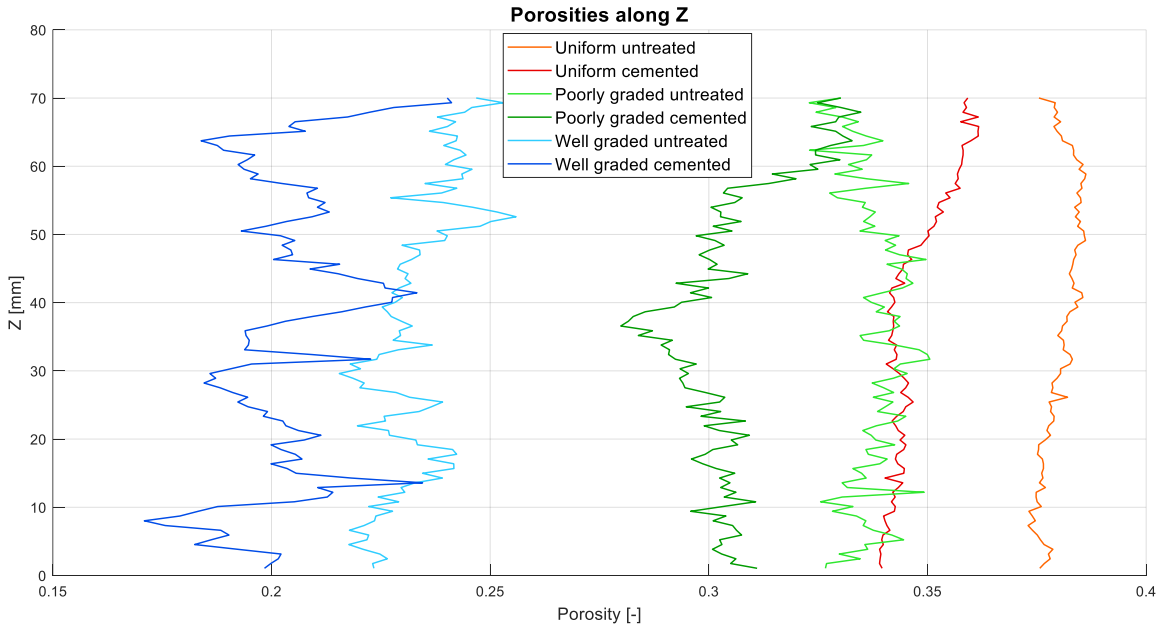

Figure 6.5 - Porosity change along the height of the cemented and untreated columns

The figure shows the trends of the void volume, averaged over 100 intervals, so as to reduce the noise that the graph containing all the measures reported (4522 initial measures, such as the number slices of which the analysed column is made).

The porosity reduction is clearly observable from the shift of the curves to the left. The grains size variability translates into a variability of the porosity, demonstrated by the increased noise and by the reduced homogeneity of the curves from UN to PG to WG.

WG 1 reports greater variability than WG 2 and the porosity of the former seems to have a tendency to decrease towards the bottom of the column. PG 1 shows a minimum of porosity in the center of the sample (about 0.28), decreasing decisively from the top (where it is practically identical to PG 2), then increasing again slightly towards the bottom and reaching a porosity somewhat over 0.3, probably due to the inherent variability of the sample.

The uniform granulometry exhibits a low variability and a minimum of porosity in the center (about 0.34), yet, very similar to the value at the bottom. In any case, the reduction from top to center is evident, as in 3 cm the porosity goes from 0.36 to 0.34 approximately.

To evaluate the pre / post MICP porosity changes at top, center and bottom it is possible to refer to Table 6.2, where the reported values are calculated as voids volume fractions in the aforementioned 3 cylindrical sections and in the whole columns.

Table 6.2 - Porosity as volume fraction of top (TOP), center (MID) and bottom (BOT) sub-cylinder. Column "ALL" reports the porosity volume fraction computed on the 7 cm parallelepiped whose continuous values are shown in Figure 6.5

		Porosity (-)				**Δε (-)**				**Δε (%)**			
		ALL	**TOP**	**MID**	**BOT**	**ALL**	**TOP**	**MID**	**BOT**	**ALL**	**TOP**	**MID**	**BOT**
UN	**1**	0.35	0.34	0.33	0.32	0.03	0.03	0.05	0.05	8.74	9.17	12.66	13.18
	2	0.38	0.37	0.37	0.38								
PG	**1**	0.31	0.31	0.28	0.29	0.03	0.02	0.05	0.04	9.66	7.09	15.74	12.92
	2	0.34	0.34	0.33	0.33								
WG	**1**	0.21	0.21	0.19	0.18	0.03	0.02	0.04	0.05	11.96	9.42	19.17	20.94
	2	0.23	0.25	0.22	0.23								

The porosity reductions are calculated on the average void volume of the untreated samples, as the particle size distribution inside the mold is not exactly the same. In the UN, the total porosity goes from 0.38 to 0.35. The greatest reduction is actually recorded at the bottom of the column, going from 0.37 (average) to 0.32, for a reduction of 13.18%,

against 9.17% at the top. This difference between the two extremes is however small when compared to PG and WG. The first confirms, also with this calculation of the 3D volume fraction, a maximum reduction of 15.74% in the center. At the top, the porosity goes from 0.34 (average) to 0.31, limiting the reduction to 7.09%. At the bottom of the PG there is a difference of 0.04 (12.92%) while the total void fraction passes from 0.34 to 0.31, with a decrease (9.66%) comparable to that of the UN (8.74%).

The WG proves to be the most variable. The average porosity decreases from 0.23 to 0.21 (-11.96%). The greatest reductions are observed at the bottom and center, respectively of 20.94% and 19.17%, with a decrease from 0.23 (average) to 0.18 at the lowermost. At the top, the porosity is only reduced by 9.42%.

6.3.2. Pore volume skeleton

Through a specific Avizo function, it was possible to reproduce the void volume skeleton of the treated samples. This technique allows to roughly evaluate the pore size distribution by means of a rendering of pores and throats thicknesses. At the same time, it is possible to evaluate the potential flow paths.

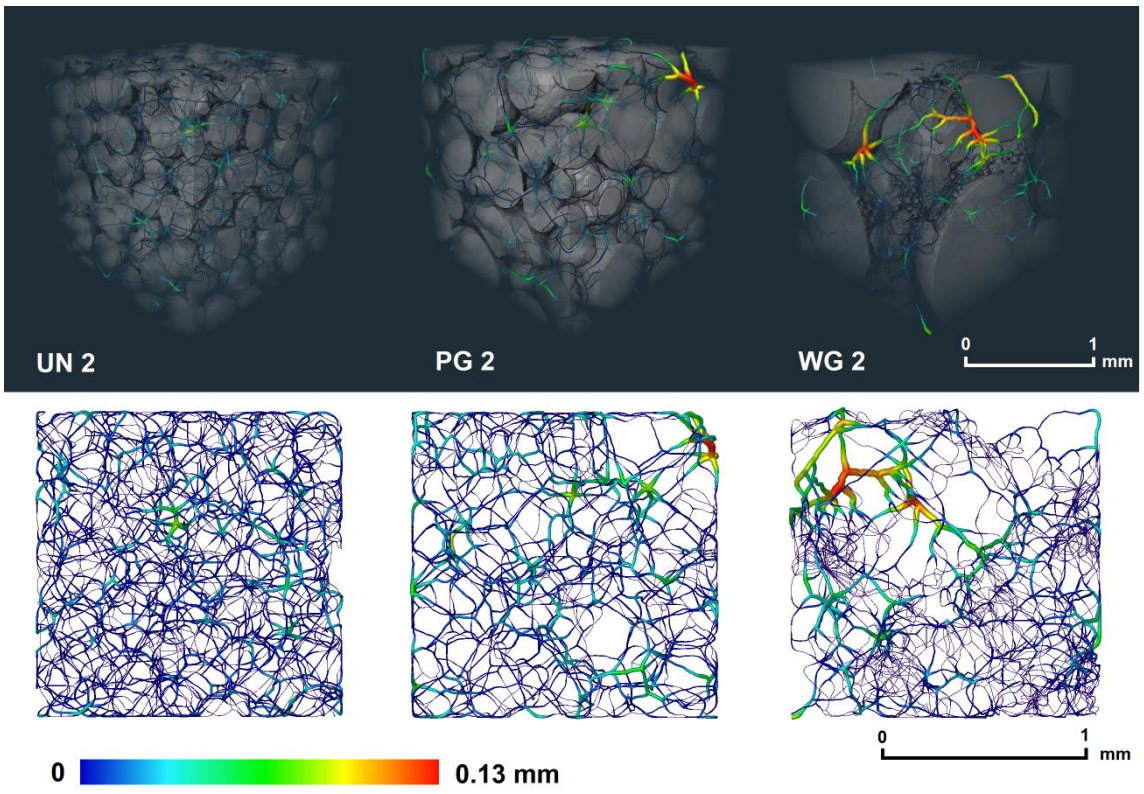

Figure 6.6 - 3D granulometries rendering with skeletonization of the pore volume (top) and skeleton front view (bottom). From the left: UN, PG, WG. For clarity: the lines represent the pores and pore throats; lines colours and thickness allow for an estimate of the pore size distribution

Figure 6.6 shows the result of the "skeletonization" within a 3D rendering of the granulometries under study and through a frontal view.

One can immediately notice the greater variability of the WG porosity compared to the PG, and even more so, to the UN. The latter reports mostly constant hues and less than 0.07 mm thicknesses. Its pore throats network is then much denser and more regular than that of the other granulometries.

In the WG it is observable how a part of the sub-sample shows a dense and thin pore net (bottom-right), while in the upper right part, the size of the pores exceeds 0.13 mm and the throats become sparser.

The PG appears to be a cross between WG and UN, with partial skeleton regularity and slightly variable pore size, even reaching 0.13 mm in a portion of the sample.

6.3.3. Discussion

The change in porosity along the Z axis reflects the definition of the granulometries: the better graded they are, the more variable the porosity is.

On average, the numerically calculated void volumes are 0.38, 0.34 and 0.23 for the untreated samples of UN, PG and WG respectively. If we compare these results with the laboratory-estimated values (UN = 0.36, PG = 0.31, WG = 0.22), a good agreement is observed. It can be said that the calculation with Avizo slightly underestimates the porosity. This depends on the binarization threshold used, as well as on the fact that the calculation in the laboratory was made in an approximate way, and perhaps on portions not containing the same percentages of grains.

Again, referring to the total column porosity, the porosity variability after cementation slightly increased, at the macroscopic scale. The uniform granulometry reports an almost linear decrease towards the CS injection point, suggesting an augmented presence of calcite.

The lower porosity in the center of the PG can also be converted into CC and compared with empirical measurements. For the moment, from this behavior we can infer a greater deposition in the median meeting point between CS and BS.

In the WG it is already possible to notice a strong variability in the untreated sample, due to fines segregation, which locally decrease the porosity. Indeed, the void volume seems to decrease slightly from top to bottom, suggesting a greater presence of the smaller grains in the lower part, deposited due to the force of gravity.

Finally, WG II shows a very high variability, with values between 0.18 and 0.24. It is difficult to make physical sense of these result, but it was certainly affected by the poor image quality. In any case, a reduction has been correctly highlighted and a slight trend of lower porosity towards the bottom is foreseeable.

For the UN and PG samples, it was possible to perform a second-degree polynomial interpolation to highlight the trend of the porosity change. The WG did not lend itself to this expedient, given the stochastic variability of its void volume along the Z axis.

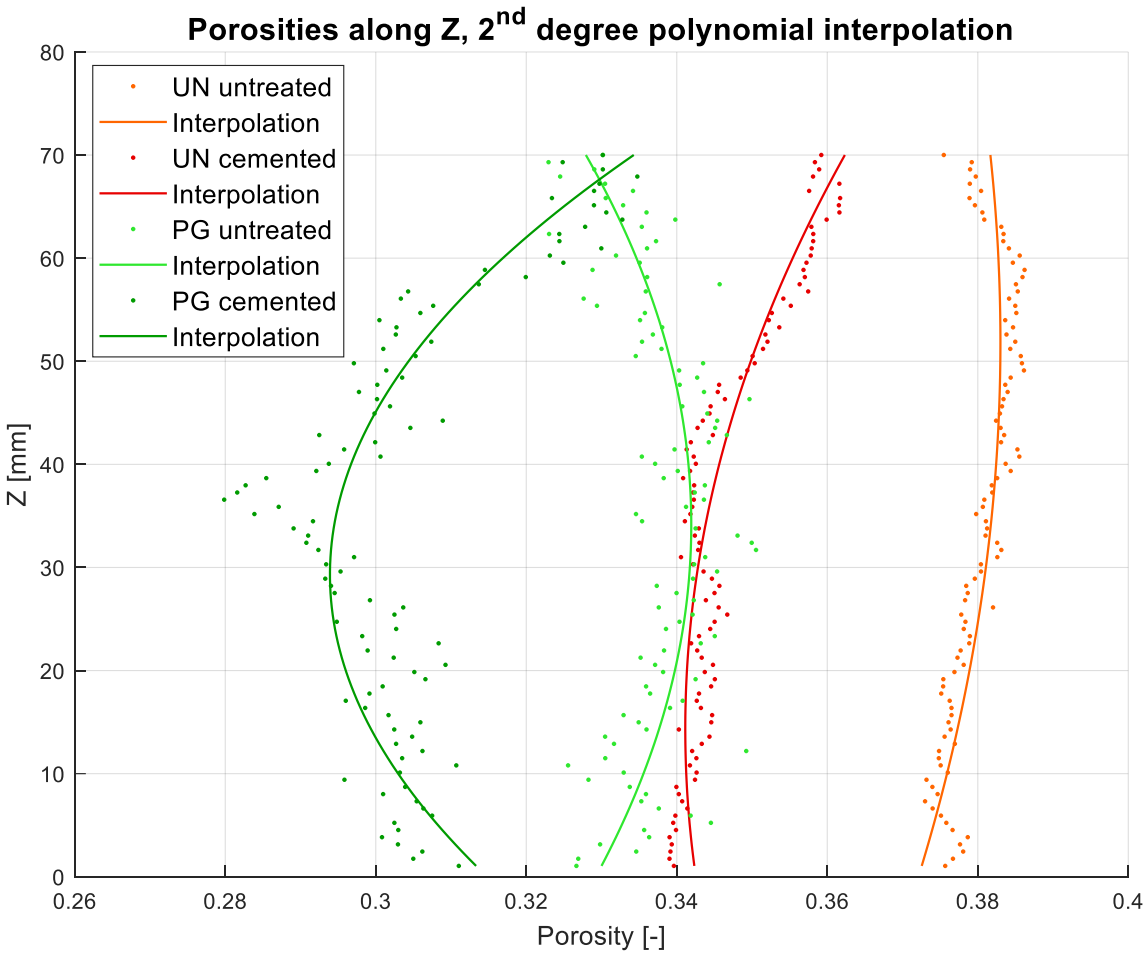

Figure 6.7 - Second degree polynomial interpolation of UN and PG porosity change along the columns, before and after cementation

The result of the interpolation can be seen in the Figure 6.7. The uniform granulometry clearly highlights the reduction in porosity towards the bottom, with a lower rate of decrease starting from the center. This leads us to think that the cementation is fairly uniform between bottom and center, and then decreases towards the top. The UN untreated, instead, has a fairly regular void volume, with a slightly opposite trend to the UN 1, which anyway is not considered in the CC calculation.

The minimum porosity in the center of PG 1 is very evident: it then grows towards the top and towards the bottom. At the top, in particular, the void volume is very similar to that of the non-cemented sample, suggesting minimal calcite deposition. Also in this case the untreated sample seems to have a slightly mirror-like trend compared to PG 1, but in any case, much more uniform.

As for the pore skeleton (Figure 6.6), the UN exhibits a very high uniformity of thicknesses and colours. There are channels with a conceivable width of around 0.04 mm, but no preferential flow paths are highlighted. This means that the reactants had the opportunity to reach every part of the sample in a uniform manner, and this was reflected in the homogeneous porosity reduction and, as we will see in following chapter, in a uniform calcite deposition.

In the PG there is a minimum thicknesses variability, but the network becomes sparser and the average size is greater. A smaller number of available passages suggests the flowing of the reactants into the pores and throats of larger width (up to 0.13 mm), with consequent increased deposition in those locations, and minimal presence of calcite where the solutions are never found to pass. However, this variability is not observable either empirically or numerically, as it manifests itself at a microscopic level.

Finally, the WG skeleton confirms what has been observed and hypothesized for the fine's segregation and the passage of fluids. From the analysed sub-sample, the presence of preferential flow channels, much larger than others is evident. They are found almost isolated and in areas with a high presence of coarse grains and few fines.

Reactants are therefore likely to exclusively pass into these thicker pores and throats. Unlike the PG, in which a certain continuity of these flow channels was observed, in the WG they are often found to merge into more dense and subtle networks, in which the passage of solutions is forced but slowed down, causing an increase in residence time and

possibly an augmented calcium carbonate precipitation in these areas of high fines content.

6.3.4. Conclusion

Numerical analyses of porosity and pore skeleton variation confirmed some previous hypotheses and highlighted new results.

The void volume fractions calculated with Avizo proved to be in line with those measured in the laboratory, giving reliability to the numerical results. The greater the granulometry gradation, the lower the porosity, because the voids of the larger spheres are filled by the smaller ones.

The mean porosity change following cementation is 8.74% for UN, 9.66% for PG and 11.96% for WG. The magnitude of the change is similar for the three granulometries, but the variation along the height of the column is different.

The WG reported the greatest variability, but due to image quality issues, its trend cannot be given a confident meaning. In any case, the $CaCO_3$ crystals seem to have deposited with extreme variability in the whole sample, and in a more accentuated way towards the CS injection point. The PG reported the greatest change in porosity in the center, with a strong difference from the top and bottom. The cemented UN showed instead the lowest porosity at the bottom, but with a much lower variability.

The void volume skeletonization allowed us to infer a uniform flow path and therefore a homogeneous distribution of calcium carbonate at a microscopic level for the UN and inhomogeneous for PG and WG. For the latter in particular, the presence of fines accumulation areas was confirmed. In these zones, the confluence of the reactants coming from the large preferential channels and the accumulation of $CaCO_3$ was presumed. This is reinforced by the presence, at the moment of the opening of the WG 1 column, of large cemented fragments, characterized by a high presence of small diameter beads.

To conclude, porosity analyses seem to represent a valid tool for the qualitative calcite content numerical estimation and its distribution along the samples. Skeletonization can instead be useful for understanding the flowing channels trend and morphology and for interpreting the permeability results of Chapter 6.5.

6.4. Calcium carbonate content

The calcite content evaluation was made by means of the variation between the porosity of the cemented sample and the average porosity of the untreated one. The continuous analyses are carried out on the 7 cm parallelepipedal sub-samples, the discrete ones on the sub-cylinders.

6.4.1. Results

The results of the numerical investigations on calcium carbonate content are reported in Table 6.3 in a discrete format, while the trend of the CC along the height of the columns is shown in Figure 6.8.

The granulometry that shows the greatest CC is the UN, followed by the PG and the WG. The estimates deriving from the average of the calculations on the cylindrical sub-samples overestimate those of the parallelepipedal sub-samples by 1-2 percentage points.

For the former, CCs of 7.58%, 6.59% and 5.49% are reported, respectively for UN, PG and WG. The latter, on the other hand, assume $CaCO_3$ contents of 5.87%, 5.41% and 3.99% respectively.

If we refer to the 3 portions representing the top, center and bottom of the samples, the highest CCs for each category are found at the bottom for the UN (8.56%) and the WG (6.97%) and in the center for the PG (8.70%).

Table 6.3 - Numerically calculated Calcite content from parallelepiped sub-sample (ALL), top (TOP), center (MID) and bottom (BOT) sub-cylinders. "MEAN" is the average of the three sub-cylinders

	Calcite content (%)				
	ALL	**TOP**	**MID**	**BOT**	**MEAN**
UN	5.87	5.96	8.23	8.56	7.58
PG	5.41	3.92	8.70	7.14	6.59
WG	3.99	3.13	6.38	6.97	5.49

From the continuous analysis of Figure 6.8, it can be seen how along the height of the columns the CCs tend to be alternately greater and smaller in the three granulometries. At the top and bottom, the UN reports the highest values of the three, while in the center the PG shows the highest CC.

The WG is once again characterized by an extreme variability of results. It reports a $CaCO_3$ content span between 0% and 8.7%, with an average of 5.49%. The trend of the

UN is instead much more linear and shows an increase in CC from the top to the bottom, with an inflection of the curve starting from the center.

Finally, the PG has very low CC at the top (up to 1%), to then reach an evident maximum of about 9.4% in the center and decrease again towards about 5% in the bottom.

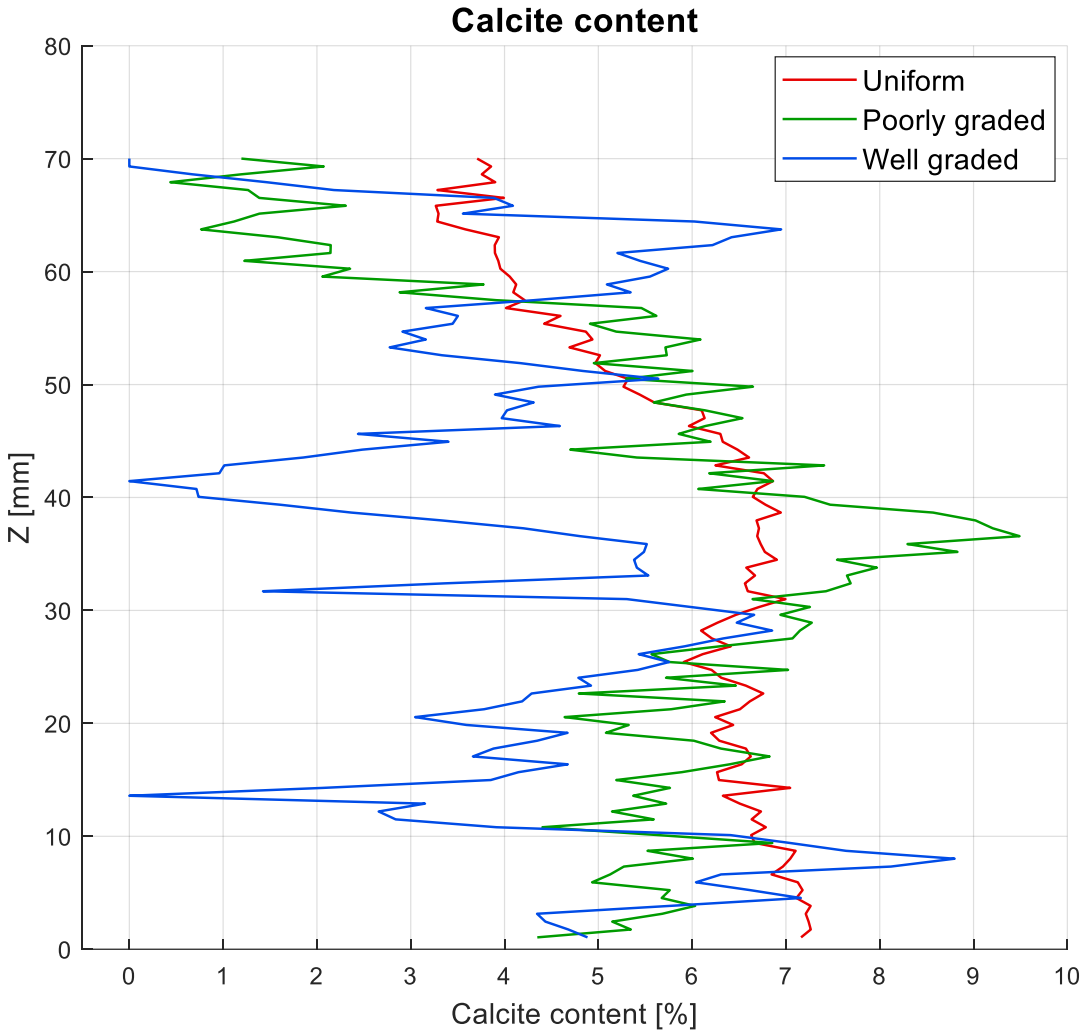

Figure 6.8 - Calcite content along the height of the UN, PG and WG samples

Looking at the estimated variability in the three portions of the columns (Figure 6.9), it is evident that the UN is characterized by slightly changing CC within the sub-samples, with a clear maximum at the top.

This unpredictability is much greater in PG and WG. The first reports CCs covering 7 percentage points only at the top, with the 25th and 75th percentiles encompassing a range of about 4 percentage points. The mutability decreases considerably in the center and bottom, limiting itself to about 5 percentage points in the center and less than three percentage points at the bottom, with much of the variability within the whiskers.

The WG is very inconstant in the whole sample. Within each sub-cylinder there is a CC variability of 7 percentage points. The one between the different portions of the column is much less marked.

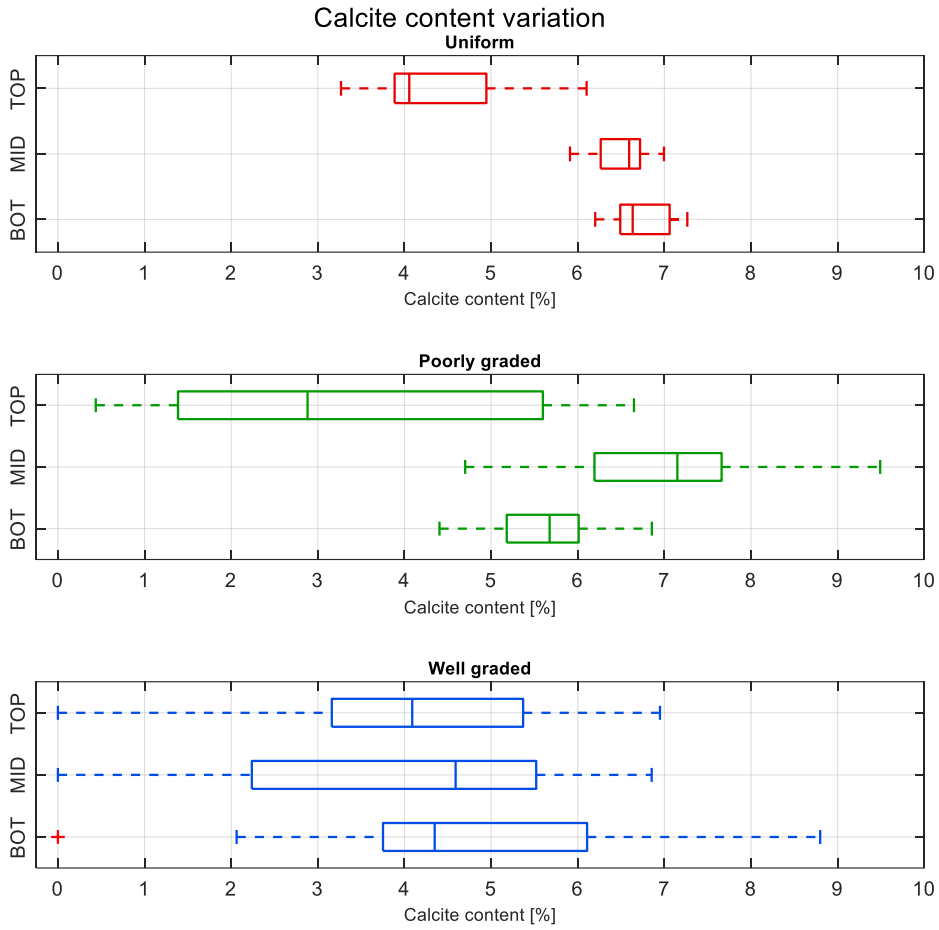

Figure 6.9 - Boxplots representing the continuous measurements variability in parallelepipedal sub-samples. On each box, the central mark indicates the median, and the bottom and top edges of the box indicate the 25th and 75th percentiles, respectively. The whiskers extend to the most extreme data points not considered outliers. The "+" symbol indicates an outlier.

6.4.2. Discussion

The hierarchy of the numerically calculated calcite contents is the same as that resulting from the acid digestion measurements. The values, however, are largely greater in the first case. The extent of the overestimation can be assessed in Figure 6.10.

At the top, the biggest difference is present in the UN, with acid digestion indicating a CC of 4.63% and the numerical calculation estimating 5.96%. The overestimation is much higher in the middle of all samples. The WG has a difference greater than 3 percentage points and the PG even greater than 4, more than 100% more. At the bottom

the differences remain very high, with more than 4 percentage points in the WG (almost 200% more), a little more contained in PG and UN.

Although these results remain consistent with what has been reported in the literature for similar treatments, the overestimation is, especially in some portions of the samples, not acceptable, as it leads to overestimation of the soil mechanical properties. In fact, it is believed that the empirical calculation by means of acid digestion is more reliable, as it allows to carry out a practical check during the analysis. Therefore, it is believed that the numerical analysis shall be improved.

The causes of the overestimation may be due to high uncertainty of the thresholding, mainly due to the low image quality. Another point to consider is the method used to numerically evaluate the CC, which takes into account only an average porosity of the untreated reference sample. The porosity changes of the treated columns are therefore always translated into an increase of CC, while in some cases they could be due to a different grain size distribution in the given portion.

A separate discussion must instead be made for the WG, in which the image quality of the treated column has certainly led to the overestimation of the CC for the reasons explained in Chapter 6.1.

More similar values would have been obtained by shortening the binarization threshold in the cemented samples. In this study, probably, the halo at the edges of the grains – due to the limitations in image quality – led to consider a solid phase volume in the treated samples greater than the real one, with consequent CC overestimation.

For a more precise binarization, maintaining the same method of CC calculation, it would have been necessary to scan the same granulometry before and after the treatment (but this was difficult in terms of organization), and secondly to calibrate the numerically estimated porosity with the real one.

In the case of this study, the quickly calculated porosities were not accurate and representative enough to proceed in this way. A reliable measurement directly performed on the samples in question would have made possible a more effective thresholding.

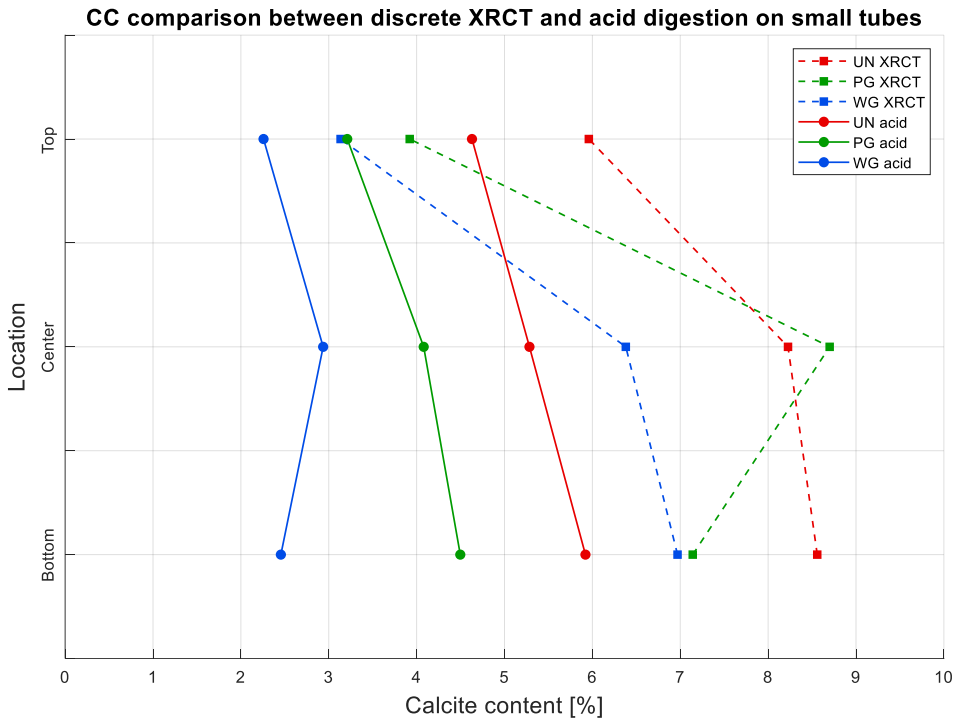

Figure 6.10 - Calcite content comparison between the numerical and empirical (acid digestion) results

What is useful of the numerical analysis is the shown CC trend at the top, center and bottom. When compared with empirical calculations (Figure 6.10), it is quite similar. The UN, in particular, reports in both cases an increasing CC from top to bottom, although the numerical estimate shows an inflection in the center.

The PG presents an evident maximum of CC in the center in the numerical analyses, while in the empirical calculations only one inflection point is highlighted, with the CC continuously increasing from top to bottom. It is possible that in the center of the PG there was a portion with greater content of fines and therefore increased solid volume. However, it is clear that the precipitation is largely lower at the top, probably due to clogging phenomena and reduced reactants delivery to the areas furthest from the CS injection point. The decrease in CC is then much greater from center to top than from top to center.

Finally, the WG presents this time a maximum in the center according to the empirical results, which is absent according to the XRCT estimates, reporting an increasing CC towards the bottom of the column. This result is certainly an artifact, due to the fact that the image quality at WG 1 bottom was the lower, causing an increase in the solid volume and CC estimates. The minimum at the top can still be considered a consistent result.

Considering instead only the numerical result, the continuous trend of the $CaCO_3$ content observable in Figure 6.8 allows for some observations to be made.

The UN granulometry once again demonstrates a certain uniformity of results. From the bottom to the center the CC is always between 6% and 7% and then goes against a linear decrease towards the top. In this case, given the sample's high porosity, it can be assumed that evident clogging phenomena are not present. The decrease could be due to a lower $CaCl_2$ and urea content in the CS that reached the top, due to an increased precipitation in the first few centimetres. In any case, given the quite evident and sudden decrease, an accentuated reduction in porosity around 40 mm cannot be excluded.

The CC trend in the PG column is very peculiar. As mentioned, it could be due to an increased solid volume in that area. However, the calcite content goes from an average of 6% between center and bottom to 1% at the top. This result is an indicator of clogging in the first half of the column and also suggests finding a treatment alternative to achieve similar values across the sample.

Finally, the WG presents a behaviour that is too far from the empirical measure to enable a discussion. The decrease towards the top is very high and the CC at the bottom is certainly overestimated. The trend between center and top could be the real one, even if empirical estimates suggest a much less marked decrease.

To complete the discussion on the calcite content variability in the columns we can refer to the boxplots in Figure 6.9. The limits of the 25th and 75th percentile in the UN are very narrow and reflect the granulometry uniformity. Such low variability with respect to the median value, combined with the empirical results make the numerical trend reliable. It can also be noted that the median value is sometimes quite distant from the average one, suggesting the presence of more or less strongly cemented areas, which cause the latter to vary. The median, on the other hand, is less affected by this internal variability.

The PG reports an extreme irregularity at the top, probably due to the coexistence of a still consistent cementation near the center and very low near the BS inlet. There is therefore the greatest decrease in CC in the top portion, probably due to clogging phenomena. In the center and bottom, especially excluding whiskers, the CC remains in a contained range, while extreme CC values are still present very far from the median in the center, outside the 25th and 75th percentiles.

The WG, as mentioned, does not allow for a consistent discussion. The variability is decidedly high in each portion of the column, covering calcite contents from 0% to 9%. The median values are all very similar, as opposed to the averages. Surely, the great variability is partly the result of the granulometry morphological characteristics. To what extent the trend is due to these properties rather than binarization errors is not, however, possible to understand.

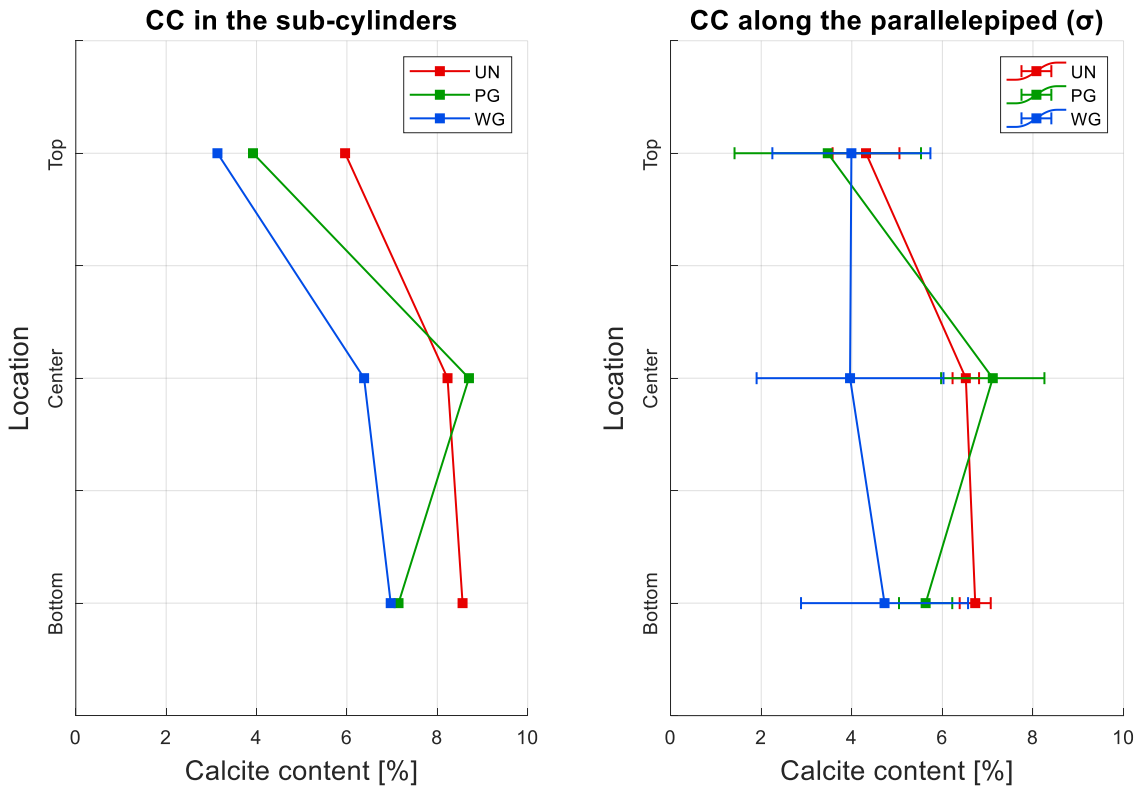

Figure 6.11 - Calcite content comparison between discrete numerical estimations in the sub-cylinders and mean values with standard deviation at top, center and bottom of the parallelepipedal sub-volume

To conclude, it is possible to make a comparison between the numerical estimates made on the sub-cylinders and those on the parallelepiped that excludes the edges (Figure 6.11).

Firstly, the CCs in cylindrical volumes are almost always greater, with the exception of the WG at the top. This is probably due to increased cementation at the sample's edges, between the beads and the column walls. This greater presence of $CaCO_3$ was actually found by opening the specimens and can be explained by the presence of a greater volume of voids and therefore of a preferential flow path at the edges, where more precipitation occurred. Chemical phenomena related to the material of which the molds (PP) were composed could also be investigated. The extent of the overestimation is around 1-2 percentage points.

As for the CC trend, UN and PG report practically the same one between top, center and bottom, with the only difference of a leftward curves shift in the case of the parallelepiped. The CC at the top of the PG seems to be the one whose estimate is more similar in the two sub-volumes, but it suffers from a great deal of variability.

Finally, the WG presents a different trend in the two cases. At the top there is an even higher CC in the parallelepiped estimates. This could be due to the presence of a segregation of fines and therefore an area of greater solid content away from the edges, then converted into greater CC than that estimated in the cylindrical volumes. As again evidenced by the error bars, the variability is always too high to rely on these assumptions.

6.4.3. Conclusion

The numerical analysis of the calcite content was based on the difference in porosity between a cemented and an untreated sample. This technique allowed to observe the variances between the three granulometries and to appreciate in a qualitative and almost continuous way the CC trend along the height of the columns. The result was a confirmation of increasing CC and decreasing variability from WG to PG to UN.

The greatest $CaCO_3$ relative presence was observed at the bottom of UN and WG and at the center of the PG. It is therefore possible to confirm that the cementation was never completely uniform but always lower at the columns top, far from the CS injection point. The CC begins to decrease decisively starting from the center of the samples, due to clogging phenomena or accelerated precipitation at the bottom and poor reactants delivery to the top. The maximum CC in PG the center, although it could be a symptom of increased bacterial concentration or CS slowing in that area, is not confirmed by empirical measurements.

In general, the low CC variability found in the UN confirms that the homogeneity of the pore size distribution results in a homogeneous reactants delivery, although the uniform achievement of the latter up to the top is limited by a greater precipitation at the bottom.

On the other hand, PG and WG are much more variable in particle size, with a consequent effect on the distribution of calcite in the samples. The WG, in particular, reports the greatest variability, certainly caused by the fine's segregation within it but just as likely by the image binarization problems.

As for the values estimated from the numerical analyses, the CC was always higher than that deriving from acid digestion. This is due to the technique used to estimate the amount of $CaCO_3$, which has obvious limits. For a more effective binarization it would be necessary to calibrate the thresholds on the basis of porosities previously calculated with precision. To exactly define the CC in a certain area it would then be necessary to compare the same sample before and after cementation.

The overestimation resulting from the numerical calculations is therefore considered less precise than the empirical results. For comparisons between the CC observed in this study with respect to the results of the literature, the comments are therefore limited to the case of acid digestion. The study of XRCT images remains an excellent tool for a qualitative and confirmatory study. With some improvements in the technique and the methods it could be possible to reach a much higher precision and reliability.

To conclude, the comparison between the CC in the parallelepipeds and the one in the sub-cylinders, allowed us to ascertain an accentuated precipitation at the sample's edges, at the interface with the column wall. This result could be the consequence of a preferential flow path in this area of greater porosity. In the real case of treatment of a control volume in an open space, this effect would not be present, so the results excluding the edges could be more representative of that situation.

6.5. Permeability changes

The permeability changes caused by the treatment were assessed by measuring the absolute permeability of 7 mm side cubic sub-samples and observing the pressures and flow velocities trends inside them, before and after MICP treatment. The numerically estimated permeability was compared with the analytical results deriving from the application of the Kozeny-Carman equations.

Only the results deriving from the connected porosity analysis are presented and discussed below, as no appreciable differences were observed with the simulations on non-connected porosity (see Chapter 3.5.6 to understand the difference between the two volumes).

6.5.1. Results

Table 6.4 reports the results of the numerical calculation, which are displayed in Figure 6.12, as regards the cemented samples. Absolute permeability is almost always in the order of magnitude of 10^{-11} m^2. The highest values are found in the PG along the entire

column, with an average permeability of 1.06E-10 m^2 in the uncemented sample and 8.90E-11 m^2 after treatment. The UN follows, passing from an average of 8.52E-11 m^2 before treatment to 7.44E-11 m^2 after MICP. The lowest permeability is found in the WG, which presents 4.66E-11 m^2 before injections and 3.75E-11 m^2 in the cemented sample.

The permeabilities of UN and PG are very similar in the center, where there is also the PG minimum (7.55E-11 m^2). The UN instead has a slightly decreasing trend towards the CS inlet, but with very similar permeabilities in the center and bottom.

The WG reports a minimum of permeability in the center (3.12E-11 m^2) and higher values at the top, but especially at the bottom (4.50E-11 m^2).

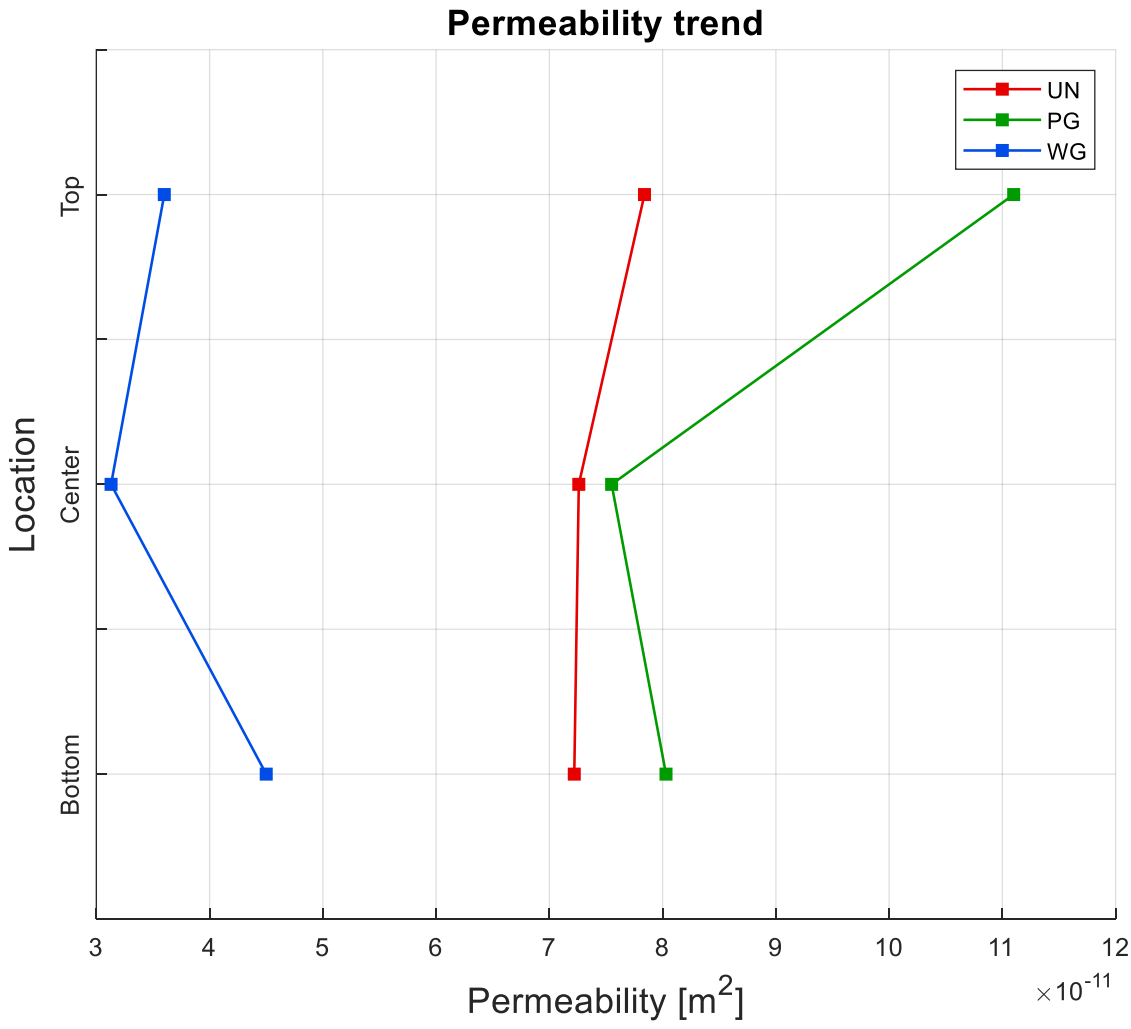

Figure 6.12 - Permeability at top, center and bottom of the treated samples

As for the percentage reduction in permeability following treatment, it is on average greater in the WG (19.62%), followed by the PG (16.10%) and the UN (12.61%). The

greatest reductions in each granulometry occur at the bottom of the UN (15.16%) and in the center of the PG (28.80%) and the WG (32.75%).

Table 6.4 - Numerically calculated absolute permeability in treated and untreated samples and relative reduction

		Absolute permeability (m^2)				Permeability reduction (%)			
		MEAN	**TOP**	**MID**	**BOT**	**MEAN**	**TOP**	**MID**	**BOT**
UN	**1**	7.44E-11	7.84E-11	7.26E-11	7.22E-11	12.61	7.98	14.69	15.16
	2	8.52E-11	8.32E-11	8.92E-11	8.31E-11				
PG	**1**	8.90E-11	1.11E-10	7.55E-11	8.03E-11	16.10	-4.73	28.80	24.22
	2	1.06E-10	9.49E-11	1.11E-10	1.12E-10				
WG	**1**	3.75E-11	3.60E-11	3.13E-11	4.50E-11	19.62	22.65	32.75	3.47
	2	4.66E-11	4.60E-11	4.95E-11	4.43E-11				

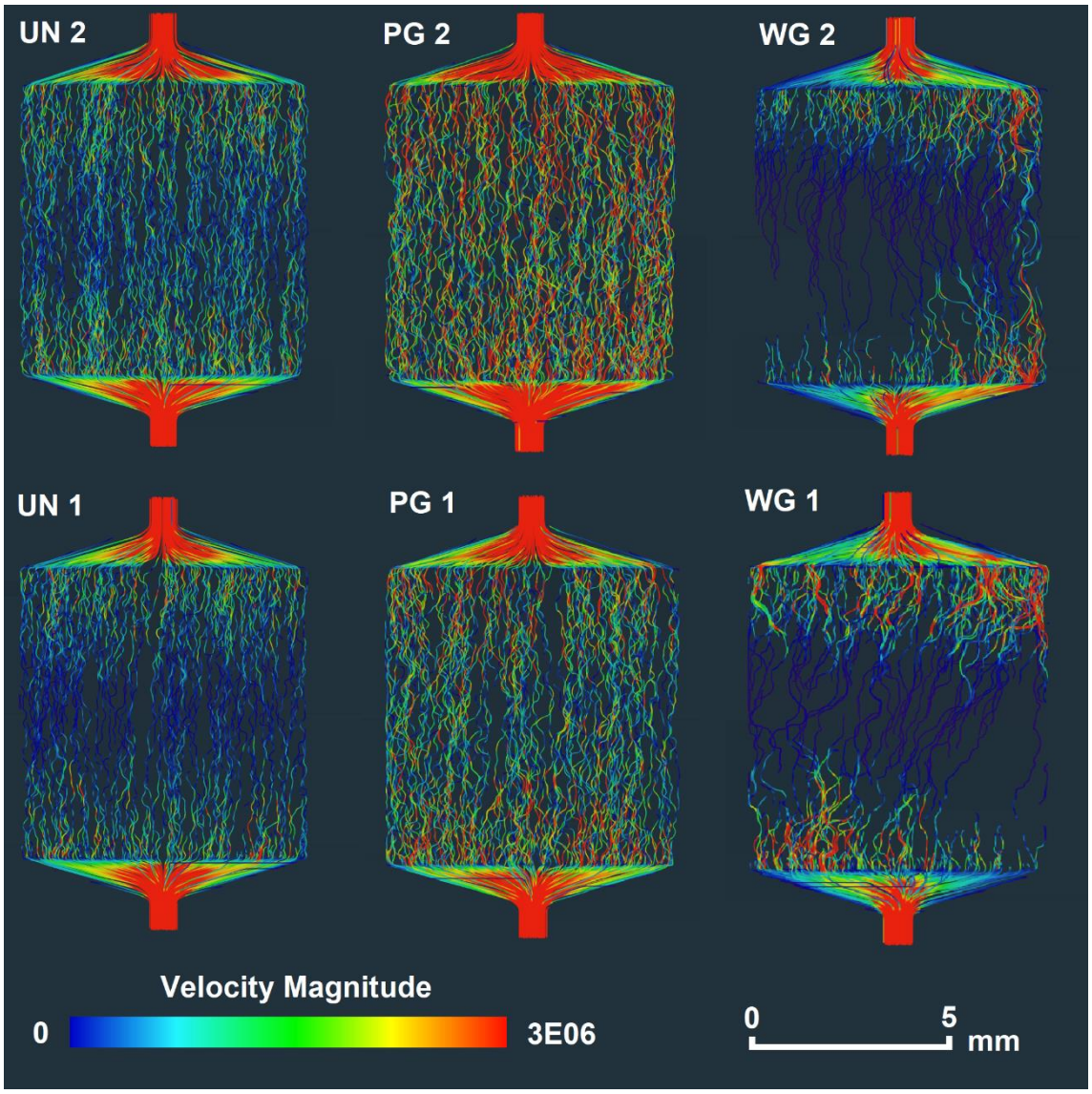

Figure 6.13 - Flow paths and velocity magnitude inside the granulometries. Sub-samples are taken from the bottom of the columns

Referring to Figure 6.13, it is possible to observe the trend of the velocities and the simulated flow paths inside the solid matrix.

The higher velocity in the PG is evident from the prevailing red hues, which slightly veer towards blue in the UN, and completely in the WG. The flow paths of the UN are more uniform than those of the PG, in which there are greater radii of curvature, although the general direction is always the vertical one. In the WG, on the other hand, the flow paths have very inhomogeneous directions, especially in WG 1, in which the vertical direction is often lost, in favour of diagonal flows.

Regarding the difference between treated and untreated samples, both in the UN and in the PG a general decrease of the velocities is clearly observed, without a particular change of flow path taking place. In the WG, as mentioned, the flows change direction, while the velocity magnitude decreases only slightly.

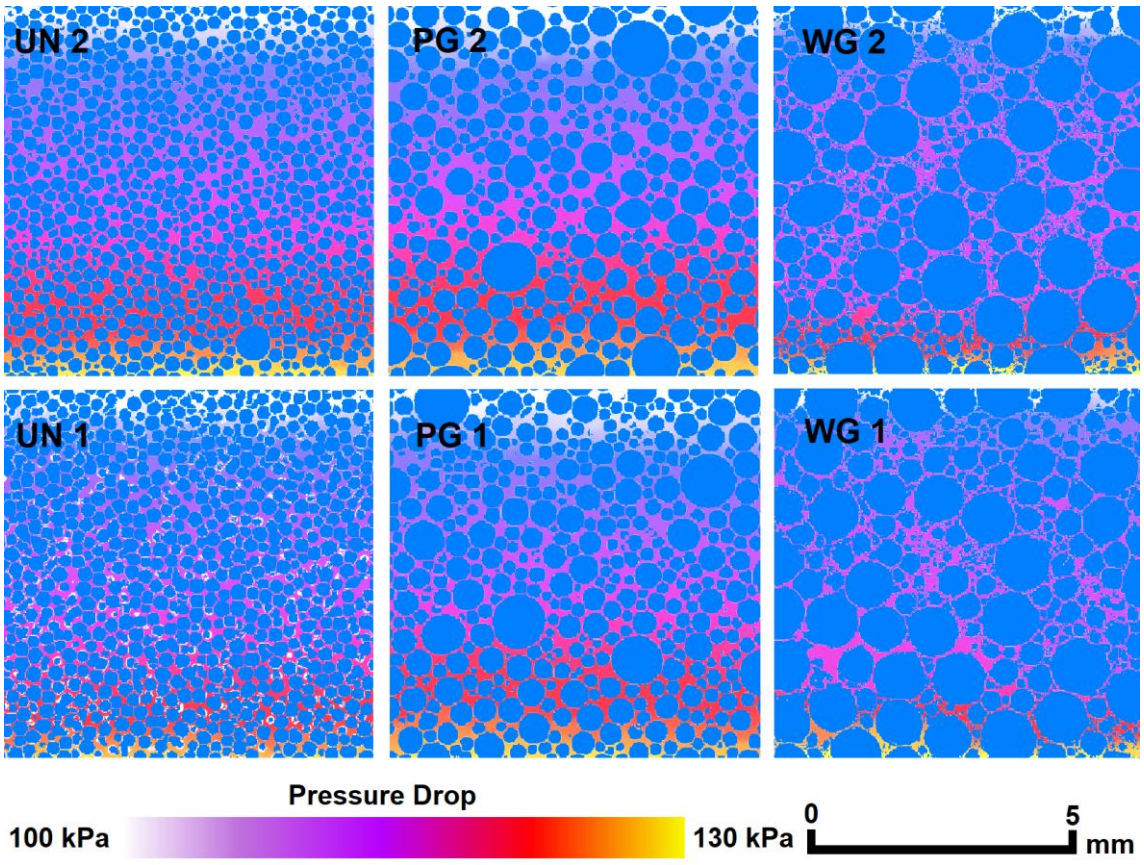

Figure 6.14 - Pressure drop in the 420 side sub-cubes from the columns bottom before and after cementation. 100 kPa and 130 kPa are imposed respectively at the top and bottom of the sub- samples

In Figure 6.14 the pressure gradients in the sub-samples are represented, imposing a difference of 30 kPa between top and bottom. There are no significant differences

between the pre and post treatment samples. However, it can be noted that in the WG the pressure tends to decrease faster in the first millimetres, while in the UN and PG the pressure drop is more gradual.

Finally, Table 6.5 shows the permeability values calculated with the Kozeny-Carman equation (3.12). The highest permeability is found in this case in the uniform granulometry (k = 6.28E-11 in UN 2), followed by PG (k = 5.49E-11 in UN 2) and, with one order of magnitude less, by WG (k = 9.32E-12 in UN 2). The trend between top, center and bottom is very similar to that of the numerical calculation. The reduction in permeability is maximum in the UN (27.57%), followed by the PG (25.62%) and the WG (22.44%).

Table 6.5 - Permeability estimates from Kozeny-Carman equation

Permeability from Kozeny Carman (m^2)						
		MEAN	**TOP**	**MID**	**BOT**	**Reduction (%)**
WG	**1**	7.23E-12	7.07E-12	8.11E-12	6.50E-12	22.44
	2	9.32E-12	1.21E-11	8.37E-12	7.47E-12	
PG	**1**	4.09E-11	4.71E-11	3.73E-11	3.82E-11	25.62
	2	5.49E-11	5.79E-11	5.72E-11	4.98E-11	
UN	**1**	4.55E-11	5.21E-11	4.28E-11	4.15E-11	27.57
	2	6.28E-11	6.53E-11	6.57E-11	5.74E-11	

6.5.2. Discussion

The numerical analysis on the samples absolute permeability reported approximately values with an order of magnitude of 10^{-11}. This result is in line with the average permeability of silty sand and clean sand mixed soils (Stranne et al., 2019), in accordance with the definition of our granulometries.

The higher permeability observed in PG is the consequence of a higher D_{60} and probably larger pores. Although the porosity of UN is greater, other factors play a key role in defining the permeability, such as grain size and tortuosity (Stack, 2015). The flow paths inside the PG therefore find larger channels in which the fluid flows faster, creating preferential pathways. In the UN, the permeability is slightly lower probably because the pore size distribution uniformity leads to a homogeneous flow in all the pores, and to a reduced speed.

In WG, the permeability is by far the lowest. Although there are certainly preferential flow paths where the small grains are present in lower quantities, the porosity in the fines clusters is so low and the flow so disadvantaged that the total permeability is lower.

It is possible that by performing the analysis on another portion of the WG sample with low fines content, the permeability would become the highest of all. Samples are still within a REV for the grain size, but segregation clusters can greatly change the result. In Figure 6.15 the preferential paths followed by the flow in the WG are evident, both in the cemented and in the untreated sample. In WG 1 the flow lines are even oblique, as the fluid tries to bypass a zone of minimal permeability. In WG 2 it is very clear how some lines are interrupted, due to a velocity equal to zero in correspondence with a cluster of fines that prevents the passage of the fluid, which then flows with greater speed in the right part of the image, in which probably there is a greater porosity.

However, a clear decrease in velocity between WG 2 and WG 1 is not evident, which instead is very clear in the poorly graded granulometry. In the latter, in fact, we observe in the PG 2 a velocity magnitude that reaches 3E06 and a very dense network of flow lines. In PG 1 the hues turn towards blue, highlighting a decrease in velocity. The flow paths are also less dense, emphasising some restricted areas of no flow (Figure 6.15).

For the UN, the same observations made for the PG apply, as the hues change to lower velocities and the flow lines become less dense in the cemented sample.

Specific interest is put on the recurring spatial characteristics and the radius of curvature of the flow paths in the three granulometries. For the UN, flow paths are very uniform and almost straight, as the variability of the pore size is minimal, and the grains are very small compared to the reference volume. This is the cause of the more homogenous distribution of calcite, since the reactants are transported evenly across the entire width and length of the sample.

The PG yields flow lines with greater radius of curvature and often higher velocities. This greater irregularity, due to the non-constant presence of large and fine particles, could result in an inhomogeneous delivery of CS at the micro scale, due to locally higher speeds and preferential channels. However, the high permeability suggests the possibility of reactants delivery even at considerable distances.

The irregularity found in the flow lines of the WG is instead extreme, and suggests the presence of strongly preferential flow paths, with consequent inhomogeneous precipitation also at the column scale.

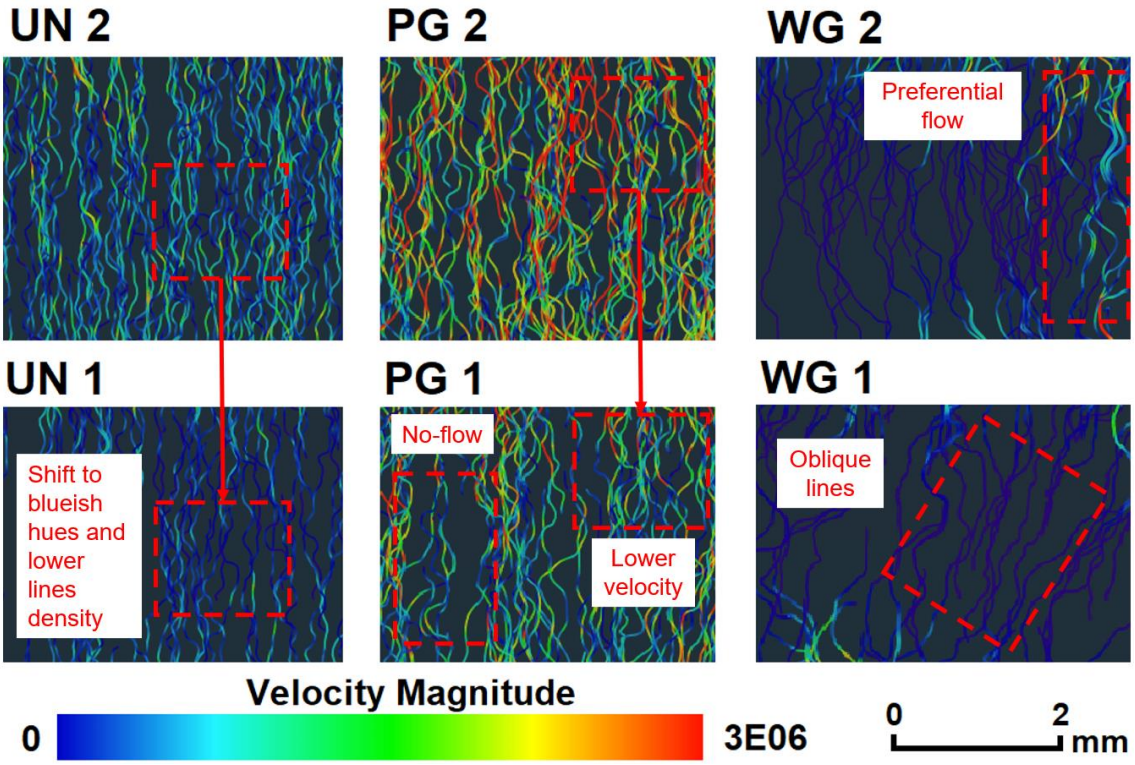

Figure 6.15 - Flow lines and velocity change detail in the three granulometries

As for the different permeability at the top, center and bottom, it reflects the trend of porosity and calcite content in the different portions. The permeability of the PG is however always the highest, with a maximum at the top where the cementation was very low and a minimum at the center where the calcite content was the highest. The difference in permeability between the two portions is about 32%, which can be considered not high in absolute terms but among the highest observed in this study. Also in the UN there is the inverse trend of that of the calcite content, but the variability along the column is limited.

Finally, in the WG, the trend is not consistent with that of the CC, as a maximum permeability is observed at the bottom. These results are certainly influenced by clusters of ends within the sub-samples.

As regards the permeability reduction following the MICP treatment, the variability along the column has the same trend discussed for the permeability of the cemented samples. The negative value at PG 1 top is probably due to very little or no cementation in the

cemented column fragment under study and to a limited presence of fines, which makes its porosity and average grain diameter greater than those of the untreated sample.

In general terms, the greatest reduction in permeability occurs in the WG, followed by PG and UN. This result suggests a strong cementation within the clusters of fines and consequent manifestation of localized clogging phenomena, with a decrease in the equivalent flow channel area.

Regarding the comparison between the decrease in permeability registered in this study and other works related to MICP effects, good consistency has been observed. The reduction of permeability within the same sample is related to the CC, in accordance with results previously reported in literature (Cheng et al., 2013; Dadda et al., 2017; Qabany and Soga, 2013; Zamani and Montoya, 2016).

However, Cheng et al. (2013), Dadda et al. (2017) and Van Paassen (2009), reported reductions of up to 70%, but with higher CCs. Qabany and Soga (2013), on the other hand, for a CC around 2% observed a reduction of 20%.

The results of this study do not differ much from those in the literature and could be very close to those of Cheng et al. (2013), Dadda et al. (2017) and Van Paassen (2009) for higher CC.

These are substantial reductions in permeability but not greater than an order of magnitude. It can be therefore said that the MICP treatment does not substantially modify the permeability of the soils and certainly to a much lesser extent than traditional cement improvements (Cheng et al., 2013). Further injections would be possible, given the maintenance of good permeability. If the aim of the treatment were to reduce this latter, more injections and the use of higher concentrations would be necessary.

From the observations, it emerged that the clusters of fines can create areas of accentuated cementation and clogging. An injection of CS solutions containing fine aggregates (similarly to what Li et al. (2019) suggested) could favour a greater cementation and a more consistent decrease in permeability.

As for the pressure gradient (Figure 6.14), the more sudden drop of the WG is due to the lower permeability in areas with a high content of small grains and obstructed flow. This decrease is much more gradual in PG and UN, given the more homogeneous and free flow.

Finally, the numerical and analytical permeability estimates performed with the Kozeny-Carman relation, do not differ much, and almost always remain within the same order of magnitude. This is due to the fact that the diameter and porosity used in equation (3.12) are also a result obtained with Avizo.

The reduction hierarchies in the three granulometries are instead quite different. The Kozeny-Carman estimates show a greater reduction for UN, followed by PG and WG, in descending order of CC. The analytical calculation is in fact mainly based on two properties (grain size and porosity) which are functions of the calcite content. The tortuosity and the existence of flow paths with minimum permeability play instead a fundamental role in Avizo's simulation. The effect of tortuosity in the Kozeny-Carman equation is enclosed in a variable that has not been changed for the three granulometries, as its estimate is extremely difficult, but it is strongly influenced by the pore and throats size distribution. The numerical result is therefore different, and perhaps more precise, as it takes into account the sample anisotropy and the existence of preferential pathways and localized flow slowdowns.

6.5.3. Conclusion

The numerical permeability analysis and the simulation of flow lines are an effective non-invasive tool to understand the hydraulic properties of a soil.

The results showed a variability of the permeability as a function of both the calcite content and the granulometry. The PG turned out to be the most permeable, followed by UN and WG. The variability along the column is once again a function of the CC and of the grain size distribution, which determines the sample tortuosity. The presence of fines agglomerates can significantly affect the modification of a soil permeability, both before and after the MICP treatment.

The flow lines within the UN are regular and evenly distributed. The PG instead promotes pathways with a greater radius of curvature and some preferential channels that suggest an inhomogeneous $CaCO_3$ distribution at the micro-scale. Nevertheless, the presence of channels with a rather high permeability suggests the possibility for the reactants to reach considerable distances, with the limit of excessive clogging near the CS injection point.

The flow lines irregularity is greatest in the WG, where the effect of fines clusters is evident. They form areas of very low permeability and divert the incident flow or slow it

down a lot, probably therein causing a greater cementation, with an inhomogeneity that manifests at the scale of the column.

In general terms, the reduction in permeability following the MICP treatment was appreciable but contained, settling between 22% and 28% for CC between 2% and 6%, consistently with similar studies. These are reductions that do not substantially modify the hydraulic properties of the soil and are decidedly inferior to those caused by traditional treatments.

To conclude, the comparison of the numerical results with the analytical calculations by means of the Kozeny-Carman equation reported results with a similar order of magnitude but highlighted how the tortuosity plays a fundamental role in the calculation of permeability and must be carefully evaluated when using the analytical method.

6.6. Failure mechanism

This chapter follows the analysis on the micro-UCS test (Chapter 5.4) performed on the sample of uniform granulometry, analysing the failure mechanism and the response of the specimen to the load.

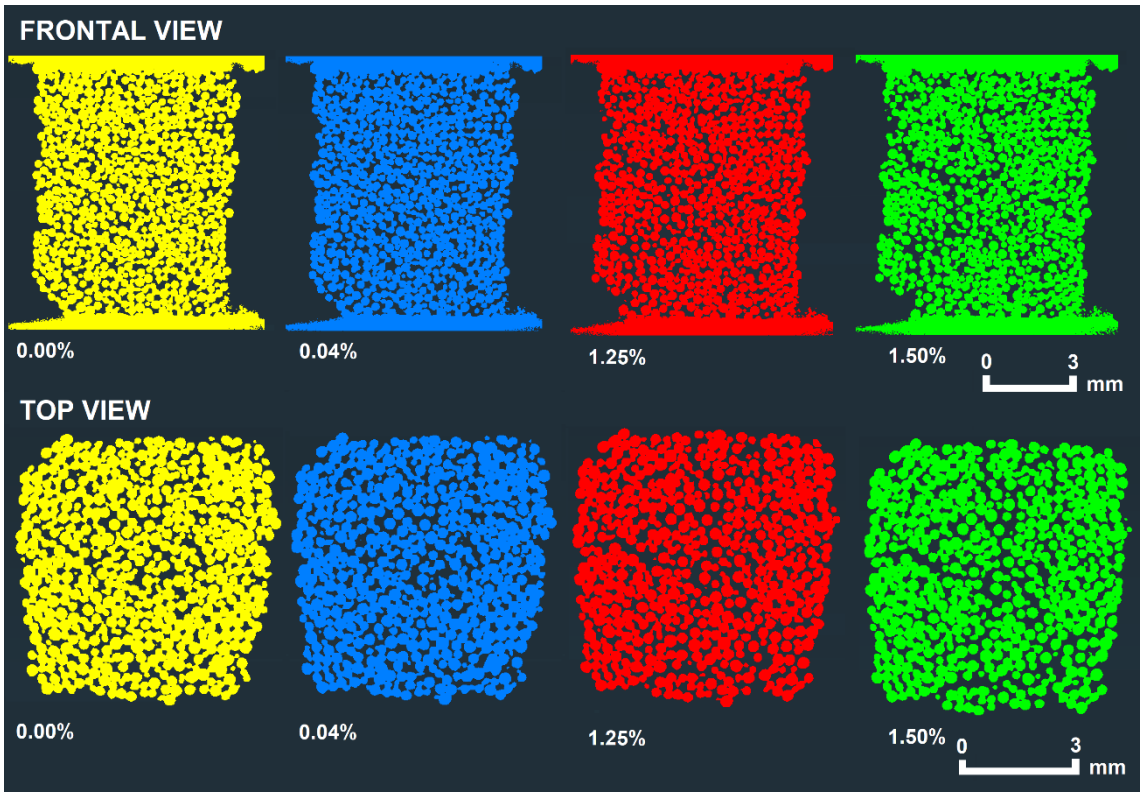

Figure 6.16 - Binarized frontal and top views of the sample during loading. In yellow the unloaded specimen, in blue 0.04% axial strain, in red the failure, in green 1.5% axial strain

In Figure 6.16 are reported the 4 scans that were performed, in binarized frontal and top views. At first sight the fractures in the sample at failure are already distinguishable. The specimen remains almost intact up to the axial strain of 1.5%.

By observing Figure 6.17, instead, it is possible to observe the displacement of the solid matrix in correspondence with the different loading steps.

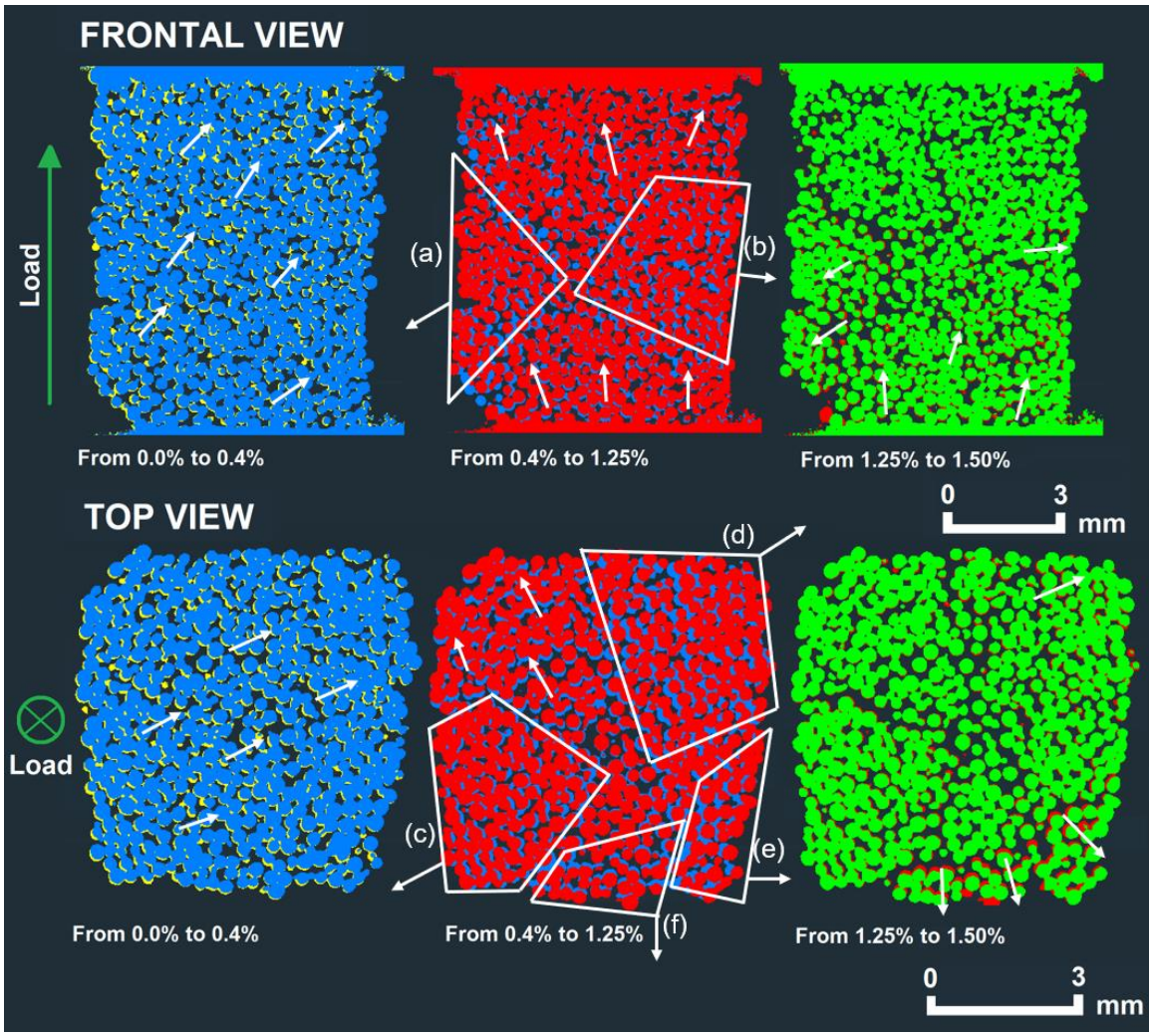

Figure 6.17 - Superposition of the slices at the different loadings in frontal and top views. The white arrows indicate the displacement directions, the white polygons show the displacement of entire blocks following failure. 0.0% = yellow, 0.4% = blue, 1.25% = red, 1.5% = green.

In the elastic branch it is possible to notice the absence of crack formation and an almost uniform displacement of all the beads in the load direction, with a slight tendency to bending the specimen to the right, confirmed by the top view, in which a stiff preferential displacement is highlighted by the white arrows.

Between the axial strain 0.4% and 1.25% the formation of the failure surfaces (highlighted by the outline of the polygons) is appreciable. The displacement near the top and bottom

surfaces is minimal and the formation of rigid fragments moving from the breakage plans can be noted. In particular, the pieces indicated with (a) and (b) are evident: they move in the radial direction, sliding on the failure surfaces under the compression of the specimen. In the top view it is clear that this displacement is radial, with the fragments moving away from the center of the sample. The failure mechanism can be defined of double shear type (Chakraborty et al., 2019), characterized indeed by the formation of rigid bodies remaining intact after failure.

The portions indicated with (e) and (f), clearly continue to move even in softening part. In this latter phase, the greatest movements are observed in correspondence with the fragments separated following failure, while in the part opposite to the loading surface the displacement is null.

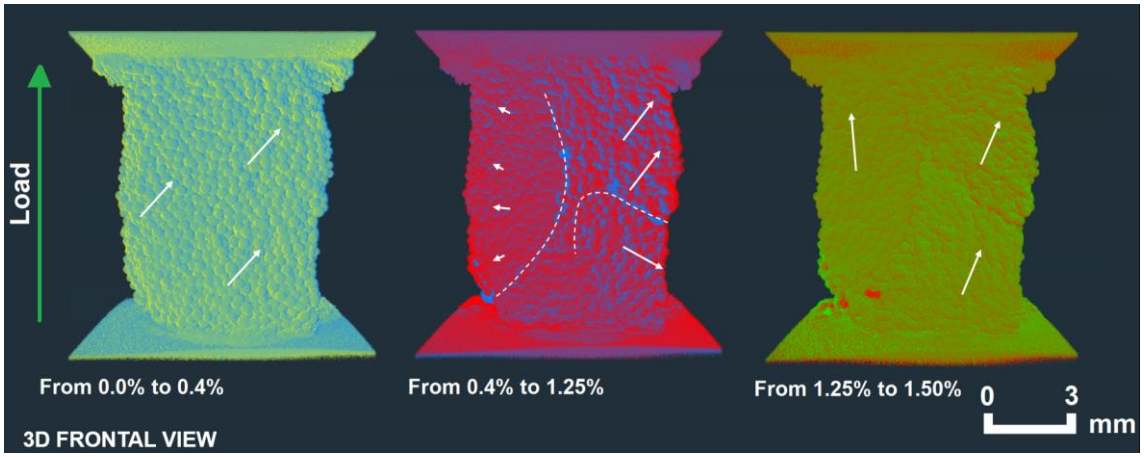

Figure 6.18 - 3D front view with renderings superposition between the different loading phases. The white arrows indicate the displacement of the specimen, the dashed lines highlight possible failure surfaces. 0.0% = yellow, 0.4% = blue, 1.25% = red, 1.5% = green

The Figure 6.18 confirms the rigid compression of the whole sample in the elastic phase and the formation of fragments in radial displacement, at failure. In the softening phase the sample continues to compress and the fragments to move like rigid blocks.

6.6.1. Conclusion

The execution of the scans in the different loading phases allowed the identification of plastic volumetric deformations and of the predominant failure planes. In the elastic phase, a rigid compression of the whole sample was observed, while at failure the formation of rigid fragments sliding on the two predominant failure surfaces was captured, resulting into dilation. The failure mode resembles to that of double shear, typical in soft rocks.

The failure was of a brittle type and the failure planes were numerous and generally oblique, giving rise to wedge-shaped fragments. However, a large part of the specimen remained intact (Figure 5.24). As loading continued, following failure, the intact fragments that separated from the specimen continued to move stiffly and the sample to compress homogeneously.

By measuring the change in the sample total volume, it would be possible to calculate the volumetric strain, even with the current resolution. For an observation of the failure mechanism at the $CaCO_3$ crystal scale, however, the resolution should reach at least 4 μm, which is not possible with the current test setup.

7. Conclusions and Perspectives

The experimental work carried out in this study made it possible to follow all the steps underlying the MICP technology, from bacterial cultivation, to solutions' injection, to process monitoring and subsequent tests. It covers different scientific fields: from biology, to chemistry and physics, to mechanics, trying to reach the full understanding of a technology that sees the geotechnical application of soil improvement as its final goal.

We meant to observe the peculiarities of the treatment at the microscale, by means of the numerical analysis of XRCT images, bringing to light the effects of the soil pore-scale heterogeneities on the MICP treatment. These outcomes served as verification for the results of chemical monitoring and physical analysis.

In the following two chapters we want to summarize and comment on the main results of this study, as well as collect the perspectives that can be derived from it.

7.1. Summary of findings

The effect that soil pore-scale heterogeneities have on the homogeneity and extent of the bio-cementation treatment was investigated by creating ad-hoc three granulometries, a well-graded (WG), a poorly-grade (PG) and a uniform (UN), with the intention of reproducing sands, whose variability of heterogeneity is reflected in the variability of their pores' size, where $CaCO_3$ precipitation takes place. The WG presents a wide spectrum grain size distribution variability, restricted instead in the PG and extremely limited in the UN. These characteristics lead to different porosity and permeability, which have been found to influence the MICP.

The treatment saw the injection on the first day of the bacterial solution (BS) from the top of the test columns, while the cementation solution (CS) was injected, with eleven repetitions, from the bottom. The main findings are summarized below for the experimental and numerical part of the study.

7.1.1. Experimental results

The monitoring of the pH and EC of the effluents proved to be a highly effective tool to evaluate the actual presence of the ureolysis reaction, and qualitatively predict its magnitude. In this study, bacterial activity was observed for the entire duration of treatment, with the most consistent decline apparently from days 7/8.

These observations were confirmed by the chemical analysis of the ions in solution (Ca^{2+}, NH_4^+, TIC), which are able to provide the first quantitative indications on the bacterial activity and on the amount of precipitated $CaCO_3$. They confirmed a good ureolysis rate (up to 10 mM of hydrolysed urea per hour), at least until day 6, highlighting the continuous bacterial activity, even with a rather not sufficient magnitude for the complete ions' precipitation to $CaCO_3$ in the last days of treatment.

By means of the chemical analyses it was possible to bring to light the first differences between the granulometries. The trend of the chemical reaction efficiency (always greater than 50%) and of the bacterial activity is in fact continuously decreasing in all the granulometries, but in the WG an almost constant behavior is reported in the last 3 days of injection. This was translated into a greater bacterial density within that sample, due to the highest number of contact points among the three granulometries, and to the presence of areas with a high content of fines, behaving as filters of the bacterial cells, which remained in greater relative quantity attached to the solid matrix. The filtering processes can, therefore, lead to greater bacterial attachment, although this can manifest unevenly.

The high bacterial density in the well-graded sample could also be inferred from the observations of the SEM images, which revealed the widespread presence of $CaCO_3$ crystals was found in all the contact points between the grains, which were numerous in the portions with a high content of fine.

The absolute quantity of $CaCO_3$ crystals precipitated according to the chemical estimates, was found to be a function of the sample porosity, with even greater evidence as regards the calcite content, which was estimated to be maximum in the UN, followed by PG and WG. The estimated mass of precipitated $CaCO_3$, normalized by the void ratio, revealed instead a greater relative precipitation in the WG, followed by the PG and the UN.

The empirical CC measurement by means of acid digestion, proved to be strongly in agreement with chemical estimates, reporting the same hierarchy of $CaCO_3$ content among the different granulometries and with lower values from 15 to 25%, rendering chemical monitoring a tool of sufficient precision for the estimation of the precipitated calcium carbonate, without the slightest disturbance to the sample.

The injection technique allowed for the treatment of the entire column, although a higher $CaCO_3$ concentration was recorded at the bottom of the samples, towards the point of CS injection. This observation suggested the presence of clogging phenomena, with

consequent reduced delivery of the reactants towards the points furthest from the inlet. The effect is reduced when the porosity, and therefore the permeability, are higher: this is the reason why the 50 mL UN sample showed a maximum of CC in the center of the column, where probably the bacterial concentration was higher and CS arrived easily. The WG, on the other hand, has the opposite behavior, confirming the great influence of the high fine's content areas, causing the formation of transport preferential channels, leading to inhomogeneous delivery and precipitation of reactants.

The smaller columns showed a slightly different CC trend, especially in the WG where the segregation of fines is less evident, reducing the inhomogeneity effect. However, a preferential precipitation towards the bottom was generally confirmed, in agreement with previous studies (Konstantinou et al., 2021b; Noiriel et al., 2016; Rowshanbakht et al., 2016).

Therefore, from the CC empirical analysis the importance of a good porosity for the effective transport of the solutions was deduced, which, in case of preferential precipitation, interfere with the treatment homogeneity by activating clogging phenomena. The presence of areas with reduced porosity and permeability, and minimal pore size, confirmed the generation of preferential flow paths in which the fluid flows faster, with reduced precipitation, and clusters of fines that act as filters for both bacterial biomass and the cementation solution, leading to an increased and inhomogeneous precipitation in the slowdown and stagnation areas.

The SEM observations, in addition to confirming the preferential precipitation of the crystals at the contact points between the particles, where the greatest bacterial presence is hypothesized, offered further possibilities of discussion.

From them we gained understanding about the micro-scale failure mechanism, consisting of the detachment of the crystals at the interface with the glass. Furthermore, the low reactant concentrations have been confirmed to lead to the formation of small, uniformly distributed crystals. These have been observed in the form of calcite, with sporadic presence of amorphous $CaCO_3$ where a higher rate of precipitation may have taken place (UN).

The spheres of intermediate size showed the presence of a uniform thin layer of crystals, while the smaller reported their presence exclusively at the contact points, cementing large portions of the WG sample in an extensive but fragile manner. The larger beads,

instead, exhibited a less dense crystals distribution, probably in the limited points of contact with other smaller spheres.

It was concluded that areas with high content of fines are easier to cement, given the small size of the crystals necessary for their bridging, but the acquired strength could be limited. The presence of crystals almost exclusively at the grains' contact points or in the form of very thin layers, led to hypothesize their low influence on permeability.

To conclude, we would like to emphasise how in the context of the micro-UCS test, the uniform sample subjected to the load reported a UCS of about 250 kPa, which can be considered a satisfying result achieved by a granulometry without initial strength and composed of spherical beads. The failure was of a brittle type, with the formation of at least two failure planes and the presence of a clear elastic response phase, with a trend similar to that of the reloading stage, after failure.

7.1.2. Numerical results

The numerically computed granulometric curves proved to be decidedly consistent with the real ones. Their shift to the right was the result of the MICP treatment. The UN granulometry reported a uniform shift, symptom of a homogenous cementation, with an average increase of less than 10 um, equal to the thickness of a thin crystalline layer. The greater the variability of the granulometry, the more inhomogeneous was the precipitation on the different grain sizes, with a more important curves shift at the intermediate diameters in the PG, validating the SEM observations. Cementation of grains smaller than 106 μm led to complicated binarization, due to the apparent particles' merging, translated into a WG curve shift of difficult interpretation.

By comparing the numerically calculated porosities with those defined in the laboratory, it was possible to evaluate the goodness of the numerical calculation, resulting to be highly consistent, with a maximum underestimation of 10% in Avizo's estimates.

The derived porosity change following the treatment was in the order of 10% on average, with little difference between the samples. However, the reduction was variable along the columns, reflecting the definition of the granulometries: the better graded they were, the more variable the porosity was.

The study of the void volume skeleton provided important considerations on the possible behavior of the reactants flowing within the solid matrix. The great uniformity of the UN

skeleton led to hypothesize a homogeneous distribution of $CaCO_3$ inside it, at the microscopic level. Calcite precipitation is instead believed to be more heterogeneous for PG and WG, due to the formation of preferential pathways, in which the reagents are transported but the precipitation is scarce. In the WG, above all, the presence of accumulation areas of fines was confirmed. In these zones, the confluence of the reactants coming from the large preferential channels and the accumulation of $CaCO_3$ was hypothesized.

As for the calcite content numerically measured, it again confirmed the hierarchy resulting from the analysis with acid digestion, with the maximum CC in UN (7.58%), followed by PG (6.59%) and WG (5.49%), mainly because of the different volume of reagents involved.

The distribution of calcium carbonate content turned out to be inhomogeneous, along the height of the column. A lower content was always found at the columns' top, far from the CS injection point, suggesting the presence of clogging phenomena towards the bottom (in UN and WG) and the center (in PG) of the columns, or an accelerated precipitation at the lowermost, with poor delivery of reactants to the top.

In general, the low CC variability found in the UN confirmed that the pore size distribution homogeneity results in a uniform reactants delivery, while the micro-heterogeneities of PG and WG, leads to a greater variability at the pore scale.

The presence of $CaCO_3$ was greater at the edges of the samples. Increased precipitation at the matrix-column wall interface could be due to chemical phenomena related to the material of the molds, or to the greater porosity locally present in those areas, and consequent higher volume of reactants.

Numerical estimates were always higher than those empirically obtained, with a maximum of 216% more for the WG, due to thresholding challenges, and with an average of 150% more for UN and PG. These major errors render the XRCT results of this study a useful tool for evaluating trends and for qualitative analysis only.

The numerical permeability analysis resulted to be an effective non-invasive tool to explore the hydraulic properties of a soil.

Permeability varied as a function of both CC and granulometry, resulting higher in the PG, followed by UN and WG. Along the columns, the variations are mainly due to $CaCO_3$

crystals and beads size distributions, which affect the sample tortuosity, with maximum evidence in the case of agglomerates of fines.

The flow velocities in PG were found to be the highest, due to the presence of larger pores, which lead to the establishment of preferential flow paths and locally uneven CC distribution. In the UN, on the other hand, although the velocities are lower, preferential channels are absent, and precipitation can occur more homogeneously. The maximum irregularity was found in the WG, in which the low permeability areas confirmed to be able to divert the incident flow or slow it down a lot, probably therein causing a greater cementation, with an inhomogeneity that manifests at the scale of the column.

The reduction in permeability, according to numerical estimates, was always in the order of 10-20% and increasing with increasing GSD variability. Slightly higher (20-30%) were the results obtained from the Kozeny-Carman equations. The difference was considered due to the influence of tortuosity, more effectively taken into account by Avizo. In general, the decrease in permeability following the treatment is small, especially when compared with the effects of a traditional cement soil improvement.

The numerical analysis of the failure mechanism revealed the presence of an evident elastic response phase, following which failure occurred. The latter was of brittle type, with the formation of rigid fragments, sliding on two predominant failure surfaces, and resulting into dilation. The failure mode was, therefore, identified as double shear type, typical in soft rocks.

7.1.3. General observations

This study has provided some answers on the MICP behavior at the microscopic level. The chemical and physical monitoring of the reaction, together with the numerical analyses, made it possible to observe the influence that the pore-scale soil heterogeneities have on the result of the treatment.

Chemical analyses proved to be an excellent tool for undisturbed investigations of the reaction, providing a highly indicative estimate of the extent of precipitation and of the final calcite content inside the samples.

The calcium carbonate content calculation by means of acid digestion was a good starting point on which to base the pore-scale investigations deriving from the numerical analysis.

Through the study of XRCT images, it was possible to observe the distribution of calcite along the height of the treated samples and on the different sizes of the beads. The pore skeleton and permeability analyses were fundamental to understand the behavior of the reactants inside the solid matrices, whose local velocities and volumes are the factors determining the $CaCO_3$ preferential precipitation and the CC distribution at both the pore and the column level.

Finally, scanning electron microscopy investigations have proved to be an essential tool for confirming or refuting the experimental and numerical results, showing the distribution of crystals at the microscopic level and their morphology.

From the analysis of the treatment results on three granulometries of increasing GSD gradation, was possible to draw some important conclusions.

First, due to the lower bacterial activity drop observed in the WG at the end of the treatment with respect to the other granulometries, a greater relative bacterial presence in the sample was hypothesized. This is considered a consequence of the higher content of fine and contacts points between the grains, representing favourable characteristics to the attachment of bacterial cells.

The variability in the granulometry influences the homogeneity of the treatment, with a uniform soil characterized by more homogenous cementation than a poorly-graded and even more so against a well-graded one. This trend is the consequence of the rheological behavior of the reactants within the solid matrices. Greater variability, and in particular a localized presence of fines, can cause locally reduced permeabilities and the generation of preferential pathways, in which reactants are mostly transported. In correspondence with the low permeability areas, filtering phenomena and local slowdowns of the flow occur. The passage of the solutions is forced there, with consequent increased precipitation. In the case of uniform flows, even with lower average velocities, the calcite distribution is much more homogeneous.

Precipitation increased near the CS injection point, with considerably lower $CaCO_3$ concentrations at greater distances, regardless of granulometry. Clogging phenomena are, therefore, conceivable at the scale of the column. Alternatively, a lower delivery at high distances may be due to a lack of reactants in the solution reaching these portions of the column, due to increased precipitation in the first parts.

The scanning electron microscopy analyses showed a preferential and uniform precipitation on the beads between 200 and 300 μm, localized at the contact points for the smaller diameter beads and more scattered on the larger spheres. This could indicate the influence of the pore size in which precipitation occurs, disadvantaged for very large diameters and for very small spaces, in which reactants and bacteria undergo filtering effects.

Calcite has always been found at the particle-particle contact points. Its extension in aggregates has never reached such dimensions as to occlude the pores. The minimal reduction in permeability observed after the treatment is a consequence of this distribution of crystals.

The same investigations made it possible to observe the failure mechanism at a microscopic scale, represented by the detachment of the crystals from the smooth surfaces of the glass spheres. At a macroscopic level, the failure mechanism due to uniaxial load was of brittle type, with the formation of at least two failure surfaces and rigid fragments sliding on them.

The limits of the study are represented by the resolution of the images and the contrast between calcite and glass, which were not sufficient to detect the single $CaCO_3$ crystals, whose distribution in the three-dimensional space has not been possible to study numerically. The analysis of the precipitation along the height of the column, although quite detailed, still represents a two-dimensional investigation. However, the simulations of the flow velocities and the pore skeleton study allowed the formulation of hypotheses on the 3D behavior of MICP.

The treatment of a single series of samples for each specimen size did not allow to completely validate the results, although the outcomes of the analysis on the two dimensions under study were concordant. The treatment of triplicates in parallel would have provided greater consistency to the results.

Finally, the poor quality of the well-graded cemented sample XRCT images did not allow to precisely explore the numerical results of the treatment for that granulometry, leading to a certain overestimation of the CC.

7.2. Perspectives

The results obtained from this preliminary study of the effect of pore-scale heterogeneity on the efficiency of MICP treatment proved promising for further investigation. Therefore, experimental replication to validate the observations of this work is suggested. In this case, the granulometries under study could be modified, in order to avoid rough segregation of fines.

In case of use of base material different from glass beads, the void ratio could be adjusted, in order to treat samples of the same relative density. However, glass spheres proved to be a highly effective material for achieving standardization of results.

Secondly, it is considered important to extend the numerical investigation to a three-dimensional space. This further investigation is suggested to be designed with the use of a base material with different refractive index than calcite, to be able to achieve the segmentation of precipitated calcium carbonate crystals and define their spatial distribution with precision, with respect to the pore-scale heterogeneities. Observing three-dimensionally the area of $CaCO_3$ preferential precipitation, in relation to the local velocities of the solutions, would allow to definitively link the rheological consequences deriving from the pore-scale heterogeneities with calcite precipitation kinetics. It would also be possible to better understand the link between soil grain radius and calcite preferential deposition, which for the moment has only been given an explanation related to filtering processes and to the link between total surface energy and nucleation.

To conclude, the execution of a greater number of UCS tests on all the granulometries under study and on different portions of the columns, would allow to investigate the mechanical differences between the granulometries and at varying CCs. This would provide with additional information on the distribution of the loads, on the cementation efficiency in total strength increase and on the failure mechanisms.

These and further investigations would provide some of the required answers for a full understanding of the MICP at the microscale, starting from the biological behavior at the different morphological conditions deriving from the pore size distribution, up to the local factors determining the result of the ureolysis reaction.

By fully understanding the factors influencing the calcium carbonate precipitation and its spatial distribution at the pore-scale, one could predict the effects of a certain treatment strategy on the cementation outcome, and definitively transfer the technology to the field-

scale, where other challenges will be faced to consolidate the MICP technology in a world where the demand for environmental-friendly alternatives to traditional techniques is clear.

References

Al Qabany, A., Soga, K., Santamarina, C., 2012. Factors Affecting Efficiency of Microbially Induced Calcite Precipitation. Journal of Geotechnical and Geoenvironmental Engineering 138, 992–1001. https://doi.org/10.1061/(ASCE)GT.1943-5606.0000666

Amarger, N., 2002. Genetically modified bacteria in agriculture. Biochimie 84, 1061–1072. https://doi.org/10.1016/S0300-9084(02)00035-4

Anbu, P., Kang, C.-H., Shin, Y.-J., So, J.-S., 2016. Formations of calcium carbonate minerals by bacteria and its multiple applications. SpringerPlus 5, 250. https://doi.org/10.1186/s40064-016-1869-2

ASTM D2166 / D2166M-16, 2016. Standard Test Method for Unconfined Compressive Strength of Cohesive Soil. ASTM International, West Conshohocken. https://doi.org/10.1520/D2166_D2166M-16

ASTM D2487-17e1, 2017. Standard Practice for Classification of Soils for Engineering Purposes (Unified Soil Classification System). ASTM International, West Conshohocken. https://doi.org/10.1520/D2487-06

ATCC® 11859™, n.d. Sporosarcina pasteurii (Miquel) Yoon et al. ATCC ® 11859™ [WWW Document]. URL https://www.lgcstandards-atcc.org/products/all/11859.aspx?geo_country=ch#generalinformation (accessed 5.11.21).

Bajaj, S., Singh, D.K., 2015. Biodegradation of persistent organic pollutants in soil, water and pristine sites by cold-adapted microorganisms: Mini review. International Biodeterioration & Biodegradation 100, 98–105. https://doi.org/10.1016/j.ibiod.2015.02.023

Bam, L., Miller, J., Becker, M., 2020. A Mineral X-ray Linear Attenuation Coefficient Tool (MXLAC) to Assess Mineralogical Differentiation for X-ray Computed Tomography Scanning. Minerals 10, 441. https://doi.org/10.3390/min10050441

Castillo-Carvajal, L.C., Sanz-Martín, J.L., Barragán-Huerta, B.E., 2014. Biodegradation of organic pollutants in saline wastewater by halophilic microorganisms: a review. Environ Sci Pollut Res 21, 9578–9588. https://doi.org/10.1007/s11356-014-3036-z

Cement Sustainability Initiative [WWW Document], 2018. . Global Cement. URL https://www.globalcement.com/news/itemlist/tag/Cement%20Sustainability%20Initiative?start=10 (accessed 6.15.21).

Cement technology roadmap plots path to cutting CO2 emissions 24% by 2050 - News [WWW Document], 2018. . IEA. URL https://www.iea.org/news/cement-technology-roadmap-plots-path-to-cutting-co2-emissions-24-by-2050 (accessed 6.15.21).

Chakraborty, S., Bisai, R., Palaniappan, S.K., Pal, S.K., 2019. Failure Modes of Rocks under Uniaxial Compression Tests: An Experimental Approach. Journal of Advances in Geotechnical Engineering 2, 1–8. https://doi.org/10.5281/zenodo.3461773

Cheng, L., 2012. Innovative ground enhancement by improved microbially induced CaCO3 precipitation technology (phd). Cheng, Liang <https://researchrepository.murdoch.edu.au/view/author/Cheng, Liang.html> (2012) Innovative ground enhancement by improved microbially induced CaCO3 precipitation technology. PhD thesis, Murdoch University. Murdoch University.

Cheng, L., Cord-Ruwisch, R., Shahin, M., 2013. Cementation of sand soil by microbially induced calcite precipitation at various degrees of saturation. Canadian Geotechnical Journal 50, 81–90. https://doi.org/10.1139/cgj-2012-0023

Cheng, L., Shahin, M.A., Mujah, D., 2017. Influence of Key Environmental Conditions on Microbially Induced Cementation for Soil Stabilization. Journal of Geotechnical and Geoenvironmental Engineering 143, 04016083. https://doi.org/10.1061/(ASCE)GT.1943-5606.0001586

Chou, C.-W., Seagren, E.A., Aydilek, A.H., Lai, M., 2011. Biocalcification of Sand through Ureolysis. Journal of Geotechnical and Geoenvironmental Engineering 137, 1179–1189. https://doi.org/10.1061/(ASCE)GT.1943-5606.0000532

Chu, J., Ivanov, V., Naeimi, M., Stabnikov, V., Liu, H.-L., 2014. Optimization of calcium-based bioclogging and biocementation of sand. Acta Geotech. 9, 277–285. https://doi.org/10.1007/s11440-013-0278-8

Clarà Saracho, A., Haigh, S., Soga, K., Farsang, S., Redfern, S., Marek, E., 2020a. Characterisation of CaCO3 phases during strain-specific ureolytic precipitation. Scientific Reports 10. https://doi.org/10.1038/s41598-020-66831-y

Clarà Saracho, A., Haigh, S.K., Ehsan Jorat, M., 2020b. Flume study on the effects of microbial induced calcium carbonate precipitation (MICP) on the erosional behaviour of fine sand. Géotechnique 1–15. https://doi.org/10.1680/jgeot.19.P.350

Cui, M.-J., Zheng, J.-J., Zhang, R.-J., Lai, H.-J., Zhang, J., 2017. Influence of cementation level on the strength behaviour of bio-cemented sand. Acta Geotech. 12, 971–986. https://doi.org/10.1007/s11440-017-0574-9

Dadda, A., Geindreau, C., Emeriault, F., du Roscoat, S.R., Garandet, A., Sapin, L., Filet, A.E., 2017. Characterization of microstructural and physical properties changes in biocemented sand using 3D X-ray microtomography. Acta Geotech. 12, 955–970. https://doi.org/10.1007/s11440-017-0578-5

Das, B.M., Sivakugan, N., 2011. Maximum and minimum void ratios and median grain size of granular soils: their importance and correlations with material properties, in: Shahin, M.A., Nikraz, H.R. (Eds.), . Presented at the ICAGE 2011 International Conference on Advances in Geotechnical Engineering, Curtin University, Perth, WA, Australia, pp. 59–73.

De Belie, N., Muynck, W., 2008. Crack repair in concrete using biodeposition 777–781. https://doi.org/10.1201/9781439828403.ch107

Dejong, J., Montoya, B., Boulanger, R., 2013. Dynamic response of liquefiable sand improved by microbial-induced calcite precipitation. Géotechnique 63, 302–312. https://doi.org/10.1680/geot.SIP13.P.019

DeJong, J.T., Fritzges, M.B., Nüsslein, K., 2006. Microbially Induced Cementation to Control Sand Response to Undrained Shear. Journal of Geotechnical and Geoenvironmental Engineering 132, 1381–1392. https://doi.org/10.1061/(ASCE)1090-0241(2006)132:11(1381)

DeJong, J.T., Mortensen, B.M., Martinez, B.C., Nelson, D.C., 2010. Bio-mediated soil improvement. Ecological Engineering, Special Issue: BioGeoCivil Engineering 36, 197–210. https://doi.org/10.1016/j.ecoleng.2008.12.029

Dupraz, C., Visscher, P.T., 2005. Microbial lithification in marine stromatolites and hypersaline mats. Trends in Microbiology 13, 429–438. https://doi.org/10.1016/j.tim.2005.07.008

Duraisamy, Y., 2016. Strength And Stiffness Improvement Of Bio-Cemented Sydney Sand.

Ergun, S., 1952. Fluid flow through packed columns [WWW Document]. URL http://dns2.asia.edu.tw/~ysho/YSHO-English/2000%20Engineering/PDF/Che%20Eng%20Pro48,%2089.pdf (accessed 5.28.21).

Fauriel, S., 2012. Multiphysical Modelling of Soils with a Focus on Microbially Induced Calcite Precipitation [WWW Document]. Infoscience. https://doi.org/10.5075/epfl-thesis-5413

Feng, K., Montoya, B.M., 2016. Influence of Confinement and Cementation Level on the Behavior of Microbial-Induced Calcite Precipitated Sands under Monotonic Drained Loading. Journal of Geotechnical and Geoenvironmental Engineering 142, 04015057. https://doi.org/10.1061/(ASCE)GT.1943-5606.0001379

Feng, K., Montoya, B.M., Evans, T.M., 2017. Discrete element method simulations of bio-cemented sands. Computers and Geotechnics 85, 139–150. https://doi.org/10.1016/j.compgeo.2016.12.028

Gao, C.H., Zekri, A., 2011. Applications of Microbial-Enhanced Oil Recovery Technology in the Past Decade. Energy Sources, Part A: Recovery, Utilization, and Environmental Effects 33, 972–989. https://doi.org/10.1080/15567030903330793

Gao, Y., Hang, L., He, J., Chu, J., 2019. Mechanical behaviour of biocemented sands at various treatment levels and relative densities. Acta Geotech. 14, 697–707. https://doi.org/10.1007/s11440-018-0729-3

Gomez, M.G., Martinez, B.C., DeJong, J.T., Hunt, C.E., deVlaming, L.A., Major, D.W., Dworatzek, S.M., 2015. Field-scale bio-cementation tests to improve sands. Proceedings of the Institution of Civil Engineers - Ground Improvement 168, 206–216. https://doi.org/10.1680/grim.13.00052

Hammes, F., Boon, N., De Villiers, J., Verstraete, W., Siciliano, S.D., 2003. Strain-specific ureolytic microbial calcium carbonate precipitation. Applied and Environmental Microbiology 69, 4901–4909. https://doi.org/10.1128/AEM.69.8.4901-4909.2003

Hammes, F., Verstraete*, W., 2002. Key roles of pH and calcium metabolism in microbial carbonate precipitation. Re/Views in Environmental Science and Bio/Technology 1, 3–7. https://doi.org/10.1023/A:1015135629155

Ivanov, V., Chu, J., 2008. Applications of microorganisms to geotechnical engineering for bioclogging and biocementation of soil in situ. Rev Environ Sci Biotechnol 7, 139–153. https://doi.org/10.1007/s11157-007-9126-3

Karol, R.H., 2003. Chemical Grouting And Soil Stabilization, Revised And Expanded. CRC Press.

Kim, H.K., Park, S.J., Han, J.I., Lee, H.K., 2013. Microbially mediated calcium carbonate precipitation on normal and lightweight concrete. Construction and Building Materials, 25th Anniversary Session for ACI 228 – Building on the Past for the Future of NDT of Concrete 38, 1073–1082. https://doi.org/10.1016/j.conbuildmat.2012.07.040

Konstantinou, C., Biscontin, G., Jiang, N.-J., Soga, K., 2021a. Application of microbially induced carbonate precipitation (MICP) to form bio-cemented artificial sandstone. Journal of Rock Mechanics and Geotechnical Engineering 13. https://doi.org/10.1016/j.jrmge.2021.01.010

Konstantinou, C., Wang, Y., Biscontin, G., Soga, K., 2021b. The role of bacterial urease activity on the uniformity of carbonate precipitation profiles of bio-treated coarse sand specimens. Scientific Reports 11, 6161. https://doi.org/10.1038/s41598-021-85712-6

Kruczek, B., 2014. Carman–Kozeny Equation, in: Drioli, E., Giorno, L. (Eds.), Encyclopedia of Membranes. Springer Berlin Heidelberg, Berlin, Heidelberg, pp. 1–3. https://doi.org/10.1007/978-3-642-40872-4_1995-1

Kucharski, E.S., Cord-Ruwisch, R., Whiffin, V.S., Al-Thawadi, S., 2006. Microbial biocementation [WWW Document]. Patent. URL https://researchrepository.murdoch.edu.au/id/eprint/9464/ (accessed 3.6.21).

Lade, P., Liggio, C.D., Yamamuro, J., 1998. Effects of non-plastic fines on minimum and maximum void ratios of sand. https://doi.org/10.1520/GTJ11373J

Lauchnor, E.G., Topp, D.M., Parker, A.E., Gerlach, R., 2015. Whole cell kinetics of ureolysis by Sporosarcina pasteurii. J Appl Microbiol 118, 1321–1332. https://doi.org/10.1111/jam.12804

Lazar, I., Petrisor, I.G., Yen, T.F., 2007. Microbial Enhanced Oil Recovery (MEOR). Petroleum Science and Technology 25, 1353–1366. https://doi.org/10.1080/10916460701287714

Li, T., Li, M., Jing, X., Xiao, W., Cui, Q., 2019. Influence mechanism of pore-scale anisotropy and pore distribution heterogeneity on permeability of porous media. Petroleum Exploration and Development 46, 594–604. https://doi.org/10.1016/S1876-3804(19)60039-X

Lin, H. (Thomas), Suleiman, M., Brown, D., Kavazanjian, E., 2015. Mechanical Behavior of Sands Treated by Microbially Induced Carbonate Precipitation. Journal of Geotechnical and Geoenvironmental Engineering 142, 04015066. https://doi.org/10.1061/(ASCE)GT.1943-5606.0001383

Liu, S., Wen, K., Armwood, C., Bu, C., Li, C., Amini, F., Li, L., 2019. Enhancement of MICP-Treated Sandy Soils against Environmental Deterioration. Journal of Materials in Civil Engineering 31, 04019294. https://doi.org/10.1061/(ASCE)MT.1943-5533.0002959

Mahawish, A., Bouazza, A., Gates, W.P., 2018. Effect of particle size distribution on the bio-cementation of coarse aggregates. Acta Geotech. 13, 1019–1025. https://doi.org/10.1007/s11440-017-0604-7

Martinez, B.C., DeJong, J.T., 2012. Bio-Mediated Soil Improvement: Load Transfer Mechanisms at the Micro- and Macro- Scales 242–251. https://doi.org/10.1061/41025(338)26

Martinez, B.C., DeJong, J.T., Ginn, T.R., 2014. Bio-geochemical reactive transport modeling of microbial induced calcite precipitation to predict the treatment of sand in one-dimensional flow. Computers and Geotechnics 58, 1–13. https://doi.org/10.1016/j.compgeo.2014.01.013

Martinez, B.C., DeJong, J.T., Ginn, T.R., Montoya, B.M., Barkouki, T.H., Hunt, C., Tanyu, B., Major, D., 2013. Experimental Optimization of Microbial-Induced Carbonate Precipitation for Soil Improvement. Journal of Geotechnical and Geoenvironmental Engineering 139, 587–598. https://doi.org/10.1061/(ASCE)GT.1943-5606.0000787

McGeary, R., 1961. Mechanical Packing of Spherical Particles. Journal of the American Ceramic Society 44, 513–522. https://doi.org/10.1111/j.1151-2916.1961.tb13716.x

Mitchell, J.K., Santamarina, J.C., 2005. Biological Considerations in Geotechnical Engineering. Journal of Geotechnical and Geoenvironmental Engineering 131, 1222–1233. https://doi.org/10.1061/(ASCE)1090-0241(2005)131:10(1222)

Molins, S., Trebotich, D., Steefel, C.I., Shen, C., 2012. An investigation of the effect of pore scale flow on average geochemical reaction rates using direct numerical simulation. Water Resources Research 48. https://doi.org/10.1029/2011WR011404

Mortensen, B.M., DeJong, J.T., 2012. Strength and Stiffness of MICP Treated Sand Subjected to Various Stress Paths 4012–4020. https://doi.org/10.1061/41165(397)410

Mortensen, B.M., Haber, M.J., DeJong, J.T., Caslake, L.F., Nelson, D.C., 2011. Effects of environmental factors on microbial induced calcium carbonate precipitation. Journal of Applied Microbiology 111, 338–349. https://doi.org/10.1111/j.1365-2672.2011.05065.x

Mujah, D., Cheng, L., Shahin, M., 2019. Microstructural and Geomechanical Study on Biocemented Sand for Optimization of MICP Process. Journal of Materials in Civil Engineering 31. https://doi.org/10.1061/(ASCE)MT.1943-5533.0002660

Nemati, M., Greene, E.A., Voordouw, G., 2005. Permeability profile modification using bacterially formed calcium carbonate: comparison with enzymic option. Process Biochemistry 40, 925–933. https://doi.org/10.1016/j.procbio.2004.02.019

Nemati, M., Voordouw, G., 2003. Modification of porous media permeability, using calcium carbonate produced enzymatically in situ. Enzyme and Microbial Technology 33, 635–642. https://doi.org/10.1016/S0141-0229(03)00191-1

Noiriel, C., Steefel, C.I., Yang, L., Ajo-Franklin, J., 2012. Upscaling calcium carbonate precipitation rates from pore to continuum scale. Chemical Geology 318–319, 60–74. https://doi.org/10.1016/j.chemgeo.2012.05.014

Noiriel, C., Steefel, C.I., Yang, L., Bernard, D., 2016. Effects of pore-scale precipitation on permeability and flow. Advances in Water Resources 95, 125–137. https://doi.org/10.1016/j.advwatres.2015.11.013

OECD Environmental Outlook to 2050: The Consequences of Inaction - Key Facts and Figures - OECD [WWW Document], 2012. . OECD. URL https://www.oecd.org/env/indicators-modelling-

outlooks/oecdenvironmentaloutlookto2050theconsequencesofinaction-keyfactsandfigures.htm (accessed 6.15.21).

Oliveira, P.J.V., Freitas, L.D., Carmona, J.P.S.F., 2017. Effect of Soil Type on the Enzymatic Calcium Carbonate Precipitation Process Used for Soil Improvement. Journal of Materials in Civil Engineering 29, 04016263. https://doi.org/10.1061/(ASCE)MT.1943-5533.0001804

Onoda, G.Y., Liniger, E.G., 1990. Random loose packings of uniform spheres and the dilatancy onset. Phys. Rev. Lett. 64, 2727–2730. https://doi.org/10.1103/PhysRevLett.64.2727

Pan, X., Chu, J., Yang, Y., Cheng, L., 2020. A new biogrouting method for fine to coarse sand. Acta Geotechnica 15. https://doi.org/10.1007/s11440-019-00872-0

Pouliquen, O., Nicolas, M., Weidman, P.D., 1997. Crystallization of non-Brownian Spheres under Horizontal Shaking. Phys. Rev. Lett. 79, 3640–3643. https://doi.org/10.1103/PhysRevLett.79.3640

Proaño, L., Sarmiento, A.T., Figueredo, M., Cobo, M., 2020. Techno-economic evaluation of indirect carbonation for CO2 emissions capture in cement industry: A system dynamics approach. Journal of Cleaner Production 263, 121457. https://doi.org/10.1016/j.jclepro.2020.121457

Qabany, A. al, Soga, K., 2013. Effect of chemical treatment used in MICP on engineering properties of cemented soils. Géotechnique 63, 331–339. https://doi.org/10.1680/geot.SIP13.P.022

Rebata-Landa, V., 2007. Microbial Activity in Sediments: Effects on Soil Behavior.

Rowshanbakht, K., Khamehchiyan, M., Sajedi, R., Nikudel, M., 2016. Effect of injected bacterial suspension volume and relative density on carbonate precipitation resulting from microbial treatment. Ecological Engineering 89, 49–55. https://doi.org/10.1016/j.ecoleng.2016.01.010

Santosh, K., Ramachandran, S.K., Ramakrishnan, V., Bang, S.S., 2001. Remediation of concrete using microorganisms. American Concrete Institute Journal 98, 3–9.

Skinner, H.C.W., Jahren, A.H., 2003. Biomineralization. Treatise on Geochemistry 8, 682. https://doi.org/10.1016/B0-08-043751-6/08128-7

Srivastava, S., 2003. Understanding Bacteria. Springer Science & Business Media.

Stack, A.G., 2015. Precipitation in Pores: A Geochemical Frontier. Reviews in Mineralogy and Geochemistry 80, 165–190. https://doi.org/10.2138/rmg.2015.80.05

Stocks-Fischer, S., Galinat, J.K., Bang, S.S., 1999. Microbiological precipitation of CaCO3. Soil Biology and Biochemistry 31, 1563–1571. https://doi.org/10.1016/S0038-0717(99)00082-6

Stranne, C., O'Regan, M., Jakobsson, M., Brüchert, V., Ketzer, M., 2019. Can anaerobic oxidation of methane prevent seafloor gas escape in a warming climate? Solid Earth 10, 1541–1554. https://doi.org/10.5194/se-10-1541-2019

Terzis, D., 2017. Kinetics, Mechanics and Micro-structure of Bio-cemented Soils 246.

Terzis, D., Bernier-Latmani, R., Laloui, L., 2016. Fabric characteristics and mechanical response of bio-improved sand to various treatment conditions. Géotechnique Letters 6, 50–57. https://doi.org/10.1680/jgele.15.00134

Terzis, D., Laloui, L., 2019. A decade of progress and turning points in the understanding of bio-improved soils: A review. Geomechanics for Energy and the Environment 19, 100116. https://doi.org/10.1016/j.gete.2019.03.001

Terzis, D., Laloui, L., 2018. 3-D micro-architecture and mechanical response of soil cemented via microbial-induced calcite precipitation. Sci Rep 8, 1416. https://doi.org/10.1038/s41598-018-19895-w

ThermoFisher SCIENTIFIC [WWW Document], n.d. URL //www.thermofisher.com/uk/en/home/industrial/electron-microscopy/electron-microscopy-instruments-workflow-solutions/3d-visualization-analysis-software.html (accessed 5.21.21).

Van Hamme, J.D., 2004. Bioavailability and Biodegradation of Organic Pollutants — A Microbial Perspective, in: Singh, A., Ward, O.P. (Eds.), Biodegradation and Bioremediation, Soil Biology. Springer, Berlin, Heidelberg, pp. 37–56. https://doi.org/10.1007/978-3-662-06066-7_3

Van Paassen, L., Ghose, R., Van der Linden, T.J.M., Van der Star, W.R.L., Van Loosdrecht, M.C.M., 2010. Quantifying Biomediated Ground Improvement by Ureolysis: Large-Scale Biogrout Experiment. Journal of Geotechnical and

Geoenvironmental Engineering 136, 1721–1728. https://doi.org/10.1061/(ASCE)GT.1943-5606.0000382

Van Paassen, L.A., 2009. Biogrout, ground improvement by microbial induced carbonate precipitation.

Van Tittelboom, K., De Belie, N., De Muynck, W., Verstraete, W., 2010. Use of bacteria to repair cracks in concrete. CEMENT AND CONCRETE RESEARCH 40, 157–166. https://doi.org/10.1016/j.cemconres.2009.08.025

Venda Oliveira, P.J., da Costa, M.S., Costa, J.N.P., Nobre, M.F., 2015. Comparison of the Ability of Two Bacteria to Improve the Behavior of Sandy Soil. Journal of Materials in Civil Engineering 27, 06014025. https://doi.org/10.1061/(ASCE)MT.1943-5533.0001138

Wang, Y., 2019. Microbial-Induced Calcium Carbonate Precipitation: from micro to macro scale (Thesis). University of Cambridge. https://doi.org/10.17863/CAM.35552

Wang, Y., Liu, H., Zhang, Z., Xiao, P., He, X., Xiao, Y., 2019. Study on Low-Strength Biocemented Sands Using a Temperature-Controlled MICP (Microbially Induced Calcite Precipitation) Method: Proceedings of the 5th GeoChina International Conference 2018 – Civil Infrastructures Confronting Severe Weathers and Climate Changes: From Failure to Sustainability, held on July 23 to 25, 2018 in HangZhou, China. pp. 15–26. https://doi.org/10.1007/978-3-319-95771-5_2

Wang, Y., Soga, K., DeJong, J.T., Kabla, A.J., 2021. Effects of Bacterial Density on Growth Rate and Characteristics of Microbial-Induced CaCO3 Precipitates: Particle-Scale Experimental Study. Journal of Geotechnical and Geoenvironmental Engineering 147, 04021036. https://doi.org/10.1061/(ASCE)GT.1943-5606.0002509

Whiffin, V.S., 2004. Microbial CaCO3 precipitation for the production of biocement (phd). Whiffin, Victoria S. <https://researchrepository.murdoch.edu.au/view/author/Whiffin, Victoria.html> (2004) Microbial CaCO3 precipitation for the production of biocement. PhD thesis, Murdoch University. Murdoch University.

Whiffin, V.S., Paassen, L.A. van, Harkes, M.P., 2007. Microbial carbonate precipitation as a soil improvement technique. GEOMICROBIOL.J. 24, 417–423. https://doi.org/10.1080/01490450701436505

Xiao, Y., Wang, Y., Wang, S., Evans, T.M., Stuedlein, A.W., Chu, J., Zhao, C., Wu, H., Liu, H., 2021. Homogeneity and mechanical behaviors of sands improved by a temperature-controlled one-phase MICP method. Acta Geotech. https://doi.org/10.1007/s11440-020-01122-4

Yadav, V., Batham, S., Acharya, A., Paul, R., 2014. Approach to accurate circle detection: Circular Hough Transform and Local Maxima concept. Presented at the 2014 International Conference on Electronics and Communication Systems, ICECS 2014, pp. 1–5. https://doi.org/10.1109/ECS.2014.6892577

Yoon, J.H., Lee, K.C., Weiss, N., Kho, Y.H., Kang, K.H., Park, Y.H., 2001. Sporosarcina aquimarina sp. nov., a bacterium isolated from seawater in Korea, and transfer of Bacillus globisporus (Larkin and Stokes 1967), Bacillus psychrophilus (Nakamura 1984) and Bacillus pasteurii (Chester 1898) to the genus Sporosarcina as Sporosarcina globispora comb. nov., Sporosarcina psychrophila comb. nov. and Sporosarcina pasteurii comb. nov., and emended description of th. International Journal of Systematic and Evolutionary Microbiology, 51, 1079–1086. https://doi.org/10.1099/00207713-51-3-1079

Zamani, A., Montoya, B.M., 2018. Undrained Monotonic Shear Response of MICP-Treated Silty Sands. Journal of Geotechnical and Geoenvironmental Engineering 144, 04018029. https://doi.org/10.1061/(ASCE)GT.1943-5606.0001861

Zamani, A., Montoya, B.M., 2016. Permeability Reduction Due to Microbial Induced Calcite Precipitation in Sand 94–103. https://doi.org/10.1061/9780784480120.011

Zwietering, M.H., Jongenburger, I., Rombouts, F.M., Riet, K. van 't, 1990. Modeling of the Bacterial Growth Curve. Appl. Environ. Microbiol. 56, 1875–1881.